

A COMPARATIVE STUDY OF THE FITTING PERFORMANCE OF
HYPERELASTIC CONSTITUTIVE MODELS

A THESIS SUBMITTED TO
THE GRADUATE SCHOOL OF NATURAL AND APPLIED SCIENCES
OF
MIDDLE EAST TECHNICAL UNIVERSITY

BY

YASHAR BADIENIA

IN PARTIAL FULFILLMENT OF THE REQUIREMENTS
FOR
THE DEGREE OF MASTER OF SCIENCE
IN
MECHANICAL ENGINEERING

SEPTEMBER 2019

Approval of the thesis:

**A COMPARATIVE STUDY OF THE FITTING PERFORMANCE OF
HYPERELASTIC CONSTITUTIVE MODELS**

submitted by **YASHAR BADIENIA** in partial fulfillment of the requirements for the degree of **Master of Science in Mechanical Engineering Department, Middle East Technical University** by,

Prof. Dr. Halil Kalıpçılar
Dean, Graduate School of **Natural and Applied Sciences**

Prof. Dr. M. A. Sahir Arıkan
Head of Department, **Mechanical Engineering**

Assoc. Prof. Dr. Hüsnü Dal
Supervisor, **Mechanical Engineering, METU**

Examining Committee Members:

Prof. Dr. Suha Oral
Mechanical Engineering, METU

Assoc. Prof. Dr. Hüsnü Dal
Mechanical Engineering, METU

Prof. Dr. Serkan Dağ
Mechanical Engineering, METU

Assoc. Prof. Dr. Ercan Gürses
Aerospace Engineering, METU

Assoc. Prof. Dr. Barış Sabuncuoğlu
Mechanical Engineering, Hacettepe University

Date: 11.09.2019

I hereby declare that all information in this document has been obtained and presented in accordance with academic rules and ethical conduct. I also declare that, as required by these rules and conduct, I have fully cited and referenced all material and results that are not original to this work.

Name, Surname: Yashar Badienia

Signature :

ABSTRACT

A COMPARATIVE STUDY OF THE FITTING PERFORMANCE OF HYPERELASTIC CONSTITUTIVE MODELS

Badienia, Yashar

M.S., Department of Mechanical Engineering

Supervisor: Assoc. Prof. Dr. Hüsnü Dal

September 2019, 207 pages

Hyperelastic materials are widely used over the last decades. Studies on molecular structure and stress-stretch response of such materials goes back to 1940. Since then, many researchers have developed various material models to represent the response of hyperelastic materials undergoing different loading scenarios. Generally phenomenological and micromechanically based material models are the two main categories considered during the modeling steps. Among the hyperelastic material models micromechanically based network models are known to have high performance and reliability over the purely phenomenological models dealing with the analysis of unfilled rubber. Number of available experimental data sets under different loading cases, maximum stretch level reached by each loading case, and additives with percentage of fillers, on the other hand, play an important role choosing the appropriate model for further analysis of technical rubber. Therefore, a well defined hyperelastic material model should have physically interpretable and minimum number of parameters. During the last decades number of hyperelastic material models has been increased, therefore, comparison among the material models and choosing an appropriate one

turns to be crucial factor for researchers of the field. One may access to large number of review papers comparing strength and weakness of constitutive material models, implying the importance of making decision between different types of constitutive models suiting the specific analysis. In this study, fitting performance of 40 hyper-elastic material models has been presented. In order to obtain parameters for each constitutive model a genetic algorithm is developed. Further improvement of the results are achieved using FMINCON utility of MATLAB. Four set of distinct and well known data for uniaxial tensile, equi-biaxial, pure shear, and biaxial tension loads has been considered during parameter optimization.

Keywords: Hyperelasticity, parameter optimization, rubber-like material, genetic algorithm, multi-objective optimization

ÖZ

HİPERELASTİK BÜNYE MODELLERİNİN EĞRİ UYDURMA PERFORMANSLARININ KARŞILAŞTIRILMALI ANALİZİ

Badienia, Yashar

Yüksek Lisans, Makina Mühendisliği Bölümü

Tez Yöneticisi: Doç. Dr. Hüsnü Dal

Eylül 2019 , 207 sayfa

Son yıllarda hiperelastik malzemeler yaygın olarak kullanılmaktadır. Bu tür malzemelerin moleküler yapısı ve gerilim-gerinim tepkisi üzerine çalışmalar 1940'lı yıllara dayanmaktadır. 1940'lardan yana birçok araştırmacı farklı yükleme senaryoları altında hiperelastik malzemelerin tepkisini temsil etmek adına çeşitli malzeme modelleri geliştirmiştir. Genel olarak fenomenolojik ve mikromekanik tabanlı malzeme modelleri, modelleme aşamalarında dikkate alınan iki ana kategoridir. Hiperelastik malzeme modelleri arasında mikromekanik tabanlı ağ modellerinin, fenomenolojik modellere kıyasla yüksek performans ve güvenilirliğe sahip olduğu bilinmektedir. Farklı yükleme durumları altındaki mevcut deneysel verilerin sayısı, bu yüklemeler esnasında malzemenin ulaştığı maksimum uzama seviyesi ve dolgu katkı maddelerin oranı, teknik kauçuk analizi için uygun modelin seçiminde önemli bir rol oynamaktadır. Bu nedenle, iyi tanımlanmış bir hiperelastik malzeme modelinin fiziksel olarak yorumlanabilir ve minimum parametre sayısına sahip olması gerekmektedir. Son yıllarda, hiperelastik malzeme modellerinin sayısında artış gözlenmektedir. Bu artış sebebiyle, malzeme modelleri arasında kıyaslama yaparak uygun modelin seçilmesi,

bu alanda çalışan arařtırmacılar için önem arz etmektedir. Literatürde bu tür malzeme modellerinin güçlü ve zayıf yönlerini inceleyen çok sayıda deęerlendirme makalesi mevcuttur, bu da belirli bir analize uygun farklı malzeme modelleri arasında seçim ve karar almanın önemini ortaya koymaktadır. Bu çalışmada, 40 hiperelastik malzeme modelinin en iyileme ve eğri uydurma performansı sunulmuştur. Bu modellerin deęişkenlerini elde etmek amacıyla genetik algoritma kodu geliştirilmiştir. Genetik algoritma aracılığıyla elde edilen sonuçlarının iyilemesi ise MATLAB'ın FMINCON yardımcı programı kullanılarak elde edilmiştir. Parametre optimizasyonu sırasında, tek eksenli, eşit-çift eksenli, saf kayma ve çift eksenli çekme yükleri için dört farklı veri seti dikkate alınmıştır.

Anahtar Kelimeler: hiperelastisite, deęişken optimizasyonu, kauçuk türü malzeme, genetik algoritma, çok-amaçlı optimizasyon

To my family

ACKNOWLEDGMENTS

Firstly, I would like to express my sincere thanks and appreciation to my supervisor Assoc. Prof. Dr. Hüsni Dal for his motivation, support, and share of his enormous knowledge during my graduate studies. Despite my slight knowledge about the subject at the beginning of the studies, he believed in me and gave me a chance to be part of his project. His consistency and persistence during the project gave me total energy to continue my research. I cannot imagine being able to reach where I am without his continuous help. I am very grateful for his patience and for always treating me as a colleague.

I was blessed to be a member of computational micromechanics lab, where I have met many dear friends who have made my M.Sc. program very entertaining. I had a great opportunity to work among very bright lab mates who gave me fruitful suggestions and comments during my research studies and most importantly their endless friendship. I would like to especially thank Kemal Açıkgöz for sharing his experiences regardless of the time and condition. They were always available to discuss my disorienting problems cheerfully.

I also would like to thank my amazing friends Payam Parvizi, Yaser Mohamadi, Oğuzhan Güner, Yasemin Bilgen and Hamid Majidi Balaneji for their unbroken encouragement and companionship. They were always beside me in my happiness and sadness. During these years, far from my hometown, they were my second family. We might not be able to see each other more often in the future, but they will be always my best friends.

My deepest thanks go to my parents and siblings for their unconditional love and encouragement throughout my life. I would not have been able to achieve anything in my life without them being by my side along the way. The enlightened vision and determination of my parents helped me to pursue my goals and take strong steps by leaning on them without a second thought. Also, I was fortunate to grow up in

a family with amazing siblings. Being the youngest, I had the opportunity to learn from them all, and I am extremely thankful for that. This study would not be finished without their patience and encouragement.

TABLE OF CONTENTS

ABSTRACT	v
ÖZ	vii
ACKNOWLEDGMENTS	x
TABLE OF CONTENTS	xii
LIST OF TABLES	xviii
LIST OF FIGURES	xxviii
LIST OF ABBREVIATIONS	xxxvi
CHAPTERS	
1 INTRODUCTION	1
1.1 Overview and Background	1
1.2 Elasticity of Rubber-like Materials	3
1.3 Motivation and Contribution	4
1.4 Scope and Outline	4
2 LITERATURE REVIEW	7
3 PRELIMINARIES ON CONTINUUM MECHANICS AND HYPERELAS- TICITY	17
3.1 Basic concepts in Continuum Mechanics	17
3.1.1 Kinematics	18

3.1.2	Stress Expressions	22
3.1.3	Boundary value problems	28
3.2	Hyperelasticity	28
3.2.1	Lagrangian and Eulerian setting	29
3.2.2	Incompressible hyperelasticity	32
3.2.3	Deformation modes	33
3.2.3.1	Uniaxial tension deformation mode	34
3.2.3.2	Equibiaxial tension deformation mode	35
3.2.3.3	Pure shear deformation mode	36
3.2.3.4	Biaxial tension deformation mode	37
3.2.4	Invariant based incompressible hyperelastic material models .	38
3.2.5	Principle stretch based incompressible hyperelastic material models	39
4	HYPERELASTIC MATERIAL MODELS	41
4.1	Phenomenological Material Models	41
4.1.1	First Invariant Base Models	42
4.1.1.1	neo-Hooke model	42
4.1.1.2	Yeoh model	42
4.1.1.3	Gent model	43
4.1.1.4	Yeoh-Fleming model	43
4.1.1.5	Two-Term model	43
4.1.1.6	Exp-Ln model	44
4.1.2	First and Second Invariant Base Models	45

4.1.2.1	Mooney model	45
4.1.2.2	Isihara model	45
4.1.2.3	Biderman model	46
4.1.2.4	Gent-Thomas model	46
4.1.2.5	Hart-Smith model	46
4.1.2.6	Alexander model	47
4.1.2.7	James model	48
4.1.2.8	Haines-Wilson model	48
4.1.2.9	Swanson model	48
4.1.2.10	Kilian (van der Waals) model	49
4.1.2.11	Yamashita-Kawabata model	50
4.1.2.12	Lion model	50
4.1.2.13	Diani-Rey model	50
4.1.2.14	Haupt-Sedlan model	51
4.1.2.15	Chavelier-Marco model	52
4.1.2.16	Pucci-Saccomandi model	52
4.1.2.17	Amin model	52
4.1.2.18	Beda model	53
4.1.2.19	Carroll model	53
4.1.2.20	Nunes model	54
4.1.3	Principle Stretch Base Models	54
4.1.3.1	Valanis-Landel model	54
4.1.3.2	Ogden model	55

4.1.3.3	Slip-Link model	55
4.1.3.4	Constrained-Junction model	56
4.1.3.5	Shariff model	57
4.1.3.6	Attard-Hunt model	58
4.1.3.7	Bechir model	58
4.1.4	Mixed Invariant and Principle Stretch Based Models	59
4.1.4.1	WFB model	59
4.2	Micro-mechanics based material models	60
4.2.1	Entropy, free energy, and force definitions for single chain	61
4.2.2	Three-chain model	63
4.2.3	Arruda-Boyce model	63
4.2.4	Tube model	64
4.2.5	Extended-Tube model	65
4.2.6	Micro-sphere model	66
4.2.7	Khiem (network averaging tube) model	70
5	PARAMETER OPTIMIZATION	73
5.1	Parameter optimization preliminaries	73
5.2	Genetic Algorithm Approach	74
6	RESULTS AND DISCUSSION	79
6.1	Ranking of hyperelastic material models	79
6.2	Results of hyperelastic material models	83
6.2.1	Micro-sphere model results	83
6.2.2	Alexander model results	85

6.2.3	Diani and Rey model results	87
6.2.4	Extended tube model results	89
6.2.5	Shariff model results	91
6.2.6	Carroll model results	93
6.2.7	Network averaging tube model results	95
6.2.8	Chevalier and Marco model results	97
6.2.9	Ogden model results	99
6.2.10	Amin model results	101
6.2.11	James model results	103
6.2.12	Haines-Wilson model results	105
6.2.13	Attard and Hunt model results	107
6.2.14	4-term Bechir model results	109
6.2.15	Pucci and Saccomandi model results	111
6.2.16	Biderman model results	113
6.2.17	Kilian (van der Waals) model results	115
6.2.18	Yamashita and Kawabata model results	117
6.2.19	Lion model results	119
6.2.20	Beda model results	121
6.2.21	Hart-Smith model results	123
6.2.22	Haupt and Sedlan model results	125
6.2.23	Exp-Ln model results	127
6.2.24	Yeoh model results	129
6.2.25	Two-term model results	131

6.2.26	Yeoh-Fleming model results	133
6.2.27	Arruda-Boyce model results	135
6.2.28	Gent model results	137
6.2.29	Three-chain model results	139
6.2.30	Mooney model results	141
6.2.31	Isihara model results	143
6.2.32	Nunes model results	145
6.2.33	Tube model results	147
6.2.34	Slip-link model results	149
6.2.35	Swanson model results	151
6.2.36	Gent-Thomas model results	153
6.2.37	Constrained-junction model results	155
6.2.38	WFB model results	157
6.2.39	neo-Hooke model results	159
6.2.40	Valanis-Landel model results	161
7	CONCLUDING REMARKS	163
	REFERENCES	165
A	EQUIBIAXIAL TENSION RESULTS FOR HYPERELASTIC MODELS .	173
B	PURE SHEAR RESULTS FOR HYPERELASTIC MODELS	189
C	STRAIN ENERGY FUNCTIONS FOR HYPERELASTIC MODELS . . .	205

LIST OF TABLES

TABLES

Table 6.1	First 20 models are sorted based on simultaneous quality of fit values.	81
Table 6.2	Last 20 models are sorted based on simultaneous quality of fit values.	82
Table 6.3	Simultaneous fitting results for Micro-Sphere model.	84
Table 6.4	Uniaxial tension results for Micro-Sphere model.	84
Table 6.5	Biaxial tension results for Micro-Sphere model.	84
Table 6.6	Simultaneous fitting results for Alexander model.	86
Table 6.7	Uniaxial tension fitting results for Alexander model.	86
Table 6.8	Biaxial tension results for Alexander model.	86
Table 6.9	Simultaneous fitting results for Diani and Ray model.	88
Table 6.10	Uniaxial tension results for Diani and Ray model.	88
Table 6.11	Biaxial tension results for Diani and Ray model.	88
Table 6.12	Simultaneous fitting results for Extended-Tube model.	90
Table 6.13	Uniaxial tension results for Extended-Tube model.	90
Table 6.14	Biaxial tension results for Extended-Tube model.	90
Table 6.15	Simultaneous fitting results for Shariff model.	92
Table 6.16	Uniaxial tension results for Shariff model.	92
Table 6.17	Biaxial tension results for Shariff model.	92

Table 6.18	Simultaneous fitting results for Carroll model.	94
Table 6.19	Uniaxial tension results for Carroll model.	94
Table 6.20	Biaxial tension results for Carroll model.	94
Table 6.21	Simultaneous fitting results network averaging tube model.	96
Table 6.22	Uniaxial tension results network averaging tube model.	96
Table 6.23	Biaxial tension results network averaging tube model.	96
Table 6.24	Simultaneous fitting results for Chevalier and Marco model.	98
Table 6.25	Uniaxial tension results for Chevalier and Marco model.	98
Table 6.26	Biaxial tension results for Chevalier and Marco model.	98
Table 6.27	Simultaneous fitting results for Ogden model.	100
Table 6.28	Uniaxial tension results for Ogden model.	100
Table 6.29	Biaxial tension results for Ogden model.	100
Table 6.30	Simultaneous fitting results for Amin model.	102
Table 6.31	Uniaxial tension results for Amin model.	102
Table 6.32	Biaxial tension results for Amin model.	102
Table 6.33	Simultaneous fitting results for James model.	104
Table 6.34	Uniaxial tension results for James model.	104
Table 6.35	Biaxial tension results for James model.	104
Table 6.36	Simultaneous fitting results for Haines and Wilson model.	106
Table 6.37	Uniaxial tension results for Haines and Wilson model.	106
Table 6.38	Biaxial tension results for Haines and Wilson model.	106
Table 6.39	Simultaneous fitting results for Attard and Hunt model.	108

Table 6.40	Uniaxial tension results for Attard and Hunt model.	108
Table 6.41	Biaxial tension results for Attard and Hunt model.	108
Table 6.42	Simultaneous fitting results for 4-term Bechir model.	110
Table 6.43	Uniaxial tension results for 4-term Bechir model.	110
Table 6.44	Biaxial tension results for 4-term Bechir model.	110
Table 6.45	Simultaneous fitting results for Pucci and Saccomandi model. . . .	112
Table 6.46	Uniaxial tension results for Pucci and Saccomandi model.	112
Table 6.47	Biaxial tension results for Pucci and Saccomandi model.	112
Table 6.48	Simultaneous fitting results for Biderman model.	114
Table 6.49	Uniaxial tension results for Biderman model.	114
Table 6.50	Biaxial tension results for Biderman model.	114
Table 6.51	Simultaneous fitting results for Kilian (van der Waals) model. . . .	116
Table 6.52	Uniaxial tension results for Kilian (van der Waals) model.	116
Table 6.53	Biaxial tension results for Kilian (van der Waals) model.	116
Table 6.54	Simultaneous fitting results for Yamashita and Kawabata model. . .	118
Table 6.55	Uniaxial tension results for Yamashita and Kawabata model.	118
Table 6.56	Biaxial tension results for Yamashita and Kawabata model.	118
Table 6.57	Simultaneous fitting results for Lion model.	120
Table 6.58	Uniaxial tension results for Lion model.	120
Table 6.59	Biaxial tension results for Lion model.	120
Table 6.60	Simultaneous fitting results for Beda model.	122
Table 6.61	Uniaxial tension results for Beda model.	122

Table 6.62	Biaxial tension results for Bada model.	122
Table 6.63	Simultaneous fitting results for Hart-Smith model.	124
Table 6.64	Uniaxial tension results for Hart-Smith model.	124
Table 6.65	Biaxial tension results for Hart-Smith model.	124
Table 6.66	Simultaneous fitting results for Haupt and Sedlan model.	126
Table 6.67	Uniaxial tension results for Haupt and Sedlan model.	126
Table 6.68	Biaxial tension results for Haupt and Sedlan model.	126
Table 6.69	Simultaneous fitting results for Exp-Ln model.	128
Table 6.70	Uniaxial tension results for Exp-Ln model.	128
Table 6.71	Biaxial tension results for Exp-Ln model.	128
Table 6.72	Simultaneous fitting results for Yeoh model.	130
Table 6.73	Uniaxial tension results for Yeoh model.	130
Table 6.74	Biaxial tension results for Yeoh model.	130
Table 6.75	Simultaneous fitting results for two-term model.	132
Table 6.76	Uniaxial tension results for two-term model.	132
Table 6.77	Biaxial tension results for two-term model.	132
Table 6.78	Simultaneous fitting results for Yeoh-Fleming model.	134
Table 6.79	Uniaxial tension results for Yeoh-Fleming model.	134
Table 6.80	Biaxial tension results for Yeoh-Fleming model.	134
Table 6.81	Simultaneous fitting results for Arruda-Boyce model.	136
Table 6.82	Uniaxial tension results for Arruda-Boyce model.	136
Table 6.83	Biaxial tension results for Arruda-Boyce model.	136

Table 6.84	Simultaneous fitting results for Gent model.	138
Table 6.85	Uniaxial tension results for Gent model.	138
Table 6.86	Biaxial tension results for Gent model.	138
Table 6.87	Simultaneous fitting results for three-chain model.	140
Table 6.88	Uniaxial tension results for three-chain model.	140
Table 6.89	Biaxial tension results for three-chain model.	140
Table 6.90	Simultaneous fitting results for Mooney model.	142
Table 6.91	Uniaxial tension results for Mooney model.	142
Table 6.92	Biaxial tension results for Mooney model.	142
Table 6.93	Simultaneous fitting results for Isihara model.	144
Table 6.94	Uniaxial tension results for Isihara model.	144
Table 6.95	Biaxial tension results for Isihara model.	144
Table 6.96	Simultaneous fitting results for Nunes model.	146
Table 6.97	Uniaxial tension results for Nunes model.	146
Table 6.98	Biaxial tension results for Nunes model.	146
Table 6.99	Simultaneous fitting results for tube model.	148
Table 6.100	Uniaxial tension results for tube model.	148
Table 6.101	Biaxial tension results for tube model.	148
Table 6.102	Simultaneous fitting results for slip-link model.	150
Table 6.103	Uniaxial tension results for slip-link model.	150
Table 6.104	Biaxial tension results for slip-link model.	150
Table 6.105	Simultaneous fitting results for Swanson model.	152

Table 6.106 Uniaxial tension results for Swanson model.	152
Table 6.107 Biaxial tension results for Swanson model.	152
Table 6.108 Simultaneous fitting results for Gent-Thomas model.	154
Table 6.109 Uniaxial tension results for Gent-Thomas model.	154
Table 6.110 Biaxial tension results for Gent-Thomas model.	154
Table 6.111 Simultaneous fitting results for constrained-junction model.	156
Table 6.112 Uniaxial tension results for constrained-junction model.	156
Table 6.113 Biaxial tension results for constrained-junction model.	156
Table 6.114 Simultaneous fitting results for weight function based (WFB) model.	158
Table 6.115 Uniaxial tension results for weight function based (WFB) model. . .	158
Table 6.116 Biaxial tension results for weight function based (WFB) model. . .	158
Table 6.117 Simultaneous fitting results for neo-Hooke model.	160
Table 6.118 Uniaxial tension results for neo-Hooke model.	160
Table 6.119 Biaxial tension results for neo-Hooke model.	160
Table 6.120 Simultaneous fitting results for Valanis-Landel model.	162
Table 6.121 Uniaxial tension results for Valanis-Landel model.	162
Table 6.122 Biaxial tension results for Valanis-Landel model.	162
Table A.1 Equibiaxial tension results for Micro-Sphere model.	174
Table A.2 Equibiaxial tension fitting results for Alexander model.	174
Table A.3 Equibiaxial tension results for Diani and Ray model.	174
Table A.4 Equibiaxial tension results for Extended-Tube model.	175
Table A.5 Equibiaxial tension results for Shariff model.	175

Table A.6	Equibiaxial tension results for Carroll model.	175
Table A.7	Equibiaxial tension results network averaging tube model.	176
Table A.8	Equibiaxial tension results for Chevalier and Marco model.	176
Table A.9	Equibiaxial tension results for Ogden model.	176
Table A.10	Equibiaxial tension results for Amin model.	177
Table A.11	Equibiaxial tension results for James model.	177
Table A.12	Equibiaxial tension results for Haines and Wilson model.	177
Table A.13	Equibiaxial tension results for Attard and Hunt model.	178
Table A.14	Equibiaxial tension results for 4-term Bechir model.	178
Table A.15	Equibiaxial tension results for Pucci and Saccomandi model.	178
Table A.16	Equibiaxial tension results for Biderman model.	179
Table A.17	Equibiaxial tension results for Kilian (van der Waals) model.	179
Table A.18	Equibiaxial tension results for Yamashita and Kawabata model.	179
Table A.19	Equibiaxial tension results for Lion model.	180
Table A.20	Equibiaxial tension results for Beda model.	180
Table A.21	Equibiaxial tension results for Hart-Smith model.	180
Table A.22	Equibiaxial tension results for Haupt and Sedlan model.	181
Table A.23	Equibiaxial tension results for Exp-Ln model.	181
Table A.24	Equibiaxial tension results for Yeoh model.	181
Table A.25	Equibiaxial tension results for two-term model.	182
Table A.26	Equibiaxial tension results for Yeoh-Fleming model.	182
Table A.27	Equibiaxial tension results for Arruda-Boyce model.	182

Table A.28	Equibiaxial tension results for Gent model.	183
Table A.29	Equibiaxial tension results for three-chain model.	183
Table A.30	Equibiaxial tension results for Mooney model.	183
Table A.31	Equibiaxial tension results for Isihara model.	184
Table A.32	Equibiaxial tension results for Nunes model.	184
Table A.33	Equibiaxial tension results for tube model.	184
Table A.34	Equibiaxial tension results for slip-link model.	185
Table A.35	Equibiaxial tension results for Swanson model.	185
Table A.36	Equibiaxial tension results for Gent-Thomas model.	185
Table A.37	Equibiaxial tension results for constrained-junction model.	186
Table A.38	Equibiaxial tension results for weight function based (WFB) model.	186
Table A.39	Equibiaxial tension results for neo-Hooke model.	186
Table A.40	Equibiaxial tension results for Valanis-Landel model.	187
Table B.1	Pure shear results for Micro-Sphere model.	190
Table B.2	Pure Shear results for Alexander model.	190
Table B.3	Pure shear results for Diani and Ray model.	190
Table B.4	Pure shear results for Extended-Tube model.	191
Table B.5	Pure shear results for Shariff model.	191
Table B.6	Pure shear results for Carroll model.	191
Table B.7	Pure shear results network averaging tube model.	192
Table B.8	Pure shear results for Chevalier and Marco model.	192
Table B.9	Pure shear results for Ogden model.	192

Table B.10	Pure shear results for Amin model.	193
Table B.11	Pure shear results for James model.	193
Table B.12	Pure shear results for Haines and Wilson model.	193
Table B.13	Pure shear results for Attard and Hunt model.	194
Table B.14	Pure shear results for 4-term Bechir model.	194
Table B.15	Pure shear results for Pucci and Saccomandi model.	194
Table B.16	Pure shear results for Biderman model.	195
Table B.17	Pure shear results for Kilian (van der Waals) model.	195
Table B.18	Pure shear results for Yamashita and Kawabata model.	195
Table B.19	Pure shear results for Lion model.	196
Table B.20	Pure shear results for Beda model.	196
Table B.21	Pure shear results for Hart-Smith model.	196
Table B.22	Pure shear results for Haupt and Sedlan model.	197
Table B.23	Pure shear results for Exp-Ln model.	197
Table B.24	Pure shear results for Yeoh model.	197
Table B.25	Pure shear results for two-term model.	198
Table B.26	Pure shear results for Yeoh-Fleming model.	198
Table B.27	Pure shear results for Arruda-Boyce model.	198
Table B.28	Pure shear results for Gent model.	199
Table B.29	Pure shear results for three-chain model.	199
Table B.30	Pure shear results for Mooney model.	199
Table B.31	Pure shear results for Isihara model.	200

Table B.32	Pure shear results for Nunes model.	200
Table B.33	Pure shear results for tube model.	200
Table B.34	Pure shear results for slip-link model.	201
Table B.35	Pure shear results for Swanson model.	201
Table B.36	Pure shear results for Gent-Thomas model.	201
Table B.37	Pure shear results for constrained-junction model.	202
Table B.38	Pure shear results for weight function based (WFB) model.	202
Table B.39	Pure shear results for neo-Hooke model.	202
Table B.40	Pure shear results for Valanis-Landel model.	203
Table C.1	Free energy functions of first 20 models sorted by quality of fit metric.	206
Table C.2	Free energy functions of the remaining 20 models sorted by quality of fit metric.	207

LIST OF FIGURES

FIGURES

Figure 3.1	Mathematical description of the motion of a body \mathcal{B} in \mathbb{R}^3	18
Figure 3.2	Line, area, and volume elements on a material point \mathcal{P} at \mathbf{X} . . .	19
Figure 3.3	Deformation gradient mapping.	19
Figure 3.4	Rotation, left and right stretch tensors.	20
Figure 3.5	Definition of metric tensors. a) current metric in Lagrangian configuration; b) reference metric in Eulerian configuration.	21
Figure 3.6	Covariant pull-back and push-forward operations between the material and spatial strain tensors.	22
Figure 3.7	Representation of body forces on deformed and undeformed states.	23
Figure 3.8	Representation for Cauchy's Lemma.	24
Figure 3.9	Stress components on the surfaces of unit cube.	25
Figure 3.10	Traction components on a tetrahedron.	25
Figure 3.11	Definition of stress tensors. Relationship between stresses. . . .	27
Figure 3.12	Initial boundary value problem.	28
Figure 3.13	Uniaxial tension deformation	34
Figure 3.14	Equibiaxial tension deformation	35
Figure 3.15	Pure shear deformation	36

Figure 3.16	Biaxial tension deformation	37
Figure 4.1	Micro-state of an undeformed chain	60
Figure 4.2	Forces derived from Gaussian and non-Gaussian statistics result in an asymptotic behavior when approaching extensibility limit $\lambda_r \rightarrow 1$ [1]. Here, $L = Nl$	62
Figure 4.3	Three chain model representative network structure.	63
Figure 4.4	Eight chain model representative network structure.	64
Figure 4.5	Micro-sphere kinematic variables.	67
Figure 4.6	Affine transformation of a chain	68
Figure 5.1	Pictorial representations of types of mutations, a) standalone mutation operator, b) multiple-mutations operator	75
Figure 5.2	Pictorial representation of cross-over operator.	76
Figure 5.3	Parameter identification procedure.	77
Figure 6.1	Micro-Sphere model prediction for a) uniaxial tension, b) com- bination of uniaxial, equibiaxial, and pure shear loadings usning Treloar data c) biaxial tension loading for $\lambda_1 : 1.04 - 1.24$, d) biaxial tension loading for $\lambda_1 : 1.3 - 3.7$ using Kawabata data.	83
Figure 6.2	Alexander's model prediction for a) uniaxial tension, b) combi- nation of uniaxial, equibiaxial, and pure shear loadings usning Treloar data c) biaxial tension loading for $\lambda_1 : 1.04 - 1.24$, d) biaxial tension loading for $\lambda_1 : 1.3 - 3.7$ using Kawabata data.	85
Figure 6.3	Diani and Ray's model prediction for a) uniaxial tension, b) combination of uniaxial, equibiaxial, and pure shear loadings usning Treloar data c) biaxial tension loading for $\lambda_1 : 1.04 - 1.24$, d) biaxial tension loading for $\lambda_1 : 1.3 - 3.7$ using Kawabata data.	87

Figure 6.4	Extended-Tube model prediction for a) uniaxial tension, b) combination of uniaxial, equibiaxial, and pure shear loadings using Treloar data c) biaxial tension loading for $\lambda_1 : 1.04 - 1.24$, d) biaxial tension loading for $\lambda_1 : 1.3 - 3.7$ using Kawabata data.	89
Figure 6.5	Shariff model prediction for a) uniaxial tension, b) combination of uniaxial, equibiaxial, and pure shear loadings using Treloar data c) biaxial tension loading for $\lambda_1 : 1.04 - 1.24$, d) biaxial tension loading for $\lambda_1 : 1.3 - 3.7$ using Kawabata data.	91
Figure 6.6	Carroll model prediction for a) uniaxial tension, b) combination of uniaxial, equibiaxial, and pure shear loadings using Treloar data c) biaxial tension loading for $\lambda_1 : 1.04 - 1.24$, d) biaxial tension loading for $\lambda_1 : 1.3 - 3.7$ using Kawabata data.	93
Figure 6.7	Network averaging tube model prediction for a) uniaxial tension, b) combination of uniaxial, equibiaxial, and pure shear loadings using Treloar data c) biaxial tension loading for $\lambda_1 : 1.04 - 1.24$, d) biaxial tension loading for $\lambda_1 : 1.3 - 3.7$ using Kawabata data.	95
Figure 6.8	Chevalier and Marco's model prediction for a) uniaxial tension, b) combination of uniaxial, equibiaxial, and pure shear loadings using Treloar data c) biaxial tension loading for $\lambda_1 : 1.04 - 1.24$, d) biaxial tension loading for $\lambda_1 : 1.3 - 3.7$ using Kawabata data.	97
Figure 6.9	Ogden model prediction for a) uniaxial tension, b) combination of uniaxial, equibiaxial, and pure shear loadings using Treloar data c) biaxial tension loading for $\lambda_1 : 1.04 - 1.24$, d) biaxial tension loading for $\lambda_1 : 1.3 - 3.7$ using Kawabata data.	99
Figure 6.10	Amin model prediction for a) uniaxial tension, b) combination of uniaxial, equibiaxial, and pure shear loadings using Treloar data c) biaxial tension loading for $\lambda_1 : 1.04 - 1.24$, d) biaxial tension loading for $\lambda_1 : 1.3 - 3.7$ using Kawabata data.	101

Figure 6.11	James model prediction for a) uniaxial tension, b) combination of uniaxial, equibiaxial, and pure shear loadings using Treloar data c) biaxial tension loading for $\lambda_1 : 1.04 - 1.24$, d) biaxial tension loading for $\lambda_1 : 1.3 - 3.7$ using Kawabata data.	103
Figure 6.12	Haines-Wilson model prediction for a) uniaxial tension, b) combination of uniaxial, equibiaxial, and pure shear loadings using Treloar data c) biaxial tension loading for $\lambda_1 : 1.04 - 1.24$, d) biaxial tension loading for $\lambda_1 : 1.3 - 3.7$ using Kawabata data.	105
Figure 6.13	Attard and Hunt model prediction for a) uniaxial tension, b) combination of uniaxial, equibiaxial, and pure shear loadings using Treloar data c) biaxial tension loading for $\lambda_1 : 1.04 - 1.24$, d) biaxial tension loading for $\lambda_1 : 1.3 - 3.7$ using Kawabata data.	107
Figure 6.14	Bechir model prediction for a) uniaxial tension, b) combination of uniaxial, equibiaxial, and pure shear loadings using Treloar data c) biaxial tension loading for $\lambda_1 : 1.04 - 1.24$, d) biaxial tension loading for $\lambda_1 : 1.3 - 3.7$ using Kawabata data.	109
Figure 6.15	Pucci and Saccomandi's model prediction for a) uniaxial tension, b) combination of uniaxial, equibiaxial, and pure shear loadings using Treloar data c) biaxial tension loading for $\lambda_1 : 1.04 - 1.24$, d) biaxial tension loading for $\lambda_1 : 1.3 - 3.7$ using Kawabata data.	111
Figure 6.16	Biderman model prediction for a) uniaxial tension, b) combination of uniaxial, equibiaxial, and pure shear loadings using Treloar data c) biaxial tension loading for $\lambda_1 : 1.04 - 1.24$, d) biaxial tension loading for $\lambda_1 : 1.3 - 3.7$ using Kawabata data.	113
Figure 6.17	Kilian (van der Waals) model prediction for a) uniaxial tension, b) combination of uniaxial, equibiaxial, and pure shear loadings using Treloar data c) biaxial tension loading for $\lambda_1 : 1.04 - 1.24$, d) biaxial tension loading for $\lambda_1 : 1.3 - 3.7$ using Kawabata data.	115

Figure 6.18	Yamashita and Kawabata's model prediction for a) uniaxial tension, b) combination of uniaxial, equibiaxial, and pure shear loadings usning Treloar data c) biaxial tension loading for $\lambda_1 : 1.04 - 1.24$, d) biaxial tension loading for $\lambda_1 : 1.3 - 3.7$ using Kawabata data.	117
Figure 6.19	Lion model prediction for a) uniaxial tension, b) combination of uniaxial, equibiaxial, and pure shear loadings usning Treloar data c) biaxial tension loading for $\lambda_1 : 1.04 - 1.24$, d) biaxial tension loading for $\lambda_1 : 1.3 - 3.7$ using Kawabata data.	119
Figure 6.20	Beda's model prediction for a) uniaxial tension, b) combination of uniaxial, equibiaxial, and pure shear loadings usning Treloar data c) biaxial tension loading for $\lambda_1 : 1.04 - 1.24$, d) biaxial tension loading for $\lambda_1 : 1.3 - 3.7$ using Kawabata data.	121
Figure 6.21	Hart-Smith model prediction for a) uniaxial tension, b) combination of uniaxial, equibiaxial, and pure shear loadings usning Treloar data c) biaxial tension loading for $\lambda_1 : 1.04 - 1.24$, d) biaxial tension loading for $\lambda_1 : 1.3 - 3.7$ using Kawabata data.	123
Figure 6.22	Haupt and Sedlan's model prediction for a) uniaxial tension, b) combination of uniaxial, equibiaxial, and pure shear loadings usning Treloar data c) biaxial tension loading for $\lambda_1 : 1.04 - 1.24$, d) biaxial tension loading for $\lambda_1 : 1.3 - 3.7$ using Kawabata data.	125
Figure 6.23	Exp-Ln model prediction for a) uniaxial tension, b) combination of uniaxial, equibiaxial, and pure shear loadings usning Treloar data c) biaxial tension loading for $\lambda_1 : 1.04 - 1.24$, d) biaxial tension loading for $\lambda_1 : 1.3 - 3.7$ using Kawabata data.	127
Figure 6.24	Yeoh model prediction for a) uniaxial tension, b) combination of uniaxial, equibiaxial, and pure shear loadings usning Treloar data c) biaxial tension loading for $\lambda_1 : 1.04 - 1.24$, d) biaxial tension loading for $\lambda_1 : 1.3 - 3.7$ using Kawabata data.	129

Figure 6.25	Two-Term model prediction for a) uniaxial tension, b) combination of uniaxial, equibiaxial, and pure shear loadings using Treloar data c) biaxial tension loading for $\lambda_1 : 1.04 - 1.24$, d) biaxial tension loading for $\lambda_1 : 1.3 - 3.7$ using Kawabata data.	131
Figure 6.26	Yeoh-Fleming model prediction for a) uniaxial tension, b) combination of uniaxial, equibiaxial, and pure shear loadings using Treloar data c) biaxial tension loading for $\lambda_1 : 1.04 - 1.24$, d) biaxial tension loading for $\lambda_1 : 1.3 - 3.7$ using Kawabata data.	133
Figure 6.27	Arruda-Boyce model prediction for a) uniaxial tension, b) combination of uniaxial, equibiaxial, and pure shear loadings using Treloar data c) biaxial tension loading for $\lambda_1 : 1.04 - 1.24$, d) biaxial tension loading for $\lambda_1 : 1.3 - 3.7$ using Kawabata data.	135
Figure 6.28	Gent model prediction for a) uniaxial tension, b) combination of uniaxial, equibiaxial, and pure shear loadings using Treloar data c) biaxial tension loading for $\lambda_1 : 1.04 - 1.24$, d) biaxial tension loading for $\lambda_1 : 1.3 - 3.7$ using Kawabata data.	137
Figure 6.29	Three-Chain model prediction for a) uniaxial tension, b) combination of uniaxial, equibiaxial, and pure shear loadings using Treloar data c) biaxial tension loading for $\lambda_1 : 1.04 - 1.24$, d) biaxial tension loading for $\lambda_1 : 1.3 - 3.7$ using Kawabata data.	139
Figure 6.30	Mooney model prediction for a) uniaxial tension, b) combination of uniaxial, equibiaxial, and pure shear loadings using Treloar data c) biaxial tension loading for $\lambda_1 : 1.04 - 1.24$, d) biaxial tension loading for $\lambda_1 : 1.3 - 3.7$ using Kawabata data.	141
Figure 6.31	Isihara model prediction for a) uniaxial tension, b) combination of uniaxial, equibiaxial, and pure shear loadings using Treloar data c) biaxial tension loading for $\lambda_1 : 1.04 - 1.24$, d) biaxial tension loading for $\lambda_1 : 1.3 - 3.7$ using Kawabata data.	143

Figure 6.32	Nunes model prediction for a) uniaxial tension, b) combination of uniaxial, equibiaxial, and pure shear loadings using Treloar data c) biaxial tension loading for $\lambda_1 : 1.04 - 1.24$, d) biaxial tension loading for $\lambda_1 : 1.3 - 3.7$ using Kawabata data.	145
Figure 6.33	Tube model prediction for a) uniaxial tension, b) combination of uniaxial, equibiaxial, and pure shear loadings using Treloar data c) biaxial tension loading for $\lambda_1 : 1.04 - 1.24$, d) biaxial tension loading for $\lambda_1 : 1.3 - 3.7$ using Kawabata data.	147
Figure 6.34	Slip-Link model prediction for a) uniaxial tension, b) combination of uniaxial, equibiaxial, and pure shear loadings using Treloar data c) biaxial tension loading for $\lambda_1 : 1.04 - 1.24$, d) biaxial tension loading for $\lambda_1 : 1.3 - 3.7$ using Kawabata data.	149
Figure 6.35	Swanson model prediction for a) uniaxial tension, b) combination of uniaxial, equibiaxial, and pure shear loadings using Treloar data c) biaxial tension loading for $\lambda_1 : 1.04 - 1.24$, d) biaxial tension loading for $\lambda_1 : 1.3 - 3.7$ using Kawabata data.	151
Figure 6.36	Gent-Thomas model prediction for a) uniaxial tension, b) combination of uniaxial, equibiaxial, and pure shear loadings using Treloar data c) biaxial tension loading for $\lambda_1 : 1.04 - 1.24$, d) biaxial tension loading for $\lambda_1 : 1.3 - 3.7$ using Kawabata data.	153
Figure 6.37	Constrained Junction model prediction for a) uniaxial tension, b) combination of uniaxial, equibiaxial, and pure shear loadings using Treloar data c) biaxial tension loading for $\lambda_1 : 1.04 - 1.24$, d) biaxial tension loading for $\lambda_1 : 1.3 - 3.7$ using Kawabata data.	155
Figure 6.38	Weight Function Based (WFB) model prediction for a) uniaxial tension, b) combination of uniaxial, equibiaxial, and pure shear loadings using Treloar data c) biaxial tension loading for $\lambda_1 : 1.04 - 1.24$, d) biaxial tension loading for $\lambda_1 : 1.3 - 3.7$ using Kawabata data.	157

Figure 6.39 neo-Hooke model prediction for a) uniaxial tension, b) combination of uniaxial, equibiaxial, and pure shear loadings using Treloar data c) biaxial tension loading for $\lambda_1 : 1.04 - 1.24$, d) biaxial tension loading for $\lambda_1 : 1.3 - 3.7$ using Kawabata data. 159

Figure 6.40 Valanis-Landel model prediction for a) uniaxial tension, b) combination of uniaxial, equibiaxial, and pure shear loadings using Treloar data c) biaxial tension loading for $\lambda_1 : 1.04 - 1.24$, d) biaxial tension loading for $\lambda_1 : 1.3 - 3.7$ using Kawabata data. 161

LIST OF ABBREVIATIONS

ABBREVIATIONS

UT	Uniaxial Tension
ET	Equibiaxial Tension
PS	Pure Shear
BT	Biaxial Tension
WFB	Weight Function Based
PDMS	Polydimethylsiloxane
TRESNEI	Trust-Region Solver for non-linear Equations and Inequalities
DCI	Digital Image Correlation
qofsim	Quality of Fit Value for Simultaneous Fits
nop	Number of Parameters

CHAPTER 1

INTRODUCTION

The aim of this study is to catch optimum values for parameters used in different hyperelastic material models. 40 hyperelastic material models of different kinds have been considered. Well known Treloar's data set for uniaxial tension, equi-biaxial tension, and pure shear [2] are used for parameter setting. For biaxial tension test, however, parameters are optimized taking Kawabata's experimental data [3] in consideration. Parameters are set roughly by genetic algorithm, and further improvements are reached through FMINCON utility of MATLAB. Novelty of this work is using multi-objective optimization multiplying error expression by weight factors. With the mentioned weight it is aimed to reach optimum fitting capacity of models under consideration.

1.1 Overview and Background

Natural rubber are known to be taken from Hevea Brasiliensis tree which may, in general, called as rubber tree. Rubber tree is widely grew in south American countries. Ancient civilizations like Maya, Aztec, and Olmec are known to be the first civilizations witch discovered rubber, and it goes back to around 1600 BCE. Early natural rubber materials were in unvulcanized form that was not practically usable because they affect by weather conditions. Industrial usage of rubber as vulcanized form was introduced as the eraser of pencil marks. Afterwards, tire manufacturers used filled rubber compounds in their manufacturing lines. Nowadays rubber-like materials has wide range of applications. To name some of the most commonly fields of usage for rubber-like materials, automotive and aerospace industries, motion and

power transmission components, like conveyor belts, sealing components, tires can be addressed.

Phenomenological and micro-mechanically based material models are the two main groups in hyperelastic modeling paradigms. Deriving the expressions of phenomenological material models, mathematical expressions are constructed by fitting the expressions to the material response data curve. The constructed material models are generally expressed in terms of deformation gradient invariants, principal stretches, or combination of them. Noting that the derived expression should fulfill the requirements of objectivity and material frame indifference. Micro-mechanical mechanical material models, however, are mostly defined in terms of micro-structure of chain network of polymeric material. Statistical approach is considered while deriving the constitutive equations of this group. Among the different types of material models, micro-mechanically motivated models are known to possess deeper and interpretable characteristics for unfilled rubber-like materials. Micro-structure of rubbery polymers consists of long chain molecules and micro-mechanical approach deals with the end-to-end distance through the chain length and its distribution function. The research studies on micro-mechanics of physically motivated models has began around 1940s. On that days, Mooney [4] started investigating ideal rubber material modeling, treating the response of material in mathematical manner by proposing the well-known Mooney's strain energy function. Kuhn and Gr \ddot{u} n in 1942 developed the first Gaussian distribution approach of rubbery polymers. At the same time Wall [5] has assumed a statistical approach to relate the molecular entropy of rubber-like material in macroscopic manner and related the findings to single chain. In 1943 Treloar make benefit of the findings by Wall, Mooney, and Kuhn & Gr \ddot{u} n and established the well-known neo-Hooke model [2]. The considered approaches used Gaussian distributions which are not suitable for predicting material response at higher strain values. Therefore, a need for non-Gaussian approach over some stretch level (limiting chain extensibility) while modeling the behavior of rubber-like materials became a crucial matter. Affinity assumption was considered by researchers of the time developing the micro-mechanically based material models. Wang & Guth's three-chain model [6], four-chain model of Flory and Rehner [7], full network model of Treloar and Riding [8], and Arruda-Boyce's eight-chain model [9] can be named as the ones

with non-Gaussian and affinity approach aspects. Combining the previous assumptions and being inspired from the full-network model proposed by Treloar and Riding, Miehe and coworkers [1] developed a non-affine approach together with topological tube-like constraints.

Evolution of phenomenological models for rubber-like materials has begun after the first work on free energy function proposed by Mooney [4]. The researches dealing with purely mathematical approaches mostly take an idea from the Mooney's work. Rivlin and Saunders [10] made a generalization on Mooney's model and introduced power series form of Mooney type models. Hereafter, we will name the form proposed by Rivlin and Saunders as Mooney's generalized form. There are variety of models expanded and derived considering different forms of Mooney's generalized form. Starting point for modeling of phenomenological models on the other hand can be related to the neo-Hooke model [2].

1.2 Elasticity of Rubber-like Materials

Hyperelasticity is the term most commonly used to define the rubber-like materials. The reason for this definition is that the elastomeric materials can bear high strain values with almost full recovery upon unloading. The elastic deformation applied to that kind of materials can even reach the values like 700% in a fully recoverable manner. Elastic behavior of such materials makes the constitutive relations be independent of the deformation history curve but dependent on the current state of deformation. In these cases, mostly rate independent strain approaches are considered. The stress-strain curve for hyperelastic materials is generally named as S-curve. This is because of the fact that when applying tension, the material first softens and then stiffens generating S-shape. Mostly the volume ratio for hyperelastic materials undergoing large deformations are taken as constant, thus incompressibility assumption holds ($J=1$). Objectivity condition is yet another requirement for the constitutive relations of hyperelastic materials, meaning that, during rigid body rotations, material's constitutive relations should remain unchanged [11].

1.3 Motivation and Contribution

By the increase in number of hyperelastic material models making comparison between the models and choosing appropriate one for further analysis become a crucial problem. The first step to compare material models is identifying material parameters and observe the deviations from material response curve. Over the last two decades many review papers have been published aiming to find reliable and accurate material parameters which result in minimum deviation from actual response of the material. The works done by Boyce and Arruda [12], Marckmann and Verron [13], Steinmann et al. [14], Hossain and Steinmann [15], and Beda [16] [17] are some of the review contexts in literature worth noticing. Number of experimental data-sets for distinct loading cases and conditions, maximum stretch level applied during each loading scenario, and filler percentage and additive are three main factors that critically affect the results obtained for each constitutive relation. By the increase in number of model parameters, stability of optimized parameters also become a challenging issue. In order to overcome the stability problem one may have different search mechanisms that ensures the reliability of set parameters. One of the best ways is to first roughly estimate the constant of constitutive models by methods like genetic algorithm and use the obtained parameters as starting point for gradient decent base optimization tools. It should be taken into the consideration that, constitutive relations are preferred to have less amount of material parameters with physical meanings. The validity range for each constitutive model response is yet the other issue. Validity region should be specified for each material model to make sure that the solution for analysis are set in the precise manner. In this study it is tried to give the suitable region valid for each constitutive model which is rarely seen in most of the review studies.

1.4 Scope and Outline

This thesis is aimed to find parameters for 40 constitutive relations used in hyper-elasticity. Both phenomenological and micro-mechanically based formulations will be considered and comparison between different models will be done, weakness and strengths of each model will be discussed. Moreover, the valid range for each mate-

rial model will be set. The other aspect of the study is to make an objective ranking between the 40 constitutive relations. Sorting is done according to fitting quality of models using chi-square method.

Brief introduction is provided this chapter (Chapter 1). Literature review is presented in Chapter 2. After referring to the previous studies on the rubber-like materials, common concepts and definitions in hyperelasticity will be given in Chapter 3. Preliminaries for incompressible isotropic hyperelastic materials will be mentioned and two main representation of that kind of materials will be considered. Chapter 4 is devoted to the categorization and definitions of the mentioned 40 material models. Two main categories for constitutive relations are presented and sub-groups are mentioned in detail. Chapter 5 is related to the parameter optimization methods. First part of this chapter starts with genetic algorithm and remaining part gives some useful points on multi-start utility of Matlab. Results and observations of this study is taken into the account in Chapter 6. Then, a brief discussion over the findings are presented. In the last chapter (Chapter 7), concluding remarks will be shown.

CHAPTER 2

LITERATURE REVIEW

The studies on mechanical response of hyperelastic material response goes back to 1940's. Mooney was one of the pioneers to realize that hyperelastic materials' reaction to the applied stretch differs from the response observed on metallic samples. He distinguished that Hooke's law is not sufficient to estimate the stress-strain related behavior of elastomeric compounds. Therefore, the term superelasticity was first used by Mooney considering homogeneous and hysteresis free behavior of rubber-like materials. In his paper for the first time it is postulated that rubber-like materials are isotropic, incompressible, and traction in simple shear loading can be analytically related to the shear [4]. Mooney used the experimental data of Gerke [18] to set the observations and propose the well-known Mooney model. Developments in theoretical aspects of rubber elasticity considering molecular statistical approach, however, became attractive in 1940's. Neo-Hooke model developed by Treloar in 1943 [2], proposing the idea given by Wall [5], is known to be the first and simple approach using molecular chain statistics. The following assumptions were proposed by Treloar while deriving his theory: chain network is assumed to have N number of molecules of equal length, molecules' end-to-end distance is approximated by Kuhn's Gaussian statistical mechanics formulation, deformation is affine, and material is incompressible. Then Flory and Rehner [7] developed four-chain model for Gaussian network of molecular chains. Following the previous works, especially the one proposed Flory and Rehner, Treloar proposed a non-Gaussian four-chain network in 1946 [19]. Statistical behavior of Gaussian network is deeply studied in the paper presented by James [20]. James stated that Gaussian network of polymeric materials are composed of chains, with number of segments, connected to each other at junction points. One end of chains are also considered to be fixed on a surface of cubic network. Rivlin

and Saunders In 1951 , made a generalization on phenomenological modeling of hyperelastic materials. They introduced mathematical invariant based formulations and a power series general form of Mooney's type. Most of the phenomenological material models in literature are alternative form of the mentioned generalized formula. Isihara and coworkers [21] assumed a strain energy function for approximation of the rubber-like material's response. They expanded the theory derived by James and solved their approximated Langevin's type strain energy function by James' method. Although starting point for derivation of Isihara's model is molecular chain statistics of Gaussian (micro-mechanical approach) type, the obtained model at the end represents an alternative form of Mooney's generalized formula. That is why Isihara's model is mostly considered as a phenomenological model. Wang and Guth in 1952 [6] developed a robust derivation for non-Gaussian conformation of molecular chains on principle stretch directions. They introduced three-chain model of non-Gaussian type as a result of their work. Biderman in 1958 [22] make use of generalized Mooney's model and introduced a phenomenological model considering I_1 and I_2 invariants. Gent and Thomas (1958) also used the idea given by Mooney and introduced an expression for strain energy function in terms of first and second invariant of deformation [23]. The proposed model contains first power of I_1 and a simple logarithmic term containing I_2 . Hart-Smith in 1966 [24] extended the theoretical aspects of [10] and [23], aimed to find elasticity constants of a natural rubber sample. For this reason suitable partial derivatives of free energy function with respect to first and second invariants are given. Another form of strain energy function for natural rubber is introduced by Valanis and Landel in 1967 [25] postulating that strain energy function of rubber-like materials can be analytic and separable function of stretch ratios rather than invariants. Additive split which is considered by Valanis and Landel have the form, $\psi(\lambda_1, \lambda_2, \lambda_3) = \psi(\lambda_1) + \psi(\lambda_2) + \psi(\lambda_3)$. Apart from being a model it is assumed to be a hypothesis introduced by Valanis and Landel. Combining the Revlin and Saunder's theory with the Hart-Smith's material model, Alexander [26] came up with a new constitutive relation of invariant type. The model is developed in 1968 and it is aimed to catch the experimental data points over full range of loading curve. The proposed relation contains I_2 term which is set by the approximated curve fitting on experiments conducted on inflated balloon. A power series form of principle stretch based material model is derived by Ogden in 1972.

The constitutive relation of Ogden [27] is known to obey the Valanis and Landel hypothesis. Three-term expansion of the Ogden's series is suggested by the author which gives reasonable results in analysis of natural rubber. Again using generalized Mooney's expression, in 1975, James, Green and Simpson developed a phenomenological model of containing 5 material constants [28]. Their model consists of third order for first invariant, and order one is considered for second invariant of deformation. A similar approach is presented by Haines and Wilson [29] in 1979. The suggested model has 6 material parameters with order of three for first invariant and order of two for second invariant terms. In 1981 Ball and coworkers developed a model called slip-link [30]. Concept of entanglements and topological constraints are mathematically explained in their work. The obtained model is principle stretch based with three material constants. One year later, similar approach to the slip-link is proposed by Erman and Flory [31]. The resulted model known as constrained junction is composed of two parts, namely phantom and constraint parts. The junctions are considered to be considered to move due to existence of neighboring chains. The phantom part is governed by neo-Hooke equation. The cross-linking part of free energy function, on the other hand, is given as power series containing logarithmic expressions of principle stretches. Another phenomenological model is proposed in 1985 by Swanson [32]. The constitutive relation has invariant base base summations terms. Also incompressibility term is added to improve the curve fitting performance of the model. Least square method is used for this aim. In 1986, Kilian and coworkers introduced a constitutive model considering van der Waals forces due to the interactions of molecular chains [33]. The proposed model is generally known as van der Waals or Kilian model. A penalty factor is also used to related degree of swelling during the deformation. Yeoh model [34] is another well-known phenomenological model derived in early 1990's. The simple structure of the constitutive equation is taken from generalized Mooney's formula considering first three term expansion of series for first invariant. Regression analysis for curve fitting on experimental data is investigated by Yeoh. Yamashita and Kawabata [35], in the beginning of 1992, also worked on mathematical formulation of stress-strain behavior of rubber-like materials. The derived expression for material response consists of three parameters that form the S-shape curve quite resealable. As it was stated before, Gaussian distribution cannot generally generate the S-shape and predict the stress-stretch response at

moderate to high deformation ranges. For this reason, Treloar noticed the a factor governing the chain extensibility limit [36]. The disadvantages of Gaussian distribution treatment made need for non-Gaussian approach based on Langevin statistics as mandatory. Arruda and Boyce in 1993 noted drawbacks and strengths of previous theories and developed the renowned eight-chain or Arruda-Boyce model [9]. As name of the model implies, the network structure is composed of eight number of chains linked to each other at the center of a cube and the other ends are considered to be connected to edges of cube. Another hyperelastic material model emphasizing on chain extensibility limit is devoped in 1996 by Gent [37]. The constitutive equation is first invariant based with additional term for limiting the extension of I_1 . Following the work by Edwards and Vilgis [38] and Doi [39], in 1997 Heinrich and Kaliske published an article introducing tube model [40]. The molecular network of the chains are assumed to be constrained by neighboring chains shaping a tube. Strain energy of the tube model composed of two parts, namely cross-link and entanglement based parts. Topology of constraints and entanglements are the basis of forming the free energy function of tube model. Thermodynamical properties of rubber-like materials in different temperatures are investigated by Lion [41]. The model proposed by Lion in 1997, contains also viscoelastic representation. The general Mooney's form is taken into the hand and constructed the basis of the phenomenological Lion's model. Investigating the advantages and disadvantages of the previous studies on phenomenological material models, in 1997, Yeoh and Fleming [42] published their findings as a first invariant based material model. The concept which are studied are mostly taken from Mooney-Rivlin representations [10], however an exponential term is considered while deriving the constitutive relation. In their model it is attempted to catch the material data curve at small and moderate stretch values. In 1999, Lambert Diani and Rey [43], using Treloar's data [44], fitted an expression that suits response curve of rubber-like material quite well. They split free energy expression into two series expansions of first and second invariants. The aim was to capture the S-shape curve together with estimation of results at small, moderate and high strain regimes. Kaliske and Heinrich developed the Extended tube model in 1999 [45]. The idea is taken from the tube model with extension to the high deformation range. Constraints due to chain entanglements are shown to have prominent cause on catching the stress-strain behavior and improve the results in high strain values rather than limiting chain

extensibility. For the cross-link part also formulations are extended from Gaussian to non-Gaussian treatments. Shariff in 2000 [46], developed a purely mathematical formulation to represent the material response. The proposed phenomenological constitutive relation is principle stretch base and given as in series expansion form. Phenomenological modeling of viscoelastic and viscoplastic behavior of rubber-like materials considering the Mooney-Rivlin form is proposed by Haupt and Sedlan in 2001 [47]. Following the experimental investigations on hyperelastic material behavior, Chevalier and Marco [48] developed a constitutive expression in 2002. The starting point of modeling is known to be Mooney-Rivlin expression, however some modifications are done considering second invariant term. The displacement field is captured and tracked by digital image correlations and a phenomenological expression is fitted to the response curve. In order to improve the results of Gent's model [37] and make the model to capture S-turn, Pucci and Saccomandi made modifications on Gent's constitutive relation [49]. One may note that the obtained results demonstrate combination of Gent [37] and Gent-Thomas's model [23]. First invariant part is taken from Gent's model and the second invariant part, which is responsible for S-turn, is taken from Gent-Thomas's model. In 2004, a new approach for constitutive modeling of rubber-like materials is introduced by Miehe and coworkers [1]. The proposed model is named as micro-sphere. The novelty of the approach is non-affine micro-to-macro transition formulation of the represented network model. Basically, non-affine stretch part, non-affine tube part, and micro-to-macro transition of state variables on the micro-sphere are the three main steps considered developing the micro-sphere model. Non-affine stretch part improves the fitting capacity of eight-chain model by introducing a non-affine stretch parameter p . Extending the finding by Doi and Edwards [50], none-affine tube part is developed defining a variable for tube-area-contraction, ν . Closed form of the micro-sphere mode is obtained by averaging the non-affine stretch and tube parts on the micro-sphere of 21 discrete set of orientations. Taking advantage of Valanis-Landel hypothesis, in 2004, Attard and Hunt [51] introduced a principle stretch based model. Stress formulations are presented in both Eulerian and Lagrangian settings. Compressibility term is also added considering neo-Hookean strain energy form. Considering the model proposed by Yamashita and Kawabata [35], Amin and coworkers [52] (2006) introduced a modified phenomenological model aiming simulation of high damping rubber behavior

under uniaxial compression and pure shear. Fitting performance of the model and parameter identification is done using least-square residual minimization. In 2006 another constitutive model is presented by Bechir and coworkers [53]. Obeying the Valanis-landel hypothesis, modifications on neo-Hookean and Ogden models are considered. Choosing the first invariant of Seth-Hill strain measure higher order polynomial terms are added to neo-Hooke model yielding a constitutive relation which we name it as Bechir model. Comparing the outcomes from Gent-Thomas formulation, Beda (2007) introduced a phenomenological invariant based model [16] competing with the Gent-Thomas findings. One may also notice that a polynomial term, like the one used by Yamashita and Kawabata [35], is added to improve the performance of Gent-Thomas model. In 2010, Oscar Lopez-Pamies introduced a first invariant based constitutive relation named as two-term model [54]. The attempt is to catch material response in low and intermediate deformation ranges. Generalized form of two-term model is given as an infinite polynomial series, however, as its name implies, the writer choose two term expansion series to capture the material response in the desired regions. Limitations on parameters also are given by the writer. Brief comparison with first invariant based models, like Arruda-Boyce and Gent model, is also supplied. In 2011, a simple yet accurate phenomenological invariant based model is proposed by Carroll [55]. Carroll model consists of three terms, each having certain considerations while developing the constitutive model. For the first term, taking the Treloar data and distinguishing Gaussian material response in simple extension for stretches below 4.5, neo-Hookean type strain energy function is estimated. Second and third terms are approximated identifying residual stress in simple and equibiaxial extension data of Treloar [44], respectively. In 2011, Nunes [56] used Mooney's idea to model the hyperelastic material response at low deformation region. Thus the proposed model cannot generate S-shape curve. The experiments are done on polydimethylsiloxane (PDMS) and material response under pure shear loading is analyzed. Exp-Ln model [57] was derived in 2013. As its name implies, the constitutive relation consists of two separate parts (exponential and logarithmic parts). Additive decomposition of exponential and logarithmic parts are done to generate the S-shape curve. The exponential term is a positive function and the logarithmic part is considered as negative. Writers aim to catch the material response in full range of deformation by adding the mentioned terms. Neo-Hookean term is considered to

dominate the small strain response. Parameters 'a' and 'b' demonstrate the chain extensibility limit and dominating parameter in moderate strain regimes, respectively. Khiem and Itskov in 2016 [58] introduced a micromechanical model based on analytical network averaging of tube model. The non-affine deformation is considered and Rayleigh distribution function for non-Gaussian chains are applied. The network averaging tube model can be considered as a full-network model of micro-sphere type, however, probability density function is provided as the first order approximation of the Rayleigh distribution function rather than inverse Langevin approximation. In Khiem and Itskov approach polymeric chains are assumed to be composed of identical coarse-grained segments. Recently (2017) Korba and Barkey [59] proposed a material model named as weight function based model (WFB). The constitutive relation is assumed to be a function of principle stretch (λ). As the name implies, a non-linear weighting function is introduced as a multiplicative factor to shape the S-turn (transition point) of the material response curve. In their work, simultaneous fitting is not applied and the results are presented for uniaxial, pure shear and biaxial loading separately.

Having brief introduction to the 40 hyperelastic constitutive models used in this study, and before starting the next section, some well-known review studies (since 2000) in this context is going to be presented.

Boyce and Arruda in their paper on constitutive models of rubber elasticity, reviewed 10 hyperelastic material models [12]. Three category of statistical mechanical, invariant, and principle stretch based modeling of hyperelastic material response together with examples for each category is supplied. The considered models are fitted to the uniaxial experimental data of Treloar [44], obtaining material constants, stress-strain response of the material is observed on equibiaxial and pure shear curves. Gaussian and non-Gaussian behavior of the five chain statistical based models are described and drawbacks for Gaussian approach is deeply explained. The compressibility effects on elastic material response of rubber-like materials also investigated and included in their work.

Marckmann and Verron in 2006 published a paper on fitting performance of 20 hyperelastic material models. They used well-known Treloar experimental data sets [44]

for uniaxial, equibiaxial, biaxial tension, and pure shear. Furthermore, Kawabata's data set for biaxial loading [3] is also used. To obtain model parameters, genetic algorithm and gradient based approach using Levenberg-Marquardt method is applied. Here, objective function is taken as least square error function. It is tried to make use of genetic algorithm to set the initial guesses for model parameters, then the obtained values are used as initial values for gradient based approach. During the fitting, it is aimed to find unique set of parameters well suiting the Treloar and Kawabata's data. However, for most of the models considered, it is not possible to set unique parameter values. Validity range for the models that cannot fully shape the material response curve is also considered by decreasing the number of data points in uniaxial tension gradually and searching the new parameter values. Sorting the goodness of each model is also provide by the writers. First consideration during the ranking of models is the valid range for each model, apparently the models that cover full range of stress-strain curve are considered to have higher ranking. The second criteria is the number of parameters belonging to each mode, less number of parameters cause higher ranking. Third consideration is if the model can generate material response curve of Treloar and Kawabata with a unique set of parameter. The ones with unique parameter values have higher ranking. The last criteria is a priority that writers give to the physically motivated models. Statistical and micromolecular based constitutive approaches have higher ranking compared to the phenomenological ones.

Two important review papers are published in 2012 and 2013 by Stienmann and coworkers [14], and Hossain and Stienmann [15], respectively. The latter one can be considered as the extension for the first paper. In total 25 hyperelastic material models have been discussed. An import aspect of the mentioned studies is the derivations related to fourth order tangent moduli terms for each constitutive relation which is the main challenging factor in finite element analysis of technical rubber. To obtain the parameter set for each model bound constrained non-linear least square method is used. Trust-region solver for non-linear equations and inequalities, TRESNEI, utility of Matlab software is used to solve objective functions. Note also that the related works use Treloar's data set [44] only.

Recent review studies of Dal and coworkers [60], and [61], which are directly related to this thesis, can be considered as a novel approach to parameter optimization study

on rubber-like materials. It was tried to make an objective comparison among the hyper-elastic material models. Throughout the thesis details of the related studies will be supplied.

CHAPTER 3

PRELIMINARIES ON CONTINUUM MECHANICS AND HYPERELASTICITY

In this section basic concepts and preliminaries regarding continuum mechanics and its application for hyperelastic material modeling will be presented. In the first part continuum mechanics notes are going to be considered. Basic rules and concepts in hyperelasticity will be addressed in the second part of this section.

3.1 Basic concepts in Continuum Mechanics

Continuum mechanics is concerned with the mechanical behaviour of solids and fluids on the macroscopic scale. This is inline with the experimental observations made at the same scale. At continuum level we pursue with the following assumptions:

- discrete nature of particles/matter at micro-scale is ignored,
- material is uniformly distributed throughout the space,
- quantities such as density, displacement, and velocity are continuously defined (or at least piecewise continuously) as a function of position.

Continuum mechanics deals with the interactions between forces, heat fluxes and motion, and temperature variations at material point.

Unlike rigid-body mechanics where the shape change of the body is ignored during the motion, continuum mechanics studies relation between deformation and forces (body forces [force/volume], traction [force/area]) as well as the translational/rotational motion of the body.

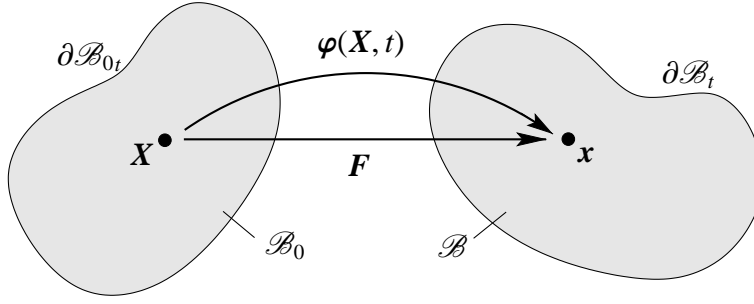


Figure 3.1: Mathematical description of the motion of a body \mathcal{B} in \mathbb{R}^3

The equations of continuum mechanics are two fold:

- i) physical law of conservation for mass, momentum, moment of momentum, and energy.
- ii) mechanical behaviour of materials, e.g. relation between stress and strain.

3.1.1 Kinematics

Following the work of [62], let a three dimensional body \mathcal{B} be consist of material points $\mathcal{P} \in \mathcal{B}$. The motion of the body can be described by the mapping

$$\chi(\mathcal{P}, t) = \begin{cases} \mathcal{B} \rightarrow \mathcal{B}(\mathcal{P}, t) \in \mathbb{R}^3 \times \mathbb{R}_+ \\ \mathcal{P} \mapsto \mathbf{x} = \chi_t(\mathcal{P}) = \chi(\mathcal{P}, t). \end{cases} \quad (3.1)$$

The current configuration of material point \mathcal{P} at time $t \in \mathbb{R}_+$ is denoted by $\mathbf{x} = \chi(\mathcal{P}, t)$. Let the configuration of \mathcal{P} at the reference time t_0 be denoted by $\mathbf{X} = \chi(\mathcal{P}, t_0) \in \mathbb{R}^3$ and $\chi_t(\mathcal{P}) = \chi(\mathcal{P}, t)$ denote the configuration at an arbitrary time t . Then the deformation map $\varphi_t = \chi_t \circ \chi_{t_0}^{-1}(\mathbf{X})$

$$\varphi_t(\mathbf{X}) = \begin{cases} \mathcal{B}_0 \rightarrow \mathcal{B} \in \mathbb{R}^3 \\ \mathbf{X} \mapsto \mathbf{x} = \varphi(\mathbf{X}, t) \end{cases} \quad (3.2)$$

maps the reference configuration $\mathbf{X} \in \mathcal{B}_0$ of \mathcal{P} onto the Eulearian counterpart $\mathbf{x} \in \mathcal{B}$ (Figure 3.1). Then, the deformation gradient

$$\mathbf{F} : T_{\mathbf{X}}\mathcal{B}_0 \rightarrow T_{\mathbf{x}}\mathcal{B}; \quad \mathbf{F} := \nabla_{\mathbf{X}}\varphi_t(\mathbf{X}) \quad (3.3)$$

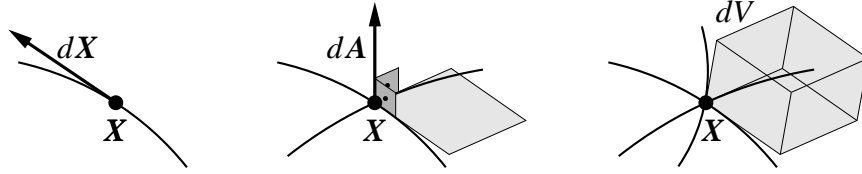


Figure 3.2: Line, area, and volume elements on a material point \mathcal{P} at X .

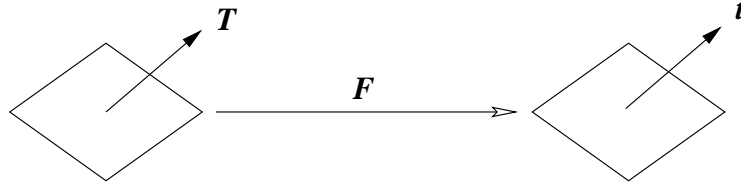


Figure 3.3: Deformation gradient mapping.

maps the unit tangent of the reference or the Lagrangian configuration onto its counterpart in the current or Eulerian configuration. Where, the gradient operators $\nabla_X[\bullet]$ and $\nabla_x[\bullet]$ denote the spatial derivatives with respect to the reference X and current x coordinates, respectively. Let dX , dA , and dV denote the infinitesimal line, area, and volume elements in the undeformed configuration (Figure 3.2). Then, the deformation gradient F , its cofactor $\text{cof}[F] = \det[F]F^{-T}$, and the Jacobian $J := \det[F] > 0$ characterize the deformation of infinitesimal line, area, and volume elements

$$dx = FdX, \quad da = \text{cof}[F]dA, \quad dv = JdV. \quad (3.4)$$

The condition $J := \det[F] > 0$ ensures the physically interpretable deformations for the deformation map φ .

$$J = \det F \begin{cases} > 0 : & \text{shrinkage/expansion (physical)} \\ = 0 : & \text{shrinkage on a mathematical point} \\ < 0 : & \text{recovering on the opposite side} \end{cases} \quad (3.5)$$

The deformation gradient maps a tangent T of Lagrangian setting onto a tangent t in current configuration (Figure 3.3). According to the deformation map, t is push-forward of Lagrangian tangent vector T and T can be considered as pull-back of t .

$$\begin{aligned}
\mathbf{t} = \mathbf{F}\mathbf{T} & : & \text{'push-forward' of } \mathbf{T} \\
\mathbf{T} = \mathbf{F}^{-1}\mathbf{t} & : & \text{'pull-back' of } \mathbf{t} \text{ (unique invertibility)}
\end{aligned}
\tag{3.6}$$

Deformation and Strain Measures

The deformation gradient can be decomposed into pure rotation and stretch inducing components.

$$\mathbf{F} = \mathbf{R}\mathbf{U} = \mathbf{V}\mathbf{R} \tag{3.7}$$

where \mathbf{R} , \mathbf{U} and \mathbf{V} are the rotation, right and left stretch tensors, respectively (Figure 3.4).



Figure 3.4: Rotation, left and right stretch tensors.

In Cartesian framework, the right and left Cauchy-Green tensors (\mathbf{C} , and \mathbf{b}) can be defined as:

$$\mathbf{C} = \mathbf{F}^T \mathbf{F} \tag{3.8}$$

and

$$\mathbf{b} = \mathbf{F}\mathbf{F}^T. \tag{3.9}$$

\mathbf{U} , \mathbf{V} , \mathbf{R} , \mathbf{C} , and \mathbf{b} are symmetric, positive-definite, proper orthogonal tensors. Right and left stretch tensors can be expressed in term of principle stretches in principle directions as follows:

$$\mathbf{U} = \sum_{i=1}^3 \lambda_i \mathbf{N}_i \otimes \mathbf{N}_i \tag{3.10}$$

and

$$\mathbf{V} = \sum_{i=1}^3 \lambda_i \mathbf{n}_i \otimes \mathbf{n}_i. \tag{3.11}$$

Where λ_i denote the principal stretches and \mathbf{N}_i , \mathbf{n}_i are principle directions in Lagrangian and Eulerian settings, respectively.

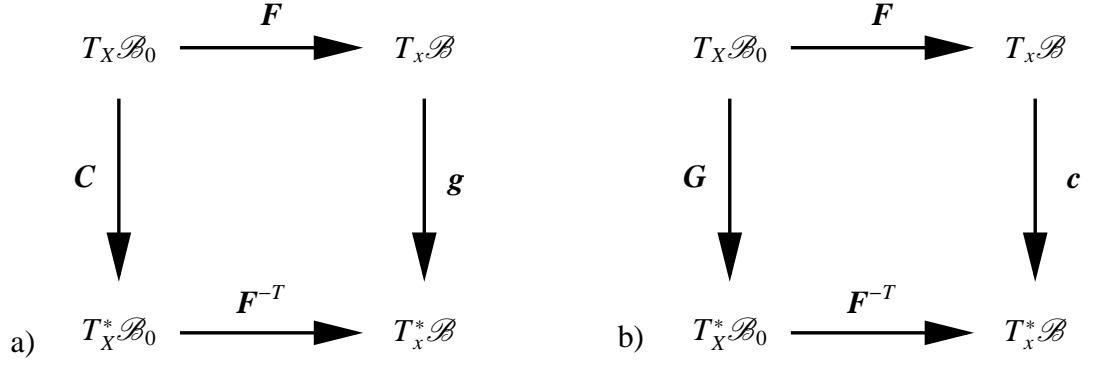


Figure 3.5: Definition of metric tensors. a) current metric in Lagrangian configuration; b) reference metric in Eulerian configuration.

Furthermore, in generalized coordinate system, reference \mathcal{B}_0 and the spatial \mathcal{B} manifolds are locally furnished with the covariant reference G and current g metric tensors in the neighborhood \mathcal{N}_X of X and \mathcal{N}_x of x , respectively. These metric tensors are required for the mapping between the covariant and contravariant objects in the Lagrangian and Eulerian manifolds.

The right Cauchy Green tensor and the inverse of the left Cauchy Green tensors can be expressed using metric tensors

$$C := F^T g F \quad (3.12)$$

and

$$c = F^{-T} G F^{-1} \quad (3.13)$$

as the pull back of the current metric g and the push forward of the Lagrangian metric G , respectively. Here notice that, the left Cauchy Green tensor or the Finger tensor is denoted by $b = c^{-1}$. For a geometric interpretation, we refer to Figures 3.5. From Figures 3.5 and 3.11 it can be concluded that the Kirchhoff stress in the Eulerian configuration is dual to g and c and the second Piola stress in Lagrangian configuration is dual to C and G . It is important to note that, $F^T(\bullet)F$ is covariant pull-back and $F^{-T}(\bullet)F^{-1}$ covariant push-forward operators.

Green-Lagrangian and Almansian strain tensors are also other strain measures which

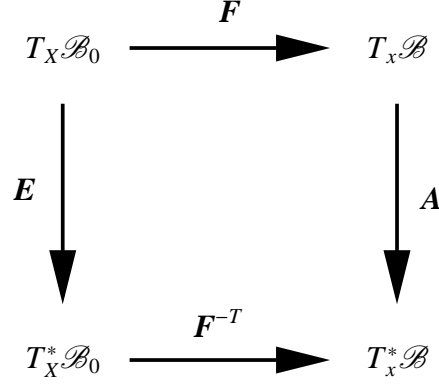


Figure 3.6: Covariant pull-back and push-forward operations between the material and spatial strain tensors.

are defined as:

$$\begin{aligned}
\mathbf{E} &= \frac{1}{2}[\mathbf{C} - \mathbf{1}] & : & \text{Green-Lagrangian Strain} \\
\mathbf{A} &= \frac{1}{2}[\mathbf{1} - \mathbf{b}^{-1}] & : & \text{Almanson Strain} \\
\mathbf{E} &= \mathbf{F}^T \mathbf{A} \mathbf{F} & : & \text{Covariant pull-back } \mathbf{F}^T(\bullet)\mathbf{F} \\
\mathbf{A} &= \mathbf{F}^{-T} \mathbf{E} \mathbf{F}^{-1} & : & \text{Covariant push-forward } \mathbf{F}^{-T}(\bullet)\mathbf{F}^{-1}.
\end{aligned} \tag{3.14}$$

Figure 3.6 describes the mapping between Green-Lagrangian and Almanson strain tensors.

3.1.2 Stress Expressions

Consider a part $\mathcal{P}_0 \subset \mathcal{B}_0$ cut out of the reference configuration \mathcal{B}_0 and its spatial counterpart $\mathcal{P}_t \subset \mathcal{B}_t$, with boundaries $\partial \mathcal{P}_0$ and $\partial \mathcal{P}_t$, respectively (Figure 3.7). Then the resultant body force can be described as:

$$\text{Resultant body force: } \int_{\mathcal{P}} \rho \mathbf{b} \, dv = \int_{\mathcal{P}_0} \rho_o \mathbf{b}_o \, dV \tag{3.15}$$

where $\mathbf{b}_o = \mathbf{b}$ is mass specific body force [force/unit mass] and $\mathbf{f}_o = \rho_o \mathbf{b}_o$ is the volume specific body force [force/unit volume]. From the equation (3.15) it can be seen that:

$$\int_{\mathcal{P}_0} \mathbf{f}_o \, dV = \int_{\mathcal{P}} \mathbf{f} \, dv. \tag{3.16}$$

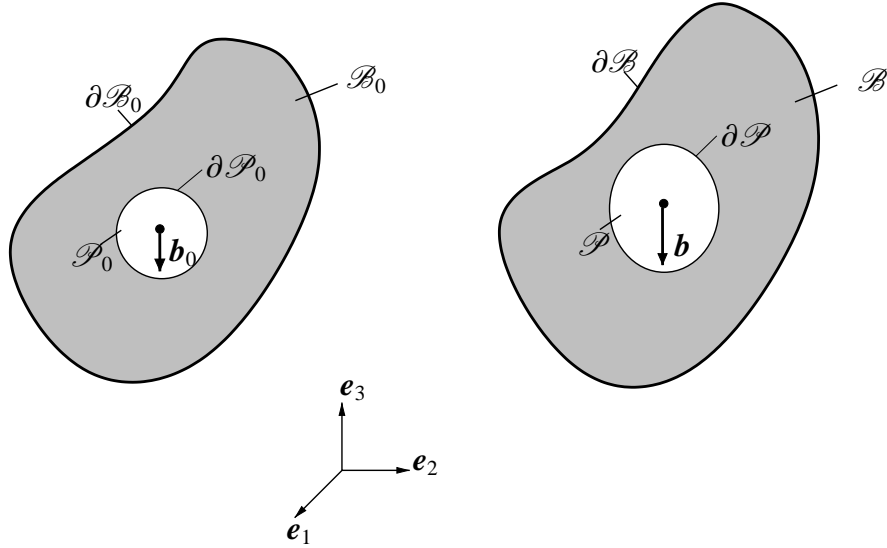


Figure 3.7: Representation of body forces on deformed and undeformed states.

Knowing that, $dv = JdV$ it can be shown that:

$$\mathbf{f}_o = J\mathbf{f}. \quad (3.17)$$

Similarly, the surface forces acting on a body \mathcal{B} are

$$\int_{\partial\mathcal{B}_t} \mathbf{t} da = \int_{\partial\mathcal{B}_0} \mathbf{T} dA, \quad (3.18)$$

where, $\partial\mathcal{B}_t$ is surface bounding the body \mathcal{B} at time t . From equations (3.16) and (3.18) total force acting on body \mathcal{B}_t in reference and current configurations are,

$$\mathbf{F}_0 = \int_{\partial\mathcal{B}_0} \mathbf{T} dA + \int_{\mathcal{B}_0} \mathbf{f}_0 dV \quad (3.19)$$

and

$$\mathbf{F}_t = \int_{\partial\mathcal{B}_t} \mathbf{t} da + \int_{\mathcal{B}_t} \mathbf{f} dv, \quad (3.20)$$

respectively.

Cauchy's Lemma

Consider a body under surface and body forces, and split the body into two parts (Figure 3.8). With the help of equation (3.20), forces action bodies \mathcal{B}_1 and \mathcal{B}_2 are

$$\mathbf{F}_1 = \int_{\partial\mathcal{B}_1^1} \mathbf{t} da + \int_{\mathcal{B}_1^1} \mathbf{f} dv + \int_{\mathcal{I}_L} \mathbf{t}(\mathbf{x}, \mathbf{n}, t) da \quad (3.21)$$

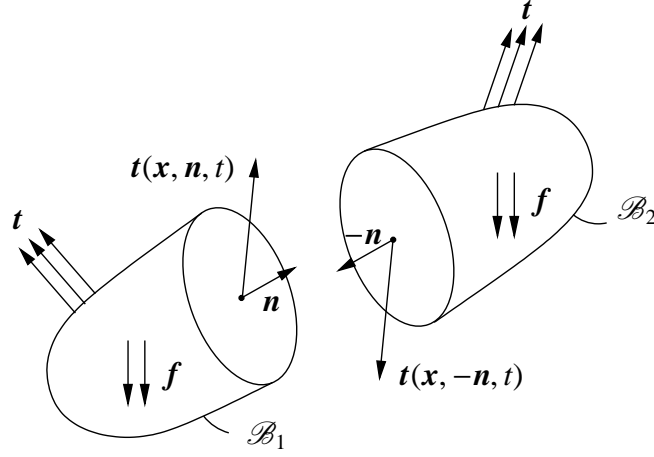


Figure 3.8: Representation for Cauchy's Lemma.

and

$$F_2 = \int_{\partial \mathcal{B}_1^2} \mathbf{t} \, da + \int_{\mathcal{B}_1^2} \mathbf{f} \, dv + \int_{\mathcal{S}_R} \mathbf{t}(\mathbf{x}, -\mathbf{n}, t) \, da \quad (3.22)$$

Total force on the body implies

$$\mathbf{F} = \mathbf{F}_1 + \mathbf{F}_2 \quad \Rightarrow \quad \int_{\mathcal{S}_L} \mathbf{t}(\mathbf{x}, \mathbf{n}, t) \, da + \int_{\mathcal{S}_R} \mathbf{t}(\mathbf{x}, -\mathbf{n}, t) \, da = \mathbf{0}. \quad (3.23)$$

Using the localization theorem one may reach the following conclusion: As $\mathcal{S}_L = \mathcal{S}_R \rightarrow 0$

$$\mathbf{t}(\mathbf{x}, \mathbf{n}, t) = -\mathbf{t}(\mathbf{x}, -\mathbf{n}, t), \quad (3.24)$$

which is known as Cauchy's fundamental lemma and corresponds to the Newton's third law of motion of action and reaction. In another word, surfaces in contact will exert the same magnitude of force with opposite directions to each other.

Cauchy's Theorem

To develop the stress tensor associated with the Cartesian frame work, consider the stress components on a unit cubical element (Figure 3.9). Let us now describe the traction vector acting on the positive surfaces in \mathbf{e}_1 , \mathbf{e}_2 , and \mathbf{e}_3 directions respectively:

$$\begin{aligned} \mathbf{t}_1 &= \sigma_{11} \mathbf{e}_1 + \sigma_{12} \mathbf{e}_2 + \sigma_{13} \mathbf{e}_3 \\ \mathbf{t}_2 &= \sigma_{21} \mathbf{e}_1 + \sigma_{22} \mathbf{e}_2 + \sigma_{23} \mathbf{e}_3 \\ \mathbf{t}_3 &= \sigma_{31} \mathbf{e}_1 + \sigma_{32} \mathbf{e}_2 + \sigma_{33} \mathbf{e}_3. \end{aligned} \quad (3.25)$$

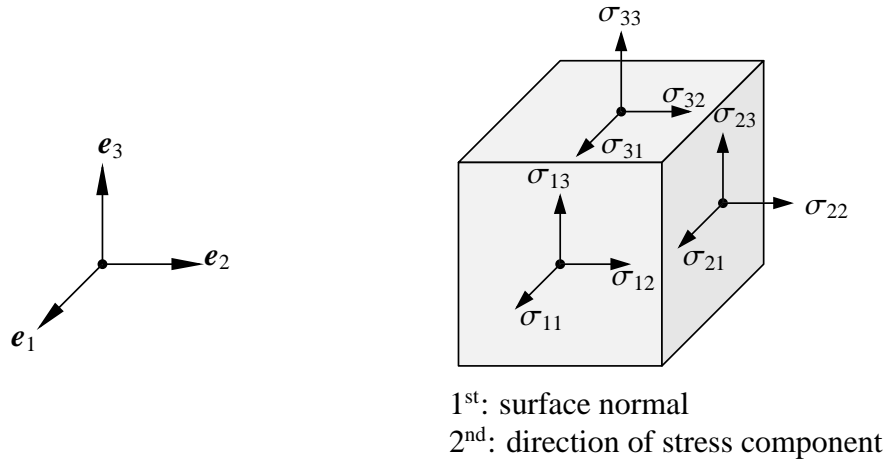


Figure 3.9: Stress components on the surfaces of unit cube.

Equation (3.25) yields,

$$t_i = \sigma_{ij} e_j \quad (3.26)$$

where there is a summation over j in equation (3.26) and

$$\sigma_{ij} = t_i e_j \quad (3.27)$$

noticing that $e_i \cdot e_j = \delta_{ij}$. Now, consider a cut out from the unit cube, which can be considered as a tetrahedron (Figure 3.10). Equilibrium of force on the deformed

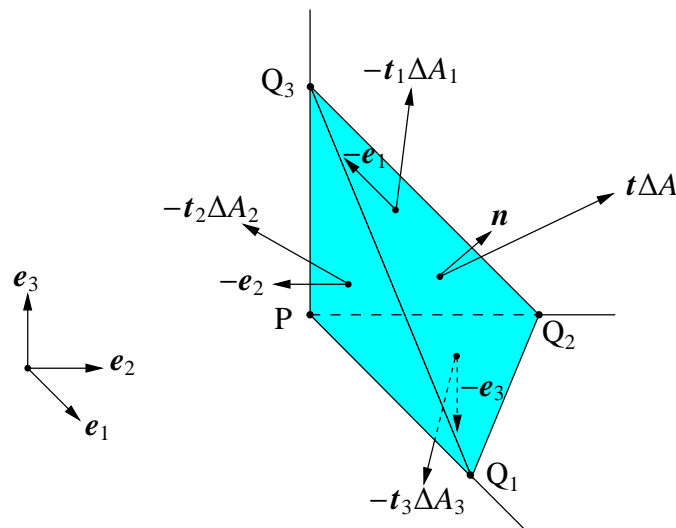


Figure 3.10: Traction components on a tetrahedron.

tetrahedron is written as:

$$t\Delta A - t_1\Delta A_1 - t_2\Delta A_2 - t_3\Delta A_3 = \mathbf{0}, \quad (3.28)$$

with $\Delta A_i = n_i \Delta A$

$$[\mathbf{t} - t_1 \mathbf{n}_1 - t_2 \mathbf{n}_2 - t_3 \mathbf{n}_3] \Delta A = \mathbf{0}. \quad (3.29)$$

Applying equation (3.26) into the above relation, the following result may be reached

$$\mathbf{t} = n_i \mathbf{t}_i = n_i \sigma_{ij} \mathbf{e}_j. \quad (3.30)$$

As a consequence, the total stress vector \mathbf{t} acts on the surface element $d\mathbf{a} \subset \partial \mathcal{P}_t$ on the deformed configuration and represents the force that the rest of the body $\mathcal{B}_t \setminus \mathcal{P}_t$ exerts on \mathcal{P}_t through $\partial \mathcal{P}_t$. Cauchy's stress theorem establishes a linear dependence between the traction and the outward surface normal

$$\mathbf{t}(\mathbf{x}, t; \mathbf{n}) = \boldsymbol{\sigma} \cdot \mathbf{n} \quad (3.31)$$

through the total Cauchy stress tensor $\boldsymbol{\sigma}$. We define the Lagrangian and Eulerian unit area elements

$$d\mathbf{A} = N dA \quad \text{and} \quad d\mathbf{a} = \mathbf{n} da, \quad (3.32)$$

where N and \mathbf{n} are the surface normals of the undeformed and deformed solid body.

Piola Identity

Cauchy stress vector $\mathbf{t}(\mathbf{x}, t; \mathbf{n})$ measures force per unit deformed area. We define the first Piola-Krichhoff stress vector $\mathbf{T}(\mathbf{X}, t; \mathbf{N})$ which is parallel to $\mathbf{t}(\mathbf{x}, t; \mathbf{n})$ but measures force per unit undeformed area

$$\mathbf{t} da = \mathbf{T} dA. \quad (3.33)$$

Then the Piola identity can be derived as follows.

$$\int_{\partial \mathcal{B}} \mathbf{n} da = \int_{\partial \mathcal{B}_0} J \mathbf{F}^{-T} \mathbf{N} dA = 0, \quad (3.34)$$

applying Gauss-divergence theorem

$$\int_{\mathcal{B}_0} \text{Div}(J \mathbf{F}^{-T}) dV = 0, \quad (3.35)$$

and using localization theorem, Piola identity is obtained (equation (3.36))

$$\text{Div}(J \mathbf{F}^{-T}) = 0. \quad (3.36)$$

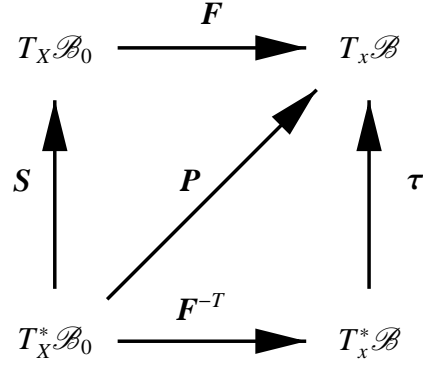


Figure 3.11: Definition of stress tensors. Relationship between stresses.

The other important concept before starting hyperelasticity concept is related to the stress tensors and their derivations which is presented below.

Various stress tensors

Consider the Piola identity $\text{Div}(J\mathbf{F}^{-T}) = 0$, applied as $\mathbf{n}da = J\mathbf{F}^{-T}\mathbf{N}dA$ which induces the definition of the nominal or the first Piola-Kirchhoff stress tensor \mathbf{P} , by setting

$$\mathbf{P}dA = \boldsymbol{\sigma}da \quad (3.37)$$

where,

$$\mathbf{P} := J\boldsymbol{\sigma}\mathbf{F}^{-T}. \quad (3.38)$$

The first and second Piola Kirchhoff stress tensor relations are obtained through transformations given in Figure 3.11, which can be summarized as,

$$\mathbf{P} = J\boldsymbol{\sigma}\mathbf{F}^{-T} = \boldsymbol{\tau}\mathbf{F}^{-T}, \quad (3.39)$$

$$\mathbf{S} = \mathbf{F}^{-1}\mathbf{P} = \mathbf{F}^{-1}\boldsymbol{\tau}\mathbf{F}^{-T}, \quad (3.40)$$

where \mathbf{S} is the pull-back of $\boldsymbol{\tau}$. One may also notice that the following relation is hold between Cauchy and Kirchhoff stress tensors

$$\boldsymbol{\tau} = J\boldsymbol{\sigma}. \quad (3.41)$$

From figures 3.5 and 3.11 it can be concluded that the Kirchhoff stress in the Eulerian configuration is dual to \mathbf{g} and \mathbf{c} and the second Piola stress in Lagrangian configuration is dual to \mathbf{C} and \mathbf{G} .

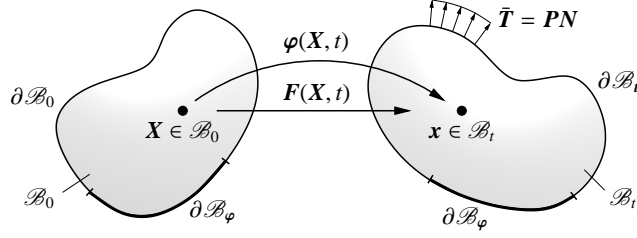


Figure 3.12: Initial boundary value problem is defined by the balance equations as well as boundary and initial conditions. Boundary of the initial and current configuration subdivided into Dirichlet and Neumann part. Traction vector given in terms of material Cauchy theorem $\bar{T} = PN$ due to the first Piola-Kirchhoff stress.

3.1.3 Boundary value problems

In purely mechanical description of continuous media, the balance equations hold for all bodies independent of the material character. In addition to these balance equations, boundary and initial conditions are imposed onto the body of interest, Figure 3.12. Types of the used conditions are given below.

$$\begin{aligned} \varphi(\mathbf{X}, t) &= \bar{\varphi}(\mathbf{X}, t) \quad \text{on} \quad \partial\mathcal{B}_\varphi; \quad \text{Dirichlet boundary condition,} \\ \mathbf{P}(\mathbf{X}, t) \cdot \mathbf{N} &= \bar{\mathbf{T}}(\mathbf{X}, t) \quad \text{on} \quad \partial\mathcal{B}_t; \quad \text{Neumann boundary condition.} \end{aligned} \quad (3.42)$$

Dirichlet boundary are also known as essential boundary conditions. Neumann boundary conditions on the other hand are generally considered as natural boundary conditions. To solve the boundary value problems there should be initial values for function, these conditions are named as initial conditions which are specified below.

$$\begin{aligned} \varphi(\mathbf{X}, t_0) &= \bar{\varphi}_0(\mathbf{X}) \quad \text{in} \quad \partial\mathcal{B}; \quad \text{displacement initial condition,} \\ \mathbf{V}(\mathbf{X}, t_0) &= \bar{\mathbf{V}}_0(\mathbf{X}) \quad \text{in} \quad \partial\mathcal{B}; \quad \text{velocity initial condition} \end{aligned} \quad (3.43)$$

3.2 Hyperelasticity

Elasticity is considered as reversible, non-dissipative response of material (no hysteresis) with memory of initial configuration. The material remembers its reference configuration and restore its original shape upon removal of external load. Rubber-like materials possess the elastic nature under loading, however, that type of materials

can resist to high stretch values while loading is applied. Hyperelasticity is the classification related to the highly non-linear material response of such materials. To simulate the hyperelastic material response in finite elasticity a governing relation named as free energy function is introduced. The basic form of free energy function is given as

$$\psi(\mathbf{F}) = \psi_{\text{vol}}(J) + \psi_{\text{iso}}(\bar{\mathbf{F}}), \quad (3.44)$$

with

$$\bar{\mathbf{F}} = J^{-\frac{1}{3}} \mathbf{F}, \quad (3.45)$$

which is additively decomposed into volumetric and isochoric parts. The first part governs the energy storage associated with volume change whereas the latter one governs the volume-preserving shape change. Rubberlike materials exhibit very stiff response to volume change. Ratio of bulk to shear modulus is large which indicates the incompressible feature for rubber-like materials. That is why, they are also known as incompressible or (nearly) quasi-incompressible materials. The energy storage due to shape change can be described in various forms

$$\psi_{\text{iso}} := \psi(\bar{\mathbf{F}}) = \tilde{\psi}(\bar{\mathbf{C}}) = \hat{\psi}(\bar{\mathbf{b}}) \quad (3.46)$$

as a function of unimodular deformation gradient, right Cauchy-Green tensor and left Cauchy-Green tensor, respectively.

3.2.1 Lagrangian and Eulerian setting

A crucial consequence of the principle of material objectivity which postulates that a constitutive relation should be invariant with respect to a change of frame, i.e., it should be independent of the observer is a reduced form that always satisfies this principle by setting

$$\psi = \bar{\psi}(\mathbf{F}^T \mathbf{g} \mathbf{F}, \mathbf{X}). \quad (3.47)$$

It can easily be proven that this equation is always objective $\bar{\psi}(\mathbf{F}^T \mathbf{Q}^T \mathbf{g} \mathbf{Q} \mathbf{F}, \mathbf{X}) = \bar{\psi}(\mathbf{F}^T \mathbf{g} \mathbf{F}, \mathbf{X})$. The reduced form of the free energy function in equation ((3.47)) then reads

$$\psi = \bar{\psi}(\mathbf{C}, \mathbf{X}) \quad \text{with} \quad \mathbf{C} = \mathbf{F}^T \mathbf{g} \mathbf{F} \quad (3.48)$$

Starting with this reduced form, an alternative constitutive expressions for the second Piola-Kirchhoff stresses \mathbf{S} and the Kirchhoff stresses $\boldsymbol{\tau}$ is obtained by reformulating the stress power

$$\mathcal{P} = \mathbf{P} : \dot{\mathbf{F}} = \mathbf{S} : \frac{1}{2} \dot{\mathbf{C}} = \boldsymbol{\tau} : \frac{1}{2} \boldsymbol{\mathfrak{L}}_v \mathbf{g} . \quad (3.49)$$

These pairs are the dual stress-strain variables in the two-point, the Lagrangian, and the Eulerian formulation, respectively. Alternative constitutive laws can now be obtained by substitution of the above introduced formulations for the stress power into the Clausius-Planck inequality

$$\mathcal{D}_0^{loc} = \mathbf{P} : \dot{\mathbf{F}} - \dot{\psi} \geq 0 \quad (3.50)$$

On the other hand, an elastic material's stress power $\mathbf{P} : \dot{\mathbf{F}}$ that deforms the material is identical to the temporal evolution of the stored energy, i.e., all work done on the material is stored $\mathcal{D}_0^{loc} = 0$. Hence, for an elastic material, one can write

$$\begin{aligned} \mathcal{D}_0^{loc} &= \mathbf{P} : \dot{\mathbf{F}} - \partial_{\mathbf{F}} \hat{\psi}(\mathbf{F}, \mathbf{X}) : \dot{\mathbf{F}} \\ &= \mathbf{S} : \frac{1}{2} \dot{\mathbf{C}} - 2\partial_{\mathbf{C}} \bar{\psi}(\mathbf{C}, \mathbf{X}) : \frac{1}{2} \dot{\mathbf{C}} \\ &= \boldsymbol{\tau} : \frac{1}{2} \boldsymbol{\mathfrak{L}}_v \mathbf{g} - 2\partial_{\mathbf{g}} \tilde{\psi}(\mathbf{g}, \mathbf{F}, \mathbf{X}) : \frac{1}{2} \boldsymbol{\mathfrak{L}}_v \mathbf{g} = 0 , \end{aligned} \quad (3.51)$$

that yield the Lagrangian and Eulerian constitutive representations of finite elasticity

$$\mathbf{S} = 2\partial_{\mathbf{C}} \hat{\psi}(\mathbf{F}^T \mathbf{g} \mathbf{F}, \mathbf{X}) \quad (3.52)$$

and

$$\boldsymbol{\tau} = 2\partial_{\mathbf{g}} \tilde{\psi}(\mathbf{g}, \mathbf{F}, \mathbf{X}). \quad (3.53)$$

The latter one is also known as the Doyle-Erickson formula of hyperelasticity.

For isotropic elastic materials the constitutive equations can be simplified and expressed in terms of principle stretches or invariants. This becomes clear if a spectral representation of the right Cauchy-Green tensor is considered that appears in the form

$$[\mathbf{C} - \lambda_{(i)}^2 \mathbf{G}] \mathbf{N}_{(i)} = \mathbf{0} \quad \Rightarrow \quad \mathbf{C} = \sum_{i=1}^3 \lambda_{(i)}^2 \mathbf{N}_{(i)} \otimes \mathbf{N}_{(i)} \quad (3.54)$$

in terms of the principal stretches $\{\lambda_{(i)}\}_{i=1,3}$ which are the eigenvalues of $\mathbf{U} := \sqrt{\mathbf{C}}$ and the Lagrangian eigenvectors $\{\mathbf{N}_{(i)}\}_{i=1,3}$. With (3.54) at hand, the symmetry condition is checked

$$\bar{\psi} \left(\sum_{i=1}^3 \lambda_{(i)}^2 (\mathbf{Q} \mathbf{N}_{(i)}) \otimes (\mathbf{Q} \mathbf{N}_{(i)}) \right) = \bar{\psi} \left(\sum_{i=1}^3 \lambda_{(i)}^2 \mathbf{N}_{(i)} \otimes \mathbf{N}_{(i)} \right) \quad \forall \mathbf{Q} \in \mathcal{G} \equiv \mathbf{SO}(3) . \quad (3.55)$$

This identity can only be satisfied, if the free energy $\bar{\psi}$ does not depend on the eigenvectors $N_{(i)}$. As a consequence, isotropic finite elastic materials depend solely on the principal stretches $\{\lambda_{(i)}\}_{i=1,3}$

$$\psi = \check{\psi}(\lambda_{(1)}, \lambda_{(2)}, \lambda_{(3)}) \quad (3.56)$$

These principal stretches are obtained by the characteristic equation of (3.54) in terms of the invariants of the right Cauchy-Green tensor

$$\det[\mathbf{C} - \lambda_{(i)}^2 \mathbf{G}] = \lambda_{(i)}^6 - I_1 \lambda_{(i)}^4 + I_2 \lambda_{(i)}^2 - I_3 = 0 \quad (3.57)$$

with the three invariants

$$I_1 = \text{tr}[\mathbf{C}] = \mathbf{C} : \mathbf{G}^{-1}, \quad (3.58)$$

$$I_2 = \frac{1}{2}(I_1^2 - \text{tr} \mathbf{C}^2) = \frac{1}{2}(I_1^2 - (\mathbf{G}^{-1} \mathbf{C} \mathbf{G}^{-1}) : \mathbf{C}), \quad (3.59)$$

$$I_3 = \det[\mathbf{C}] \rightarrow J = \sqrt{I_3} = \det[\mathbf{F}]. \quad (3.60)$$

Principle invariants (equations (3.59)-(3.60)) can also be expressed in terms of principle stretches as below

$$I_1 = \lambda_1^2 + \lambda_2^2 + \lambda_3^2, \quad (3.61)$$

$$I_2 = \lambda_1^2 \lambda_2^2 + \lambda_2^2 \lambda_3^2 + \lambda_3^2 \lambda_1^2, \quad (3.62)$$

$$I_3 = \lambda_1^2 \lambda_2^2 \lambda_3^2. \quad (3.63)$$

Then (3.56) can be recast into the alternative form

$$\psi = \check{\psi}(I_1, I_2, J) \quad (3.64)$$

Starting from (3.64), the representations of the Lagrangian and Eulerian stresses in the case of finite isotropic elasticity follows by application of the chain rule

$$\mathbf{S} = 2 \partial_{\mathbf{C}} \bar{\psi} = 2 \left[\frac{\partial \check{\psi}}{\partial I_1} \frac{\partial I_1}{\partial \mathbf{C}} + \frac{\partial \check{\psi}}{\partial I_2} \frac{\partial I_2}{\partial \mathbf{C}} + \frac{\partial \check{\psi}}{\partial J} \frac{\partial J}{\partial \mathbf{C}} \right] \quad (3.65)$$

and

$$\boldsymbol{\tau} = 2 \partial_{\mathbf{g}} \bar{\psi} = 2 \left[\frac{\partial \check{\psi}}{\partial I_1} \frac{\partial I_1}{\partial \mathbf{g}} + \frac{\partial \check{\psi}}{\partial I_2} \frac{\partial I_2}{\partial \mathbf{g}} + \frac{\partial \check{\psi}}{\partial J} \frac{\partial J}{\partial \mathbf{g}} \right]. \quad (3.66)$$

The particular expressions for the isotropic stress response are obtained by computation of the derivatives of the invariants with respect to the Lagrangian representation

of the current metric

$$\partial_{\mathbf{C}} I_1 = \mathbf{G}^{-1}, \quad (3.67)$$

$$\partial_{\mathbf{C}} I_2 = I_1 \mathbf{G}^{-1} - \mathbf{G}^{-1} \mathbf{C} \mathbf{G}^{-1}, \quad (3.68)$$

$$\partial_{\mathbf{C}} J = \frac{1}{2} J \mathbf{C}^{-1} \quad (3.69)$$

with $\mathbf{G}^{-1} = \delta^{AB} = \mathbf{I}$. The derivatives with respect to the spatial metric $\mathbf{g} = \delta_{ab} = \mathbf{I}$ follows from the push-forward operation of (3.67) through (3.69), i.e.

$$\partial_{\mathbf{g}} I_1 = \mathbf{F} \partial_{\mathbf{C}} I_1 \mathbf{F}^T = \mathbf{b}, \quad (3.70)$$

$$\partial_{\mathbf{g}} I_2 = \mathbf{F} \partial_{\mathbf{C}} I_2 \mathbf{F}^T = I_1 \mathbf{b} - \mathbf{b} \mathbf{g} \mathbf{b}, \quad (3.71)$$

$$\partial_{\mathbf{g}} J = \mathbf{F} \partial_{\mathbf{C}} J \mathbf{F}^T = \frac{1}{2} J \mathbf{g}^{-1}. \quad (3.72)$$

Substitution of (3.67) through (3.72) into (3.65) and (3.66) finally gives

$$\mathbf{S} = 2\check{\psi}_{,I_1} \mathbf{G}^{-1} + 2\check{\psi}_{,I_2} (I_1 \mathbf{G}^{-1} - \mathbf{G}^{-1} \mathbf{C} \mathbf{G}^{-1}) + \check{\psi}_{,J} J \mathbf{C}^{-1}, \quad (3.73)$$

and

$$\boldsymbol{\tau} = 2\check{\psi}_{,I_1} \mathbf{b} + 2\check{\psi}_{,I_2} (I_1 \mathbf{b} - \mathbf{b} \mathbf{g} \mathbf{b}) + \check{\psi}_{,J} J \mathbf{g}^{-1}, \quad (3.74)$$

which can be rearranged in the form

$$\mathbf{S} = 2(\check{\psi}_{,I_1} + I_1 \check{\psi}_{,I_2}) \mathbf{G}^{-1} - 2\check{\psi}_{,I_2} \mathbf{G}^{-1} \mathbf{C} \mathbf{G}^{-1} + J \check{\psi}_{,J} \mathbf{C}^{-1}, \quad (3.75)$$

and

$$\boldsymbol{\tau} = 2(\check{\psi}_{,I_1} + I_1 \check{\psi}_{,I_2}) \mathbf{b} - 2\check{\psi}_{,I_2} \mathbf{b} \mathbf{g} \mathbf{b} + J \check{\psi}_{,J} \mathbf{g}^{-1} \quad (3.76)$$

These are the general Lagrangian and Eulerian formulations of isotropic elasticity in invariants.

3.2.2 Incompressible hyperelasticity

In the fully incompressible limit where $J = \det \mathbf{F} \rightarrow 1$ the free energy function can be written as

$$\Psi = \psi(\mathbf{F}) = \tilde{\psi}(\mathbf{C}) = \hat{\psi}(\mathbf{b}). \quad (3.77)$$

In line with the general form for free energy function, equation (3.44), the Kirchhoff stresses are also decomposed into volumetric and isochoric parts

$$\boldsymbol{\tau} = \boldsymbol{\tau}_{\text{vol}} + \boldsymbol{\tau}_{\text{iso}} \quad (3.78)$$

along with definitions,

$$\boldsymbol{\tau} = \hat{\boldsymbol{\tau}} - p\mathbf{1}. \quad (3.79)$$

where

$$\hat{\boldsymbol{\tau}} = 2\mathbf{F} \frac{\partial \psi}{\partial \mathbf{C}} \mathbf{F}^T = 2\mathbf{b} \frac{\partial \psi}{\partial \mathbf{b}} \quad (3.80)$$

Here, the isochoric stresses can be evaluated from the free energy function through the relation for $\hat{\boldsymbol{\tau}}$. An arbitrary scalar parameter p , which is known as hydrostatic pressure term, is introduced in stress expressions that has to be determined from the equilibrium condition.

Also recall that for incompressible hyperelastic materials ($j = 1$), then equation (3.41) reduces to

$$\boldsymbol{\tau} = \boldsymbol{\sigma}. \quad (3.81)$$

Now, substituting equation (3.80) in (3.79) yields Kirchhoff or Cauchy stresses in Lagrangian setting as

$$\boldsymbol{\tau} = 2\mathbf{F} \frac{\partial \psi}{\partial \mathbf{C}} \mathbf{F}^T - p\mathbf{1} \quad (3.82)$$

and Eulerian settings as

$$\boldsymbol{\tau} = 2\mathbf{b} \frac{\partial \psi}{\partial \mathbf{b}} - p\mathbf{1}. \quad (3.83)$$

then the first-Piola Kirchhoff stress tensor reads,

$$\mathbf{P} = \frac{\partial \psi}{\partial \mathbf{F}} - p\mathbf{F}^{-T} \quad (3.84)$$

3.2.3 Deformation modes

In literature, for hyperelastic material characterization, four deformation modes are considered more often. These are Uniaxial Tension (UT), Equibiaxial Tension (ET), Pure Shear (PS), and Biaxial Tension (BT). In continuum mechanics stress formulations for these deformation modes utilize incompressibility ($J=1$) consideration. In this part all deformation modes are going to be studied. The deformation gradient, finger tensor, and the Kirchhoff stresses corresponding to the respective deformation modes will be mentioned.

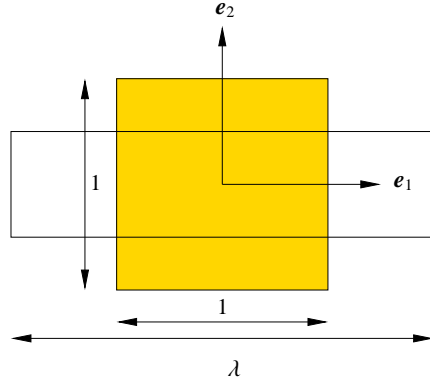


Figure 3.13: Uniaxial tension deformation

3.2.3.1 Uniaxial tension deformation mode

In uniaxial loading mode, the dumbbell shaped test specimen is fixed between fixtures of test set-up. Material is stretch with low rate of applied stretched. Specimen is elongated in e_1 direction and is free to shrink in e_2 and e_3 directions. Therefore, stretch in axial direction, e_1 , is denoted by λ_1 and stretched values in second and third directions can be observed as $1/\sqrt{\lambda}$. As a result, components of deformation gradient for uniaxial extension mode can be written as:

$$[\mathbf{F}]_{ij} = \begin{bmatrix} \lambda & & \\ & \frac{1}{\sqrt{\lambda}} & \\ & & \frac{1}{\sqrt{\lambda}} \end{bmatrix}. \quad (3.85)$$

Using equation (3.9), $\mathbf{b} = \mathbf{F}\mathbf{F}^T$, components of finger tensor in uniaxial tension case become

$$[\mathbf{b}]_{ij} = \begin{bmatrix} \lambda^2 & & \\ & \frac{1}{\lambda} & \\ & & \frac{1}{\lambda} \end{bmatrix}. \quad (3.86)$$

Applying the boundary conditions, considering that surfaces with their normal in e_2 and e_3 directions are stress free surfaces, the components of Kirchhoff stress tensor for uniaxial tension loading becomes

$$[\boldsymbol{\tau}]_{ij} = \begin{bmatrix} \tau & & \\ & 0 & \\ & & 0 \end{bmatrix}. \quad (3.87)$$

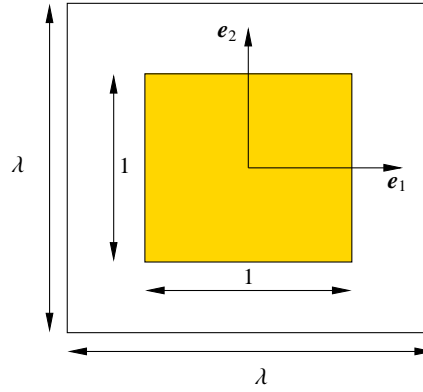


Figure 3.14: Equibiaxial tension deformation

Figure 3.13 represents a schematic for the uniaxial tension loading. For the deformation driven process (uniaxial tension), λ is known whereas τ is unknown.

3.2.3.2 Equibiaxial tension deformation mode

Equibiaxial extension loading is applied on a square sheet of rubber specimen. Equal stretches are applied to the specimen in first and second directions, e_1 and e_2 , simultaneously by the value of λ . The third direction e_3 is kept free to contract. From the incompressibility condition, $j = 1$, the stretch value in third direction would be equal to $1/\lambda^2$. Therefore, components of deformation gradient for equibiaxial extension mode can be written as:

$$[\mathbf{F}]_{ij} = \begin{bmatrix} \lambda & & \\ & \lambda & \\ & & \frac{1}{\lambda^2} \end{bmatrix}. \quad (3.88)$$

Again, using equation (3.9), $\mathbf{b} = \mathbf{F}\mathbf{F}^T$, components of finger tensor in equibiaxial tension case become

$$[\mathbf{b}]_{ij} = \begin{bmatrix} \lambda^2 & & \\ & \lambda^2 & \\ & & \frac{1}{\lambda^4} \end{bmatrix}. \quad (3.89)$$

Applying the boundary conditions, considering that surface with its normal in e_3 direction is stress free surfaces, the components of Kirchhoff stress tensor for equibiax-

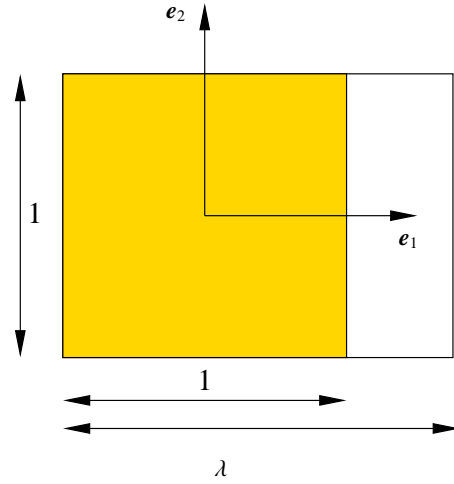


Figure 3.15: Pure shear deformation

ial tension loading becomes

$$[\tau]_{ij} = \begin{bmatrix} \tau & & \\ & \tau & \\ & & 0 \end{bmatrix}. \quad (3.90)$$

Figure 3.14 represents a schematic for the equibiaxial tension loading. For the deformation driven process (equibiaxial tension), λ is known whereas τ is unknown.

3.2.3.3 Pure shear deformation mode

During the pure shear deformation, stretch is applied in first direction, e_1 , while the specimen is constrained to deform in second direction e_2 . The specimen is kept free to deform or contract in third direction, e_3 . Used specimen is mostly wide strip of rubber. Therefore, applied stretches are λ , 1, and $1/\lambda$ in first, second, and third directions, respectively. Then, the components of deformation gradient for pure shear loading become

$$[F]_{ij} = \begin{bmatrix} \lambda & & \\ & 1 & \\ & & \frac{1}{\lambda} \end{bmatrix}. \quad (3.91)$$

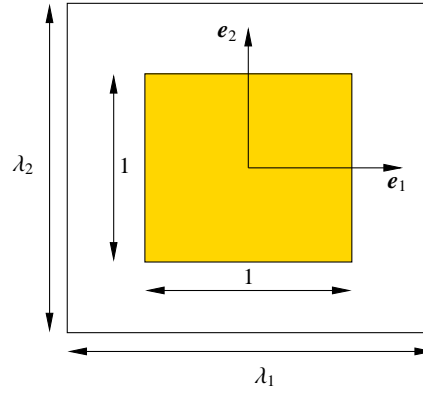


Figure 3.16: Biaxial tension deformation

Again, using equation (3.9), $\mathbf{b} = \mathbf{F}\mathbf{F}^T$, components of finger tensor in pure shear case become

$$[\mathbf{b}]_{ij} = \begin{bmatrix} \lambda^2 & & \\ & 1 & \\ & & \frac{1}{\lambda^2} \end{bmatrix}. \quad (3.92)$$

Applying the boundary conditions, considering that surface with its normal in \mathbf{e}_3 direction is stress free surfaces, the components of Kirchhoff stress tensor for pure shear loading become

$$[\boldsymbol{\tau}]_{ij} = \begin{bmatrix} \tau_1 & & \\ & \tau_2 & \\ & & 0 \end{bmatrix}. \quad (3.93)$$

Figure 3.15 represents a schematic for the pure shear loading. For the deformation driven process (pure shear), λ is known whereas τ_1 and τ_2 are unknowns.

3.2.3.4 Biaxial tension deformation mode

Biaxial loading is, in general, like equibiaxial loading case. However, deformation driven stretches are different in first and second directions. The specimen is deformed in first direction, \mathbf{e}_1 , by stretch value which is equal to λ_1 , while the stretch in second direction, \mathbf{e}_2 , is different from the first one and denoted by λ_2 . The material is kept free to contract in the third direction, \mathbf{e}_3 . Then the components of deformation gradient

tensor for biaxial extension loading become

$$[\mathbf{F}]_{ij} = \begin{bmatrix} \lambda_1 & & \\ & \lambda_2 & \\ & & \frac{1}{\lambda_1 \lambda_2} \end{bmatrix}. \quad (3.94)$$

$$[\mathbf{b}]_{ij} = \begin{bmatrix} \lambda_1^2 & & \\ & \lambda_2^2 & \\ & & \frac{1}{\lambda_1^2 \lambda_2^2} \end{bmatrix}. \quad (3.95)$$

Applying the boundary conditions, considering that surface with its normal in \mathbf{e}_3 direction is stress free surfaces, the components of Kirchhoff stress tensor for Biaxial tension loading becomes

$$[\boldsymbol{\tau}]_{ij} = \begin{bmatrix} \tau_1 & & \\ & \tau_2 & \\ & & 0 \end{bmatrix}. \quad (3.96)$$

Figure 3.16 represents a schematic for the biaxial tension loading. For the deformation driven process (biaxial extension), λ_1 , λ_2 , and λ_3 are known whereas τ_1 and τ_2 are unknowns.

3.2.4 Invariant based incompressible hyperelastic material models

The general form for stress expressions are given in Equations (3.65) and ((3.66)). On the other hand, for isotropic hyperelasticity, constitutive form depends on the first and second invariants, and due to incompressibility $J=1$. Dependency of free energy function to the first two invariants implies the following form for Kirchhoff,

$$\boldsymbol{\tau} = 2 \left(\frac{\partial \psi}{\partial I_1} + I_1 \frac{\partial \psi}{\partial I_2} \right) \mathbf{b} - 2 \frac{\partial \psi}{\partial I_2} \mathbf{b}^2 - p \mathbf{1} \quad (3.97)$$

and nominal stress,

$$\mathbf{P} = 2 \mathbf{F} \left(\left[\frac{\partial \psi}{\partial I_1} + I_1 \frac{\partial \psi}{\partial I_2} \right] \mathbf{1} - \frac{\partial \psi}{\partial I_2} \mathbf{C} \right) - p \mathbf{F}^{-T}. \quad (3.98)$$

In principle directions last two equations can be written in terms of principle stretches,

$$\tau_i = 2 \left(\lambda_i^2 \frac{\partial \psi}{\partial I_1} - \frac{1}{\lambda_i^2} \frac{\partial \psi}{\partial I_2} \right) - p \quad \text{where } i = 1, 2, 3 \quad (3.99)$$

and nominal stress,

$$P_i = 2 \left(\lambda_i \frac{\partial \psi}{\partial I_1} - \frac{1}{\lambda_i^3} \frac{\partial \psi}{\partial I_2} \right) - \frac{1}{\lambda_i} P \quad \text{where } i = 1, 2, 3. \quad (3.100)$$

Corresponding to the respective deformation modes, and using Equation (3.100); the first Piola-Kirchhoff stresses are expressed as follows:

- Uniaxial tension expressions

$$\begin{aligned} P_{22} &= P_{33} = 0, \\ P_{11} &= P = 2 \left(\lambda - \frac{1}{\lambda^2} \right) \left(\frac{\partial \psi}{\partial I_1} + \frac{\partial \psi}{\partial I_2} \frac{1}{\lambda} \right). \end{aligned} \quad (3.101)$$

- Equibiaxial tension expressions

$$\begin{aligned} P_{33} &= 0, \\ P_{11} &= P_{22} = P = 2 \left(\lambda - \frac{1}{\lambda^5} \right) \left(\frac{\partial \psi}{\partial I_1} + \frac{\partial \psi}{\partial I_2} \frac{1}{\lambda^2} \right). \end{aligned} \quad (3.102)$$

- Pure shear expressions

$$\begin{aligned} P_{33} &= 0, \\ P_{11} &= P_1 = 2 \left(\lambda - \frac{1}{\lambda^3} \right) \left(\frac{\partial \psi}{\partial I_1} + \frac{\partial \psi}{\partial I_2} \right), \\ P_{22} &= P_2 = 2 \left(1 - \frac{1}{\lambda^2} \right) \left(\frac{\partial \psi}{\partial I_1} + \lambda^2 \frac{\partial \psi}{\partial I_2} \right). \end{aligned} \quad (3.103)$$

- Biaxial tension expressions

$$\begin{aligned} P_{33} &= 0, \\ P_{11} &= P_1 = 2 \left(\lambda_1 - \frac{1}{\lambda_1^3 \lambda_2^2} \right) \left(\frac{\partial \psi}{\partial I_1} + \frac{\partial \psi}{\partial I_2} \lambda_2^2 \right), \\ P_{22} &= P_2 = 2 \left(\lambda_2 - \frac{1}{\lambda_1^2 \lambda_2^3} \right) \left(\frac{\partial \psi}{\partial I_1} + \frac{\partial \psi}{\partial I_2} \lambda_1^2 \right). \end{aligned} \quad (3.104)$$

3.2.5 Principle stretch based incompressible hyperelastic material models

Some hyperelastic models have functional representations exclusively in terms of principle stretches. Herein, the free energy function has the following form,

$$\psi = \hat{\psi}(\lambda_1, \lambda_2, \lambda_3) \quad (3.105)$$

For purely incompressible material behavior, the Kirchhoff stress tensor reads,

$$\boldsymbol{\tau} = \sum_{a=1}^3 \hat{\psi}_{,\lambda_a} \lambda_a \mathbf{n}_a \otimes \mathbf{n}_a - p \mathbf{1}. \quad (3.106)$$

The derivatives of $\hat{\psi}$ with respect to principle stretches can be defined as,

$$\alpha_1 := \hat{\psi}_{,\lambda_1} = \frac{\partial \hat{\psi}}{\partial \lambda_1}, \quad (3.107)$$

$$\alpha_2 := \hat{\psi}_{,\lambda_2} = \frac{\partial \hat{\psi}}{\partial \lambda_2}, \quad (3.108)$$

$$\alpha_3 := \hat{\psi}_{,\lambda_3} = \frac{\partial \hat{\psi}}{\partial \lambda_3}. \quad (3.109)$$

Corresponding to the respective deformation modes, and using Equation (3.106); the first Piola-Kirchhoff stresses are obtained as follows:

- Uniaxial tension expressions

$$\begin{aligned} P_{22} &= P_{33} = 0, \\ P_{11} &= P = \alpha_1 - \frac{\alpha_2}{\lambda^{\frac{3}{2}}}. \end{aligned} \quad (3.110)$$

- Equibiaxial tension expressions

$$\begin{aligned} P_{33} &= 0, \\ P_{11} &= P_{22} = P = \alpha_1 - \frac{\alpha_3}{\lambda^3}. \end{aligned} \quad (3.111)$$

- Pure shear expressions

$$\begin{aligned} P_{33} &= 0, \\ P_{11} &= P_1 = \alpha_1 - \frac{\alpha_3}{\lambda^2}, \\ P_{22} &= P_2 = \alpha_2 - \frac{\alpha_3}{\lambda}. \end{aligned} \quad (3.112)$$

- Biaxial tension expressions

$$\begin{aligned} P_{33} &= 0, \\ P_{11} &= P_1 = \alpha_1 - \frac{\alpha_3}{\lambda_1^2 \lambda_2}, \\ P_{22} &= P_2 = \alpha_1 - \frac{\alpha_3}{\lambda_1 \lambda_2^2}. \end{aligned} \quad (3.113)$$

CHAPTER 4

HYPERELASTIC MATERIAL MODELS

Generally phenomenological and micromechanically based material models are the two main categories considered during the modeling steps. In this section 40 hyperelastic material model belonging to each category with corresponding free energy functions will be presented. Description for each model is given according to the publication date. Giving some necessary information about each model, parameter optimization scheme and results for the models under consideration will be provided in next chapters.

4.1 Phenomenological Material Models

Phenomenological hyperelastic material models are also divided into different groups. Invariant based material models, principle stretch based models, and combination of invariants and principle stretch models are among the phenomenological formulation for rubber-like materials. Invariant based models can further be divided into first invariant based, I_1 , and combination of first and second invariant, I_2 , based models. To find first Piola-Kirchhoff stresses on invariant based models, it is necessary to take first derivative of strain energy functions with respect to I_1 , and I_2 , then substitute the obtained results in equations (3.101) for uniaxial extension, (3.102) for equibiaxial extension, (3.103) for pure shear, (3.104) for biaxial extension. For principle stretch based models on the other hand, the first Piola-Kirchhoff stresses are obtained by taking first derivative of strain energy functions with respect to λ_1 , λ_2 , and λ_3 , and substituting the obtained results into the equations (3.110) for uniaxial extension, (3.111) for equibiaxial extension, (3.112) for pure shear, (3.113) for biaxial extension.

For each model the mentioned derivatives are provided.

4.1.1 First Invariant Base Models

4.1.1.1 neo-Hooke model

Considering the assumptions postulated by Wall [5] that are incompressibility for the bulk response of the material, Kuhn's Gaussian distribution [63] for end-to-end distances of molecular chains, and identical chain lengths for all molecules, Treloar [2] proposed the following physically motivated free energy function,

$$\psi = \frac{1}{2}nkT(\lambda_1^2 + \lambda_2^2 + \lambda_3^2 - 3), \quad (4.1)$$

where n is the chain density per unit volume, k is the Boltzmann constant and T is the absolute temperature. Observe that, with $\mu = nkT$, the model can be written as

$$\psi = \frac{\mu}{2}(I_1 - 3). \quad (4.2)$$

Hence, the model has only one parameter that corresponds to the initial slope for the nonlinear response of rubber-like materials for all three loading cases. Therefore, it can be concluded that the assumed distribution function for the end-to-end distances of molecular chains is Gaussian type. First derivative of ψ with respect to the invariants are

$$\frac{\partial\psi}{\partial I_1} = \frac{\mu}{2}, \quad \text{and} \quad \frac{\partial\psi}{\partial I_2} = 0. \quad (4.3)$$

4.1.1.2 Yeoh model

By omitting the terms containing second invariants, Yeoh [34] proposed a first invariant based expansion of Mooney-Rivlin's [10] form up to three term,

$$\psi = C_{10}(I_1 - 3) + C_{20}(I_1 - 3)^2 + C_{30}(I_1 - 3)^3 \quad (4.4)$$

where C_{10} , C_{20} , and C_{30} are the model parameters. First derivative of ψ with respect to the invariants are

$$\frac{\partial\psi}{\partial I_1} = C_{10} + 2C_{20}(I_1 - 3) + 3C_{30}(I_1 - 3)^2, \quad \text{and} \quad \frac{\partial\psi}{\partial I_2} = 0. \quad (4.5)$$

4.1.1.3 Gent model

Following the works of Treloar [2], Gent [37] proposed,

$$\psi = -\frac{\mu}{2} J_m \ln \left(1 - \frac{I_1 - 3}{J_m} \right) \quad (4.6)$$

for energy function. Here, $I_1 - 3 := J_1$ originally was used for abbreviation, and J_m is the chain extensibility limit. It reduces to neo-Hooke for small strains. For $J_1 = J_m$, corresponding to the fully stretched state, stresses become infinite. First derivative of ψ with respect to the invariants are

$$\frac{\partial \psi}{\partial I_1} = \frac{\mu}{6} \left(\frac{J_m - 3}{J_m - I_1} \right), \quad \text{and} \quad \frac{\partial \psi}{\partial I_2} = 0. \quad (4.7)$$

4.1.1.4 Yeoh-Fleming model

Combining results of [Yeoh] and [Gent] models, [Yeoh-Fleming] proposed,

$$\psi = \frac{A}{B} (I_m - 3) (1 - e^{-BR}) - C_{10} (I_m - 3) \ln(1 - R) \quad (4.8)$$

with

$$R = \frac{(I_1 - 3)}{(I_m - 3)} \quad (4.9)$$

as the free energy function. The model's idea is to combine two different models for targeting both small strains and large strains. Since the finite extensibility of network chains is suspected to be the main mechanism at large strains, Yeoh-Fleming included chain extensibility limit with the second term analogous to Gent's model. The first term follows the reasoning behind the Yeoh model for small strains where the dominating effect is believed to be caused by network flaws, such as entanglements. First derivative of ψ with respect to the invariants are

$$\frac{\partial \psi}{\partial I_1} = A \exp(-BR) + C_{10} \left(\frac{I_m - 3}{I_m - I_1} \right), \quad \text{and} \quad \frac{\partial \psi}{\partial I_2} = 0. \quad (4.10)$$

4.1.1.5 Two-Term model

Ogden's form [27] where individual stretch values are raised to model parameters α_i as power, was investigated by Oscar Lopez-Pamies [54]. Instead, in two-term model,

raised the first invariant to the material parameters α_i , that is

$$\psi = \sum_{i=1}^M \frac{3^{1-\alpha_i}}{2\alpha_i} \mu_i (I_1^{\alpha_i} - 3^{\alpha_i}). \quad (4.11)$$

In this work we expanded the summation for $M = 2$, and utilized the following form for the strain energy function,

$$\psi = \frac{3^{1-\alpha_1}}{2\alpha_1} \mu_1 (I_1^{\alpha_1} - 3^{\alpha_1}) + \frac{3^{1-\alpha_2}}{2\alpha_2} \mu_2 (I_1^{\alpha_2} - 3^{\alpha_2}). \quad (4.12)$$

The main reasoning of Lopez-Pamis for the two-term model was to capture full range material response, mathematical convenience, and model to possess physically interpretable parameters. First derivative of ψ with respect to the invariants are

$$\frac{\partial \psi}{\partial I_1} = \frac{\mu_1}{2} (3^{1-\alpha_1}) (I_1^{\alpha_1-1}) + \frac{\mu_2}{2} (3^{1-\alpha_2}) (I_1^{\alpha_2-1}), \quad \text{and} \quad \frac{\partial \psi}{\partial I_2} = 0. \quad (4.13)$$

4.1.1.6 Exp-Ln model

The exponential and linear terms are individually contribute to the free energy function in exp-ln model [57] as follows,

$$\psi = A \left[\frac{1}{a} \exp(a (I_1 - 3)) + b (I_1 - 2) (1 - \ln (I_1 - 2)) - \frac{1}{a} - b \right] \quad (4.14)$$

where, $A = \frac{nkT}{2}$, and the parameter a governs the chain extensibility limit. The parameter b governs the response around small and moderate deformations. By polynomial expansion it can be written as,

$$\psi = A (I_1 - 3) + A \sum_{i=2}^M \frac{a^{i-1} + (-1)^{i-1} (i-2)! b}{i!} (I_1 - 3)^i \quad (4.15)$$

which is a special case of Mooney-Rivlin's expansion formula,

$$\psi = \sum_{i=0}^{M_1} \sum_{j=0}^{M_2} C_{ij} (I_1 - 3)^i (I_2 - 3)^j. \quad (4.16)$$

First derivative of ψ with respect to the invariants are

$$\frac{\partial \psi}{\partial I_1} = A [\exp(a (I_1 - 3)) - b \ln (I_1 - 2)], \quad \text{and} \quad \frac{\partial \psi}{\partial I_2} = 0. \quad (4.17)$$

4.1.2 First and Second Invariant Base Models

4.1.2.1 Mooney model

Mooney introduced a phenomenological strain energy density function based on the properties, such as the isotropy of the material, isochoric deformations, and (linear or nonlinear)-proportionality of traction to the shear for pure shear,

$$\psi = \frac{G}{4} \sum_{i=1}^3 \left(\lambda_i - \frac{1}{\lambda_i} \right)^2 + \frac{H}{4} \sum_{i=1}^3 \left(\lambda_i^2 - \frac{1}{\lambda_i^2} \right). \quad (4.18)$$

This model is the baseline for further phenomenological development, and significantly it introduced the second invariant in the free energy density function. A more familiar form for the Mooney's model [4] is as follows,

$$\psi = C_{10} (I_1 - 3) + C_{01} (I_2 - 3). \quad (4.19)$$

First derivative of ψ with respect to the invariants are

$$\frac{\partial \psi}{\partial I_1} = C_{10}, \quad \text{and} \quad \frac{\partial \psi}{\partial I_2} = C_{01}. \quad (4.20)$$

4.1.2.2 Isihara model

Isihara [21] recognized the non-Gaussian character of the network structure which is missing in neo-Hookean approach, and proposed the following semi-empirical free energy density function as,

$$\psi = C_{10} (I_1 - 3) + C_{20} (I_1 - 3)^2 + C_{01} (I_2 - 3). \quad (4.21)$$

From the form of the proposed constitutive relation it can be depicted that the Isihara's model is an special form of Mooney-Rivlin's generalized formula. Therefore, first derivative of ψ with respect to the invariants are

$$\frac{\partial \psi}{\partial I_1} = C_{10} + 2C_{20} (I_1 - 3), \quad \text{and} \quad \frac{\partial \psi}{\partial I_2} = C_{01}. \quad (4.22)$$

4.1.2.3 Biderman model

Biderman [22] considered higher order terms for I_1 and one term for I_2 , and proposed the following form,

$$\psi = C_{10} (I_1 - 3) + C_{01} (I_2 - 3) + C_{20} (I_1 - 3)^2 + C_{30} (I_1 - 3)^3. \quad (4.23)$$

which is a special case of [Rivlin-Saunders]'s expansion formula,

$$\psi = \sum_{i=0}^{M_1} \sum_{j=0}^{M_2} C_{ij} (I_1 - 3)^i (I_2 - 3)^j. \quad (4.24)$$

Following the regular procedure, first derivative of ψ with respect to the invariants are

$$\frac{\partial \psi}{\partial I_1} = C_{10} + 2C_{20} (I_1 - 3) + 3C_{30} (I_1 - 3)^2, \quad \text{and} \quad \frac{\partial \psi}{\partial I_2} = C_{01}. \quad (4.25)$$

4.1.2.4 Gent-Thomas model

Investigating the forms of neo-Hooke and Mooney's free energy density functions, Gent and Thomas [23] proposed a strain energy function of the form,

$$\psi = C_1 (I_1 - 3) + C_2 \ln\left(\frac{I_2}{3}\right). \quad (4.26)$$

Modified network theory is also used to depict the dependence of $\frac{\partial \psi}{\partial I_2}$ on I_2 . Then, the first derivative of ψ with respect to the invariants are

$$\frac{\partial \psi}{\partial I_1} = C_1, \quad \text{and} \quad \frac{\partial \psi}{\partial I_2} = \frac{C_2}{I_2}. \quad (4.27)$$

4.1.2.5 Hart-Smith model

Aiming for the full deformation range, Hart-Smith [24] utilized derivatives of free energy function for direct formulation, i.e.,

$$\frac{\partial \psi}{\partial I_1} = G \exp(k_1 (I_1 - 3)^2) \quad \text{and} \quad \frac{\partial \psi}{\partial I_2} = G \frac{k_2}{I_2}. \quad (4.28)$$

In its free energy density representation,

$$\psi = G \left\{ \int e^{k_1 (I_1 - 3)^2} dI_1 + k_2 \ln\left(\frac{I_2}{3}\right) \right\} \quad (4.29)$$

where, the partial derivative with respect to I_1 is considered as an exponential relation and the derivative does not contain any I_2 term. Similarly, the partial derivative with respect to I_2 does not contain any I_1 term. Thus, the derivatives are decoupled and I_1 and I_2 effects can be observed separately. Second term is equivalent to the logarithm term in Gent-Thomas model [23] (by integration). One may notice that exponential term makes the stress-strain behavior to tend upward, however the partial derivative with respect to I_2 forces the curve downward. Using the above equations as summations in equations (3.101), (3.102), and (3.103) helps to generate the S-shape curve representing hyperelastic behavior of rubber.

4.1.2.6 Alexander model

Combining the models by Rivlin-Saunders [10] and Hart-Smith [24], Alexander [26] proposed,

$$\psi = C_1 \int \exp(k[I_1 - 3]^2) dI_1 + C_2 \ln \left[\frac{(I_2 - 3) + \gamma}{\gamma} \right] + C_3 (I_2 - 3) \quad (4.30)$$

for the strain energy density function. It reduces to,

- Rivlin-Saunders theory for $k = 0$,
- Hart-Smith theory for $\gamma = 3$ and $C_3 = 0$,

The most successful model so far for Alexander was Rivlin-Saunders, and he argued that it is too restrictive to consider the summation of powers of invariants. Recognizing the need for a more elaborate theory, he understood that the Hart-Smith theory captures the observed behavior where for $I_1 \leq 12$, it may be considered a constant but above that value it should be function of I_1 . For moderate stresses, Hart-Smith theory fails for synthetic rubber neoprene. In order to compensate for the moderate stresses Alexander introduced also the Rivlin-Saunders additive term. Thus, the combination of Rivlin-Saunders and Hart-Smith provide a good agreement with the experimental results. Furthermore, first derivative of the free energy function with respect to the invariants can be obviously obtained as

$$\frac{\partial \psi}{\partial I_1} = C_1 \exp(k[I_1 - 3]^2), \quad \text{and} \quad \frac{\partial \psi}{\partial I_2} = \frac{C_2}{(I_2 - 3) + \gamma} + C_3. \quad (4.31)$$

4.1.2.7 James model

Investigating the the general Mooney-Rivlin expression and linking the experimental results conducted on natural rubber gum, James and coworkers [28] suggested the following form for strain energy density function

$$\begin{aligned}\psi = & C_{10} (I_1 - 3) + C_{01} (I_2 - 3) + C_{11} (I_1 - 3)(I_2 - 3) \\ & + C_{20} (I_1 - 3)^2 + C_{30} (I_1 - 3)^3 .\end{aligned}\quad (4.32)$$

The constitutive relation may be considered as third order expansion of Mooney's form. Regression analysis has been conducted by the writers on Mooney's plot and the best choice for free energy function is selected. To obtain the first Piola-Kirchhoff stresses, first derivative of the free energy function with respect to the invariants are as follows

$$\begin{aligned}\frac{\partial \psi}{\partial I_1} &= C_{10} + C_{11} (I_2 - 3) + 2C_{20} (I_1 - 3) + 3C_{30} (I_1 - 3)^2 , \\ \frac{\partial \psi}{\partial I_2} &= C_{01} + C_{11} (I_1 - 3) .\end{aligned}\quad (4.33)$$

4.1.2.8 Haines-Wilson model

Mooney-Rivlin generalized form and the investigations done by James and coworkers [28] are considered by Haines and Wilson [29]. The power series term is expanded up to six terms resulting the following equation for strain energy function

$$\begin{aligned}\psi = & C_{10} (I_1 - 3) + C_{01} (I_2 - 3) + C_{11} (I_1 - 3)(I_2 - 3) \\ & + C_{02} (I_2 - 3)^2 + C_{20} (I_1 - 3)^2 + C_{30} (I_1 - 3)^3 .\end{aligned}\quad (4.34)$$

Then, the first derivative of the free energy function with respect to the invariants can be obtained as

$$\begin{aligned}\frac{\partial \psi}{\partial I_1} &= C_{10} + C_{11} (I_2 - 3) + 2C_{20} (I_1 - 3) + 3C_{30} (I_1 - 3)^2 , \\ \frac{\partial \psi}{\partial I_2} &= C_{01} + C_{11} (I_1 - 3) + 2C_{02} (I_2 - 3) .\end{aligned}\quad (4.35)$$

4.1.2.9 Swanson model

Swanson [32] suggested an I_1 and I_2 decomposed series expansion for free energy function. The idea of decomposition is taken from Ogden's work [27] to derive the

strain energy function of the form,

$$\psi = \frac{3}{2} \sum_{i=1}^n \frac{A_i}{1 + \alpha_i} \left[\frac{I_1}{3} \right]^{1+\alpha_i} + \frac{3}{2} \sum_{j=1}^n \frac{B_j}{1 + \beta_j} \left[\frac{I_2}{3} \right]^{1+\beta_j} \quad (4.36)$$

In our case, we just take the first order expansion of the series to make parameter identification study. Then, the reduced form of the Swanson's model in this study is

$$\psi = \frac{3}{2} \frac{A_1}{(1 + \alpha_1)} \left[\frac{I_1}{3} \right]^{1+\alpha_1} + \frac{3}{2} \frac{B_1}{(1 + \beta_1)} \left[\frac{I_2}{3} \right]^{1+\beta_1} . \quad (4.37)$$

The first derivative of the free energy function with respect to the invariants are

$$\frac{\partial \psi}{\partial I_1} = \frac{3}{2} A_1 \left(\frac{I_1}{3} \right)^{\alpha_1} , \quad \text{and} \quad \frac{\partial \psi}{\partial I_2} = \frac{3}{2} B_1 \left(\frac{I_2}{3} \right)^{\beta_1} . \quad (4.38)$$

4.1.2.10 Kilian (van der Waals) model

Inspired from the idea of Wang and Guth [6], Kilian and coworkers [33] developed a unique representation to approximate the C_{ij} constants of Mooney-Rivlin expression [10] considering van der Waals theory and relate the idea to finite chain extensibility and fluctuations of cross-links. Functionality of cross-link degree is investigated considering a parameter "a" named as van der Waals interaction parameter. The general form of the proposed model is given in equation (4.39)

$$\psi = G \left\{ -(\lambda_m^2 - 3) [\ln(1 - \theta) + \theta] - \frac{2}{3} a \left(\frac{\tilde{I} - 3}{2} \right)^{3/2} \right\} \quad (4.39)$$

with

$$\theta = \sqrt{\frac{(\tilde{I} - 3)}{(\lambda_m^2 - 3)}} , \quad (4.40)$$

and

$$\tilde{I} = \beta I_1 + (1 - \beta) I_2 . \quad (4.41)$$

Here parameter "a" stands for van der Waals interaction. As the cross-link density increased, "a" tends to decrease. λ_m governs the limiting chain extensibility, G is modulus term, like $\frac{1}{2}nkT$ in neo-Hooke model, is used to describe swelling force. β is an empirical penalty term for weighting effects of I_1 and I_2 . Because of the complex and long formulation of the derivations, we skip that parts.

4.1.2.11 Yamashita-Kawabata model

The idea used by Yamashita and Kawabata [35] is raised from the theoretical work of Rivlin and Saunders [35]. However, the term containing C_3 has a polynomial form with power of $N + 1$.

$$\psi = C_5 (I_1 - 3) + C_2 (I_2 - 3) + \frac{C_3}{N + 1} (I_1 - 3)^{N+1} \quad (4.42)$$

The first derivative of the free energy function with respect to the invariants can easily be obtained as

$$\frac{\partial \psi}{\partial I_1} = C_5 + C_3 (I_1 - 3)^N, \quad \text{and} \quad \frac{\partial \psi}{\partial I_2} = C_2. \quad (4.43)$$

4.1.2.12 Lion model

Lion [41] aimed to develop a constitutive relation that may resemble the thermal aspects of rubber-like material models. The work consists of two part, the first part deals with the mechanical properties of material, yet the second part governs the thermal part. As the structure of the mechanical part implies, the proposed model is somehow similar to Mooney-Rivlin form. The constitutive relation has order of five for I_1 , but first order of expansion is considered for second invariant term. Then the material model is constructed as

$$\psi = C_{10} (I_1 - 3) + C_{01} (I_2 - 3) + C_{03} (I_1 - 3)^5. \quad (4.44)$$

Here, the first derivative of free energy function with respect to invariants I_1 and I_2 reads

$$\frac{\partial \psi}{\partial I_1} = C_{10} + 5C_{03} (I_1 - 3)^4, \quad \text{and} \quad \frac{\partial \psi}{\partial I_2} = C_{01}. \quad (4.45)$$

4.1.2.13 Diani-Rey model

Using the Rivlin and Saunders theory [10] together with experimental data on rubber-like materials, Diani and Rey [43] tried to estimate the functions

$$\frac{\partial \psi}{\partial I_1} = f(I_1), \quad \text{and} \quad \frac{\partial \psi}{\partial I_2} = g(I_2). \quad (4.46)$$

The free energy function was considered to have additive decomposition of I_1 and I_2 term separately. To estimate $f(I_1)$ uniaxial data of Treloar [44] is used considering $g(I_2) = 0$. The following assumption leads to an exponential polynomial power series function form for I_1 function. To derive the second invariant term, equibiaxial data set of Treloar [44] is considered by the writers. Then, the second invariant term is approximated by a exponential logarithmic function in power series expansion. The general form of the free energy function proposed by Diani and Rey is

$$\psi = \int \exp\left(\sum_{i=0}^n a_i (I_1 - 3)^i\right) dI_1 + \int \exp\left(\sum_{i=0}^m b_i (\ln(I_2))^i\right) dI_2. \quad (4.47)$$

In our study, we expand equation (4.47) considering $n = 2$ and $m = 1$. Then, the constitutive relation takes the form

$$\begin{aligned} \psi = & \int \exp\left(a_0 + a_1 (I_1 - 3) + a_2 (I_1 - 3)^2\right) dI_1 \\ & + \int \exp(b_0 + b_1 \ln(I_2)) dI_2. \end{aligned} \quad (4.48)$$

From the above equation one may notice that $f(I_1)$ and $g(I_2)$ corresponds to first derivative of strain energy function with respect to I_1 and I_2 , respectively as follow

$$\begin{aligned} \frac{\partial \psi}{\partial I_1} &= \exp\left(a_0 + a_1 (I_1 - 3) + a_2 (I_1 - 3)^2\right), \\ \frac{\partial \psi}{\partial I_2} &= \exp(b_0 + b_1 \ln(I_2)). \end{aligned} \quad (4.49)$$

4.1.2.14 Haupt-Sedlan model

Conducting experiments on cylindrical bar of rubber specimen, Haupt and Sedlan [47] aimed to develop a model governing viscoplastic and viscoelastic properties of rubber-like material. The proposed constitutive relation is in the form of Mooney-Rivlin as follow

$$\begin{aligned} \psi = & C_{10} (I_1 - 3) + C_{01} (I_2 - 3) + C_{11} (I_1 - 3)(I_2 - 3) \\ & + C_{02} (I_2 - 3)^2 + C_{30} (I_1 - 3)^3. \end{aligned} \quad (4.50)$$

To obtain the first Piola-Kirchhoff stresses, first derivative of the free energy function with respect to the invariants are

$$\begin{aligned} \frac{\partial \psi}{\partial I_1} &= C_{10} + C_{11} (I_2 - 3) + 3C_{30} (I_1 - 3)^2, \\ \frac{\partial \psi}{\partial I_2} &= C_{01} + C_{11} (I_1 - 3) + 2C_{02} (I_2 - 3). \end{aligned} \quad (4.51)$$

4.1.2.15 Chavelier-Marco model

The same procedure as Diani and Rey [43] is followed by Chevalier and Marco [48]. The I_1 term of free energy function is like the one proposed by Diani and Rey but exponential terms are neglected. I_1 term is derived considering uniaxial tension data of Treloar [44]. To estimate the I_2 term, however, pure shear data of Treloar is taken into account. The strain energy function is then suggested as

$$\psi = \int \left(\sum_{i=0}^n a_i (I_1 - 3)^i \right) dI_1 + \int \left(\sum_{i=0}^n \frac{b_i}{I_2^i} \right) dI_2. \quad (4.52)$$

Then, the first derivative of strain energy function with respect to invariants can obviously be written as

$$\frac{\partial \psi}{\partial I_1} = \sum_{i=0}^n a_i (I_1 - 3)^i, \quad \text{and} \quad \frac{\partial \psi}{\partial I_2} = \sum_{i=0}^n \frac{b_i}{I_2^i}. \quad (4.53)$$

In our formulations, n is considered to take the value of 2.

4.1.2.16 Pucci-Saccomandi model

In order to improve the fitting performance of Gent Model [37], Pucci and Saccomandi [49] applied modifications on the mentioned model. First invariant based part is taken from Gent model, second part on the other hand is taken from Gent-Thomas model [23].

$$\psi = -\frac{\mu}{2} J_m \log \left(1 - \frac{I_1 - 3}{J_m} \right) + C_2 \log \left(\frac{I_2}{3} \right) \quad (4.54)$$

The desired results are obtained through this modification. First derivative of the proposed strain energy function with respect to invariants are

$$\frac{\partial \psi}{\partial I_1} = -\frac{\mu}{2} \left(\frac{I_1 - 3}{J_m} \right), \quad \text{and} \quad \frac{\partial \psi}{\partial I_2} = \frac{C_2}{I_2}. \quad (4.55)$$

4.1.2.17 Amin model

The model proposed by Amin and coworkers [52] was aimed to simulate the behavior of rubber-like materials serving as vibration absorber. Therefore, they have try to derive a constitutive relation that suits the uniaxial compression and pure shear loading.

The suggested strain energy function has the following form

$$\psi = C_5 (I_1 - 3) + \frac{C_3}{N+1} (I_1 - 3)^{N+1} + \frac{C_4}{M+1} (I_1 - 3)^{M+1} + C_2 (I_2 - 3) . \quad (4.56)$$

Amin's model may be considered as modification for Yamashita and Kawabata's model [35]. Adding a higher order I_1 term, makes the model to possess improvement in its performance. The first derivative of free energy function with respect to I_1 and I_2 is then obtained as

$$\frac{\partial \psi}{\partial I_1} = C_5 + C_3 (I_1 - 3)^N + C_4 (I_1 - 3)^M , \quad \text{and} \quad \frac{\partial \psi}{\partial I_2} = C_2 . \quad (4.57)$$

4.1.2.18 Bada model

To improve fitting performance of Gent-Thomas model [23], a modified constitutive relation is introduced by Bada [16]. Addition of a term consisting first invariant increased fitting ability of Gent-Thomas model. The proposed model is fitted to the experimental data of Treloar [44], Rivlin and Saunders [10], Yeoh-Fleming [42], and Pak and Flory [64]. The parameter identification is applied on uniaxial data curve and fitting performance of the model is observed on the other deformation modes.

$$\psi = C_{10} (I_1 - 3) + \frac{B}{\alpha} (I_1 - 3)^\alpha + K \ln \frac{I_2}{3} \quad (4.58)$$

The first derivative of Bada's equation (4.58) with respect to invariants are as follow

$$\frac{\partial \psi}{\partial I_1} = C_{10} + B (I_1 - 3)^{\alpha-1} , \quad \text{and} \quad \frac{\partial \psi}{\partial I_2} = \frac{K}{3I_2} . \quad (4.59)$$

4.1.2.19 Carroll model

A unique procedure is followed by Carroll [55] to develop a phenomenological strain energy function of invariant based type. He considered three distinct free energy terms and additive decomposition of the related terms yield the Carroll model. The first part of the constitutive relation governs the Gaussian response of the material. The second term is fitted to uniaxial data of Treloar [44] to represent the residual stress terms that make smooth transition from low to high strain range. The third part (I_2 related part) on the other hand forces the material response to exhibit up-turn and make a S-shape curve. The third part resembles the residual stress part related to the

equibiaxial data of Treloar. As a result of the assumptions done by Carroll the final form of the constitutive relation reads

$$\psi = AI_1 + BI_1^4 + C\sqrt{I_2}. \quad (4.60)$$

The first derivative of Carroll model with respect to invariants are

$$\frac{\partial\psi}{\partial I_1} = A + 4BI_1^3, \quad \text{and} \quad \frac{\partial\psi}{\partial I_2} = \frac{C}{2\sqrt{I_2}}. \quad (4.61)$$

4.1.2.20 Nunes model

To get an equation suitable for pure shear loading, Nunes [56] suggested a model which can be considered as a modified Mooney [4] model. The fitting performance of the obtained model is verified against the sample specimen of PDMS material in pure shear loading set-up. Digital image correlation (DCI) technique is used to gather data for the related loading. The general form of Nunes model is

$$\psi = C_1(I_1 - 3) + \frac{4}{3}C_2(I_2 - 3)^{3/4}. \quad (4.62)$$

One can simply derive the first derivative of the free energy function with respect to I_1 and I_2 as

$$\frac{\partial\psi}{\partial I_1} = C_1, \quad \text{and} \quad \frac{\partial\psi}{\partial I_2} = C_2(I_2 - 3)^{-1/4}. \quad (4.63)$$

4.1.3 Principle Stretch Base Models

4.1.3.1 Valanis-Landel model

Considering of complexity of deriving strain energy in terms of invariants, Valanis and Landel [25] postulated that strain energy function of isotropic and incompressible rubber-like materials can be analytically separable function of stretch ratios rather than invariants. Additive split which is considered by Valanis and Landel have the form given in equation (4.64). Apart from being a model it is assumed to be a hypothesis introduced by Valanis and Landel.

$$\psi(\lambda_1, \lambda_2, \lambda_3) = w(\lambda_1) + w(\lambda_2) + w(\lambda_3) \quad (4.64)$$

To obtain the first Piola-Kirchhoff stress tensor it is necessary to take partial derivative of function with respect to stretch ratios. The following derivatives are proposed by Valanis and Landel to estimate the rubber-like material behavior.

$$\frac{d\psi}{d\lambda_i} = 2\mu \ln(\lambda_i) \quad \text{with } i = 1, 2, 3 \quad (4.65)$$

4.1.3.2 Ogden model

Ogden following the works by Hill, argued the complexity and weaknesses of invariants based models. The basic aim of developing Ogden's model was to estimate the mechanical response of rubber-like materials in moderate to high strain regions. The free energy function obeys the Valanis-Landel hypothesis and defined as linear combination of principle stretches. Ogden [27] proposed the following free energy function which cannot be expressed in terms of I_1 or I_2 in a closed form,

$$\psi = \sum_{n=1}^N \frac{\mu_n}{\alpha_n} (\lambda_1^{\alpha_n} + \lambda_2^{\alpha_n} + \lambda_3^{\alpha_n} - 3) . \quad (4.66)$$

First derivative of the free energy function with respect to principle stretch ratios, which is a necessary factor for obtaining first Piola-Kirchhoff stresses, takes the form

$$\frac{\partial\psi}{\partial\lambda_i} = \sum_{n=1}^N \mu_n \lambda_i^{\alpha_n-1} \quad \text{with } i = 1, 2, 3 \quad (4.67)$$

In general, as in our work, the upper limit for summation is taken as 3, ($N = 3$).

4.1.3.3 Slip-Link model

Following the work by Deam and Edwards [65], Ball et. al [30] proposed a model on elasticity of entanglements of a network. They focused their on the sliding distance between the entanglements during application of pure shear loading. They used affine approach for cross-link points and used Gaussian method to approximate the sliding freedom of chains between entanglement and cross-links. To sum up, the following strain energy function is proposed for slip-link model

$$\psi = \frac{\mu_1}{2} \sum_{i=1}^3 \lambda_i^2 + \frac{\mu_2}{2} \sum_{i=1}^3 \left[\frac{(1 + \eta) \lambda_i^2}{1 + \eta \lambda_i^2} + \ln(1 + \eta \lambda_i^2) \right] \quad \text{with } i = 1, 2, 3 . \quad (4.68)$$

The first term in equation (4.68) represents the Gaussian part and the second term stands for slipping freedom of the chains. Here, η is a measure used to approximate the freedom of sliding between a rubber link and chain movement. The first derivative of free energy function with respect to λ_i becomes

$$\frac{\partial \psi}{\partial \lambda_i} = \mu_1 \sum_{i=1}^3 \lambda_i + \mu_2 \sum_{i=1}^3 \left[\frac{(1 + \eta) \lambda_i}{(1 + \eta \lambda_i^2)^2} + \frac{\eta \lambda_i}{1 + \eta \lambda_i^2} \right] \quad \text{with } i = 1, 2, 3. \quad (4.69)$$

4.1.3.4 Constrained-Junction model

Flory and Erman in their works [66] and [31] proposed that the constitutive relations in rubber elasticity are composed of two parts, namely phantom and constrained parts.

$$\psi = \psi_{ph} + \psi_c \quad (4.70)$$

The phantom part of is related to the molecular network of the rubber and the force are assumed to be exerted directly at the junction points of the chains. They simply choose Gaussian approximation of neo-Hooke model [2] for the phantom part of the constitutive relation. The second part governs the constraints due to neighboring chains. Fluctuations of phantom part of Gaussian network is assumed to be restricted by the other chains in the network. Combination of the phantom and constrained part of the theory yields the constrained junction model of the form

$$\psi = \mu_1 (I_1 - 3) + \mu_2 \sum_{i=1}^3 [B_i + D_i - \ln(B_i + 1) - \ln(D_i + 1)], \quad (4.71)$$

where

$$B_i = \kappa^2 (\lambda_i^2 + \kappa)^{-2}, \quad (4.72)$$

and

$$D_i = \lambda_i^2 \kappa^{-1} B_i \quad (4.73)$$

The constitutive relation proposed above was aimed to catch the material response in low and moderate strain regions. Now, one can derive the related derivatives of the free energy function as

$$\frac{\partial \psi}{\partial \lambda_i} = 2\mu_1 \lambda_i + \mu_2 \left\{ \frac{\partial B_i}{\partial \lambda_i} + \frac{\partial D_i}{\partial \lambda_i} - \frac{1}{(B_i + 1)} \frac{\partial B_i}{\partial \lambda_i} - \frac{1}{(D_i + 1)} \frac{\partial D_i}{\partial \lambda_i} \right\}, \quad (4.74)$$

where

$$\frac{\partial B_i}{\partial \lambda_i} = \frac{2\kappa^2 \lambda_i}{(\lambda_i^2 + \kappa)^2} \left\{ 1 - \frac{2(\lambda_i^2 - 1)}{\lambda_i^2 + \kappa} \right\} \quad (4.75)$$

and

$$\frac{\partial B_i}{\partial \lambda_i} = 2\lambda_i \kappa^{-1} B_i + \lambda_i^2 \kappa^{-1} \frac{\partial B_i}{\partial \lambda_i} . \quad (4.76)$$

4.1.3.5 Shariff model

The proposed model by Shariff [46] is a separable function of principle stretches that obeys the Valanis-Landel hypothesis. Free energy function is derived with purely mathematical consideration. The simplest form of the strain energy function consists of two material constants, however, in literature extension to model five parameter is widely used. The compact form of Shariff model is as follow

$$\psi = E \sum_{i=0}^3 \alpha_i \phi_i , \quad (4.77)$$

with the explicit form of ϕ_i as

$$\begin{aligned} \phi_0 &= \frac{2\ln(\lambda)}{3} & \phi_1 &= \exp(1 - \lambda) + \lambda - 2, \\ \phi_2 &= \exp(\lambda - 1) - \lambda & \phi_3 &= \frac{(\lambda - 1)^3}{\lambda^{3.6}}, \\ \phi_j &= (\lambda - 1)^{j-1} & \text{for } j &= 4, 5, \dots, n . \end{aligned} \quad (4.78)$$

Fist derivative of free energy function with respect to principle stretches then become

$$\frac{\partial \psi}{\partial \lambda} = E \sum_{i=0}^3 \alpha_i \frac{\partial \phi_i}{\partial \lambda} \quad (4.79)$$

with

$$\begin{aligned} \frac{\partial \phi_0}{\partial \lambda} &= \frac{2}{3\lambda} & \frac{\partial \phi_1}{\partial \lambda} &= 1 - \exp(1 - \lambda), \\ \frac{\partial \phi_2}{\partial \lambda} &= \exp(\lambda - 1) - 1 & \frac{\partial \phi_3}{\partial \lambda} &= \frac{3(\lambda - 1)^2}{\lambda^{3.6}} - \frac{3.6(\lambda - 1)^3}{\lambda^{4.6}}, \\ \frac{\partial \phi_j}{\partial \lambda} &= (j - 1)(\lambda - 1)^{j-2} & \text{for } j &= 4, 5, \dots, n . \end{aligned} \quad (4.80)$$

4.1.3.6 Attard-Hunt model

Attard and Hunt [51] used the idea given by Rivlin and Saunders [10] together with neo-Hooke model [2] and proposed a principle stretch based model. With some modifications on Mooney-Rivlin model, a principle stretch based version of the model is formulated by the writers. As it is obvious, the Valanis-Landel hypothesis is obeyed to derive the following strain energy function

$$\psi = \sum_{n=1}^m \left[\frac{A_n}{2n} (\lambda_1^{2n} + \lambda_2^{2n} + \lambda_3^{2n} - 3) + \frac{B_n}{2n} (\lambda_1^{-2n} + \lambda_2^{-2n} + \lambda_3^{-2n} - 3) \right]. \quad (4.81)$$

Now, we can write the first derivative of strain energy function with respect to principle stretches as

$$\frac{\partial \psi}{\partial \lambda_i} = \sum_{n=1}^m \left[A_n (\lambda_i^{2n-1}) - B_n (\lambda_i^{-2n-1}) \right] \quad \text{with } i = 1, 2, 3. \quad (4.82)$$

Note also that, in our work three term expansion of the constitutive relation (4.81), which yields 6 material parameters, is used.

4.1.3.7 Bechir model

The starting point for formulation of strain energy function by Bechir [53] was the neo-Hookean strain energy terms. It was tried to generalize the neo-Hookean free energy function to well-suit the hyperelastic material response of rubber-like materials. In order to make parameter identification studies with the minimum number of experimental tests, separable form of Valanis-Landel is considered. The free energy function of Bechir's model is given as

$$\psi = C_1^1 (\lambda_1^2 + \lambda_2^2 + \lambda_3^2 - 3) + \sum_{n=2}^{\infty} \sum_{r=2}^{\infty} C_n^r (\lambda_1^{2n} + \lambda_2^{2n} + \lambda_3^{2n} - 3)^r. \quad (4.83)$$

To be consistent in the number of material parameters with other models, four term (4 material parameter) of expansion of Bechir model is taken into the account. Another interesting fact regarding the Bechir model is the similarity of the proposed model to that of Attard and Hunt [51], the only difference is the power term r in Bechir's model.

First derivative of the strain energy function with respect to λ_1 , λ_2 , and λ_3 are

$$\begin{aligned}\frac{\partial \psi}{\partial \lambda_1} &= 2C_1^1 \lambda_1 + \sum_{n=2}^{\infty} \sum_{r=2}^{\infty} 2n r C_n^r \lambda_1^{2n-1} (\lambda_1^{2n} + \lambda_2^{2n} + \lambda_3^{2n} - 3)^{r-1}, \\ \frac{\partial \psi}{\partial \lambda_2} &= 2C_1^1 \lambda_2 + \sum_{n=2}^{\infty} \sum_{r=2}^{\infty} 2n r C_n^r \lambda_2^{2n-1} (\lambda_1^{2n} + \lambda_2^{2n} + \lambda_3^{2n} - 3)^{r-1}, \\ \frac{\partial \psi}{\partial \lambda_3} &= 2C_1^1 \lambda_3 + \sum_{n=2}^{\infty} \sum_{r=2}^{\infty} 2n r C_n^r \lambda_3^{2n-1} (\lambda_1^{2n} + \lambda_2^{2n} + \lambda_3^{2n} - 3)^{r-1}.\end{aligned}\quad (4.84)$$

4.1.4 Mixed Invariant and Principle Stretch Based Models

4.1.4.1 WFB model

Weight function based (WFB) model is one of the interesting material models introduced by Korba and Barkey [59]. The aim was to make a unique approach to fit the model to uniaxial data. For this reason a weight function is added as a multiplicative factor to the first invariant part of the free energy function. Free energy function for the WFB model is given as

$$\psi = \int_1^{L_f} \left\{ F(\lambda) A(\lambda e^{-BI_1}) + C(\lambda I_1^{-D}) \right\} \left(\lambda - \frac{1}{\lambda} \right) d\lambda, \quad (4.85)$$

where

$$F(\lambda) = FP1 (\lambda^2 + FP2)^{-FP3}. \quad (4.86)$$

Here $F(\lambda)$ is the weight factor which is added to the strain energy function. In order to get the constants of equation (4.86) fitting to the test data is done and related variation of the weighting function is observed. The best suiting parameters causing minimum error is selected as

$$F(\lambda) = 2.378e8 (\lambda^2 + 15.5128)^{-7.0574}. \quad (4.87)$$

To find the first derivative of free energy function with respect to principle stretches simply integral term vanishes and one can obtain the following

$$\frac{\partial \psi}{\partial \lambda} = F(\lambda) A(\lambda e^{-BI_1}) + C(\lambda I_1^{-D}) \left(\lambda - \frac{1}{\lambda} \right) \quad (4.88)$$

4.2 Micro-mechanics based material models

Micro-mechanical models utilize the statistical mechanics techniques to explain mechanical behavior of rubber and rubber-like materials in macroscopic and microscopic scales. The rubber, inherently, consists of long polymer chains which further consist of rigid segments referred to as Kuhn segments. These segments are bonded at the end-points to each other chemically, where they have rotation with respect to each other. The chains form interconnections (via cross-linking or entanglement) that separates rubber from fluid, i.e., segments are constrained at certain points that poses a restriction of motion (rotations, see [36]) of chain that manifested as shear.

A representative chain can be seen in Figure 4.1. Where, it consists of N segments of equal length l . Thus, ideally, fully extended chain length becomes Nl . However, since it is a representative chain, one must consider average values instead of absolute quantities. Therefore, based on random walk theory [36], an undeformed chain average end-to-end distance can be considered as the root mean square value of r , that is $r_0 = \sqrt{N}l$. Two important dimensionless kinematic variables for definition of deformation of a chain are *stretch* λ and *relative stretch* λ_r , and they are constructed based on the end-to-end distance r as follows,

$$\lambda = \frac{r}{r_0}, \quad \lambda_r = \frac{\lambda}{\sqrt{N}} \quad (4.89)$$

It is obvious from the Figure 4.1 that $r_{max} = Nl$. Thus, one can obtain the range of stretch and relative stretch from equation (4.89) as $\lambda \in [0, \sqrt{N})$ and $\lambda_r \in [0, 1)$, respectively for $r \rightarrow r_{max}$.

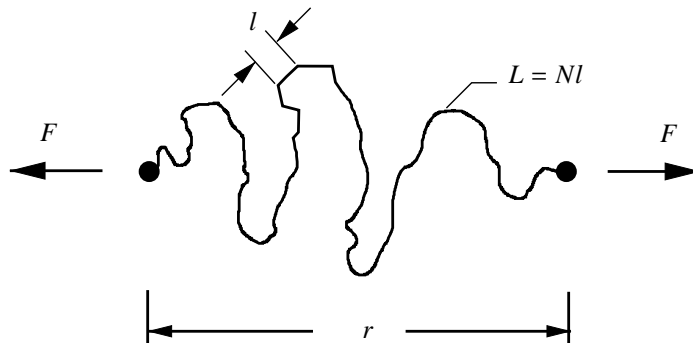


Figure 4.1: Micro-state of an undeformed chain

Using statistical mechanics arguments, the end-to-end distance can be represented as Probability Density Functions (PDFs). The Gaussian function (4.93) was the first PDF that has historical importance and was simple enough to be mathematically tractable, which led to neo-Hooke model. The so-called non-Gaussian methods are devised for explaining a physical limitation on the extensibility of rubber chains. In Gaussian theory chain end-to-end distance is not restricted in terms of elongation and consequently this limits it to small strain setting. The Gaussian statistics is valid for only $r \ll Nl$. In non-Gaussian theory, however, one can include the effect of chain extensibility limit and estimate the behavior of rubber for large strain. The well known inverse Langevin function is the single-most important PDF for rubber community which explains this phenomenon.

4.2.1 Entropy, free energy, and force definitions for single chain

In this part, we will briefly outline the development of the concepts of entropy, free energy function, and force for a single chain. The entropy of a chain is defined as the number of allowable conformations available to it. Let's focus on the kinematic variable λ for single chain. The probability of conformation of a chain to fall into the geometry defined as λ and $\lambda + d\lambda$ is,

$$dp(\lambda) = p(\lambda)d\lambda \quad (4.90)$$

From the statistical mechanics, the entropy s is defined as [36],

$$s = k \ln(p), \quad (4.91)$$

where k is the Boltzmann constant. For a purely entropic response, the free energy is described as

$$\psi = -Ts. \quad (4.92)$$

Where, T is the absolute temperature. For Gaussian statistics, p is taken as,

$$p(\lambda) = p_0 \exp\left[-\frac{3}{2}\lambda^2\right], \quad (4.93)$$

with p_0 as a normalization constant. Insertion of it into the equation (4.91) and using equation (4.92), the free energy for a single chain can be found as,

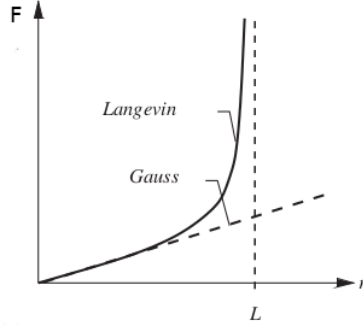


Figure 4.2: Forces derived from Gaussian and non-Gaussian statistics result in an asymptotic behavior when approaching extensibility limit $\lambda_r \rightarrow 1$ [1]. Here, $L = Nl$.

$$\psi(\lambda) = \frac{3}{2}kT\lambda^2 + \psi_0 \quad (4.94)$$

where ψ_0 is a constant. The force on a single chain due to stretch is defined as,

$$f = \frac{\partial\psi}{\partial\lambda} \quad (4.95)$$

Insertion of equation (4.94) into equation (4.95) results in,

$$f = 3kT\lambda \quad (4.96)$$

which is linear with respect to λ , see Figure 4.2. This leads to the development of the neo-Hooke model, $\psi = \frac{\mu}{2}(I_1 - 3)$, see [36]. The Langevin model, on the other hand, has the following PDF,

$$p(\lambda) = p_0 \exp \left[-N \left(\lambda_r \beta + \ln \left(\frac{\beta}{\sinh(\beta)} \right) \right) \right], \quad \text{with} \quad \beta = \mathcal{L}^{-1}(\lambda_r) \quad (4.97)$$

in terms of relative stretch λ_r . There, $\mathcal{L}(\beta) = \lambda_r = \coth\beta - \frac{1}{\beta}$ is the Langevin function. Using the definitions (4.91) and (4.92), free energy function can be found as,

$$\psi_{\mathcal{L}}(\lambda_r) = NkT \left(\lambda_r \beta + \ln \frac{\beta}{\sinh \beta} \right) + \psi_0 \quad (4.98)$$

where ψ_0 is a constant. The corresponding force for the chain reads (using (4.95)),

$$f = kT \sqrt{N} \mathcal{L}^{-1}(\lambda_r). \quad (4.99)$$

The force derived from the Langevin statistics results in an asymptotic behavior for limiting chain extension ($\lambda_r \rightarrow 1$), see Figure 4.2. This behavior allows a non-Gaussian model to fit the rubber behavior more accurately for finite strain setting.

4.2.2 Three-chain model

The three chain model is based on approximated network structure shown in Figure 4.3, where three perpendicular directions of the triad coincides with the three principal directions. Utilizing Langevin statistics (equation (4.98)), one can derive the free energy function of the three chain model as the summation of all chains contributing in three principal directions for the representative network (Figure 4.3), that is

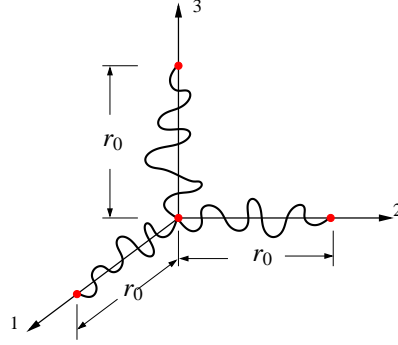


Figure 4.3: Three chain model representative network structure.

$$\Psi(\lambda_1, \lambda_2, \lambda_3) = \frac{\mu \sqrt{N}}{3} \sum_{i=1}^3 \left(\lambda_i \beta_i + \sqrt{N} \ln \left(\frac{\beta_i}{\sinh \beta_i} \right) \right), \quad \text{with } \beta_i = \mathcal{L}^{-1} \left(\frac{\lambda_i}{\sqrt{N}} \right). \quad (4.100)$$

Note that, λ_i is the stretch in the i^{th} principal direction and $\mu = nkT$ is a material parameter with n being the total number of chains statistically contributing to carry the load in all three principal directions. The division by 3 in equation (4.100) is for averaging the free energy in three principal direction. The free energy function fulfills the Valanis-Landel hypothesis

$$\Psi(\lambda_1, \lambda_2, \lambda_3) = \frac{n}{3} [\psi_{\mathcal{L}}(\lambda_1) + \psi_{\mathcal{L}}(\lambda_2) + \psi_{\mathcal{L}}(\lambda_3)] \quad (4.101)$$

4.2.3 Arruda-Boyce model

Also known as the 8-chain model, has the representative network structure as in Figure 4.4. The cube end points are considered as junction points and the center point (due to symmetry) obeys an affine transformation and remains at the geometric center of the cube during the deformation, even though it is considered statistically fluctuat-

ing [36], [9].

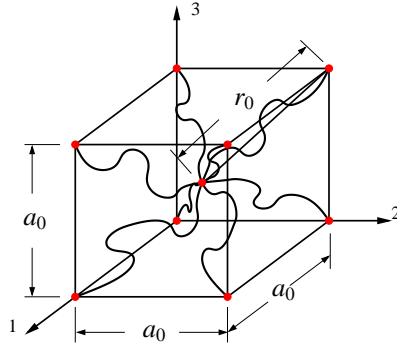


Figure 4.4: Eight chain model representative network structure.

The stretch of the diagonal formed by the principal stretches is defined as

$$\lambda_{ch} := \frac{r}{r_0} = \sqrt{(\lambda_1^2 + \lambda_2^2 + \lambda_3^2)/3} = \sqrt{I_1/3}. \quad (4.102)$$

Using the above made definition, the free energy function of the Arruda-Boyce model can be written as

$$\Psi(\lambda_{ch}) = n \cdot \psi_{\mathcal{L}}(\lambda_{ch}) \quad (4.103)$$

4.2.4 Tube model

As the name of the model implies, Heinrich and Kaliske [40] proposed that the molecular chain is constrained in a tube formed by the other chains in the network. Taking the affine coupling of network and entanglements, a non-affine assumption for deformation of tube dimension in lateral direction is made. Deformation of the molecular chains conformed in the tube is considered to be proportional to the macroscopic deformation of the network. Probability of conformation of the end-to-end distance of chain in the constraining tube is modeled by random walk distribution function

$$P(\mathbf{R}(s)) = \exp\left(-\frac{3}{2b} \int_0^L ds \left(\frac{\partial \mathbf{R}(s)}{\partial s}\right)^2\right). \quad (4.104)$$

Here " $\mathbf{R}(s)$ " is the network chain path, " b " is the Kuhn's statistical segment length, " s " is the variable used for counter, and " L " is the length of the polymeric chain under

stretch.

Elastic strain energy function is considered to be composed of two parts. First part is the strain energy function raised from the contribution of cross-links, the second part on the other hand is related to the constraints which is due to the presence of entanglements that cause variation of the tube diameter.

$$\psi = G_c I^*(2) + \frac{2G_e}{-\beta} I^*(-\beta). \quad (4.105)$$

Here " β " can be considered as a penalty parameter used for fitting the model to experimental data curve. The possible bound for β can be considered as $0 \leq \beta \leq 1$.

Then, the total shear modulus can be written as below

$$G = G_c + G_e \quad (4.106)$$

The final form of the strain energy function for tube model is suggested as

$$\psi = \sum_{i=1}^3 \frac{G_c}{2} (\lambda_i^2 - 1) + \frac{2G_e}{\beta^2} (\lambda_i^{-\beta} - 1) \quad \text{with } i = 1, 2, 3. \quad (4.107)$$

One may have notice the similarity of the proposed model with Ogden's model [27]. With $\mu_1 = G_e$, $\mu_2 = \frac{-2G_e}{\beta}$, $\alpha_1 = 2$, and $\alpha_2 = -\beta$ the 2-term Ogden model can be retained.

Finally the first derivative of the free energy function with respect to first principle stretches becomes

$$\frac{\partial \psi}{\partial \lambda_i} = \sum_{i=1}^3 G_c \lambda_i - \frac{2G_e}{\beta} \lambda_i^{-\beta-1} \quad \text{with } i = 1, 2, 3. \quad (4.108)$$

4.2.5 Extended-Tube model

An improved form of tube model [40], which is named as extended-tube model, is introduced by Kaliske ad Heinrich [45]. Unlike the previous one (tube model), the present approach do not take the Valanis-Landel hypothesis into the account. Investigating filler effect on the material response as well as molecular structure of rubber-like materials, it was distinguished that, increasing the number of filler material (carbon black or silica) cause shaping short molecular chains showing almost inextensible behavior. For moderate and large deformations, it was noted that cross-link part of the strain energy function large effect to resemble the upturn of the stress-strain curve

and make S-shape. The failure of Gaussian network theory of tube model is overcome by a new non-affine and non-Gaussian term for cross-linking part. Skipping the constraint part and replacing the cross-link part with the new function, following extended-tube model is obtained

$$\psi = \frac{G_c}{2} \left[\frac{(1 - \delta^2)(D - 3)}{1 - \delta^2(D - 3)} + \ln(1 - \delta^2(D - 3)) \right] + \frac{2G_e}{\beta^2} \sum_{i=1}^3 (\lambda_i^{-\beta} - 1). \quad (4.109)$$

with

$$\delta^2 := \langle \mathbf{R}'^2 \rangle = \alpha^2 \left(\frac{b}{d_0} \right)^2, \quad (4.110)$$

$$D = \sum_{i=1}^3 \lambda_i^2. \quad (4.111)$$

Here, α is a physical parameter that measures the inextensibility of the network chains. Then, one can say that δ is a measure used for extensibility limit in large deformations. The concept of limiting chain extensibility plays a crucial role in developing the extended-tube mode. At large deformations, where chains reach their maximum elongations, cross-links has tremendous effect to generate the behavior of rubber-like materials at high strain ranges, where constraint or entanglements do not have contribution of significant level.

Now, first derivative of strain energy function with respect to principle stretches become

$$\frac{\partial \psi}{\partial \lambda_i} = G_c \lambda_i \left\{ \frac{(1 - \delta^2)}{(1 - \delta^2(\lambda_i^2 - 3))^2} - \frac{\delta^2}{1 - \delta^2(\lambda_i^2 - 3)} \right\} \quad \text{with } i = 1, 2, 3. \quad (4.112)$$

$$- \frac{2G_e}{\beta} \lambda_i^{-\beta-1}$$

4.2.6 Micro-sphere model

Overall Framework and Definitions of Stresses and Moduli

The macroscopic free energy of the network under isothermal conditions

$$\Psi = \Psi(\hat{\mathbf{g}}; \mathbf{F})$$

Additive split of the network free energy into volumetric and isochoric parts

$$\hat{\Psi}(\mathbf{g}; \mathbf{F}) = U(J) + \bar{\Psi}(\mathbf{g}; \bar{\mathbf{F}}) \quad \text{where } \bar{\mathbf{F}} := J^{-1/3} \mathbf{F}$$

Isochoric free energy formed by the contributions from free chains and topological constraints on them

$$\bar{\Psi}(\mathbf{g}; \bar{\mathbf{F}}) = \bar{\Psi}_f(\mathbf{g}; \bar{\mathbf{F}}) + \bar{\Psi}_c(\mathbf{g}; \bar{\mathbf{F}})$$

The Doyle–Ericksen formulae give the Eulerian Kirchhoff stresses and the associated moduli

$$\boldsymbol{\tau} = 2\partial_{\mathbf{g}}\Psi(\mathbf{g}; \mathbf{F}), \quad \mathbb{C} = 4\partial_{\mathbf{g}\mathbf{g}}^2\Psi(\mathbf{g}; \mathbf{F})$$

The Kirchhoff stresses formulated through straight forward chain rule operation

$$\boldsymbol{\tau} = p\mathbf{g}^{-1} + \mathbb{P} : \bar{\boldsymbol{\tau}} \quad \text{where} \quad p := JU'(J), \quad \mathbb{P} := \mathbb{I} - \frac{1}{3}\mathbf{1} \otimes \mathbf{1}$$

The chain rule Kirchhoff stresses

$$\bar{\boldsymbol{\tau}} = \bar{\boldsymbol{\tau}}_f + \bar{\boldsymbol{\tau}}_c \text{ with } \bar{\boldsymbol{\tau}}_y := 2\partial_{\mathbf{g}}\bar{\Psi}_y(\mathbf{g}; \bar{\mathbf{F}}), \quad y = f, c$$

Definitions of Micro–State Kinematic Variables

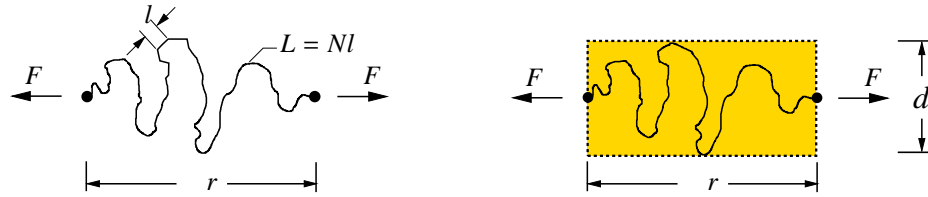


Figure 4.5: Micro-sphere kinematic variables.

Undeformed end-to-end distance of a chain,

$$r_0 = \sqrt{Nl} \tag{4.113}$$

Microscopic stretches,

$$\lambda := r/r_0 = r/\sqrt{Nl}, \quad \lambda_r := r/L = \lambda/\sqrt{N} \tag{4.114}$$

Constraining tube area contraction,

$$\nu := (d_0/d)^2 \tag{4.115}$$

Additive split of the free energy,

$$\psi(\lambda, \nu) = \psi_f(\lambda) + \psi_c(\nu) \tag{4.116}$$

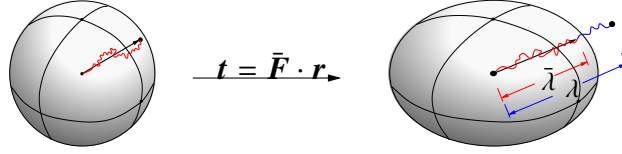


Figure 4.6: Affine transformation of a chain

Free energy of an unconstrained chain,

$$\psi_f(\lambda) = Nk\theta \left[\lambda_r \mathcal{L}^{-1}(\lambda_r) + \ln \frac{\mathcal{L}^{-1}(\lambda_r)}{\sinh \mathcal{L}^{-1}(\lambda_r)} \right] + \psi_0 \quad (4.117)$$

Free energy due to the tube-like constraint,

$$\psi_c(\nu) = \alpha k\theta N \left(\frac{l}{d_0} \right)^2 \nu + \psi_0 \quad (4.118)$$

Non-Affine Model for the Network of Unconstrained Chains

Isochoric free energy formed by the contributions from free chains and topological constraints on them

$$W = \bar{\Psi}_f(\mathbf{g}; \bar{\mathbf{F}}) + \bar{\Psi}_c(\mathbf{g}; \bar{\mathbf{g}})$$

Microscopic chain stretch,

$$\lambda = \langle \bar{\lambda} \rangle_p := \left[\frac{1}{|\mathcal{S}|} \int_{\mathcal{S}} \bar{\lambda}^p dS \right]^{1/p} \quad (4.119)$$

Contribution to the free energy,

$$\bar{\Psi}_f(\mathbf{g}; \bar{\mathbf{F}}) = n\psi_f(\langle \bar{\lambda} \rangle_p) \quad (4.120)$$

Explicit form of the free energy,

$$\bar{\Psi}_f(\mathbf{g}; \bar{\mathbf{F}}) = \mu N \left[\langle \bar{\lambda}_r \rangle_p \mathcal{L}^{-1}(\langle \bar{\lambda}_r \rangle_p) + \ln \frac{\mathcal{L}^{-1}(\langle \bar{\lambda}_r \rangle_p)}{\sinh \mathcal{L}^{-1}(\langle \bar{\lambda}_r \rangle_p)} \right], \quad \mu := nk\theta \quad (4.121)$$

Network of Constrained Chains

Another new key feature of the model is inverse non-linear relation between the microscopic tube cross section area stretch ν and the macroscopic area stretch $\bar{\nu}$

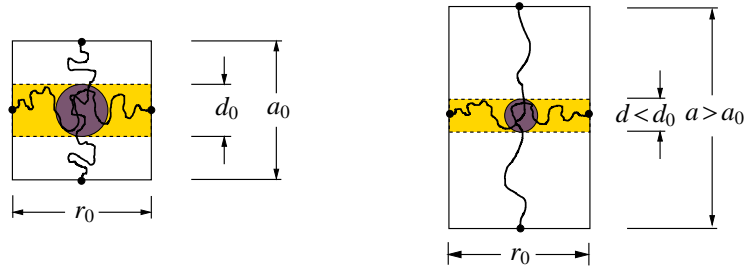
$$\nu = \left(\frac{d_0}{d} \right)^2 = (\bar{\nu})^q$$

The affine area stretch $\bar{\nu}$ of a material area element having normal \mathbf{r}^b is given by

$$\bar{\nu} = |\mathbf{n}^b|_{\mathbf{g}^{-1}} := \sqrt{\mathbf{n}^b \cdot \mathbf{g}^{-1} \mathbf{n}^b} = \sqrt{\mathbf{r}^b \cdot \bar{\mathbf{C}}^{-1} \mathbf{r}^b} \quad \text{with} \quad \mathbf{n}^b := \bar{\mathbf{F}}^{-T} \mathbf{r}^b \quad (4.122)$$

Schematically, extension of the chains being perpendicular to the chain of interest results in decrease in its admissible transverse excursions of the chain decreasing number of available conformations

Non-Affine Model for the Network of Constrained Chains



Micro-tube contraction,

$$\nu = (\bar{\nu})^q \quad (4.123)$$

Contribution to the free energy,

$$\bar{\Psi}_c(\mathbf{g}; \mathbf{F}) = \langle n \psi_c(\bar{\nu}^q) \rangle \quad (4.124)$$

Explicit form of the free energy,

$$\bar{\Psi}_c(\mathbf{g}; \mathbf{F}) = \mu N U \langle \bar{\nu}^q \rangle, \quad U := \alpha (l/d_0)^2 \quad (4.125)$$

Kirchhoff stresses,

$$\bar{\boldsymbol{\tau}}_c = -n \langle \psi'_c q \bar{\nu}^{(q-2)} \rangle \mathbf{n} \otimes \mathbf{n} \quad (4.126)$$

Material parameter q describes the non-affine relation between macro- and micro-kinematic measures.

4.2.7 Khiem (network averaging tube) model

Network averaging approach used by Khiem and Itskov [58] was proposed as an alternative form of extended-tube [45] model. Polymeric chains are considered as coarse-grained model and Rayleigh non-Gaussian distribution function is used to approximate the end-to-end distance of the chains. Applied force on the coarse-grained segment can be calculated through dumbbell model with two particle joined by finitely extensible spring. The motion of spring in undeformed state can be approximated by Schrödinger equation as

$$P_{eq} = \left\{ \frac{n}{\pi r} \sin\left(\frac{\pi r}{n}\right) \right\}^2. \quad (4.127)$$

Then, the probability density function for end-to-end distance of $\frac{\kappa}{2}n$ number of identical segments are written as

$$P_c(r) = \prod_{i=1}^{\frac{\kappa}{2}n} P_{eq} = A \left\{ \frac{n}{\pi r} \sin\left(\frac{\pi r}{n}\right) \right\}^{\kappa n}, \quad (4.128)$$

with

$$A = P_c^{\text{exact}}(n, 10^{-2}) \quad (4.129)$$

is used for normalization.

The non-Gaussian strain energy function can be written as

$$\psi_c(n, r) = -k_B T \ln(P_c(r)) = nk_B T \kappa \ln \left\{ \frac{\pi r}{n \sin\left(\frac{\pi r}{n}\right)} \right\} + C. \quad (4.130)$$

The strain energy of the topological constraints causing lateral deformation of tube is written as

$$\psi_t = -k_B T \ln P_t = k_B T \alpha \left(\frac{\pi^2 R}{3D^2} \right) \left(\frac{D}{d} \right)^2, \quad (4.131)$$

with $\left(\frac{D}{d}\right)^2$ being the tube contraction.

Averaging equations (4.130) and (4.131) yields the following strain energy function for network averaging tube model.

$$\psi = \mu_c \kappa n \ln \frac{\sin(\pi/\sqrt{n})(I_1/3)^{q/2}}{\sin((\pi/\sqrt{n})(I_1/3)^{q/2})} + \mu_t \left[\left(\frac{I_2}{3} \right)^{1/2} - 1 \right]. \quad (4.132)$$

Here, $\mu_c \kappa$ is the effective shear modulus of the network and μ_t is the shear modulus of topological constraint part. The writers prefer to use Rayleigh distribution function

instead of Langevin functions because of the difficulties encountered during the integration of Langevin functions. To get rid of integration, Rayleigh exact distribution function is used.

CHAPTER 5

PARAMETER OPTIMIZATION

5.1 Parameter optimization preliminaries

The parameter identification process is based on the description of an objective function

$$\mathcal{E}_{\text{UT}}(\boldsymbol{\zeta}) = \sum_{i=1}^{n_{\text{UT}}} (P_{11}(\boldsymbol{\zeta}, \lambda_i) - P_{11}^{\text{exp}}(\lambda_i))^2 \quad (5.1)$$

where, P_{11} is the first Piola-Kirchhoff stress and n_{UT} is the number of data points for uniaxial tension (UT) test. Similarly, the cost functions for the equibiaxial tension (ET) and pure shear (PS) tests

$$\begin{aligned} \mathcal{E}_{\text{ET}}(\boldsymbol{\zeta}) &= \sum_{i=1}^{n_{\text{ET}}} (P_{11}(\boldsymbol{\zeta}, \lambda_i) - P_{11}^{\text{exp}}(\lambda_i))^2 \\ \mathcal{E}_{\text{PS}}(\boldsymbol{\zeta}) &= \sum_{i=1}^{n_{\text{PS}}} (P_{11}(\boldsymbol{\zeta}, \lambda_i) - P_{11}^{\text{exp}}(\lambda_i))^2 \end{aligned} \quad (5.2)$$

can be defined for ET and PS experiments. The total cost function for multi-objective optimization incorporation UT, ET and PS experiments reads

$$\mathcal{E}_{\text{TOT}}(\boldsymbol{\zeta}, \boldsymbol{w}) = w_1 \mathcal{E}_{\text{UT}}(\boldsymbol{\zeta}) + w_2 \mathcal{E}_{\text{ET}}(\boldsymbol{\zeta}) + w_3 \mathcal{E}_{\text{PS}}(\boldsymbol{\zeta}) \quad (5.3)$$

with the extended parameter domain $\boldsymbol{\xi} := \{\boldsymbol{\zeta}, \boldsymbol{w}\}$ which is obtained from the minimization principle

$$\boldsymbol{\xi} = \text{Arg} \left\{ \inf_{\boldsymbol{\xi} \in \mathcal{W}} \mathcal{E}_{\text{TOT}}(\boldsymbol{\xi}) \right\}. \quad (5.4)$$

Therein, the optimization procedure is subjected to the following constraint domain

$$\mathcal{W} = \{\boldsymbol{\zeta} \mid \boldsymbol{\zeta} \in \mathcal{D} \wedge \boldsymbol{w} \mid w_i \in [0, 1]\}. \quad (5.5)$$

with $w_1 + w_2 + w_3 = 1$. The domain \mathcal{D} is the physical admissible domain for the material parameter vector $\boldsymbol{\zeta}$.

The gradient type solution is achieved by FMINCON function in MATLAB where the extended cost function

$$\mathcal{L}(\boldsymbol{\xi}, \boldsymbol{\lambda}^{\text{eq}}, \boldsymbol{\lambda}^{\text{ine}}) = \mathcal{E}_{\text{tot}}(\boldsymbol{\xi}) + \sum_i \lambda_i^{\text{ine}} g^i(\boldsymbol{\xi}) + \sum_i \lambda_i^{\text{eq}} h^i(\boldsymbol{\xi}) \quad (5.6)$$

is subjected to equality constraints $h^i(\boldsymbol{\xi})$ and the inequality constraints $g^i(\boldsymbol{\xi})$, respectively. For the optimum point of solution, the variational principle requires

$$\nabla_{\boldsymbol{\xi}} \mathcal{L}(\boldsymbol{\xi}, \boldsymbol{\lambda}^{\text{eq}}, \boldsymbol{\lambda}^{\text{ine}}) = \mathbf{0}, \quad (5.7)$$

along with the Karush-Kuhn-Tucker optimality conditions for the inequality constraints

$$\lambda_i^{\text{ine}} \geq 0 \quad g^i(\boldsymbol{\xi}) \leq 0 \quad \lambda_i^{\text{ine}} g^i(\boldsymbol{\xi}) = 0, \quad (5.8)$$

where λ_i^{ine} are the Lagrange multipliers for the inequality constraint. The equality constraint

$$h^i(\boldsymbol{\xi}) = 0 \quad (5.9)$$

is enforced by the penalty parameters λ_i^{eq} . The function call in MATLAB is as follows:

$$\boldsymbol{\xi} = \text{FMINCON}(\mathcal{E}, \boldsymbol{\xi}_0, \mathbf{A}, \mathbf{b}, \mathbf{A}_{\text{eq}}, \mathbf{b}_{\text{eq}}) \quad (5.10)$$

with equality constraint $\mathbf{A}_{\text{eq}} \boldsymbol{\xi} = \mathbf{b}_{\text{eq}}$ and the inequality constraint $\mathbf{A} \boldsymbol{\xi} \leq \mathbf{b}$. *Interior-point* algorithm used. Furthermore, \mathbf{A}_{eq} stands for coefficient matrix of equality constraint, \mathbf{b}_{eq} is right-hand side vector for equality constraint, \mathbf{A} defines the coefficient matrix for inequality constraint, \mathbf{b} is right-hand side vector for inequality constraint, and $\boldsymbol{\xi}_0$ are the initial points.

5.2 Genetic Algorithm Approach

Let a_{ij} denote a gene at location i on an ordered list $A_j = \{a_{1j}, a_{2j}, \dots, a_{nj}\}$ that denotes the j^{th} chromosome. Here, n , is the number of genes in a chromosome. A person consists of single or multiple chromosomes. A population consists of N persons. In this work, a person has a single chromosome. Therefore, j represents a person's only chromosome and it is interchangeably used for a person or a person's only chromosome throughout the paper.

The constraints are defined over each slot in A_j ,

$$a_{ij} \in \{c_i \mid c_i \in [\min_i, \max_i]\} \quad \forall i \in [1, n - 2] \quad (5.11)$$

$$a_{ij} \in \{w_i \mid w_i \in [0, 1]\} \quad \forall i \in [n - 2, n] \quad (5.12)$$

The notation $|A_{ij}| = a_{ij}$ will be used to refer to a specific gene at i^{th} slot in j^{th} chromosome,

Let's partition A_j into two important sections,

$$\begin{aligned} L_j &= \{a_{1j}, a_{2j}, \dots, a_{(n-3)j}\} \\ R_j &= \{a_{(n-2)j}, a_{(n-1)j}, a_{nj}\}, \end{aligned} \quad (5.13)$$

with $A_j = L_j \cup R_j$. The genetic algorithm parameter optimization relies on the same definition for the cost (or fitness) function as in multi-objective optimization,

$$\begin{aligned} \mathcal{E}_{GA}(L_j, R_j) &= |R_{1j}| \mathcal{E}_{UT}(L_j) + \\ &|R_{2j}| \mathcal{E}_{ET}(L_j) + \\ &|R_{3j}| \mathcal{E}_{PS}(L_j) \end{aligned} \quad (5.14)$$

The ordered lists L_j and R_j represent parameters and weights of a model, respectively. Note that, weights are subjected to the constraint,

$$\sum_{\alpha=n-2}^n a_{\alpha j} = 1 \quad (5.15)$$

The tuple, $A_t^* = \langle L_j^*, R_j^* \rangle_t$

$$A_t^* = \min(\{\mathcal{E}_{GA}(\langle L_j, R_j \rangle_t), \forall j \in [0, n]\}) \quad (5.16)$$

represents the optimal (or fittest) person (or the lowest cost) at iteration t. The meta-heuristic search for optimization requires modifications (or alterations) of the chromosomes, that is, the chromosomes are subjected to probabilistic operations known as cross-over, mutation, and selection.

Mutation operator,

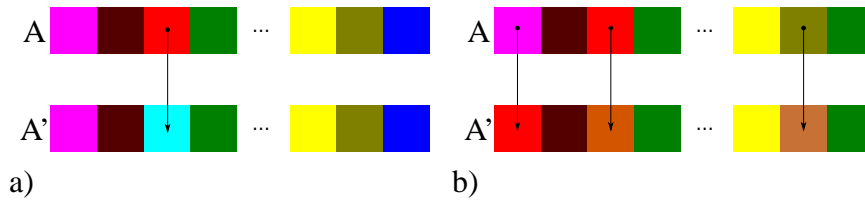


Figure 5.1: Pictorial representations of types of mutations, a) standalone mutation operator, b) multiple-mutations operator

$$\text{MUT}(A_k, s) := \text{rand}(0, 1)\alpha a_{sk} + \text{rand}(0, 1)(a_{sk} + \text{rand}\beta) \quad (5.17)$$

where, α is a proportionality constant called mutation amplitude and β is a severe direct mutation. In this operation, $s \in [1, n]$. Mutation operation is complete if,

$$a_{sk} \leftarrow \text{MUT}(A_k, s) \quad (5.18)$$

Multiple mutation operator, The generalization of mutation operator is called multiple mutations,

$$\text{MMUT}(A_k, r) := \begin{bmatrix} \text{MUT}(A_k, s_1) \\ \text{MUT}(A_k, s_1) \\ \dots \\ \text{MUT}(A_k, s_r) \end{bmatrix} \quad (5.19)$$

Then, the multiple mutations are complete if all the components are subjected to mutation.

$$\begin{bmatrix} a_{1k} \\ a_{2k} \\ \vdots \\ a_n \end{bmatrix} \leftarrow \begin{bmatrix} \text{MUT}(A_k, 1) \\ \text{MUT}(A_k, 2) \\ \vdots \\ \text{MUT}(A_n, r) \end{bmatrix} \quad (5.20)$$

Cross-over operator, For a chromosome k, a general partitioning operation is defined

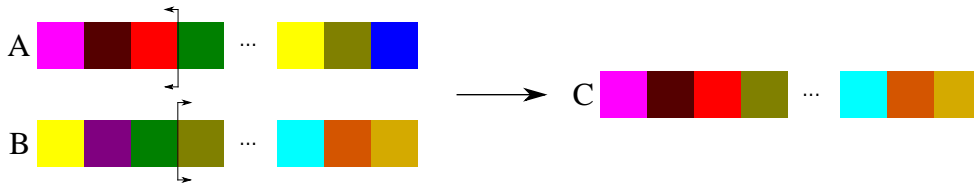


Figure 5.2: Pictorial representation of cross-over operator.

as,

$$\begin{aligned} A_{k|m^-} &= \{a_{1k}, a_{2k}, \dots, a_{(m-1)k}\} \\ A_{k|m^+} &= \{a_{mk}, a_{(m+1)k}, \dots, a_{nk}\} \end{aligned} \quad (5.21)$$

The cross-over operator is defined as,

$$\text{CO}(A_k, A_l, m^\pm) := \text{cat}(\text{MMUT}(\text{perm}(A_k, A_l))) \quad (5.22)$$

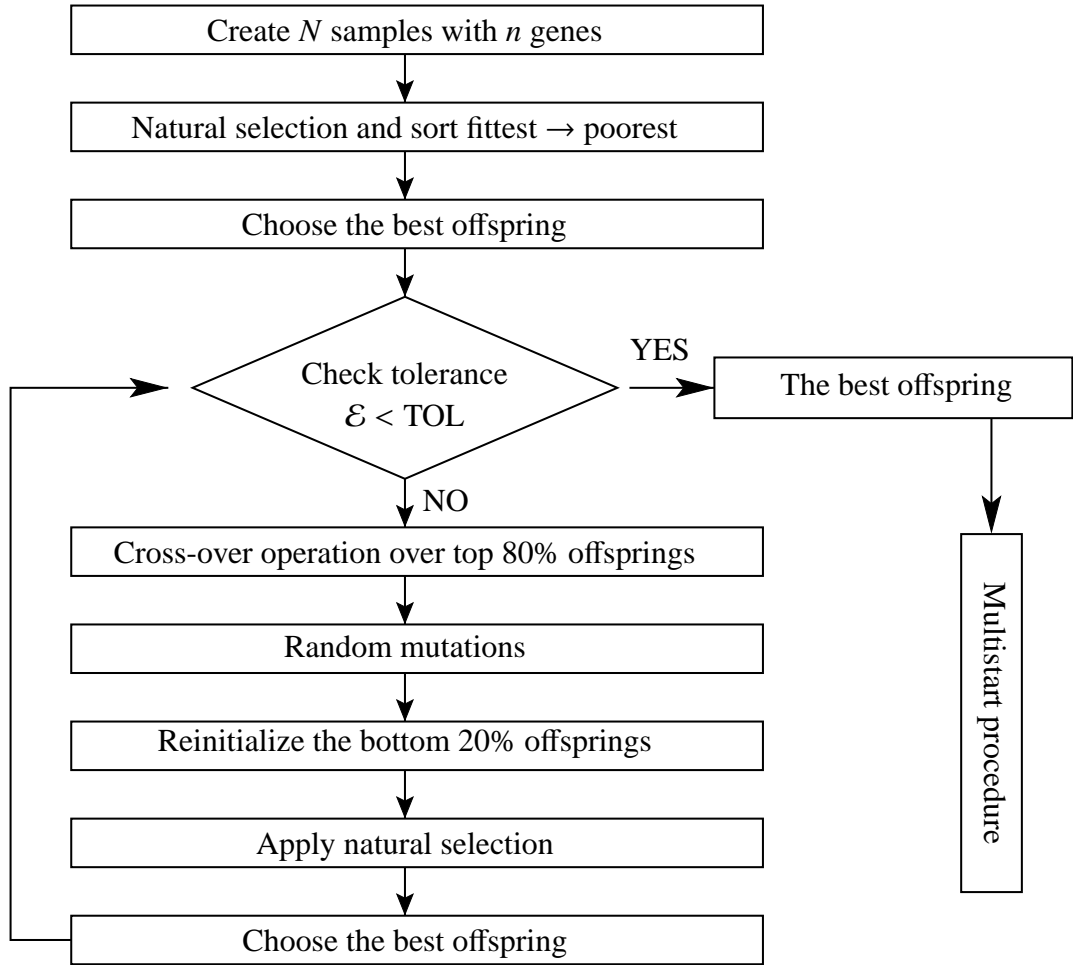


Figure 5.3: Parameter identification procedure.

where, $\text{cat}(\cdot, \cdot)$ represents concatenation of two ordered lists. $\text{perm}(A_{k|m^\pm}, A_{l|m^\pm})$ represents one of the two possible orderings, namely $\langle A_{k|m^+}, A_{l|m^-} \rangle$ and $\langle A_{k|m^-}, A_{l|m^+} \rangle$.

Selection operator,

Selection process is defined over a set of persons on their fitness (or cost) values. The ordered list $P_t = \{A_j^t \mid \forall j \in [1, N]\}$ is the list of persons at iteration t . The selection operator is defined as follows,

$$\text{SEL}(P_t, o) := \text{sort}(\mathcal{E}_{\text{GA}}(P_t))_{|o^-} \quad (5.23)$$

Validity Range Approach

The error measure \mathcal{E} is not a valid measure to assess the performance of the constitutive model, specially for the models that are not able to catch the S-shape response of the material in full range. In order to make an objective measure and compare

the models' prediction a validity range approach is introduced. Note that, the mentioned approach is applied only for simultaneous fitting. We introduce an alternative expression called as the quality of fit expression

$$\chi^2 = \sum_{i=1}^n \frac{(P_{11}(\lambda_i) - P_{11}^{\text{exp}}(\lambda_i))^2}{P_{11}^{\text{exp}}(\lambda_i)} \quad (5.24)$$

for the assessment of the performance of the model through full range of data set. This measures the relative value of model's error to the experimental data.

Region 1 : $1 < \lambda < \frac{1}{3}\lambda_{max}$

Region 2 : $1 < \lambda < \frac{2}{3}\lambda_{max}$

Region 3 : $1 < \lambda < \lambda_{max}$

where, λ_{max} is the maximum stretch levels in each experiment.

CHAPTER 6

RESULTS AND DISCUSSION

6.1 Ranking of hyperelastic material models

In this section the material models that their parameters are identified and sorted according to their quality of fit measure. The ranking is done according to the simultaneous fitting quality considered hyperelastic constitutive relations. Unlike the other works, like the one proposed by Marckmann and Verron [13], for the ranking, we did not consider number of parameters of each material model. In the same study, type of the material models are also an important factor to rank the constitutive models, they gave priority to the physically based material models. However, in our case, only quality of fit measure which provides an objective measure is taken into the account. For the models that are not able to generate the S-shape curve, the results are obtained by validity range approach. Sorted results are presented in Tables 6.1 and 6.2, where qof_{SIM} is the quality of fit values for simultaneous fits. nop denotes the number of parameters taken for each model during parameter identification. Validity range values on synthetic data for λ_{UT} , λ_{ET} , and λ_{PS} are listed in the last three columns. The range that each model is able to fit the data points are also presented.

Detailed resulting tables for each constitutive material model are presented in the next subsections. One can also reach the quality of fit values for uniaxial and biaxial fit from the presented results and sort the material models according to the obtained values. Further results for equibiaxial only and pure shear fittings are also provided in Appendices A and B.

Following observations during the parameter identification study has been concluded

- first invariant based models are not capable of reproducing UT, ET, PS test data simultaneously,
- simple uniaxial tension experiment is enough to obtain parameters for first invariant based models,
- Phenomenological models based on I_1 and I_2 are more successful than the I_1 -based models,
- the models having tube constraint or I_2 expression in the free energy function over 3 material parameters cannot be identified by simple UT-tests alone,
- UT, ET, and PS experiments are necessary to find material parameters for $\{I_1, I_2\}$ -based, principle stretch-based, and models incorporating tube constraints,
- principal stretch based models require more material parameters compared to invariant based models for the same level of fit of quality,
- micromechanically based models must have a tube-like constraint and physically motivated non-affine average network stretch,
- the most successful models have either a tube constraint in terms of negative powers of the principal stretches or a I_2 -based term.

Rank	model name	Reference	Type	nop	qof_{SIM}	Validity Range		
						λ_{UT}	λ_{ET}	λ_{PS}
1	Micro-sphere model	[1]	λ (Stat. Mech.)-based	5	0.0657	full range	full range	full range
2	Alexander model	[26]	I1,I2-based	5	0.0705	full range	full range	full range
3	Diani and Rey model	[43]	I1,I2-based	5	0.0724	full range	full range	full range
4	Extended tube model	[45]	λ -based	4	0.0812	full range	full range	full range
5	Shariff model	[46]	λ -based	5	0.0918	full range	full range	full range
6	Carroll model	[55]	I1,I2-based	3	0.1186	full range	full range	full range
7	Network averaging tube model	[58]	I1,I2-based	4	0.1366	full range	full range	full range
8	Chevallier & Marco model	[48]	I1,I2-based	6	0.1482	full range	full range	full range
9	Ogden model	[27]	λ -based	6	0.1604	full range	full range	full range
10	Amin model	[52]	I1,I2-based	6	0.1785	full range	full range	full range
11	James model	[28]	I1,I2-based	5	0.1808	full range	full range	full range
12	Hains-Wilson model	[29]	I1,I2-based	6	0.1876	full range	full range	full range
13	Attard & Hunt model	[51]	λ -based	6	0.1881	full range	full range	full range
14	Bechir-4term model	[53]	λ -and I1-based	4	0.2130	full range	full range	full range
15	Pucci & Saccomandi model	[49]	I1,I2-based	3	0.2243	full range	full range	full range
16	Biderman model	[22]	I1,I2-based	4	0.2289	full range	full range	full range
17	Kilian (van der waals) model	[33]	I1,I2-based	4	0.2404	full range	full range	full range
18	Yamashita & Kawabata model	[35]	I1,I2-based	4	0.2723	full range	full range	full range
19	Lion model	[41]	I1,I2-based	3	0.2835	full range	full range	full range
20	Beda model	[16]	I1,I2-based	4	0.3150	full range	full range	full range

Table 6.1: First 20 models are sorted based on simultaneous quality of fit values.

Rank	model name	Reference	Type	nop	qof _{SIM}	Validity Range		
						λ_{UT}	λ_{ET}	λ_{PS}
21	Hart-Smith model	[67]	I1,I2-based	3	0.3173	full range	full range	full range
22	Haupt & Sedlan model	[47]	I1,I2-based	5	0.3727	full range	full range	full range
23	Exp-Ln model	[57]	I1-based	3	0.5647	full range	full range	full range
24	Yeoh model	[34]	I1-based	3	0.5671	full range	full range	full range
25	Two-Term model	[54]	I1-based	4	0.5772	full range	full range	full range
26	Yeoh and Fleming model	[42]	I1-based	4	0.6238	full range	full range	full range
27	Arruda-Boyce model	[9]	λ (Stat. Mech.)-based	2	0.8129	full range	full range	full range
28	Gent model	[37]	I1-based	2	0.9367	full range	full range	full range
29	Three Chain model	[6]	λ (Stat. Mech.)-based	2	1.4840	full range	full range	full range
30	Mooney model	[4]	I1,I2-based	2	5.5	full range	full range	full range
31	Isihara model	[21]	I1,I2-based	3	5.5	full range	full range	full range
32	Nunes model	[56]	I1,I2-based	2	4.5	2.5	2.5	4
33	Tube model	[40]	λ -based	3	4.5	4.5	2.5	4
34	Slip-Link model	[30]	λ -based	3	4.5	2.5	2.5	4
35	Swanson-4term model	[32]	I1,I2-based	4	4.5	2.5	2.5	3.5
36	Gent-Thomas model	[23]	I1,I2-based	2	4.5	2	2	3.5
37	Constrained Junction model	[66]	λ -based	3	3.5	2.5	2.5	3
38	WFB model	[59]	λ -and I1-based	4	3	3	3	3
39	neo-Hooke model	[2]	I1-based	1	2.5	2.5	2.5	2
40	Valanis-Landel model	[25]	λ -based	1	2	1.5	1.5	2

Table 6.2: Last 20 models are sorted based on simultaneous quality of fit values.

6.2 Results of hyperelastic material models

6.2.1 Micro-sphere model results

Due to the well-defined physically motivated theory behind the micro-sphere model, and existence of a non-affine tube constraint, as it was expected, excellent agreement with experimental data is reached. Fitting results are graphically given in Figure 6.1 and numerical results for simultaneous, uniaxial and biaxial fittings are given in Tables 6.3, 6.4, and 6.5, respectively.

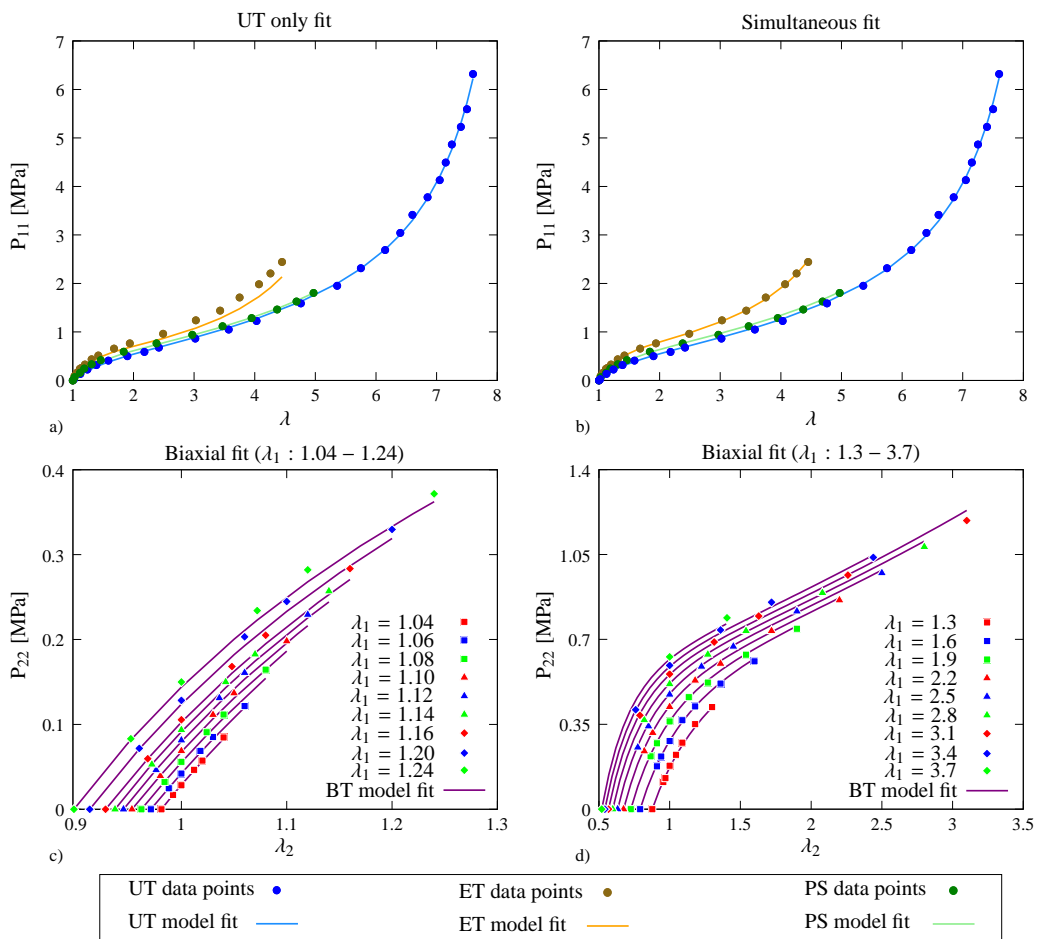


Figure 6.1: Micro-Sphere model prediction for a) uniaxial tension, b) combination of uniaxial, equibiaxial, and pure shear loadings using Treloar data c) biaxial tension loading for $\lambda_1 : 1.04-1.24$, d) biaxial tension loading for $\lambda_1 : 1.3-3.7$ using Kawabata data.

Simultaneous fitting (Treloar)					
Parameters	$\mu=0.2902$ [MPa]	$N=22.5298$	$p=1.5326$		
	$U=0.2908$	$q=0.2389$			
		Quality of fit			
	Weight	Error	Region 1	Region 2	Region 3
UT	0.4805	0.0752	0.0072	0.0117	0.0273
ET	0.3172	0.0066	0.0241	0.0249	0.0264
PS	0.2023	0.0077	0.0131	0.0135	0.0176
Total	1.0000	0.0895	0.0444	0.0501	0.0713

Table 6.3: Simultaneous fitting results for Micro-Sphere model.

UT only fit (Treloar)					
Parameters	$\mu=0.2678$ [MPa]	$N=24.8289$	$p=1.8966$		
	$U=2.8190$	$q=0.0216$			
		Quality of fit			
	Weight	Error	Region 1	Region 2	Region 3
UT	1	0.0722	0.0119	0.0168	0.0310
ET	0	0.3817	0.0366	0.0725	0.2533
PS	0	0.0071	0.0209	0.0258	0.0265
Total	1	0.4610	0.0694	0.1151	0.3108

Table 6.4: Uniaxial tension results for Micro-Sphere model.

Biaxial fit (Kawabata)			
Parameters	$\mu=0.3774$ [MPa]	$N=100.02$	$p=1.2386$
	$U=0.0728$	$q=0.0941$	
Quality of fit: 0.3930	Biaxial error: 0.1160		

Table 6.5: Biaxial tension results for Micro-Sphere model.

6.2.2 Alexander model results

It is observed in this study that the Alexander’s model has excellent simultaneous fitting capabilities, also for individual loading cases it catches the S-curve perfectly using Treloar’s data. Fitting results are graphically given in Figure 6.2 and numerical results for simultaneous, uniaxial and biaxial fittings are given in Tables 6.6, 6.7, and 6.8, respectively.

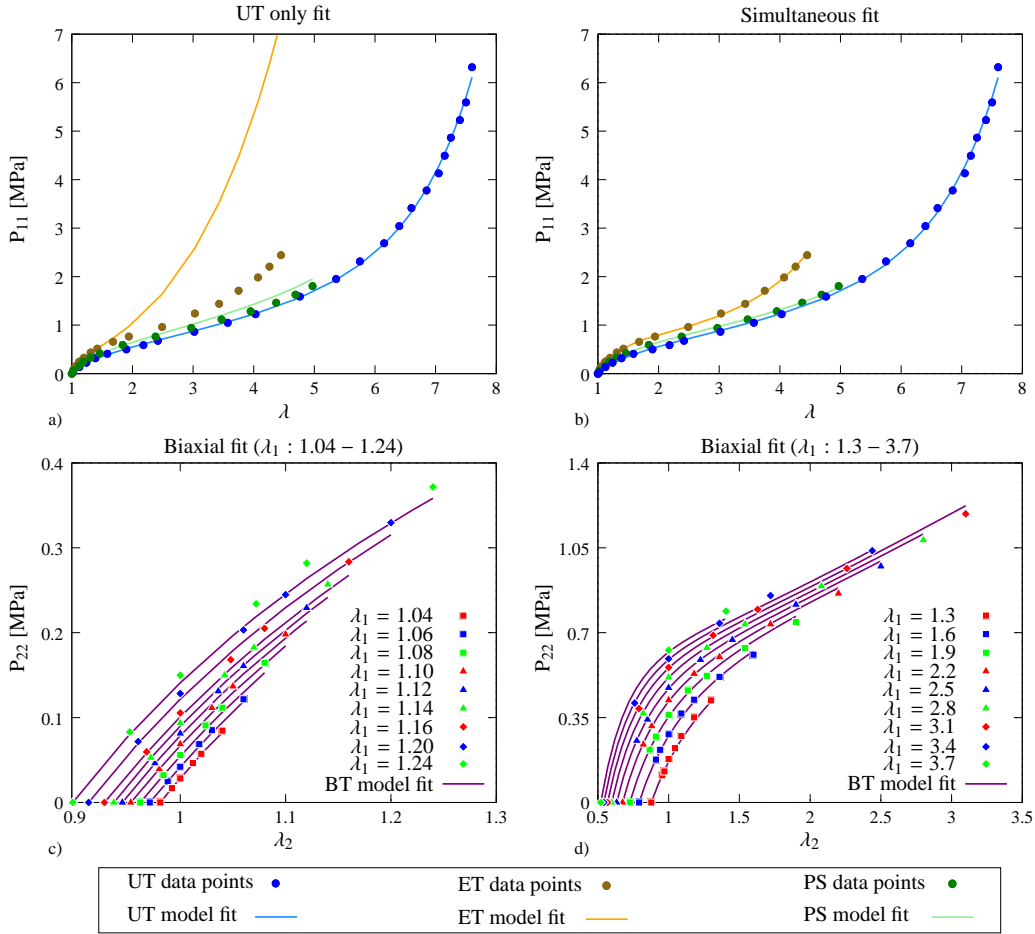


Figure 6.2: Alexander’s model prediction for a) uniaxial tension, b) combination of uniaxial, equibiaxial, and pure shear loadings using Treloar data c) biaxial tension loading for $\lambda_1 : 1.04 - 1.24$, d) biaxial tension loading for $\lambda_1 : 1.3 - 3.7$ using Kawabata data.

Simultaneous fitting (Treloar)					
Parameters	$C_1=0.1403$ [MPa]	$C_2=0.2542$ [MPa]	$C_3=0.0022$ [MPa]		
	$\gamma=5.8088$	$k=3.46e - 4$			
		Quality of fit			
	Weight	Error	Region 1	Region 2	Region 3
UT	0.3001	0.1073	0.0072	0.0094	0.0307
ET	0.3999	0.0079	0.0226	0.0236	0.0261
PS	0.3000	0.0035	0.0119	0.0123	0.0137
Total	1.0000	0.1188	0.0417	0.0453	0.0705

Table 6.6: Simultaneous fitting results for Alexander model.

UT only fit (Treloar)					
Parameters	$C_1=0.1389$ [MPa]	$C_2=0.0089$ [MPa]	$C_3=0.0300$ [MPa]		
	$\gamma=0.1390$	$k=3.49e - 4$			
		Quality of fit			
	Weight	Error	Region 1	Region 2	Region 3
UT	1	0.1045	0.0026	0.0039	0.0251
ET	0	68.1298	0.0057	0.5494	33.5362
PS	0	0.0902	0.0047	0.0059	0.0670
Total	1	68.3245	0.0130	0.5592	33.6283

Table 6.7: Uniaxial tension fitting results for Alexander model.

Biaxial fit (Kawabata)			
Parameters	$C_1=0.1570$ [MPa]	$C_2=0.2124$ [MPa]	$C_3=0.0020$ [MPa]
	$\gamma=7.6605$	$k=7.61e - 9$	
Quality of fit: 0.5078	Biaxial error: 0.1626		

Table 6.8: Biaxial tension results for Alexander model.

6.2.3 Diani and Rey model results

Obtained results for Diani and Rey model are also in good agreement with experimental data. Introducing a logarithmic power term in the proposed constitutive relation, makes the simultaneous fitting results to be in perfect agreement with experimental data in higher stretch values. Fitting results are graphically given in Figure 6.3 and numerical results for simultaneous, uniaxial and biaxial fittings are given in Tables 6.9, 6.10, and 6.11, respectively.

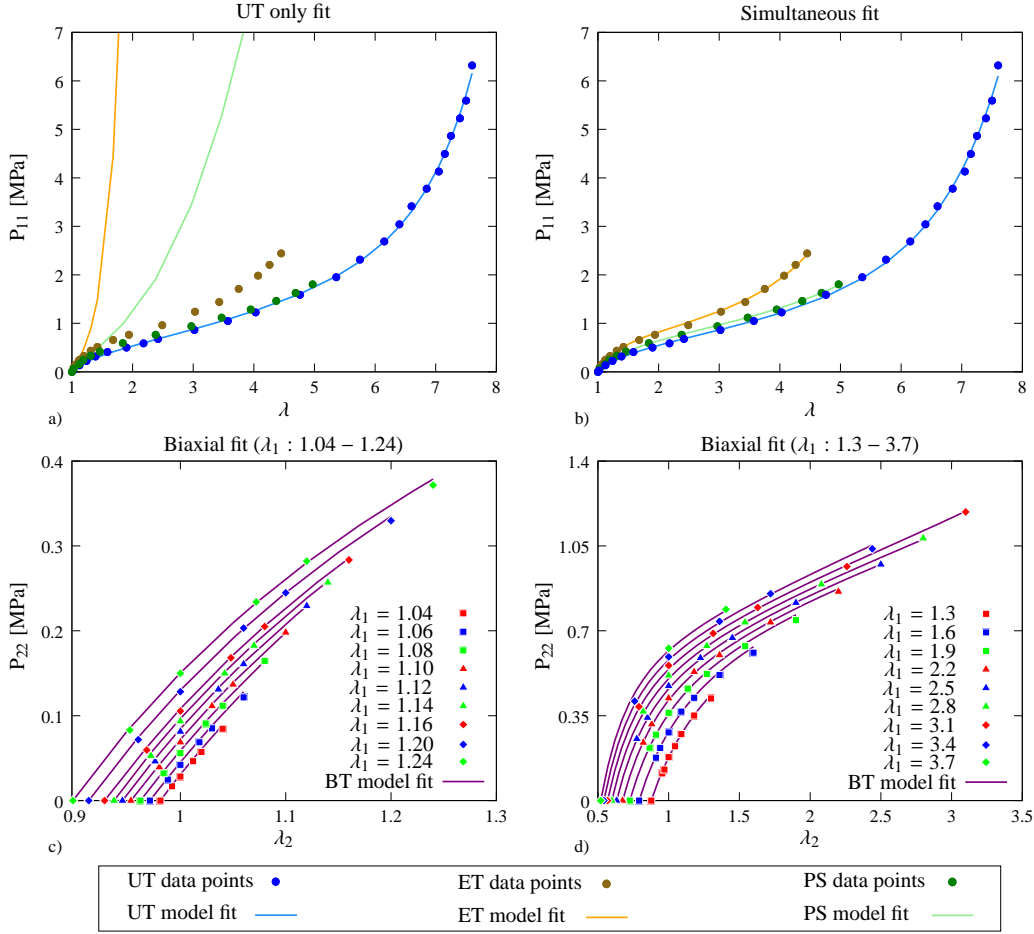


Figure 6.3: Diani and Ray's model prediction for a) uniaxial tension, b) combination of uniaxial, equibiaxial, and pure shear loadings using Treloar data c) biaxial tension loading for $\lambda_1 : 1.04-1.24$, d) biaxial tension loading for $\lambda_1 : 1.3-3.7$ using Kawabata data.

Simultaneous fitting (Treloar)					
Parameters	$exp(a_0)=0.1350$ [MPa]	$a_1=0.0018$	$a_2=3.26e-4$		
	$exp(b_0)=0.1020$ [MPa]	$b_1=-0.6250$			
			Quality of fit		
	Weight	Error	Region 1	Region 2	Region 3
UT	0.1002	0.1104	0.0065	0.0074	0.0295
ET	0.7998	0.0119	0.0220	0.0275	0.0300
PS	0.1000	0.0024	0.0120	0.0122	0.0129
Total	1.0000	0.1246	0.0405	0.0472	0.0724

Table 6.9: Simultaneous fitting results for Diani and Ray model.

UT only fit (Treloar)					
Parameters	$exp(a_0)=0.0338$ [MPa]	$a_1=0.0221$ [MPa]	$a_2=3.15e-4$ [MPa]		
	$exp(b_0)=0.0552$ [MPa]	$b_1=0.9985$			
			Quality of fit		
	Weight	Error	Region 1	Region 2	Region 3
UT	1	0.0870	0.0087	0.0118	0.0289
ET	0	$2.79e7$	0.0332	$4.54e3$	$1.25e7$
PS	0	422.3282	0.0118	2.0064	269.8971
Total	1	$2.79e7$	0.0537	$4.54e3$	$1.25e7$

Table 6.10: Uniaxial tension results for Diani and Ray model.

Biaxial fit (Kawabata)			
Parameters	$exp(a_0)=0.1723$ [MPa]	$a_1=-0.0358$ [MPa]	$a_2=0.0011$ [MPa]
	$exp(b_0)=0.0472$ [MPa]	$b_1=-0.4332$	
Quality of fit: 0.2844	Biaxial error: 0.1131		

Table 6.11: Biaxial tension results for Diani and Ray model.

6.2.4 Extended tube model results

With four number of material parameters, extended-tube model shows a high fitting performance in simultaneous fitting. Using the obtained values for material constants in uniaxial tension, one can also reach reasonable results in equibiaxial and pure shear loadings. Fitting results are graphically given in Figure 6.4 and numerical results for simultaneous, uniaxial and biaxial fittings are given in Tables 6.12, 6.13, and 6.14, respectively.

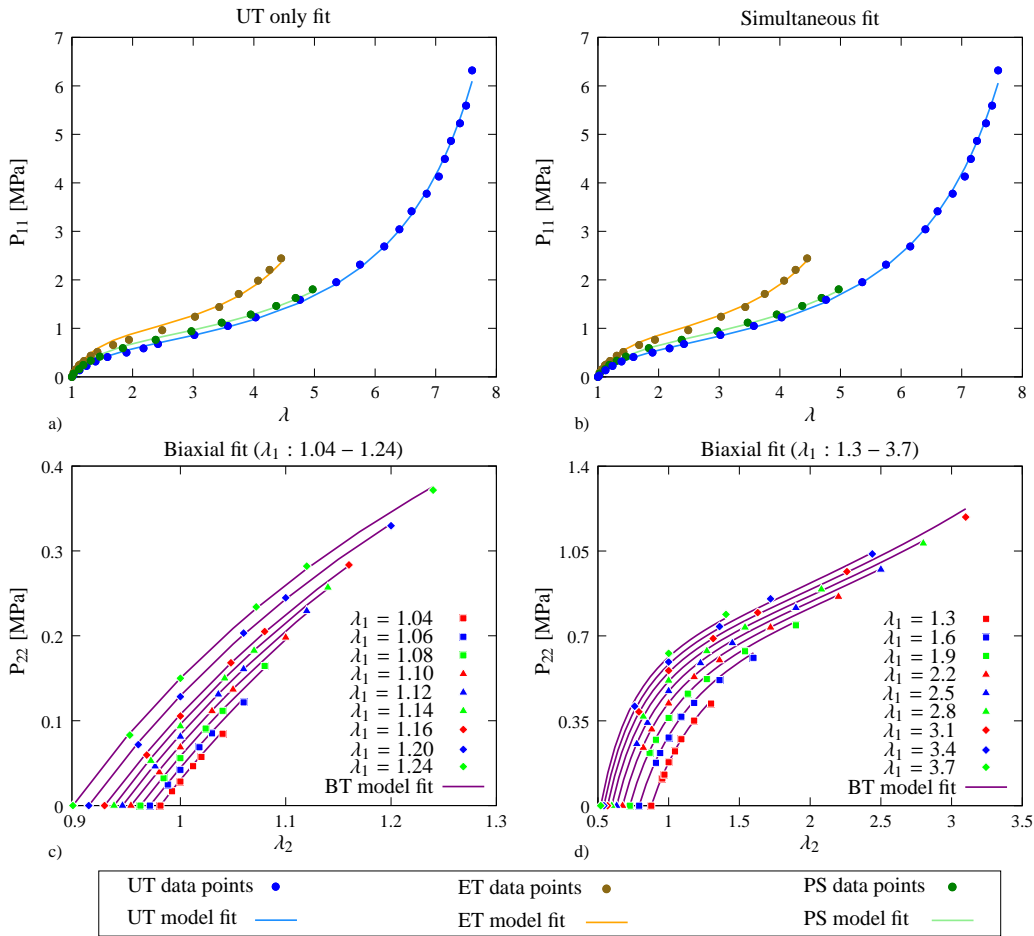


Figure 6.4: Extended-Tube model prediction for a) uniaxial tension, b) combination of uniaxial, equibiaxial, and pure shear loadings using Treloar data c) biaxial tension loading for $\lambda_1 : 1.04-1.24$, d) biaxial tension loading for $\lambda_1 : 1.3-3.7$ using Kawabata data.

Simultaneous fitting (Treloar)					
Parameters	$G_c=0.1933$ [MPa]		$\delta=0.0956$ [MPa]	$G_e=0.1997$	
	$\beta=0.1691$				
			Quality of fit		
	Weight	Error	Region 1	Region 2	Region 3
UT	0.2001	0.1350	0.0025	0.0062	0.0316
ET	0.5999	0.0262	0.0156	0.0376	0.0419
PS	0.2000	0.0031	0.0079	0.0081	0.0099
Total	1.0000	0.1644	0.0260	0.0519	0.0833

Table 6.12: Simultaneous fitting results for Extended-Tube model.

UT only fit (Treloar)					
Parameters	$G_c=0.1813$ [MPa]		$\delta=0.0971$ [MPa]	$G_e=0.2414$	
	$\beta=2.12e - 5$				
			Quality of fit		
	Weight	Error	Region 1	Region 2	Region 3
UT	1	0.1194	0.0088	0.0132	0.0361
ET	0	0.0636	0.0108	0.0714	0.0819
PS	0	0.0094	0.0076	0.0151	0.0178
Total	1	0.1924	0.0272	0.0996	0.1358

Table 6.13: Uniaxial tension results for Extended-Tube model.

Biaxial fit (Kawabata)		
Parameters	$G_c=0.2145$ [MPa]	$\delta=0.0909$ [MPa]
	$G_e=0.1833$	
	$\beta=-0.4109$	
Quality of fit: 0.3362	Biaxial error: 0.0997	

Table 6.14: Biaxial tension results for Extended-Tube model.

6.2.5 Shariff model results

Shariff model with five material parameters estimates the Treloar's data set in simultaneous fitting very well. For the uniaxial results, the obtained parameters can generate S-shape curve, however the parameters cannot be used for equibiaxial and pure shear loadings. It seems that the material model targets Treloar's data set and with other experimental data it should be used with care. Fitting results are graphically given in Figure 6.5 and numerical results for simultaneous, uniaxial and biaxial fittings are given in Tables 6.15, 6.16, and 6.17, respectively.

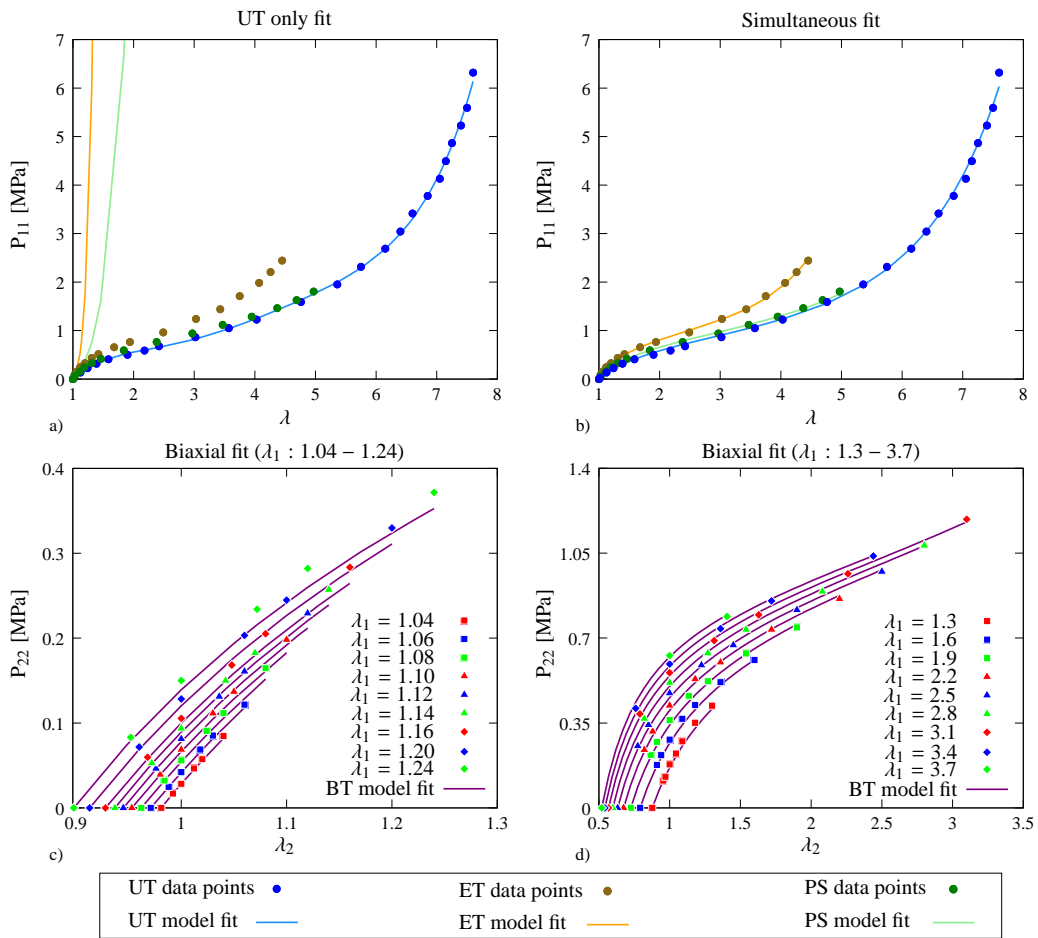


Figure 6.5: Shariff model prediction for a) uniaxial tension, b) combination of uniaxial, equibiaxial, and pure shear loadings using Treloar data c) biaxial tension loading for $\lambda_1 : 1.04 - 1.24$, d) biaxial tension loading for $\lambda_1 : 1.3 - 3.7$ using Kawabata data.

Simultaneous fitting (Treloar)					
Parameters	$E=1.1225$ [MPa]		$\alpha_1=0.9353$	$\alpha_2=0.0377$	
	$\alpha_3=7.93e-5$		$\alpha_4=0.0223$		
			Quality of fit		
	Weight	Error	Region 1	Region 2	Region 3
UT	0.2000	0.1573	0.0124	0.0193	0.0477
ET	0.2000	0.0104	0.0247	0.0291	0.0311
PS	0.6000	0.0065	0.0113	0.0121	0.0150
Total	1.0000	0.1741	0.0484	0.0604	0.0938

Table 6.15: Simultaneous fitting results for Shariff model.

UT only fit (Treloar)					
Parameters	$E=1.2538$ [MPa]		$\alpha_1=-4.1208$	$\alpha_2=0.0545$	
	$\alpha_3=10.5991$		$\alpha_4=-0.3132$		
			Quality of fit		
	Weight	Error	Region 1	Region 2	Region 3
UT	1	0.0952	0.0048	0.0087	0.0276
ET	0	$2.86e6$	1.3102	$5.38e6$	$1.29e10$
PS	0	$4.42e5$	0.5885	808.1882	$2.78e5$
Total	1	$2.86e6$	1.9034	$5.28e6$	$1.29e10$

Table 6.16: Uniaxial tension results for Shariff model.

Biaxial fit (Kawabata)				
Parameters	$E=1.1155$ [MPa]		$\alpha_1=0.8591$	$\alpha_2=0.0879$
	$\alpha_3=8.55e-6$		$\alpha_4=1.04e-4$	
Quality of fit: 0.5179	Biaxial error: 0.1480			

Table 6.17: Biaxial tension results for Shariff model.

6.2.6 Carroll model results

As stated before, Carroll's model is one of the most interesting constitutive hyper-elastic models. With only three material parameters, it approximates experimental data in simultaneous fitting with excellent performance. One may also reach good performance using uniaxial fitting results on the other two experimental data (namely, equibiaxial and pure shear loadings). Fitting results are graphically given in Figure 6.6 and numerical results for simultaneous, uniaxial and biaxial fittings are given in Tables 6.18, 6.19, and 6.20, respectively.

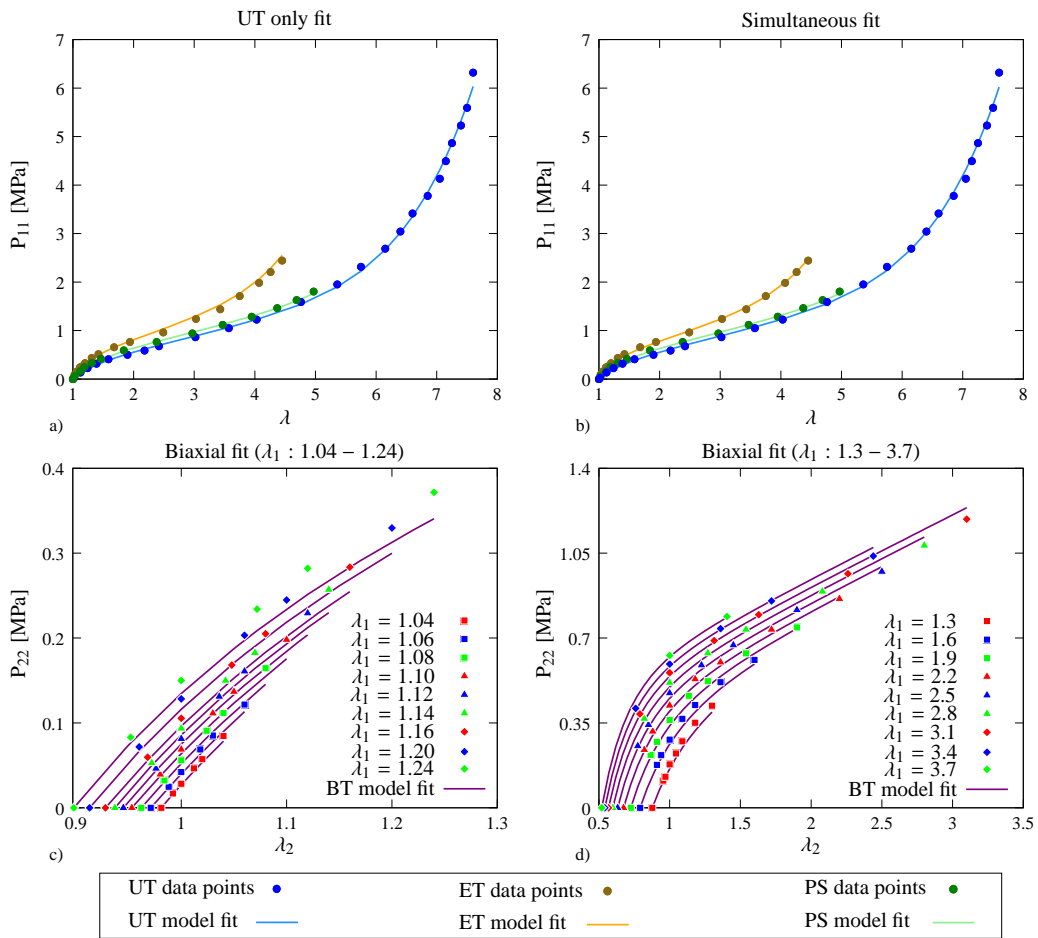


Figure 6.6: Carroll model prediction for a) uniaxial tension, b) combination of uniaxial, equibiaxial, and pure shear loadings using Treloar data c) biaxial tension loading for $\lambda_1 : 1.04 - 1.24$, d) biaxial tension loading for $\lambda_1 : 1.3 - 3.7$ using Kawabata data.

Simultaneous fitting (Treloar)					
Parameters	$A=0.1453$ [MPa]	$B=3.20e-7$ [MPa]	$C=0.1059$ [MPa]		
			Quality of fit		
	Weight	Error	Region 1	Region 2	Region 3
UT	0.3399	0.1660	0.0119	0.0152	0.0473
ET	0.3301	0.0130	0.0359	0.0464	0.0476
PS	0.3300	0.0068	0.0200	0.0223	0.0238
Total	1.0000	0.1858	0.0679	0.0839	0.1188

Table 6.18: Simultaneous fitting results for Carroll model.

UT only fit (Treloar)					
Parameters	$A=0.1431$ [MPa]	$B=3.23e-7$ [MPa]	$C=0.1265$ [MPa]		
			Quality of fit		
	Weight	Error	Region 1	Region 2	Region 3
UT	1	0.1650	0.0099	0.0131	0.0462
ET	0	0.0491	0.0304	0.0394	0.0598
PS	0	0.0057	0.0166	0.0177	0.0169
Total	1	0.2199	0.0569	0.0703	0.1256

Table 6.19: Uniaxial tension results for Carroll model.

Biaxial fit (Kawabata)			
Parameters	$A=0.1470$ [MPa]	$B=7.26e-14$ [MPa]	$C=0.1057$ [MPa]
Quality of fit: 0.7148	Biaxial error: 0.2315		

Table 6.20: Biaxial tension results for Carroll model.

6.2.7 Network averaging tube model results

With four material parameters and physically interpretable parameter sets, network averaging tube model results are in good agreement with Treloar's data set in simultaneous fitting. For the uniaxial tension also well estimations are reached. However using the parameter values in uniaxial tension can fit the equibiaxial and pure shear only in low stretch values. Fitting results are graphically given in Figure 6.7 and numerical results for simultaneous, uniaxial and biaxial fittings are given in Tables 6.21, 6.22, and 6.23, respectively.

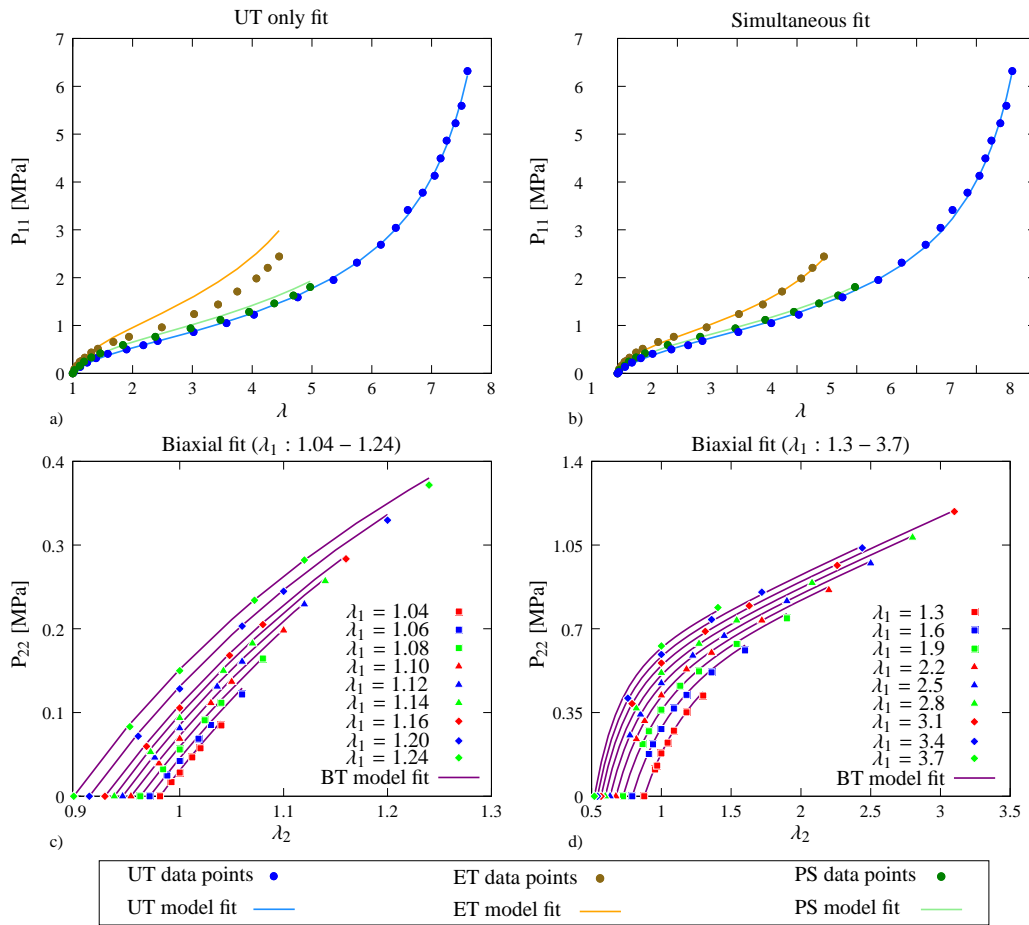


Figure 6.7: Network averaging tube model prediction for a) uniaxial tension, b) combination of uniaxial, equibiaxial, and pure shear loadings using Treloar data c) biaxial tension loading for $\lambda_1 : 1.04 - 1.24$, d) biaxial tension loading for $\lambda_1 : 1.3 - 3.7$ using Kawabata data.

Simultaneous fitting (Treloar)					
Parameters	$\mu_c k=0.0894$ [MPa] $n=21.0753$ $q=0.9518$				
	$\mu_i=0.1709$ [MPa]				
	Quality of fit				
	Weight	Error	Region 1	Region 2	Region 3
UT	0.1000	0.1177	0.0137	0.0184	0.0455
ET	0.8000	0.0207	0.0402	0.0573	0.0606
PS	0.1000	0.0104	0.0232	0.0274	0.0305
Total	1.0000	0.1489	0.0770	0.1031	0.1366

Table 6.21: Simultaneous fitting results network averaging tube model.

UT only fit (Treloar)					
Parameters	$\mu_c k=0.0673$ [MPa] $n=29.9998$ $q=1.0550$				
	$\mu_i=0.3904$ [MPa]				
	Quality of fit				
	Weight	Error	Region 1	Region 2	Region 3
UT	1	0.0684	0.0097	0.0129	0.0269
ET	0	1.5464	0.0215	0.1614	0.9384
PS	0	0.0734	0.0130	0.0142	0.0635
Total	1	1.6883	0.0442	0.1885	1.0287

Table 6.22: Uniaxial tension results network averaging tube model.

Biaxial fit (Kawabata)	
Parameters	$\mu_c k=0.1226$ [MPa] $n=27.8739$ $q=0.8318$
	$\mu_i=0.1875$ [MPa]
Quality of fit: 0.3918	Biaxial error: 0.1160

Table 6.23: Biaxial tension results network averaging tube model.

6.2.8 Chevalier and Marco model results

Chevalier and Marco’s model with six material parameter are found to have well suiting results in simultaneous fitting. That is due to the existence of second invariant term governing the moderate to high stretch ranges. In uniaxial tension fitting alone, fitting performance is also good, but the obtained parameters cannot generate equibiaxial and pure shear curves. Fitting results are graphically given in Figure 6.8 and numerical results for simultaneous, uniaxial and biaxial fittings are given in Tables 6.24, 6.25, and 6.26, respectively.

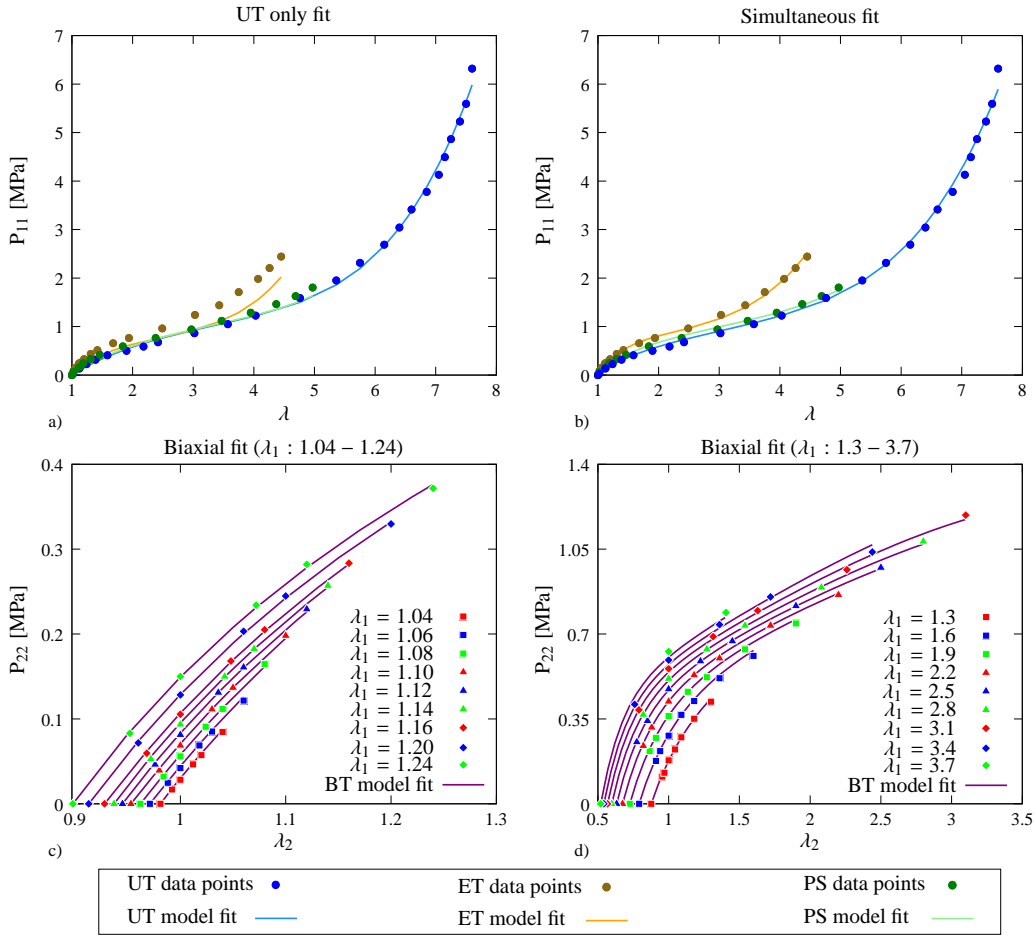


Figure 6.8: Chevalier and Marco’s model prediction for a) uniaxial tension, b) combination of uniaxial, equibiaxial, and pure shear loadings using Treloar data c) biaxial tension loading for $\lambda_1 : 1.04 - 1.24$, d) biaxial tension loading for $\lambda_1 : 1.3 - 3.7$ using Kawabata data.

Simultaneous fitting (Treloar)					
Parameters	$a_0=0.1585$ [MPa]	$a_1=-0.0023$ [MPa]	$a_2=1.18e-4$ [MPa]		
	$b_0=0.0020$ [MPa]	$b_1=0.2266$ [MPa]	$b_2=-0.4902$ [MPa]		
		Quality of fit			
	Weight	Error	Region 1	Region 2	Region 3
UT	0.3226	0.3114	0.0161	0.0255	0.0834
ET	0.5643	0.0236	0.0290	0.0324	0.0428
PS	0.1131	0.0108	0.0138	0.0174	0.0221
Total	1.0000	0.3458	0.0588	0.0753	0.1482

Table 6.24: Simultaneous fitting results for Chevalier and Marco model.

UT only fit (Treloar)					
Parameters	$a_0=0.1850$ [MPa]	$a_1=-0.0041$ [MPa]	$a_2=1.45e-4$ [MPa]		
	$b_0=6.40e-7$ [MPa]	$b_1=2.25e-6$ [MPa]	$b_2=-0.4149$ [MPa]		
		Quality of fit			
	Weight	Error	Region 1	Region 2	Region 3
UT	1	0.2481	0.0416	0.0592	0.1070
ET	0	1.0966	0.1295	0.3545	0.8649
PS	0	0.0917	0.0736	0.0932	0.1350
Total	1	1.4364	0.2447	0.5069	1.1069

Table 6.25: Uniaxial tension results for Chevalier and Marco model.

Biaxial fit (Kawabata)			
Parameters	$a_0=0.1647$ [MPa]	$a_1=-0.0041$ [MPa]	$a_2=-1.65e-7$ [MPa]
	$b_0=0.0083$ [MPa]	$b_1=0.1110$ [MPa]	$b_2=-0.1110$ [MPa]
Quality of fit: 0.3777	Biaxial error: 0.1180		

Table 6.26: Biaxial tension results for Chevalier and Marco model.

6.2.9 Ogden model results

Ogden model with six material parameters demonstrates well agreement in simultaneous fitting using Treloar’s data set. Uniaxial fitting results also estimate the material response in good manner. However, obtained parameters through uniaxial fitting can be used for pure shear throughout the curve and may be used to generate equibiaxial curve in low stretch values. Fitting results are graphically given in Figure 6.9 and numerical results for simultaneous, uniaxial and biaxial fittings are given in Tables 6.27, 6.28, and 6.29, respectively.

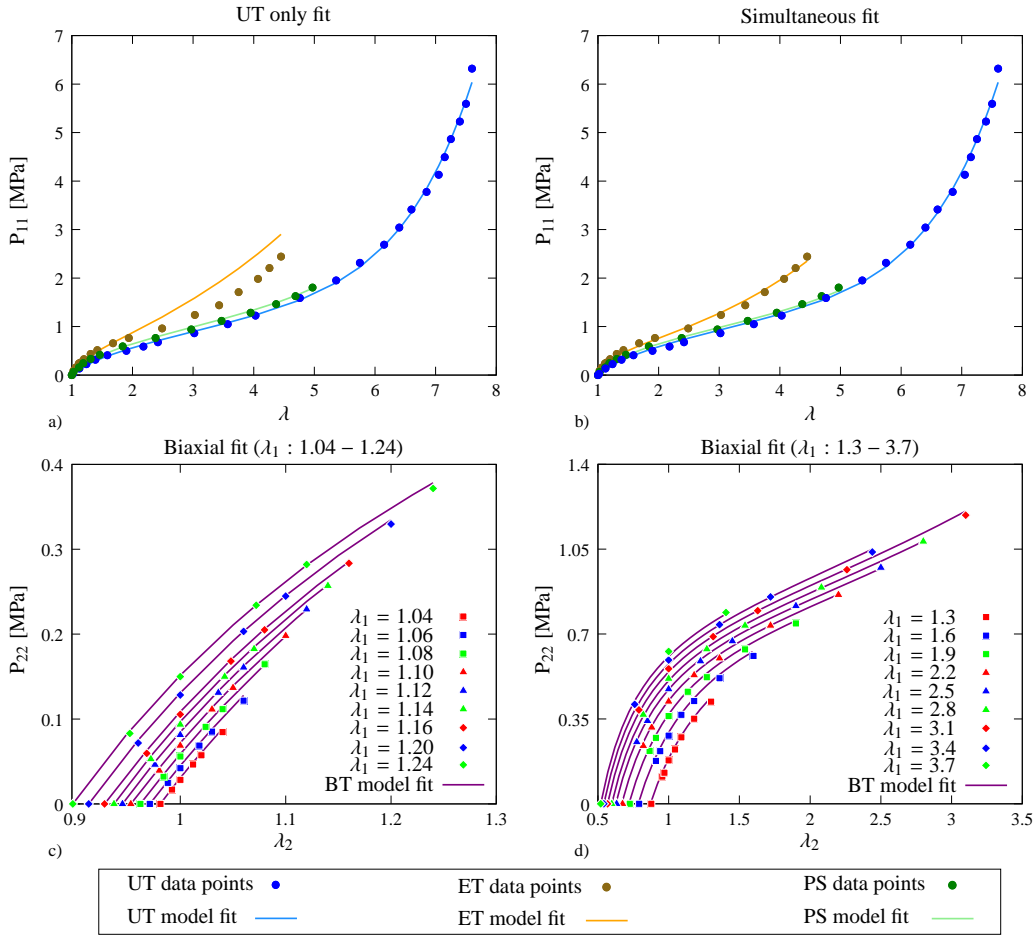


Figure 6.9: Ogden model prediction for a) uniaxial tension, b) combination of uniaxial, equibiaxial, and pure shear loadings using Treloar data c) biaxial tension loading for $\lambda_1 : 1.04 - 1.24$, d) biaxial tension loading for $\lambda_1 : 1.3 - 3.7$ using Kawabata data.

Simultaneous fitting (Treloar)					
Parameters	$\mu_1=0.3640$ [MPa]	$\mu_2=2.71e-6$ [MPa]	$\mu_3=-0.0166$ [MPa]		
	$\alpha_1=1.8729$	$\alpha_2=7.9910$	$\alpha_3=-1.8446$		
	Quality of fit				
	Weight	Error	Region 1	Region 2	Region 3
UT	0.3333	0.1720	0.0161	0.0320	0.0631
ET	0.3334	0.0423	0.0371	0.0593	0.0736
PS	0.3333	0.0106	0.0177	0.0190	0.0237
Total	1.0000	0.2249	0.0709	0.1103	0.1604

Table 6.27: Simultaneous fitting results for Ogden model.

UT only fit (Treloar)					
Parameters	$\mu_1=0.2981$ [MPa]	$\mu_2=2.68e-6$ [MPa]	$\mu_3=-0.0776$ [MPa]		
	$\alpha_1=1.9738$	$\alpha_2=7.9898$	$\alpha_3=-1.5005$		
	Quality of fit				
	Weight	Error	Region 1	Region 2	Region 3
UT	1	0.1649	0.0121	0.0173	0.0500
ET	0	1.3745	0.0360	0.1064	0.8319
PS	0	0.0093	0.0194	0.0211	0.0258
Total	1	1.5487	0.0675	0.1449	0.9077

Table 6.28: Uniaxial tension results for Ogden model.

Biaxial fit (Kawabata)			
Parameters	$\mu_1=0.5805$ [MPa]	$\mu_2=0.0057$ [MPa]	$\mu_3=-0.0170$ [MPa]
	$\alpha_1=1.2928$	$\alpha_2=4.0643$	$\alpha_3=-1.6429$
Quality of fit: 0.3128	Biaxial error: 0.0874		

Table 6.29: Biaxial tension results for Ogden model.

6.2.10 Amin model results

Amin model with six material constants represents a good agreement during the simultaneous fitting. Combination of first invariant and a first order second invariant terms force the model to make S-turn and catch the material response curve at moderate stretch values. The uniaxial fitting yields also a good estimation, however the obtained parameters cannot be used to generate equibiaxial and pure shear results. Fitting results are graphically given in Figure 6.10 and numerical results for simultaneous, uniaxial and biaxial fittings are given in Tables 6.30, 6.31, and 6.32, respectively.

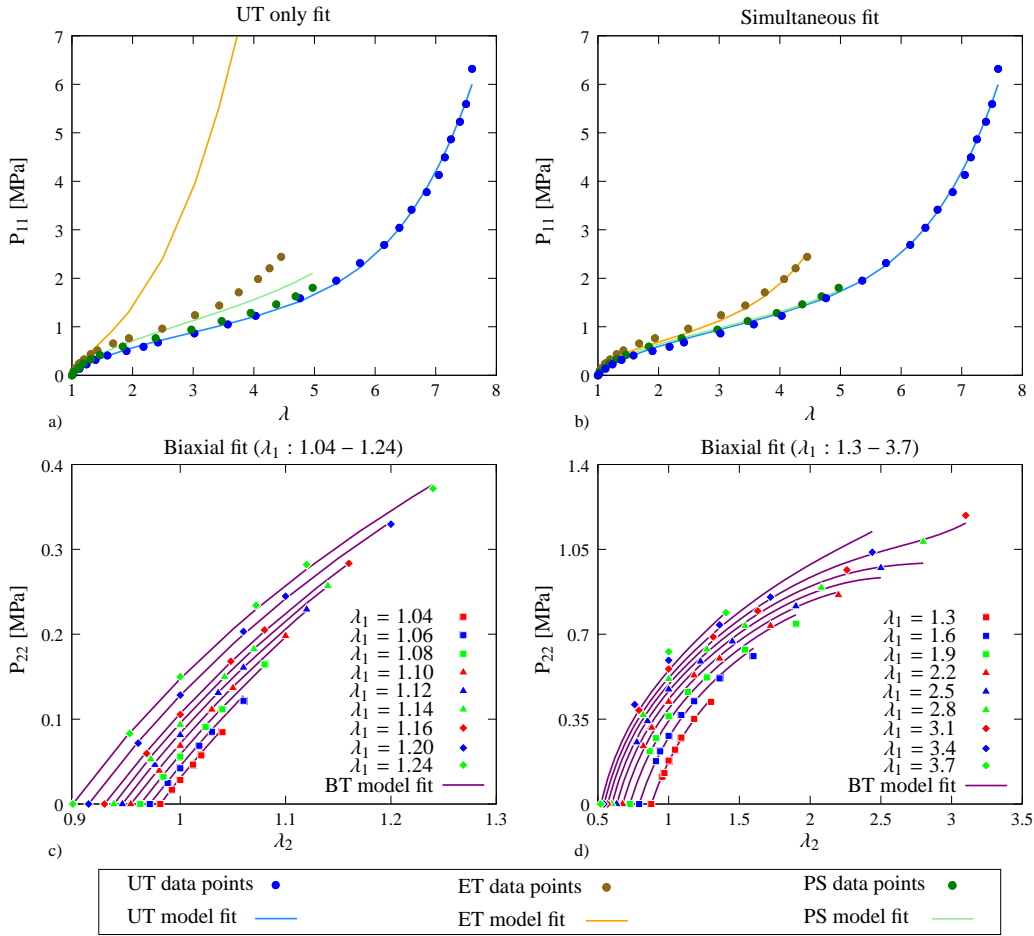


Figure 6.10: Amin model prediction for a) uniaxial tension, b) combination of uniaxial, equibiaxial, and pure shear loadings using Treloar data c) biaxial tension loading for $\lambda_1 : 1.04 - 1.24$, d) biaxial tension loading for $\lambda_1 : 1.3 - 3.7$ using Kawabata data.

Simultaneous fitting (Treloar)					
Parameters	$C_2=0.0027$ [MPa]	$C_3=2.80e-6$ [MPa]	$C_4=-94.7144$ [MPa]		
	$C_5=94.8875$ [MPa]	$M=6.64e-5$	$N=2.8413$		
			Quality of fit		
	Weight	Error	Region 1	Region 2	Region 3
UT	0.3406	0.1940	0.0159	0.0395	0.0708
ET	0.3739	0.0664	0.0220	0.0796	0.0969
PS	0.2855	0.0060	0.0073	0.0079	0.0108
Total	1.0000	0.2663	0.0452	0.1270	0.1785

Table 6.30: Simultaneous fitting results for Amin model.

UT only fit (Treloar)					
Parameters	$C_2=0.0558$ [MPa]	$C_3=6.24e-6$ [MPa]	$C_4=-4.24e-5$ [MPa]		
	$C_5=0.1340$ [MPa]	$M=1.3400$	$N=2.6573$		
			Quality of fit		
	Weight	Error	Region 1	Region 2	Region 3
UT	1	0.1905	0.0075	0.0126	0.0504
ET	0	258.4332	0.0182	2.6720	127.9011
PS	0	0.4059	0.0096	0.0293	0.3047
Total	1	259.0296	0.0352	2.7139	128.2562

Table 6.31: Uniaxial tension results for Amin model.

Biaxial fit (Kawabata)			
Parameters	$C_2=0.0187$ [MPa]	$C_3=8.78e-7$ [MPa]	$C_4=-0.0053$ [MPa]
	$C_5=0.1827$ [MPa]	$M=1.3915$	$N=4.1112$
Quality of fit: 0.8870	Biaxial error: 0.4078		

Table 6.32: Biaxial tension results for Amin model.

6.2.11 James model results

James model with five material constants predicts the material response curve in simultaneous fitting pretty well. For uniaxial loading case, response is also good, however the obtained parameter values cannot be used for equibiaxial and pure shear loadings. Estimation of Kawabata's biaxial data deviates from the actual response curve at high stretch values. Fitting results are graphically given in Figure 6.11 and numerical results for simultaneous, uniaxial and biaxial fittings are given in Tables 6.33, 6.34, and 6.35, respectively.

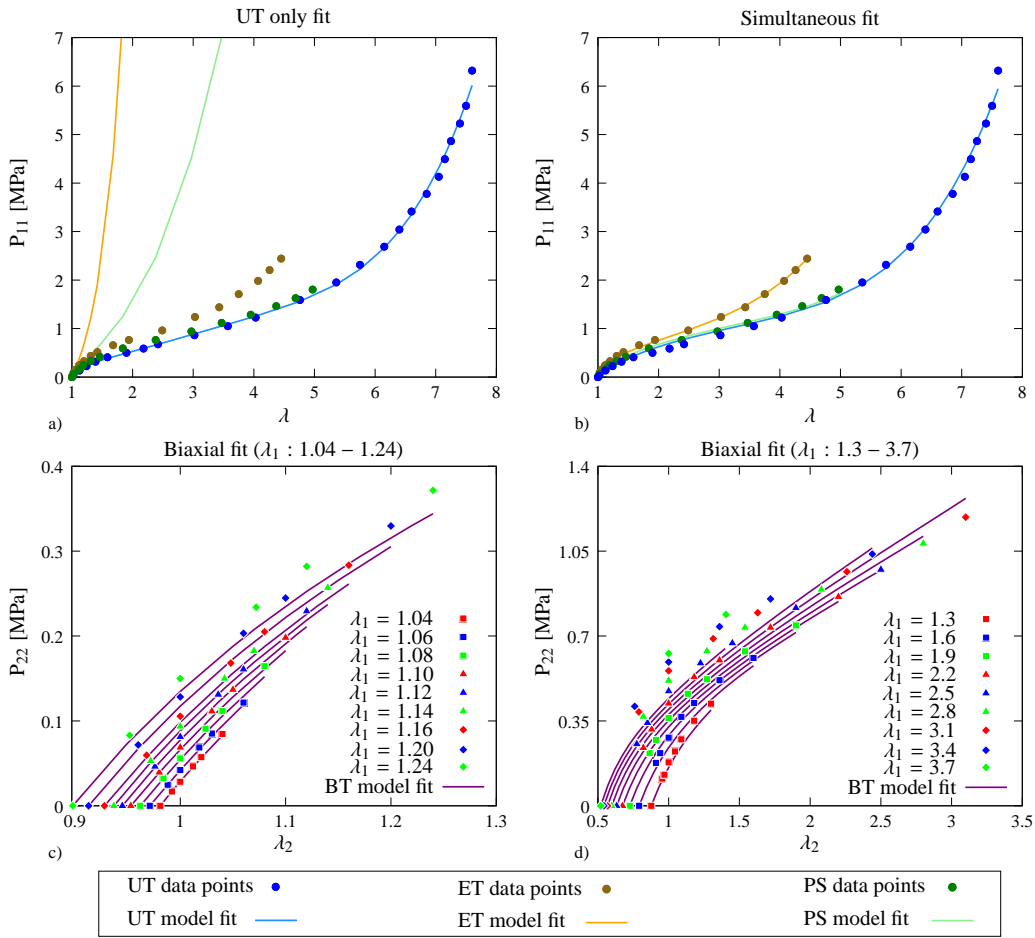


Figure 6.11: James model prediction for a) uniaxial tension, b) combination of uniaxial, equibiaxial, and pure shear loadings using Treloar data c) biaxial tension loading for $\lambda_1 : 1.04 - 1.24$, d) biaxial tension loading for $\lambda_1 : 1.3 - 3.7$ using Kawabata data.

Simultaneous fitting (Treloar)					
Parameters	$C_{10}=0.1827$ [MPa]	$C_{01}=0.0069$ [MPa]	$C_{11}=-8.40e-5$ [MPa]		
	$C_{20}=-0.0018$ [MPa]	$C_{30}=4.55e-5$ [MPa]			
	Quality of fit				
	Weight	Error	Region 1	Region 2	Region 3
UT	0.4397	0.2839	0.0376	0.0723	0.1186
ET	0.3978	0.0105	0.0252	0.0358	0.0366
PS	0.1625	0.0213	0.0098	0.0142	0.0256
Total	1.0000	0.3156	0.0726	0.1224	0.1808

Table 6.33: Simultaneous fitting results for James model.

UT only fit (Treloar)					
Parameters	$C_{10}=-0.0752$ [MPa]	$C_{01}=0.3226$ [MPa]	$C_{11}=0.0477$ [MPa]		
	$C_{20}=-0.0108$ [MPa]	$C_{30}=7.57e-5$ [MPa]			
	Quality of fit				
	Weight	Error	Region 1	Region 2	Region 3
UT	1	0.1740	0.0027	0.0064	0.0414
ET	0	$6.42e5$	0.2206	$1.06e3$	$2.99e5$
PS	0	860.3650	0.0837	4.7287	549.6365
Total	1	$6.43e5$	0.3070	$1.06e3$	$3.00e5$

Table 6.34: Uniaxial tension results for James model.

Biaxial fit (Kawabata)			
Parameters	$C_{10}=0.1827$ [MPa]	$C_{01}=0.0069$ [MPa]	$C_{11}=-8.40e-5$ [MPa]
	$C_{20}=-0.0018$ [MPa]	$C_{30}=4.55e-5$ [MPa]	
Quality of fit: 0.3900	Biaxial error: 0.1385		

Table 6.35: Biaxial tension results for James model.

6.2.12 Haines-Wilson model results

Haines-Wilson model with six material constants also has a good agreement with experimental data in simultaneous fitting. Uniaxial fitting results can also perfectly generate S-shape. However, obtained results for uniaxial fitting cannot be used to estimate equibiaxial and pure shear responses. Estimation of Kawabata's biaxial data shows good response especially in low stretch values. Fitting results are graphically given in Figure 6.12 and numerical results for simultaneous, uniaxial and biaxial fittings are given in Tables 6.36, 6.37, and 6.38, respectively.

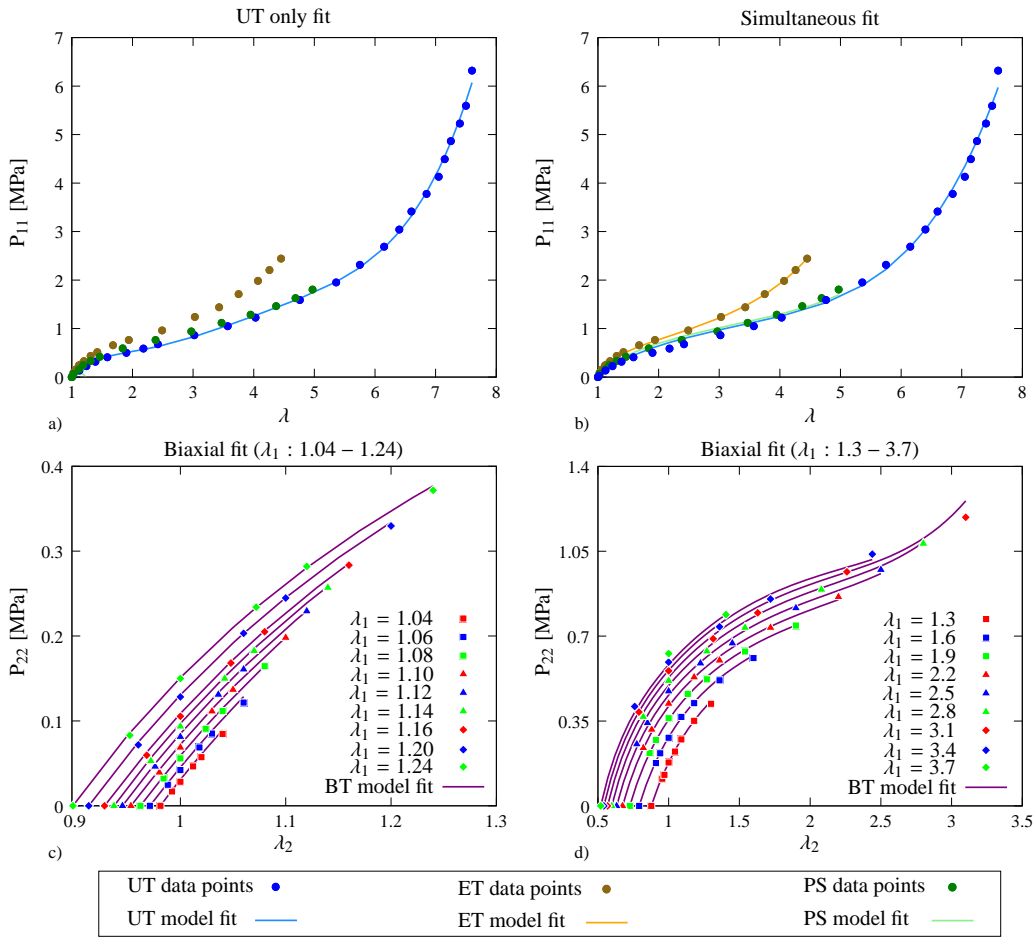


Figure 6.12: Haines-Wilson model prediction for a) uniaxial tension, b) combination of uniaxial, equibiaxial, and pure shear loadings using Treloar data c) biaxial tension loading for $\lambda_1 : 1.04-1.24$, d) biaxial tension loading for $\lambda_1 : 1.3-3.7$ using Kawabata data.

Simultaneous fitting (Treloar)					
Parameters	$C_{10}=0.1883$ [MPa]	$C_{01}=0.0070$ [MPa]	$C_{11}=-8.60e-5$ [MPa]		
	$C_{02}=0.2.30e-7$ [MPa]	$C_{20}=-0.0021$ [MPa]	$C_{30}=4.82e-5$ [MPa]		
		Quality of fit			
	Weight	Error	Region 1	Region 2	Region 3
UT	0.7994	0.2809	0.0522	0.0981	0.1425
ET	0.1005	0.0061	0.0202	0.0247	0.0253
PS	0.1001	0.0332	0.0079	0.0175	0.0349
Total	1.0000	0.3202	0.0803	0.1403	0.2027

Table 6.36: Simultaneous fitting results for Haines and Wilson model.

UT only fit (Treloar)					
Parameters	$C_{10}=0.8030$ [MPa]	$C_{01}=-0.6734$ [MPa]	$C_{11}=0.1719$ [MPa]		
	$C_{02}=-0.4665$ [MPa]	$C_{20}=-0.0302$ [MPa]	$C_{30}=1.28e-4$ [MPa]		
		Quality of fit			
	Weight	Error	Region 1	Region 2	Region 3
UT	1	0.1318	0.0072	0.0141	0.0392
ET	0	7.55e9	2.3391	1.00e6	3.38e9
PS	0	5.27e4	0.7942	205.072	3.35e4
Total	1	7.55e9	3.1405	1.00e6	3.38e9

Table 6.37: Uniaxial tension results for Haines and Wilson model.

Biaxial fit (Kawabata)			
Parameters	$C_{10}=0.1699$ [MPa]	$C_{01}=0.0324$ [MPa]	$C_{11}=-0.0024$ [MPa]
	$C_{02}=7.58e-10$ [MPa]	$C_{20}=-0.0072$ [MPa]	$C_{30}=7.01e-4$ [MPa]
Quality of fit: 0.3902	Biaxial error: 0.1385		

Table 6.38: Biaxial tension results for Haines and Wilson model.

6.2.13 Attard and Hunt model results

Attard and Hunt model with six material constants generates the material response curve in simultaneous fitting pretty well. The uniaxial fitting results are also in good agreement with Treloar’s uniaxial data. However, the results obtained through uniaxial data fitting cannot be used to estimate equibiaxial and pure shear loadings. Estimation of Kawabata’s biaxial data shows good response in low stretch values. Fitting results are graphically given in Figure 6.13 and numerical results for simultaneous, uniaxial and biaxial fittings are given in Tables 6.39, 6.40, and 6.41, respectively.

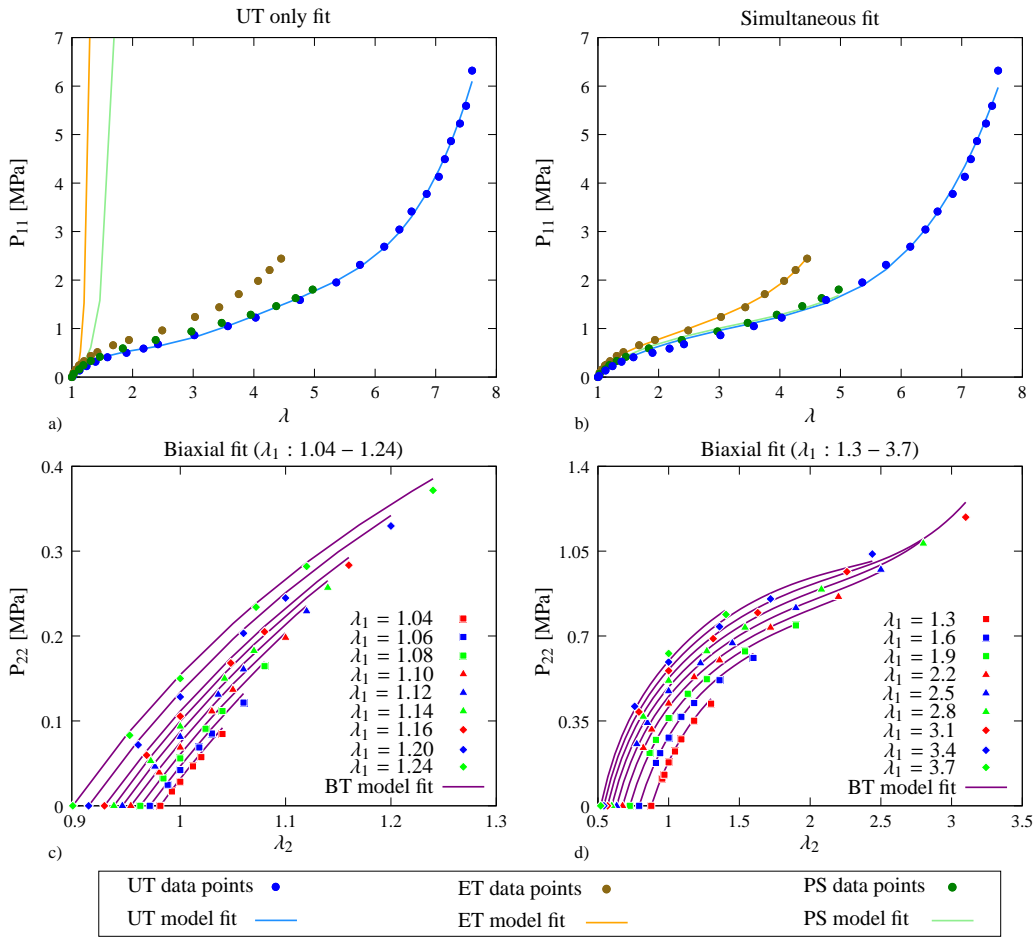


Figure 6.13: Attard and Hunt model prediction for a) uniaxial tension, b) combination of uniaxial, equibiaxial, and pure shear loadings using Treloar data c) biaxial tension loading for $\lambda_1 : 1.04-1.24$, d) biaxial tension loading for $\lambda_1 : 1.3-3.7$ using Kawabata data.

Simultaneous fitting (Treloar)					
Parameters	$A_1=0.3959$ [MPa]	$A_2=-0.0097$ [MPa]	$A_3=2.84e-4$ [MPa]		
	$B_1=0.0088$ [MPa]	$B_2=-5.62e-11$ [MPa]	$B_3=2.04e-8$ [MPa]		
		Quality of fit			
	Weight	Error	Region 1	Region 2	Region 3
UT	0.8000	0.2726	0.0429	0.0794	0.1249
ET	0.1000	0.0084	0.0217	0.0271	0.0285
PS	0.1000	0.0356	0.0085	0.0155	0.0347
Total	1.0000	0.3166	0.0731	0.1220	0.1881

Table 6.39: Simultaneous fitting results for Attard and Hunt model.

UT only fit (Treloar)					
Parameters	$A_1=0.3849$ [MPa]	$A_2=-0.1763$ [MPa]	$A_3=9.46e-4$ [MPa]		
	$B_1=6.0338$ [MPa]	$B_2=-5.2236$ [MPa]	$B_3=1.5626$ [MPa]		
		Quality of fit			
	Weight	Error	Region 1	Region 2	Region 3
UT	1	0.1220	0.0093	0.0170	0.0404
ET	0	$6.82e14$	0.3329	$1.11e9$	$2.95e14$
PS	0	$3.21e7$	0.2470	$4.98e3$	$1.94e7$
Total	1	$6.82e14$	0.5892	$1.11e9$	$2.95e14$

Table 6.40: Uniaxial tension results for Attard and Hunt model.

Biaxial fit (Kawabata)			
Parameters	$A_1=0.5017$ [MPa]	$A_2=-0.0564$ [MPa]	$A_3=0.0042$ [MPa]
	$B_1=0.0160$ [MPa]	$B_2=-9.46e-5$ [MPa]	$B_3=-1.74e-7$ [MPa]
Quality of fit: 0.4162	Biaxial error: 0.1397		

Table 6.41: Biaxial tension results for Attard and Hunt model.

6.2.14 4-term Bechir model results

Four term Bechir model with four material parameters demonstrates well agreement in simultaneous fitting using Treloar’s data set. Uniaxial fitting results also estimate the material response in good manner. However, obtained parameters through uniaxial fitting can be used for pure shear throughout the curve and may be used to generate equibiaxial curve in low stretch values. Fitting results are graphically given in Figure 6.14 and numerical results for simultaneous, uniaxial and biaxial fittings are given in Tables 6.42, 6.43, and 6.44, respectively.

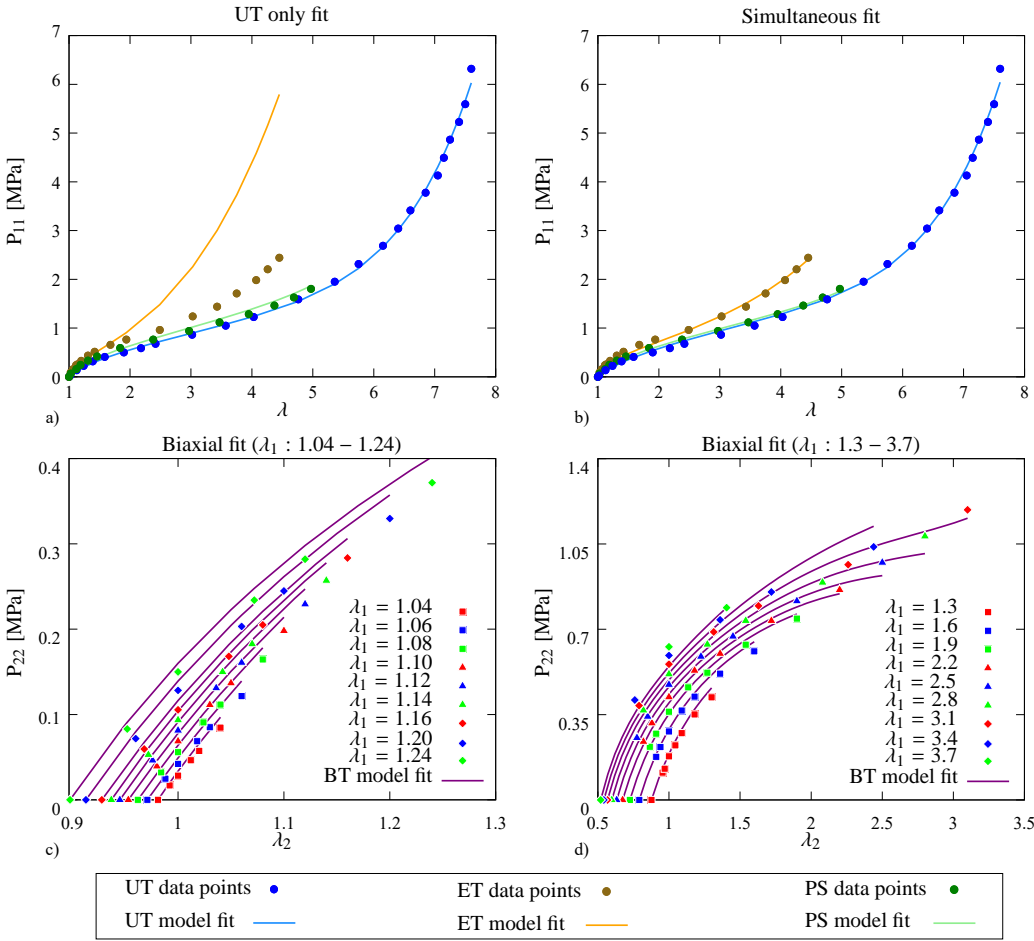


Figure 6.14: Bechir model prediction for a) uniaxial tension, b) combination of uniaxial, equibiaxial, and pure shear loadings using Treloar data c) biaxial tension loading for $\lambda_1 : 1.04 - 1.24$, d) biaxial tension loading for $\lambda_1 : 1.3 - 3.7$ using Kawabata data.

Simultaneous fitting (Treloar)					
Parameters	$C_1^1=0.1806$ [MPa]	$C_2^1=0.0024$ [MPa]	$C_1^2=-0.0027$ [MPa]		
	$C_2^2=3.47e-7$ [MPa]				
	Quality of fit				
	Weight	Error	Region 1	Region 2	Region 3
UT	0.1000	0.1731	0.0195	0.0444	0.0729
ET	0.8000	0.0435	0.0504	0.1011	0.1061
PS	0.1000	0.0121	0.0261	0.0299	0.0341
Total	1.0000	0.2287	0.0960	0.1754	0.2130

Table 6.42: Simultaneous fitting results for 4-term Bechir model.

UT only fit (Treloar)					
Parameters	$C_1^1=0.2200$ [MPa]	$C_2^1=0.0123$ [MPa]	$C_1^2=-0.0123$ [MPa]		
	$C_2^2=3.30e-7$ [MPa]				
	Quality of fit				
	Weight	Error	Region 1	Region 2	Region 3
UT	1	0.1628	0.0154	0.0197	0.0518
ET	0	34.5427	0.0434	0.3612	17.2239
PS	0	0.0379	0.0250	0.0285	0.0523
Total	1	34.7433	0.0838	0.4093	17.3280

Table 6.43: Uniaxial tension results for 4-term Bechir model.

Biaxial fit (Kawabata)			
Parameters	$C_1^1=0.2635$ [MPa]	$C_2^1=0.0020$ [MPa]	$C_1^2=-0.0107$ [MPa]
	$C_2^2=9.05e-6$ [MPa]		
Quality of fit: 0.8961	Biaxial error: 0.4033		

Table 6.44: Biaxial tension results for 4-term Bechir model.

6.2.15 Pucci and Saccomandi model results

Pucci and Saccomandi model with three material parameters generate reasonable results for simultaneous fitting. There observed some under estimation of equibiaxial data. Uniaxial fitting performance of the model is also good and the obtained parameter values can be used to estimate the other two curves. Biaxial fitting results however, deviate from the data points at high stretch values. Fitting results are graphically given in Figure 6.15 and numerical results for simultaneous, uniaxial and biaxial fittings are given in Tables 6.45, 6.46, and 6.47, respectively.

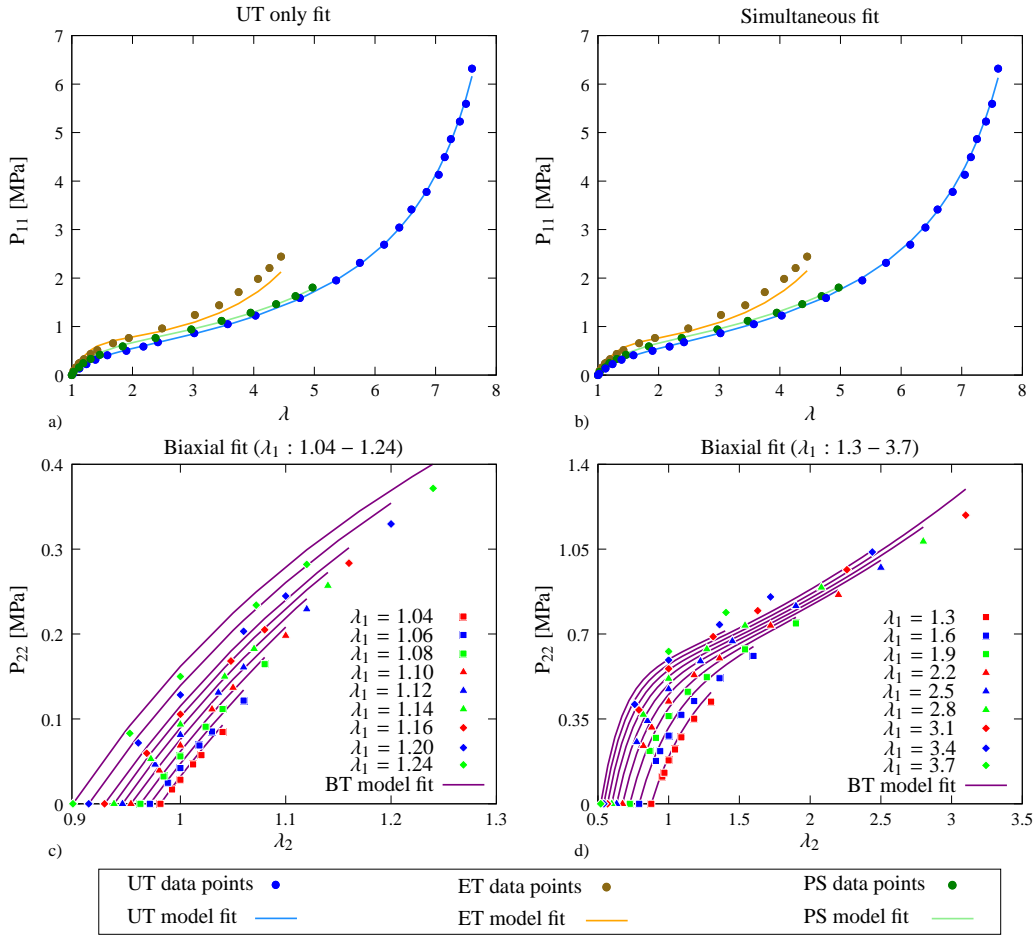


Figure 6.15: Pucci and Saccomandi's model prediction for a) uniaxial tension, b) combination of uniaxial, equibiaxial, and pure shear loadings using Treloar data c) biaxial tension loading for $\lambda_1 : 1.04 - 1.24$, d) biaxial tension loading for $\lambda_1 : 1.3 - 3.7$ using Kawabata data.

Simultaneous fitting (Treloar)					
Parameters	$C_2=0.2575$ [MPa] $\mu=0.2466$ [MPa] $J_m=82.3593$				
	Weight	Error	Quality of fit		
			Region 1	Region 2	Region 3
UT	0.1000	0.0977	0.0011	0.0018	0.0225
ET	0.8000	0.3235	0.0114	0.0334	0.1922
PS	0.1000	0.0028	0.0068	0.0090	0.0097
Total	1.0000	0.4240	0.0193	0.0441	0.2243

Table 6.45: Simultaneous fitting results for Pucci and Saccomandi model.

UT only fit (Treloar)					
Parameters	$C_2=0.2995$ [MPa] $\mu=0.2374$ [MPa] $J_m=80.9372$				
	Weight	Error	Quality of fit		
			Region 1	Region 2	Region 3
UT	1	0.0732	0.0014	0.0021	0.0168
ET	0	0.3878	0.0138	0.0603	0.2450
PS	0	0.0060	0.0095	0.0156	0.0166
Total	1	0.4670	0.0248	0.0780	0.2784

Table 6.46: Uniaxial tension results for Pucci and Saccomandi model.

Biaxial fit (Kawabata)	
Parameters	$C_2=0.1490$ [MPa] $\mu=0.3186$ [MPa] $J_m=93.5851$
Quality of fit: 0.8167	Biaxial error: 0.3922

Table 6.47: Biaxial tension results for Pucci and Saccomandi model.

6.2.16 Biderman model results

Biderman model with four material parameters generate reasonable results for simultaneous fitting. There observed some under estimation of equibiaxial data in moderate stretch values. Uniaxial fitting performance of the model is also good and the obtained parameter values can be used to estimate the pure shear only. Biaxial fitting results however, deviate from the data points at high stretch values. Fitting results are graphically given in Figure 6.16 and numerical results for simultaneous, uniaxial and biaxial fittings are given in Tables 6.48, 6.49, and 6.50, respectively.

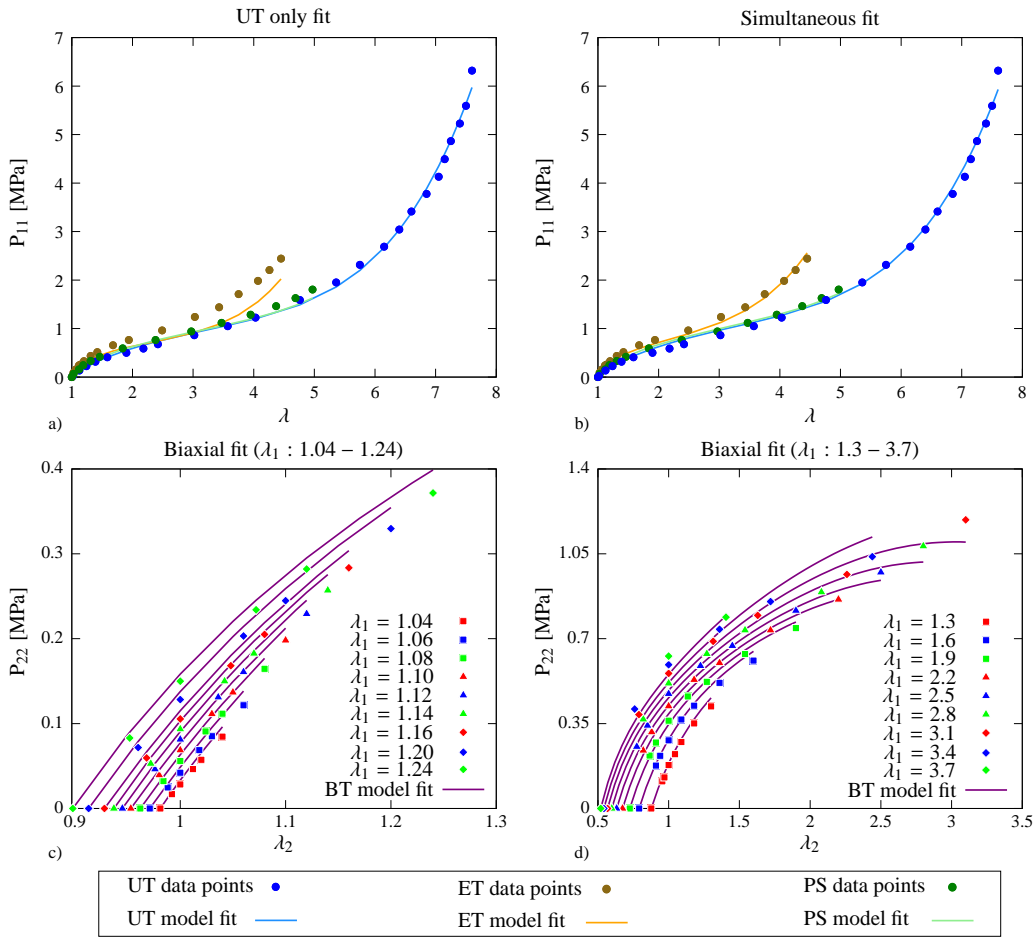


Figure 6.16: Biderman model prediction for a) uniaxial tension, b) combination of uniaxial, equibiaxial, and pure shear loadings using Treloar data c) biaxial tension loading for $\lambda_1 : 1.04-1.24$, d) biaxial tension loading for $\lambda_1 : 1.3-3.7$ using Kawabata data.

Simultaneous fitting (Treloar)					
Parameters	$C_{10}=0.1846$ [MPa]	$C_{01}=0.0029$ [MPa]	$C_{20}=-0.0018$ [MPa]		
	$C_{30}=4.50e-5$ [MPa]				
		Quality of fit			
	Weight	Error	Region 1	Region 2	Region 3
UT	0.2000	0.2958	0.0380	0.0764	0.1237
ET	0.6000	0.0632	0.0281	0.0592	0.0825
PS	0.2000	0.0167	0.0109	0.0139	0.0228
Total	1.0000	0.3757	0.0770	0.1496	0.2289

Table 6.48: Simultaneous fitting results for Biderman model.

UT only fit (Treloar)					
Parameters	$C_{10}=0.1763$ [MPa]	$C_{01}=6.16e-6$ [MPa]	$C_{20}=-0.0019$ [MPa]		
	$C_{30}=4.64e-5$ [MPa]				
		Quality of fit			
	Weight	Error	Region 1	Region 2	Region 3
UT	1	0.2530	0.0191	0.0353	0.0847
ET	0	1.0601	0.0427	0.1675	0.6946
PS	0	0.0864	0.0194	0.0213	0.0738
Total	1	1.3994	0.0812	0.2241	0.8531

Table 6.49: Uniaxial tension results for Biderman model.

Biaxial fit (Kawabata)			
Parameters	$C_{10}=0.2012$ [MPa]	$C_{01}=0.0182$ [MPa]	$C_{20}=-0.0073$ [MPa]
	$C_{30}=4.89e-5$ [MPa]		
Quality of fit: 0.9973	Biaxial error: 0.4505		

Table 6.50: Biaxial tension results for Biderman model.

6.2.17 Kilian (van der Waals) model results

Van der Waals model with four material parameters generate reasonable results for simultaneous fitting. There observed some under estimation of equibiaxial data in moderate stretch values. Uniaxial fitting performance of the model is also good but the obtained parameter values cannot be used to estimate the other two curves. Biaxial fitting results however, deviate from the data points at high stretch values. Fitting results are graphically given in Figure 6.17 and numerical results for simultaneous, uniaxial and biaxial fittings are given in Tables 6.51, 6.52, and 6.53, respectively.

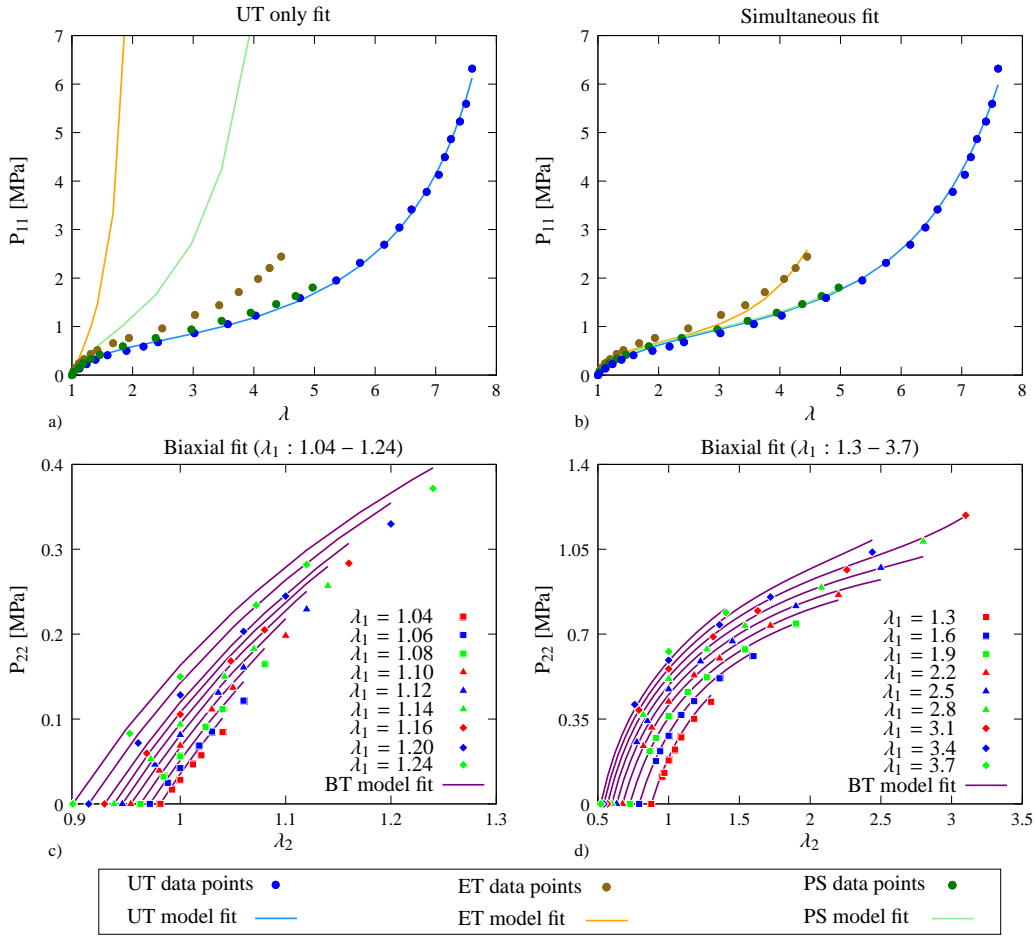


Figure 6.17: Kilian (van der Waals) model prediction for a) uniaxial tension, b) combination of uniaxial, equibiaxial, and pure shear loadings using Treloar data c) biaxial tension loading for $\lambda_1 : 1.04 - 1.24$, d) biaxial tension loading for $\lambda_1 : 1.3 - 3.7$ using Kawabata data.

Simultaneous fitting (Treloar)					
Parameters	$G=0.4064$ [MPa] $\lambda_m=10.5473$ $\beta=0.0079$ $a=0.2871$				
			Quality of fit		
	Weight	Error	Region 1	Region 2	Region 3
UT	0.1000	0.2259	0.0301	0.0568	0.0940
ET	0.8000	0.1392	0.0187	0.0783	0.1378
PS	0.1000	0.0029	0.0068	0.0074	0.0087
Total	1.0000	0.3680	0.0556	0.1425	0.2404

Table 6.51: Simultaneous fitting results for Kilian (van der Waals) model.

UT only fit (Treloar)					
Parameters	$G=0.5180$ [MPa] $\lambda_m=5.2143$ $\beta=0.8704$ $a=0.2000$				
			Quality of fit		
	Weight	Error	Region 1	Region 2	Region 3
UT	1	0.1067	0.0306	0.0347	0.0540
ET	0	4.16e4	0.1644	2.91e3	2.16e4
PS	0	7.32e3	0.0981	1.5550	4.12e3
Total	1	4.89e4	0.2931	2.91e3	2.57e4

Table 6.52: Uniaxial tension results for Kilian (van der Waals) model.

Biaxial fit (Kawabata)	
Parameters	$G=0.4705$ [MPa] $\lambda_m=12.0009$ $\beta=0.1481$ $a=0.3864$
Quality of fit: 0.5409	Biaxial error: 0.2064

Table 6.53: Biaxial tension results for Kilian (van der Waals) model.

6.2.18 Yamashita and Kawabata model results

Yamashita and Kawabata model with four material parameters generate reasonable results for simultaneous fitting. There observed some under estimation of equibiaxial data in low stretch values. Uniaxial fitting performance of the model is also good and the obtained parameter values can be used to estimate the pure shear only. Biaxial fitting results however, deviate from the data points at high stretch values. Fitting results are graphically given in Figure 6.18 and numerical results for simultaneous, uniaxial and biaxial fittings are given in Tables 6.54, 6.55, and 6.56, respectively.

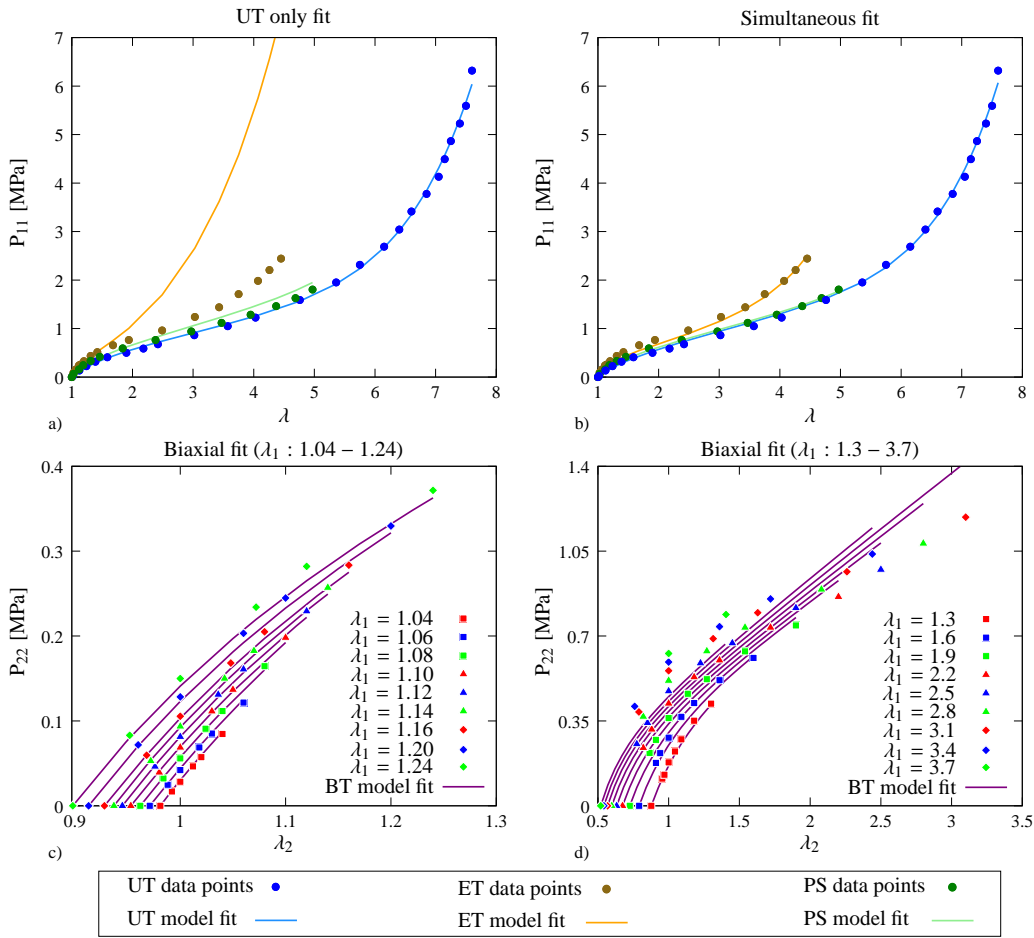


Figure 6.18: Yamashita and Kawabata's model prediction for a) uniaxial tension, b) combination of uniaxial, equibiaxial, and pure shear loadings using Treloar data c) biaxial tension loading for $\lambda_1 : 1.04 - 1.24$, d) biaxial tension loading for $\lambda_1 : 1.3 - 3.7$ using Kawabata data.

Simultaneous fitting (Treloar)					
Parameters	$C_2=0.0028$ [MPa] $C_3=05.62e - 7$ [MPa] $C_5=0.1620$ [MPa]				
	$N=3.2327$				
			Quality of fit		
	Weight	Error	Region 1	Region 2	Region 3
UT	0.1000	0.1580	0.0212	0.0499	0.0745
ET	0.8000	0.0745	0.0594	0.1453	0.1550
PS	0.1000	0.0135	0.0326	0.0397	0.0428
Total	1.0000	0.2460	0.1131	0.2350	0.2723

Table 6.54: Simultaneous fitting results for Yamashita and Kawabata model.

UT only fit (Treloar)					
Parameters	$C_2=0.0312$ [MPa] $C_3=1.91e - 6$ [MPa] $C_5=0.1466$ [MPa]				
	$N=2.9372$				
			Quality of fit		
	Weight	Error	Region 1	Region 2	Region 3
UT	1	0.1630	0.0126	0.0218	0.0525
ET	0	74.0959	0.0326	0.6845	36.5417
PS	0	0.1225	0.0175	0.0220	0.1066
Total	1	74.3814	0.0627	0.7284	36.7009

Table 6.55: Uniaxial tension results for Yamashita and Kawabata model.

Biaxial fit (Kawabata)	
Parameters	$C_2=0.0034$ [MPa] $C_3=7.59e - 25$ [MPa] $C_5=0.1966$ [MPa]
	$N=9.3826$
Quality of fit: 4.7639	Biaxial error: 2.3165

Table 6.56: Biaxial tension results for Yamashita and Kawabata model.

6.2.19 Lion model results

Lion model with three material parameters generate reasonable results for simultaneous fitting. There observed some over estimation of uniaxial data in low stretch values. Uniaxial fitting performance of the model is also good and the obtained parameter values can be used to estimate the pure shear only. Biaxial fitting results however, deviate from the data points at high stretch values. Fitting results are graphically given in Figure 6.19 and numerical results for simultaneous, uniaxial and biaxial fittings are given in Tables 6.57, 6.58, and 6.59, respectively.

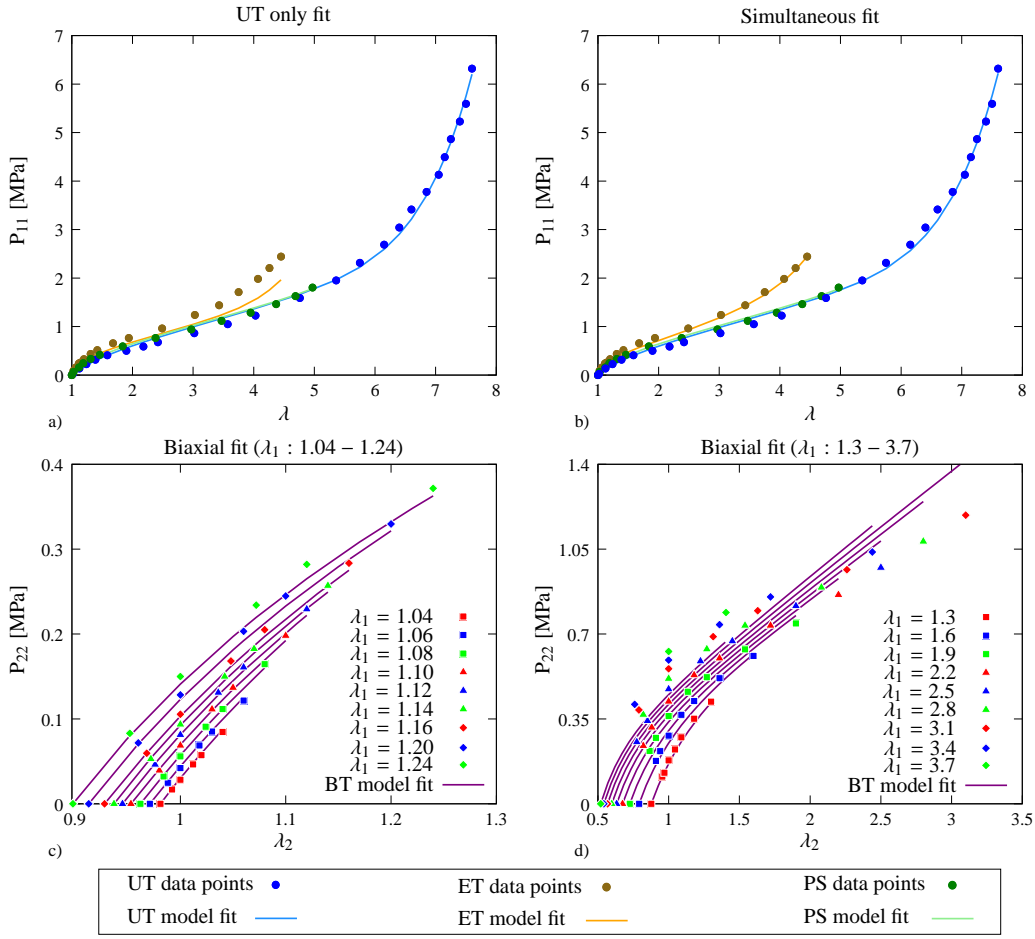


Figure 6.19: Lion model prediction for a) uniaxial tension, b) combination of uniaxial, equibiaxial, and pure shear loadings using Treloar data c) biaxial tension loading for $\lambda_1 : 1.04 - 1.24$, d) biaxial tension loading for $\lambda_1 : 1.3 - 3.7$ using Kawabata data.

Simultaneous fitting (Treloar)					
Parameters	$C_{10}=0.1689$ [MPa]	$C_{01}=0.0029$ [MPa]	$C_{03}=5.26e - 9$ [MPa]		
	Quality of fit				
	Weight	Error	Region 1	Region 2	Region 3
UT	0.1008	0.2453	0.0245	0.0871	0.1354
ET	0.7992	0.0448	0.0480	0.1007	0.1054
PS	0.1000	0.0245	0.0237	0.0268	0.0427
Total	1.0000	0.3146	0.0961	0.2146	0.2835

Table 6.57: Simultaneous fitting results for Lion model.

UT only fit (Treloar)					
Parameters	$C_{10}=0.1724$ [MPa]	$C_{01}=9.62e - 5$ [MPa]	$C_{03}=5.17e - 9$ [MPa]		
	Quality of fit				
	Weight	Error	Region 1	Region 2	Region 3
UT	1	0.2348	0.0277	0.1099	0.1469
ET	0	0.8370	0.0479	0.1245	0.5140
PS	0	0.0268	0.0229	0.0261	0.0440
Total	1	1.0985	0.0985	0.2605	0.7048

Table 6.58: Uniaxial tension results for Lion model.

Biaxial fit (Kawabata)			
Parameters	$C_{10}=0.1966$ [MPa]	$C_{01}=0.0034$ [MPa]	$C_{03}=2.00e - 15$ [MPa]
Quality of fit: 4.7639	Biaxial error: 2.3165		

Table 6.59: Biaxial tension results for Lion model.

6.2.20 Beda model results

Beda model with four material constants generate reasonable results for simultaneous fitting. There observed some under estimation of equibiaxial data in high stretch values. Uniaxial fitting performance of the model is also good and the obtained parameter values can be used to estimate the pure shear only. Biaxial fitting results however, deviate from the data points at high stretch values. Fitting results are graphically given in Figure 6.20 and numerical results for simultaneous, uniaxial and biaxial fittings are given in Tables 6.60, 6.61, and 6.62, respectively.

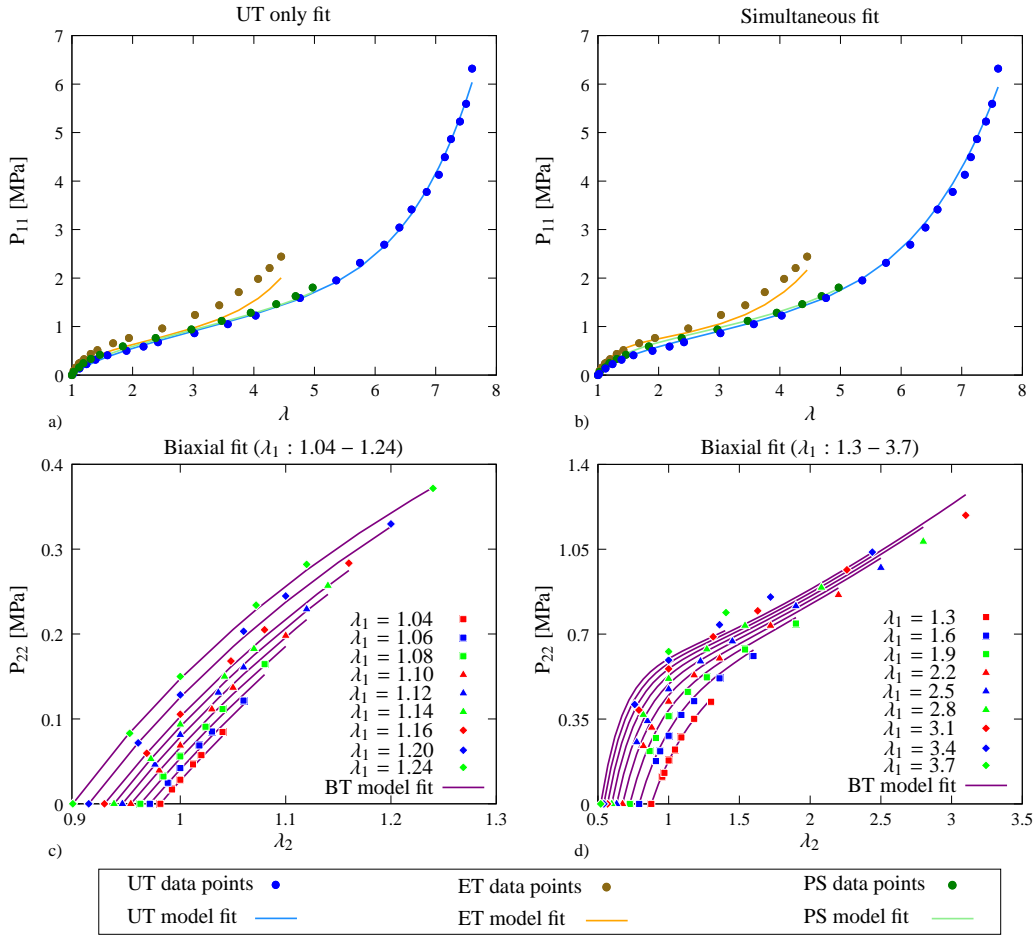


Figure 6.20: Beda's model prediction for a) uniaxial tension, b) combination of uniaxial, equibiaxial, and pure shear loadings using Treloar data c) biaxial tension loading for $\lambda_1 : 1.04 - 1.24$, d) biaxial tension loading for $\lambda_1 : 1.3 - 3.7$ using Kawabata data.

Simultaneous fitting (Treloar)					
Parameters	$C_{10} = 0.1455$ [MPa] $B = 1.12e - 5$ [MPa] $K = 0.1816$ [MPa] $\alpha = 3.4920$				
			Quality of fit		
	Weight	Error	Region 1	Region 2	Region 3
UT	0.1000	0.3097	0.0108	0.0192	0.0818
ET	0.8000	0.3793	0.0114	0.0250	0.2212
PS	0.1000	0.0043	0.0067	0.0109	0.0120
Total	1.0000	0.6933	0.0289	0.0550	0.3150

Table 6.60: Simultaneous fitting results for Beda model.

UT only fit (Treloar)					
Parameters	$C_{10} = 0.1554$ [MPa] $B = 1.04e - 6$ [MPa] $K = 0.0162$ [MPa] $\alpha = 4.0841$				
			Quality of fit		
	Weight	Error	Region 1	Region 2	Region 3
UT	1	0.1532	0.0227	0.0303	0.0596
ET	0	0.9476	0.0661	0.2192	0.6595
PS	0	0.0338	0.0391	0.0540	0.0653
Total	1	1.1346	0.1279	0.3035	0.7844

Table 6.61: Uniaxial tension results for Beda model.

Biaxial fit (Kawabata)	
Parameters	$C_{10} = 0.1209$ [MPa] $B = 0.0290$ [MPa] $K = 0.1503$ [MPa] $\alpha = 1.3124$
Quality of fit: 0.7338	Biaxial error: 0.3370

Table 6.62: Biaxial tension results for Beda model.

6.2.21 Hart-Smith model results

Hart-Smith model with three material constants generate reasonable results for simultaneous fitting. There observed some under estimation of equibiaxial data in high stretches. Uniaxial fitting performance is also good and the obtained parameter values can be used to estimate the pure shear and equibiaxial data in low stretches. Biaxial fitting results however, deviate from the data points at high stretch values. Fitting results are graphically given in Figure 6.21 and numerical results for simultaneous, uniaxial and biaxial fittings are given in Tables 6.63, 6.64, and 6.65, respectively.

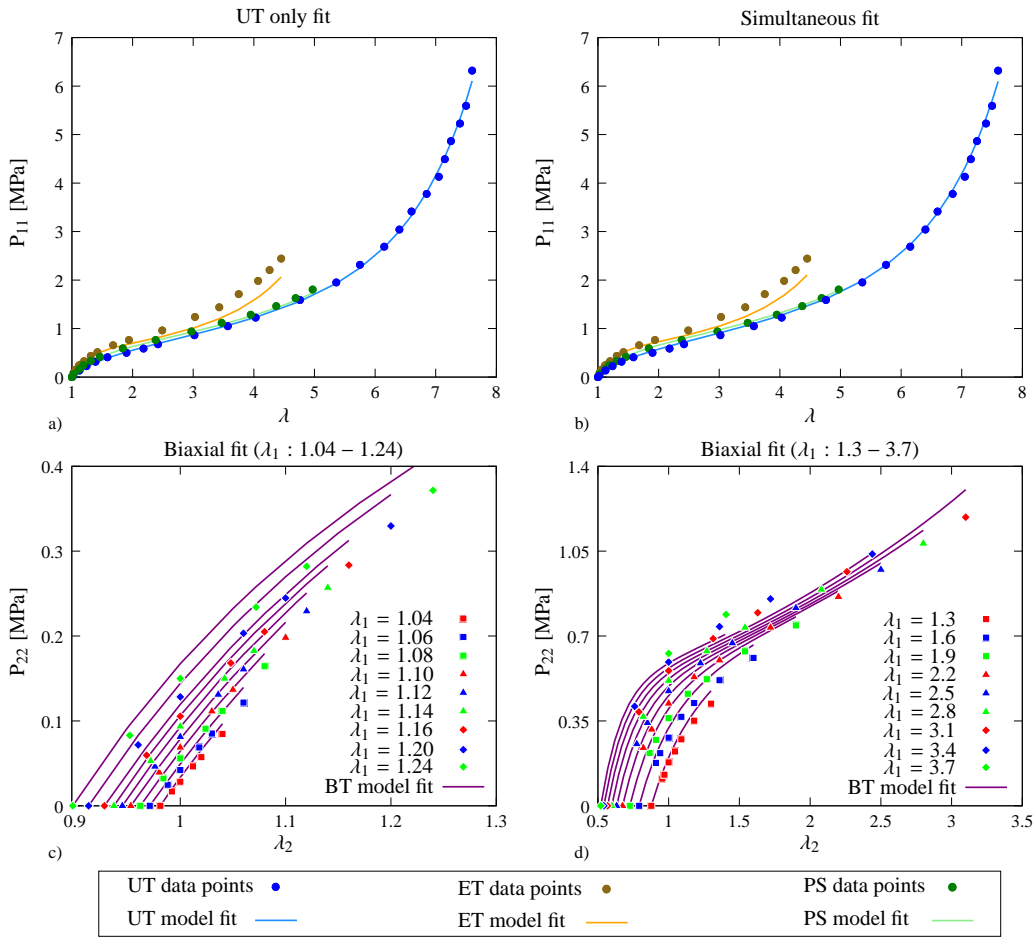


Figure 6.21: Hart-Smith model prediction for a) uniaxial tension, b) combination of uniaxial, equibiaxial, and pure shear loadings using Treloar data c) biaxial tension loading for $\lambda_1 : 1.04-1.24$, d) biaxial tension loading for $\lambda_1 : 1.3-3.7$ using Kawabata data.

Simultaneous fitting (Treloar)					
Parameters	$G=0.1466$ [MPa] $k_1=3.32e-4$ $k_2=1.0465$				
	Weight	Error	Quality of fit		
			Region 1	Region 2	Region 3
UT	0.0500	0.1376	0.0084	0.0191	0.0441
ET	0.8999	0.4679	0.0148	0.0283	0.2638
PS	0.0501	0.0025	0.0074	0.0083	0.0094
Total	1.0000	0.6080	0.0306	0.0557	0.3173

Table 6.63: Simultaneous fitting results for Hart-Smith model.

UT only fit (Treloar)					
Parameters	$G=0.1414$ [MPa] $k_1=3.44e-4$ $k_2=1.0057$				
	Weight	Error	Quality of fit		
			Region 1	Region 2	Region 3
UT	1	0.1071	0.0056	0.0070	0.0285
ET	0	0.6335	0.0210	0.0522	0.3688
PS	0	0.0132	0.0109	0.0116	0.0190
Total	1	0.7538	0.0375	0.0708	0.4163

Table 6.64: Uniaxial tension results for Hart-Smith model.

Biaxial fit (Kawabata)			
Parameters	$G=0.1694$ [MPa] $k_1=5.42e-4$ $k_2=0.8559$		
Quality of fit: 0.9457	Biaxial error: 0.4570		

Table 6.65: Biaxial tension results for Hart-Smith model.

6.2.22 Haupt and Sedlan model results

Haupt and Sedlan model with five material parameters generate reasonable results for simultaneous fitting. Uniaxial fitting performance of the model is also good but the obtained parameter values cannot be used to estimate the other two curves. Biaxial fitting results however, deviate from the data points at high stretch values. Fitting results are graphically given in Figure 6.22 and numerical results for simultaneous, uniaxial and biaxial fittings are given in Tables 6.66, 6.67, and 6.68, respectively.

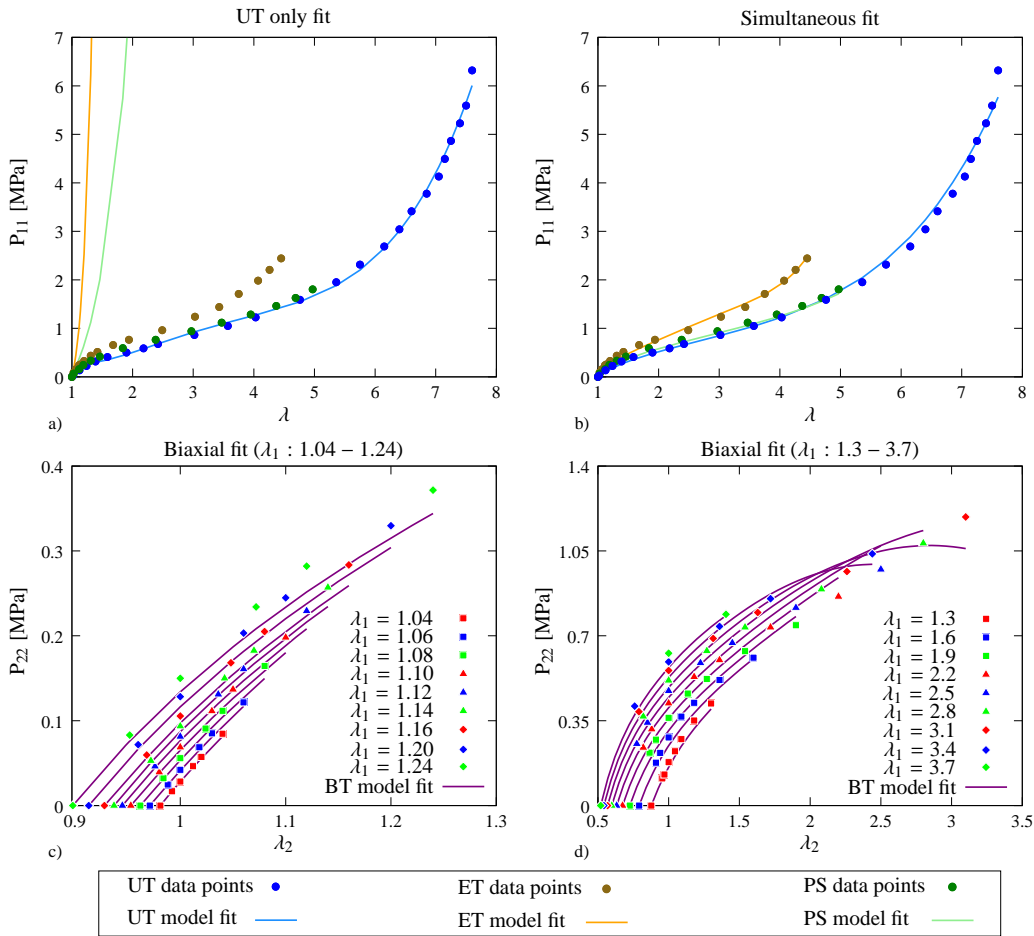


Figure 6.22: Haupt and Sedlan's model prediction for a) uniaxial tension, b) combination of uniaxial, equibiaxial, and pure shear loadings using Treloar data c) biaxial tension loading for $\lambda_1 : 1.04 - 1.24$, d) biaxial tension loading for $\lambda_1 : 1.3 - 3.7$ using Kawabata data.

Simultaneous fitting (Treloar)					
Parameters	$c_1=0.1405$ [MPa]	$c_2=0.0175$ [MPa]	$c_3=-6.45e-4$ [MPa]		
	$c_4=2.58e-5$ [MPa]	$c_5=2.75e-5$ [MPa]			
		Quality of fit			
	Weight	Error	Region 1	Region 2	Region 3
UT	0.3748	0.5919	0.0318	0.0326	0.1623
ET	0.4086	0.0515	0.0664	0.1209	0.1292
PS	0.2166	0.0450	0.0435	0.0638	0.0812
Total	1.0000	0.6885	0.1418	.02174	0.3727

Table 6.66: Simultaneous fitting results for Haupt and Sedlan model.

UT only fit (Treloar)					
Parameters	$c_1=-1.0379$ [MPa]	$c_2=1.4591$ [MPa]	$c_3=-0.0276$ [MPa]		
	$c_4=0.4103$ [MPa]	$c_5=5.06e-5$ [MPa]			
		Quality of fit			
	Weight	Error	Region 1	Region 2	Region 3
UT	1	0.2135	0.0581	0.0709	0.1121
ET	0	$6.17e9$	7.5754	$9.30e5$	$2.76e9$
PS	0	$7.76e4$	2.7533	337.6778	$4.94e4$
Total	1	$6.17e9$	10.3869	$9.30e5$	$2.76e9$

Table 6.67: Uniaxial tension results for Haupt and Sedlan model.

Biaxial fit (Kawabata)			
Parameters	$c_1=0.1746$ [MPa]	$c_2=0.0110$ [MPa]	$c_3=2.04e-9$ [MPa]
	$c_4=-6.71e-5$ [MPa]	$c_5=7.82e-6$ [MPa]	
Quality of fit: 1.6340	Biaxial error: 0.7082		

Table 6.68: Biaxial tension results for Haupt and Sedlan model.

6.2.23 Exp-Ln model results

Exp-Ln model with three material constants generate reasonable results for simultaneous fitting. Here, the lack of I_2 term in the strain energy function makes the model not suitable for simultaneous fitting. Uniaxial fitting performance of the model is reasonable but the obtained parameter values cannot be used for the other two experiments. Biaxial fitting results deviate from the data points at high stretch values. Fitting results are graphically given in Figure 6.23 and numerical results for simultaneous, uniaxial and biaxial fittings are given in Tables 6.69, 6.70, and 6.71, respectively.

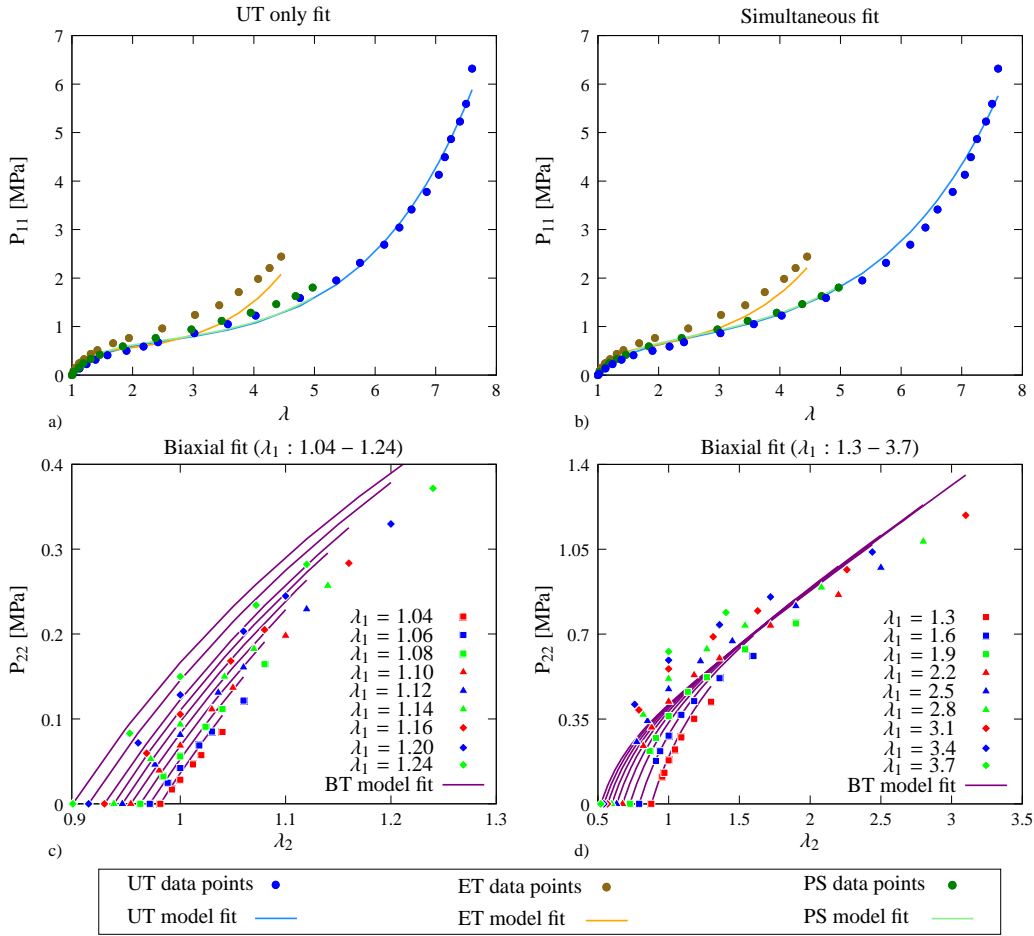


Figure 6.23: Exp-Ln model prediction for a) uniaxial tension, b) combination of uniaxial, equibiaxial, and pure shear loadings using Treloar data c) biaxial tension loading for $\lambda_1 : 1.04 - 1.24$, d) biaxial tension loading for $\lambda_1 : 1.3 - 3.7$ using Kawabata data.

Simultaneous fitting (Treloar)					
Parameters	$A=0.2182$ [MPa]	$a=0.0169$	$b=0.1978$ [MPa]		
	Quality of fit				
	Weight	Error	Region 1	Region 2	Region 3
UT	0.1000	0.7728	0.0477	0.0613	0.2409
ET	0.8000	0.4299	0.0090	0.1005	0.3069
PS	0.1000	0.0081	0.0087	0.0126	0.0168
Total	1.0000	1.2108	0.0654	0.1744	0.5647

Table 6.69: Simultaneous fitting results for Exp-Ln model.

UT only fit (Treloar)					
Parameters	$A=0.2239$ [MPa]	$a=0.0184$	$b=0.2532$ [MPa]		
	Quality of fit				
	Weight	Error	Region 1	Region 2	Region 3
UT	1	0.4099	0.0323	0.0856	0.1539
ET	0	1.1058	0.0076	0.1973	0.7470
PS	0	0.2528	0.0103	0.0197	0.1984
Total	1	1.7685	0.0502	0.3026	1.0993

Table 6.70: Uniaxial tension results for Exp-Ln model.

Biaxial fit (Kawabata)			
Parameters	$A=0.2393$ [MPa]	$a=5.63e-9$	$b=0.0299$ [MPa]
Quality of fit: 5.4195	Biaxial error: 2.5200		

Table 6.71: Biaxial tension results for Exp-Ln model.

6.2.24 Yeoh model results

Yeoh model captures the S-curve for individual loading cases, however, for simultaneous fitting it underestimates the equibiaxial and pure shear curves. This is due to the absence of second invariant terms in the strain energy function. Uniaxial fitting performance of the model is reasonable but the obtained parameter values cannot be used for the other two experiments. Fitting results are graphically given in Figure 6.24 and numerical results for simultaneous, uniaxial and biaxial fittings are given in Tables 6.72, 6.73, and 6.74, respectively.

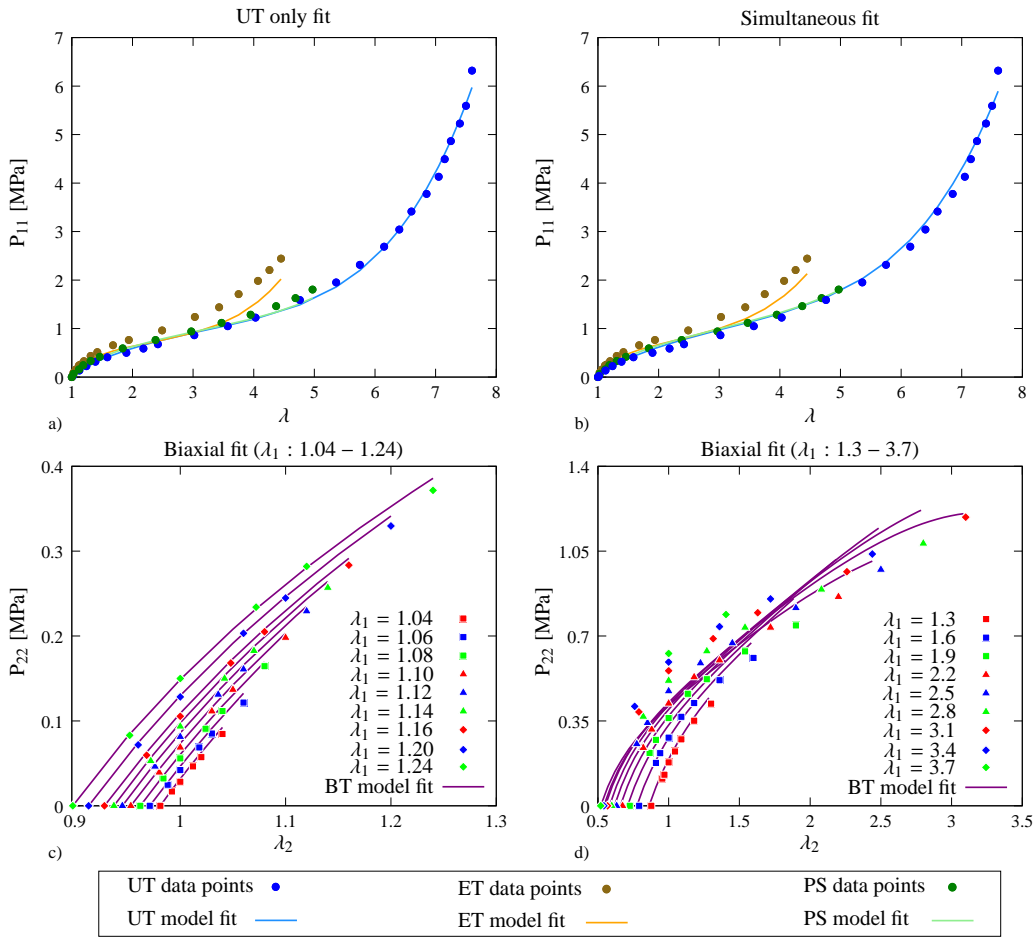


Figure 6.24: Yeoh model prediction for a) uniaxial tension, b) combination of uniaxial, equibiaxial, and pure shear loadings using Treloar data c) biaxial tension loading for $\lambda_1 : 1.04 - 1.24$, d) biaxial tension loading for $\lambda_1 : 1.3 - 3.7$ using Kawabata data.

Simultaneous fitting (Treloar)					
Parameters	$C_{10}=0.1816$ [MPa]	$C_{20}=-0.0014$ [MPa]	$C_{30}=3.95e-5$ [MPa]		
	Quality of fit				
	Weight	Error	Region 1	Region 2	Region 3
UT	0.2000	0.4467	0.0320	0.0823	0.1671
ET	0.6000	0.5579	0.0356	0.1080	0.3806
PS	0.2000	0.0065	0.0147	0.0162	0.0194
Total	1.0000	1.0110	0.0823	0.2065	0.5671

Table 6.72: Simultaneous fitting results for Yeoh model.

UT only fit (Treloar)					
Parameters	$C_{10}=0.1765$ [MPa]	$C_{20}=-0.0019$ [MPa]	$C_{30}=4.65e-5$ [MPa]		
	Quality of fit				
	Weight	Error	Region 1	Region 2	Region 3
UT	1	0.2530	0.0192	0.0356	0.0850
ET	0	1.0646	0.0426	0.1669	0.6965
PS	0	0.0864	0.0193	0.0212	0.0737
Total	1	1.4040	0.0810	0.2237	0.8551

Table 6.73: Uniaxial tension results for Yeoh model.

Biaxial fit (Kawabata)			
Parameters	$C_{10}=0.2117$ [MPa]	$C_{20}=0.0031$ [MPa]	$C_{30}=-1.48e-4$ [MPa]
Quality of fit: 4.7418	Biaxial error: 2.2867		

Table 6.74: Biaxial tension results for Yeoh model.

6.2.25 Two-term model results

Two-term model captures the S-curve for individual loading cases, however, for simultaneous fitting it underestimates the equibiaxial curves. This is due to the absence of second invariant terms in the strain energy function. Uniaxial fitting performance of the model is reasonable but the obtained parameter values cannot be used for the equibiaxial experimental data. For biaxial tension results show pure estimations. Fitting results are graphically given in Figure 6.25 and numerical results for simultaneous, uniaxial and biaxial fittings are given in Tables 6.75, 6.76, and 6.77, respectively.

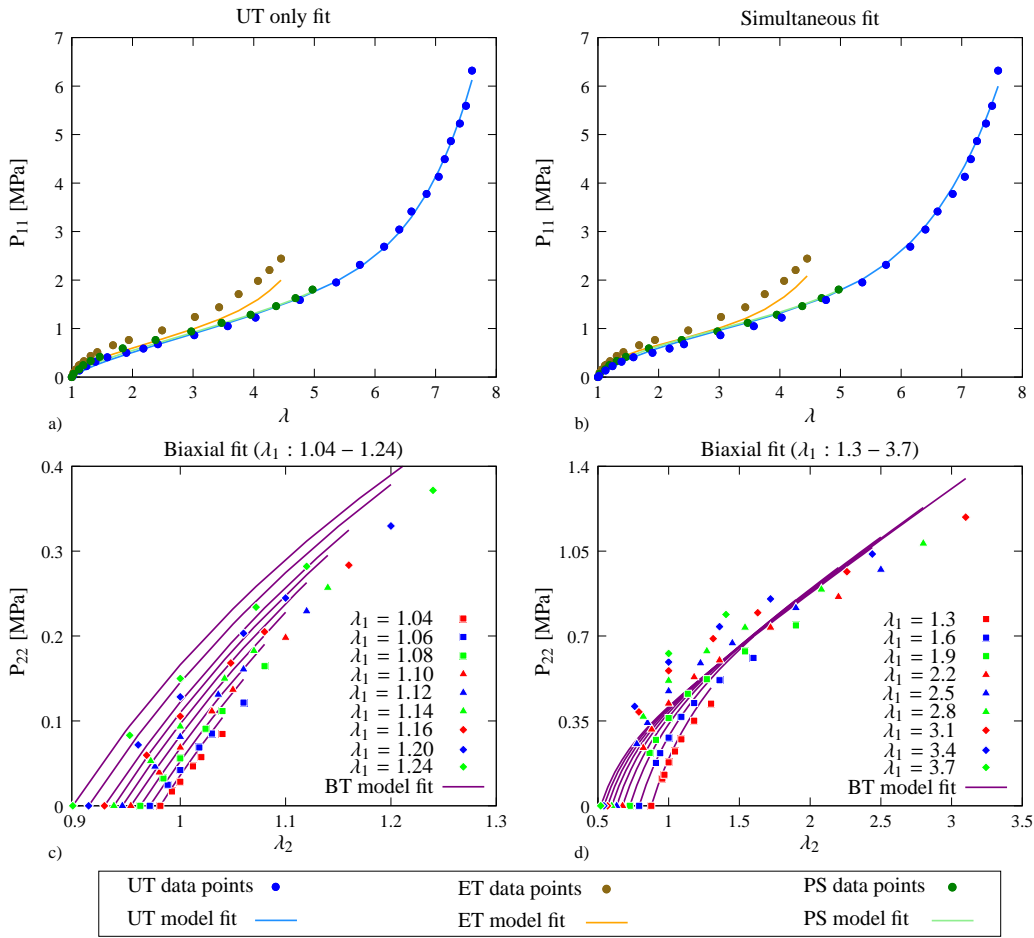


Figure 6.25: Two-Term model prediction for a) uniaxial tension, b) combination of uniaxial, equibiaxial, and pure shear loadings using Treloar data c) biaxial tension loading for $\lambda_1 : 1.04-1.24$, d) biaxial tension loading for $\lambda_1 : 1.3-3.7$ using Kawabata data.

Simultaneous fitting (Treloar)					
Parameters	$\alpha_1=0.9499$ $\mu_2=8.56e-5$ [MPa]	$\alpha_2=3.9197$	$\mu_1=0.3509$ [MPa]		
			Quality of fit		
	Weight	Error	Region 1	Region 2	Region 3
UT	0.1000	0.2770	0.0231	0.0692	0.1160
ET	0.8000	0.6362	0.0439	0.1357	0.4358
PS	0.1000	0.0081	0.0202	0.0220	0.0254
Total	1.0000	0.9213	0.0872	0.2269	0.5772

Table 6.75: Simultaneous fitting results for two-term model.

UT only fit (Treloar)					
Parameters	$\alpha_1=1.0887$ $\mu_2=3.94e-6$ [MPa]	$\alpha_2=4.9286$	$\mu_1=0.2780$ [MPa]		
			Quality of fit		
	Weight	Error	Region 1	Region 2	Region 3
UT	1	0.1296	0.0631	0.0737	0.0952
ET	0	0.9398	0.1138	0.3690	0.7638
PS	0	0.0478	0.0806	0.1297	0.1326
Total	1	1.1172	0.2576	0.5725	0.9917

Table 6.76: Uniaxial tension results for two-term model.

Biaxial fit (Kawabata)			
Parameters	$\alpha_1=0.9516$ $\mu_2=0.2379$ [MPa]	$\alpha_2=0.9516$	$\mu_1=0.2388$ [MPa]
Quality of fit: 5.3886	Biaxial error: 2.5062		

Table 6.77: Biaxial tension results for two-term model.

6.2.26 Yeoh-Fleming model results

Yeoh-Fleming model captures the S-curve for individual loading cases, however, for simultaneous fitting it underestimates the equibiaxial curves that could be improved by introducing a second invariant term. Uniaxial fitting performance of the model is reasonable but the obtained parameter values cannot be used for the equibiaxial experimental data. For biaxial tension results show pure estimations. Fitting results are graphically given in Figure 6.26 and numerical results for simultaneous, uniaxial and biaxial fittings are given in Tables 6.78, 6.79, and 6.80, respectively.

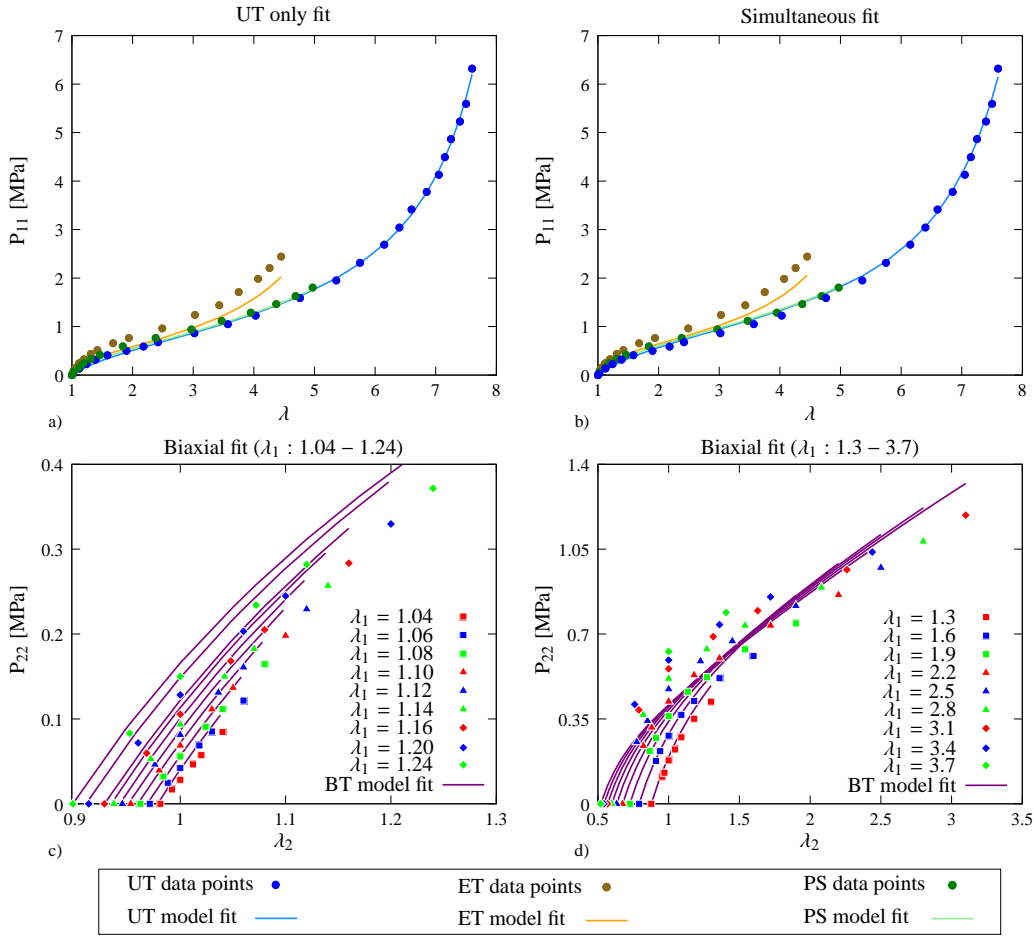


Figure 6.26: Yeoh-Fleming model prediction for a) uniaxial tension, b) combination of uniaxial, equibiaxial, and pure shear loadings using Treloar data c) biaxial tension loading for $\lambda_1 : 1.04-1.24$, d) biaxial tension loading for $\lambda_1 : 1.3-3.7$ using Kawabata data.

Simultaneous fitting (Treloar)					
Parameters	$A=0.1624$ [MPa] $B=1.0000$ $C_{10}=0.1574$ [MPa] $I_m=84.8425$				
	Quality of fit				
	Weight	Error	Region 1	Region 2	Region 3
UT	0.1000	0.1418	0.0224	0.0635	0.0846
ET	0.8000	0.6553	0.0647	0.1993	0.4881
PS	0.1000	0.0189	0.0362	0.0459	0.0511
Total	1.0000	0.8160	0.1232	0.3087	0.6238

Table 6.78: Simultaneous fitting results for Yeoh-Fleming model.

UT only fit (Treloar)					
Parameters	$A=0.1433$ [MPa] $B=0.3071$ $C_{10}=0.1114$ [MPa] $I_m=78.8497$				
	Quality of fit				
	Weight	Error	Region 1	Region 2	Region 3
UT	1	0.0844	0.0549	0.0588	0.0730
ET	0	0.8794	0.1044	0.3699	0.7344
PS	0	0.0513	0.0719	0.1207	0.1284
Total	1	1.0150	0.2312	0.5495	0.9358

Table 6.79: Uniaxial tension results for Yeoh-Fleming model.

Biaxial fit (Kawabata)	
Parameters	$A=0.2377$ [MPa] $B=1.22e4$ $C_{10}=0.0066$ [MPa] $I_m=1.83e6$
Quality of fit: 5.2781	Biaxial error: 2.4554

Table 6.80: Biaxial tension results for Yeoh-Fleming model.

6.2.27 Arruda-Boyce model results

Arruda-Boyce (eight-chain) model captures the S-curve for individual loading cases, however, for simultaneous fitting it underestimates the equibiaxial curves. Uniaxial fitting performance of the model is reasonable but the obtained parameter values cannot be used for the equibiaxial experimental data. For biaxial tension results deviate from the material response curve at high stretch values. Fitting results are graphically given in Figure 6.27 and numerical results for simultaneous, uniaxial and biaxial fittings are given in Tables 6.81, 6.82, and 6.83, respectively.

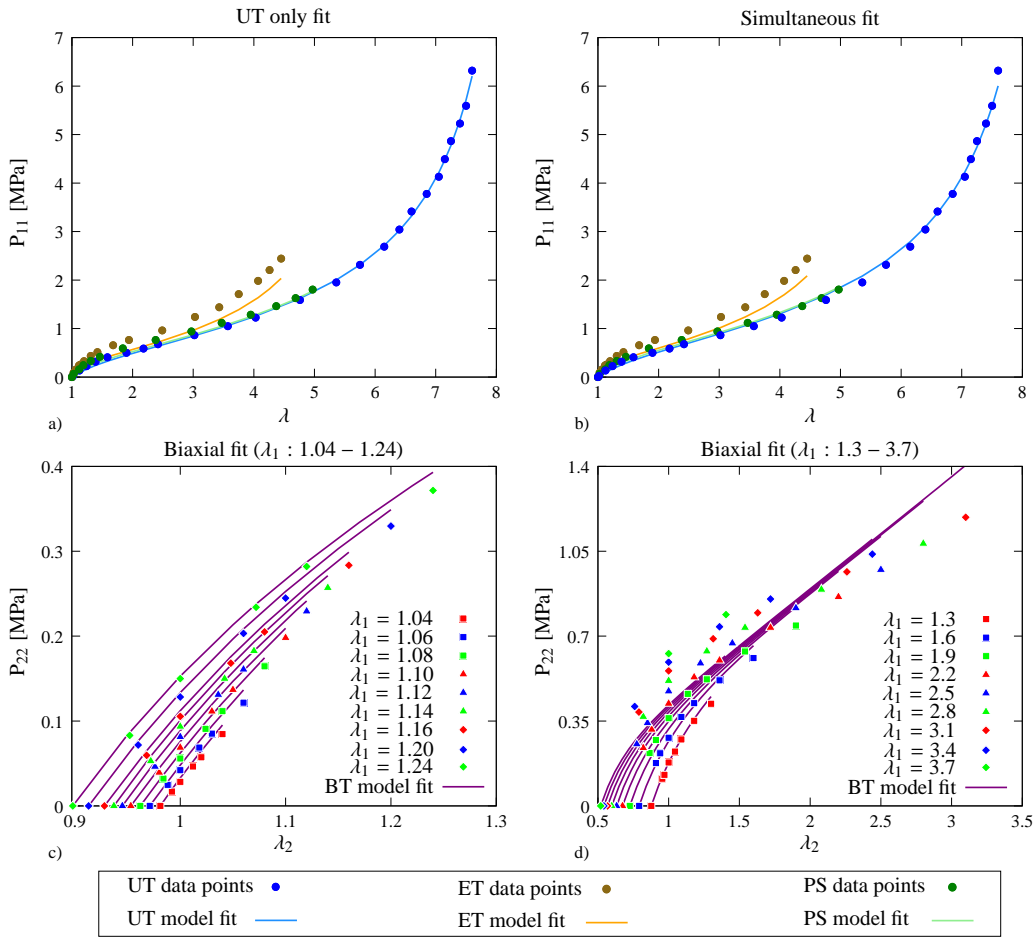


Figure 6.27: Arruda-Boyce model prediction for a) uniaxial tension, b) combination of uniaxial, equibiaxial, and pure shear loadings using Treloar data c) biaxial tension loading for $\lambda_1 : 1.04-1.24$, d) biaxial tension loading for $\lambda_1 : 1.3-3.7$ using Kawabata data.

Simultaneous fitting (Treloar)					
Parameters	$\mu=0.2821$ [MPa] $N=26.4782$				
			Quality of fit		
	Weight	Error	Region 1	Region 2	Region 3
UT	0.0100	0.2010	0.0498	0.0694	0.1074
ET	0.9800	0.6420	0.1008	0.3396	0.5891
PS	0.0100	0.0462	0.0685	0.1103	0.1164
Total	1.0000	0.8892	0.2190	0.5194	0.8129

Table 6.81: Simultaneous fitting results for Arruda-Boyce model.

UT only fit (Treloar)					
Parameters	$\mu=0.0891$ [MPa] $N=25.5927$				
			Quality of fit		
	Weight	Error	Region 1	Region 2	Region 3
UT	1	0.0870	0.0755	0.0794	0.0929
ET	0	0.8932	0.1191	0.4323	0.7898
PS	0	0.0723	0.0861	0.1538	0.1676
Total	1	1.0525	0.2808	0.6655	1.0503

Table 6.82: Uniaxial tension results for Arruda-Boyce model.

Biaxial fit (Kawabata)	
Parameters	$\mu=0.4339$ [MPa] $N=100.00$
Quality of fit: 5.5347	Biaxial error: 2.6477

Table 6.83: Biaxial tension results for Arruda-Boyce model.

6.2.28 Gent model results

Gent model with two parameters captures the S-curve for individual loading cases, however, for simultaneous fitting it underestimates the equibiaxial curves that could be improved by introducing a second invariant term. Uniaxial fitting performance of the model is reasonable but the obtained parameter values cannot be used for the equibiaxial experimental data. For biaxial tension results deviate from the material response curve at high stretch values. Fitting results are graphically given in Figure 6.28 and numerical results for simultaneous, uniaxial and biaxial fittings are given in Tables 6.84, 6.85, and 6.86, respectively.

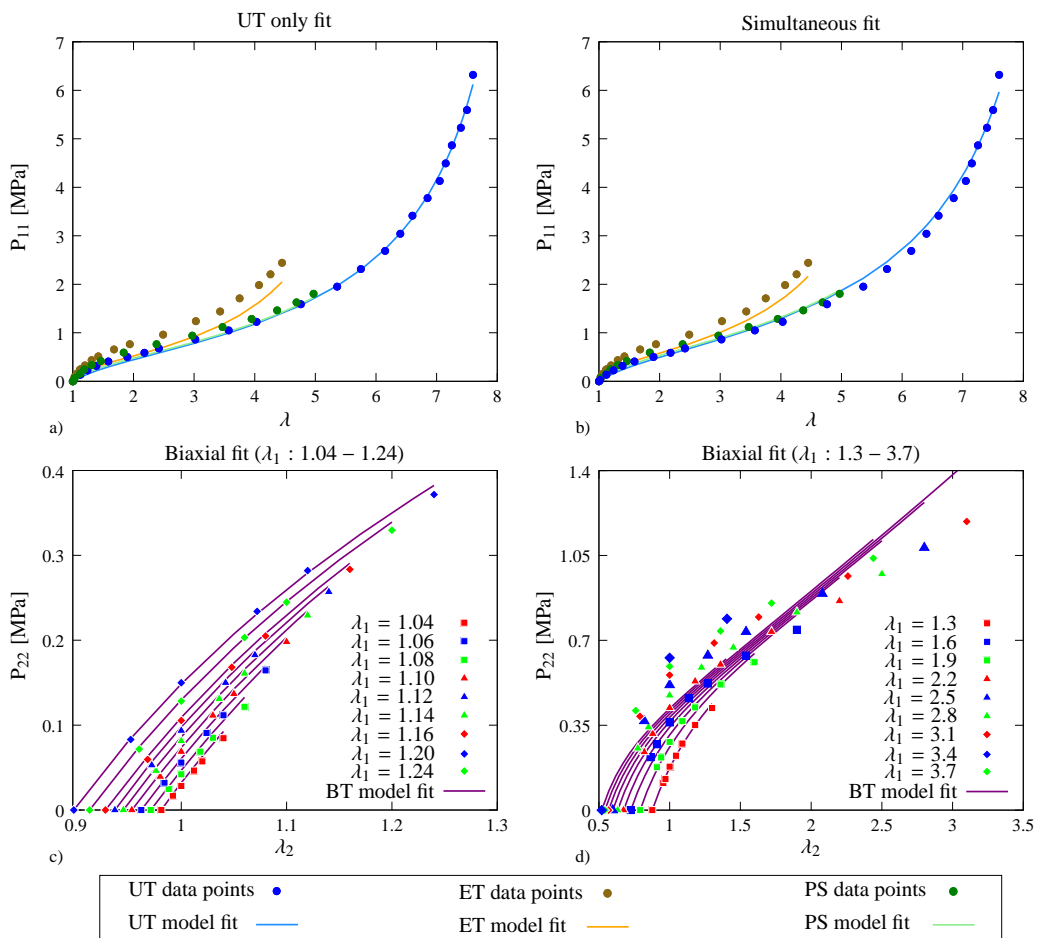


Figure 6.28: Gent model prediction for a) uniaxial tension, b) combination of uniaxial, equibiaxial, and pure shear loadings using Treloar data c) biaxial tension loading for $\lambda_1 : 1.04 - 1.24$, d) biaxial tension loading for $\lambda_1 : 1.3 - 3.7$ using Kawabata data.

Simultaneous fitting (Treloar)					
Parameters	$\mu=0.2579$ [MPa] $J_m=90.7711$				
	Weight	Error	Quality of fit		
			Region 1	Region 2	Region 3
UT	0.1000	0.3855	0.0710	0.0885	0.1817
ET	0.8000	0.5508	0.1169	0.4067	0.5978
PS	0.1000	0.0687	0.0839	0.1455	0.1572
Total	1.0000	1.0050	0.2719	0.6407	0.9367

Table 6.84: Simultaneous fitting results for Gent model.

UT only fit (Treloar)					
Parameters	$\mu=0.2307$ [MPa] $J_m=85.4462$				
	Weight	Error	Quality of fit		
			Region 1	Region 2	Region 3
UT	1	0.1491	0.1406	0.1634	0.1801
ET	0	1.0511	0.1551	0.6057	1.0092
PS	0	0.1708	0.1223	0.2473	0.3072
Total	1	1.3710	0.4179	1.0165	1.4965

Table 6.85: Uniaxial tension results for Gent model.

Biaxial fit (Kawabata)	
Parameters	$\mu=0.4116$ [MPa] $J_m=200.000$
Quality of fit: 5.7851	Biaxial error: 2.7993

Table 6.86: Biaxial tension results for Gent model.

6.2.29 Three-chain model results

Three-chain model captures the S-curve for individual loading cases, however, for simultaneous fitting it underestimates the equibiaxial curves. Uniaxial fitting performance of the model is reasonable but the obtained parameter values underestimate the equibiaxial tension and pure shear experimental data. For biaxial tension, however, results deviate from the material response curve at high stretch values. Fitting results are graphically given in Figure 6.29 and numerical results for simultaneous, uniaxial and biaxial fittings are given in Tables 6.87, 6.88, and 6.89, respectively.

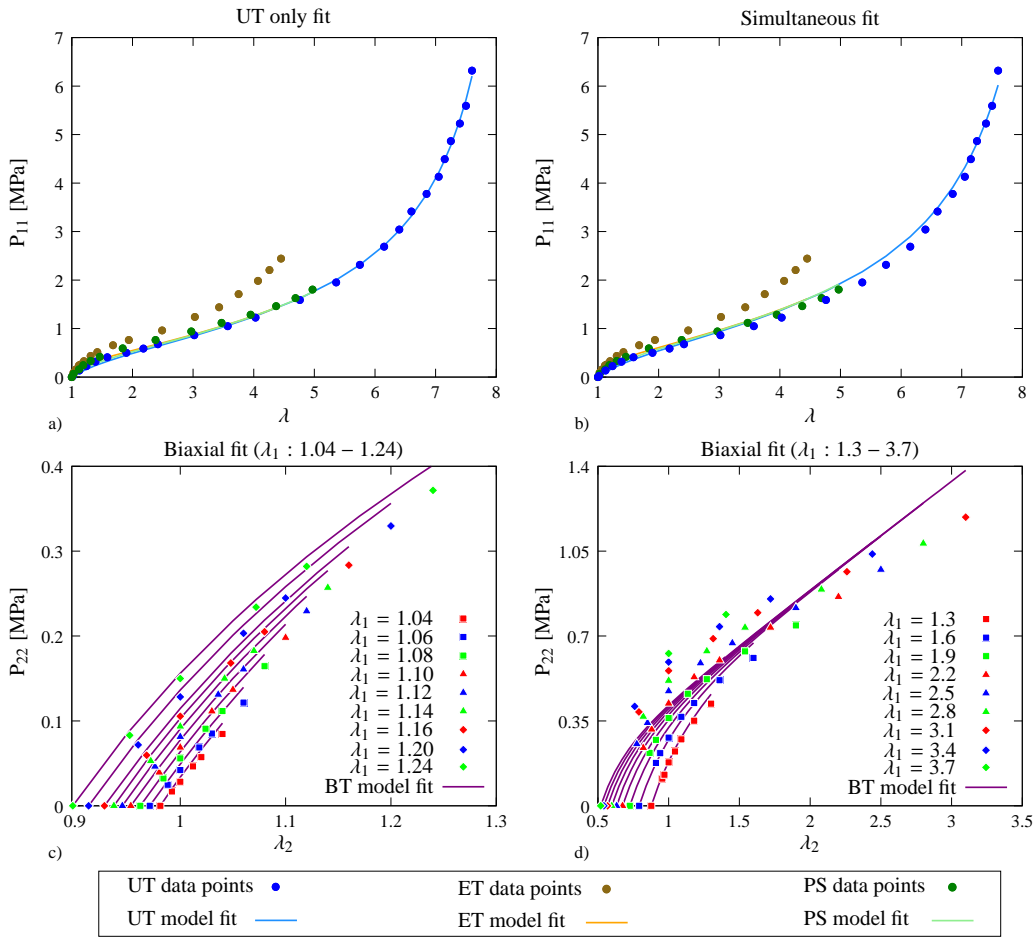


Figure 6.29: Three-Chain model prediction for a) uniaxial tension, b) combination of uniaxial, equibiaxial, and pure shear loadings using Treloar data c) biaxial tension loading for $\lambda_1 : 1.04-1.24$, d) biaxial tension loading for $\lambda_1 : 1.3-3.7$ using Kawabata data.

Simultaneous fitting (Treloar)					
Parameters	$\mu=0.2980$ [MPa] $N=80.9506$				
	Weight	Error	Quality of fit		
			Region 1	Region 2	Region 3
UT	0.2000	0.3967	0.0342	0.0986	0.1929
ET	0.6000	1.9861	0.0864	0.2951	1.1850
PS	0.2000	0.0658	0.0546	0.0792	0.1060
Total	1.0000	2.4487	0.1752	0.4730	1.4840

Table 6.87: Simultaneous fitting results for three-chain model.

UT only fit (Treloar)					
Parameters	$\mu=0.2680$ [MPa] $N=76.5519$				
	Weight	Error	Quality of fit		
			Region 1	Region 2	Region 3
UT	1	0.0877	0.0775	0.0814	0.0950
ET	0	2.9715	0.1220	0.4819	1.8206
PS	0	0.0816	0.0883	0.1597	0.1784
Total	1	3.1408	0.2879	0.7230	2.0940

Table 6.88: Uniaxial tension results for three-chain model.

Biaxial fit (Kawabata)	
Parameters	$\mu=0.1403$ [MPa] $N=0.2542$
Quality of fit: 5.3982	Biaxial error: 2.5603

Table 6.89: Biaxial tension results for three-chain model.

6.2.30 Mooney model results

Mooney model with two parameters shows poor performance for simultaneous fitting. The results cannot generate S-shape curve even in individual uniaxial fitting. The reason is summation of first order invariant based terms. Uniaxial fitting result is reasonable up to moderate stretch values. For biaxial tension results deviate from the material response curve at high stretch values. Fitting results are graphically given in Figure 6.30 and numerical results for simultaneous, uniaxial and biaxial fittings are given in Tables 6.90, 6.91, and 6.92, respectively.

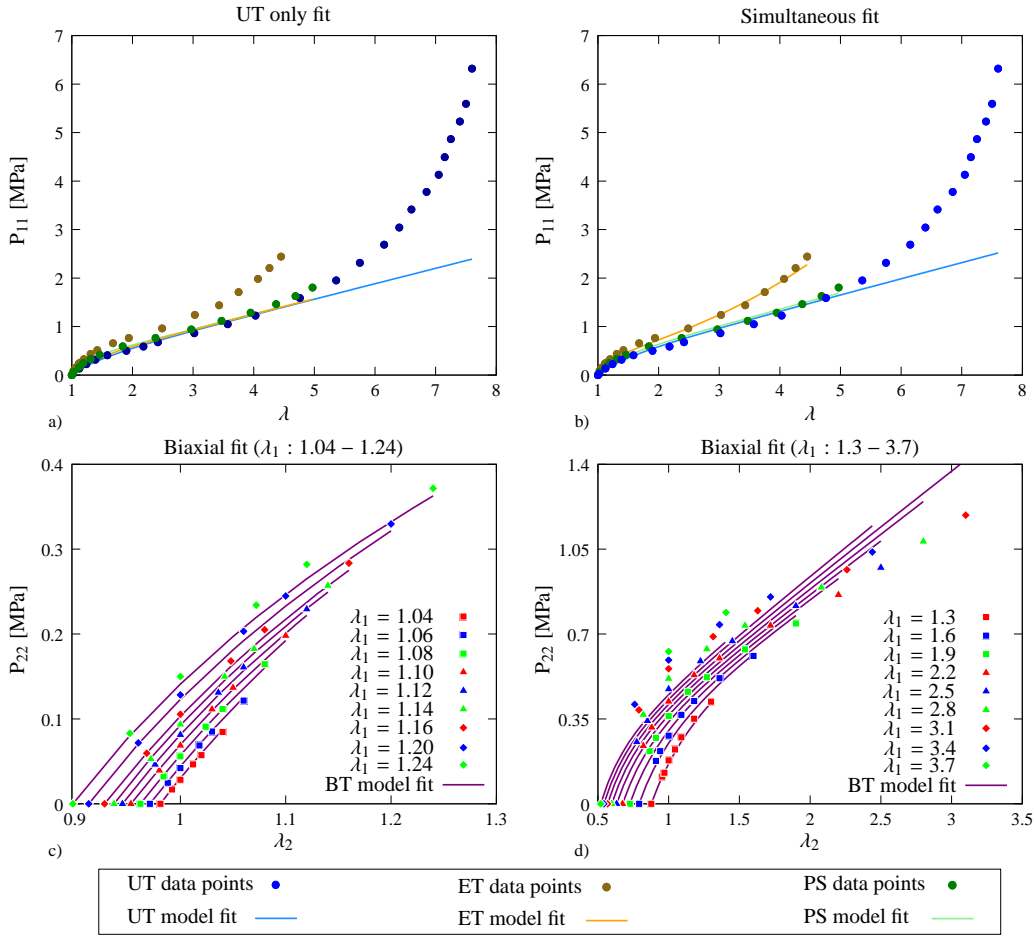


Figure 6.30: Mooney model prediction for a) uniaxial tension, b) combination of uniaxial, equibiaxial, and pure shear loadings using Treloar data c) biaxial tension loading for $\lambda_1 : 1.04-1.24$, d) biaxial tension loading for $\lambda_1 : 1.3-3.7$ using Kawabata data.

Simultaneous fitting (Treloar)					
Parameters	$C_{10}=0.1655$ [MPa] $C_{01}=0.0046$ [MPa]		Quality of fit		
	Weight	Error	Region 1	Region 2	Region 3
UT	0.2836	50.908	0.0219	0.0644	10.153
ET	0.5116	0.0750	0.0502	0.0999	0.1181
PS	0.2048	0.0306	0.0257	0.0294	0.0461
Total	1.0000	51.013	0.0978	0.1936	10.375

Table 6.90: Simultaneous fitting results for Mooney model.

UT only fit (Treloar)					
Parameters	$C_{10}=0.1577$ [MPa] $C_{01}=4.06e-6$ [MPa]		Quality of fit		
	Weight	Error	Region 1	Region 2	Region 3
UT	1	56.097	0.0254	0.0400	11.277
ET	0	2.9294	0.0735	0.2485	1.5926
PS	0	0.1097	0.0437	0.0608	0.1152
Total	1	59.136	0.1427	0.3494	12.986

Table 6.91: Uniaxial tension results for Mooney model.

Biaxial fit (Kawabata)		
Parameters	$C_{10}=0.1966$ [MPa] $C_{01}=0.0034$ [MPa]	
Quality of fit: 4.7639	Biaxial error: 2.3165	

Table 6.92: Biaxial tension results for Mooney model.

6.2.31 Isihara model results

Isihara model with three parameters shows poor performance for simultaneous fitting. The results cannot generate S-shape curve even in individual uniaxial fitting. Uniaxial fitting result is reasonable up to moderate stretch values. For biaxial tension results deviate from the material response curve even in low stretch values and poor estimation is obtained. Fitting results are graphically given in Figure 6.31 and numerical results for simultaneous, uniaxial and biaxial fittings are given in Tables 6.93, 6.94, and 6.95, respectively.

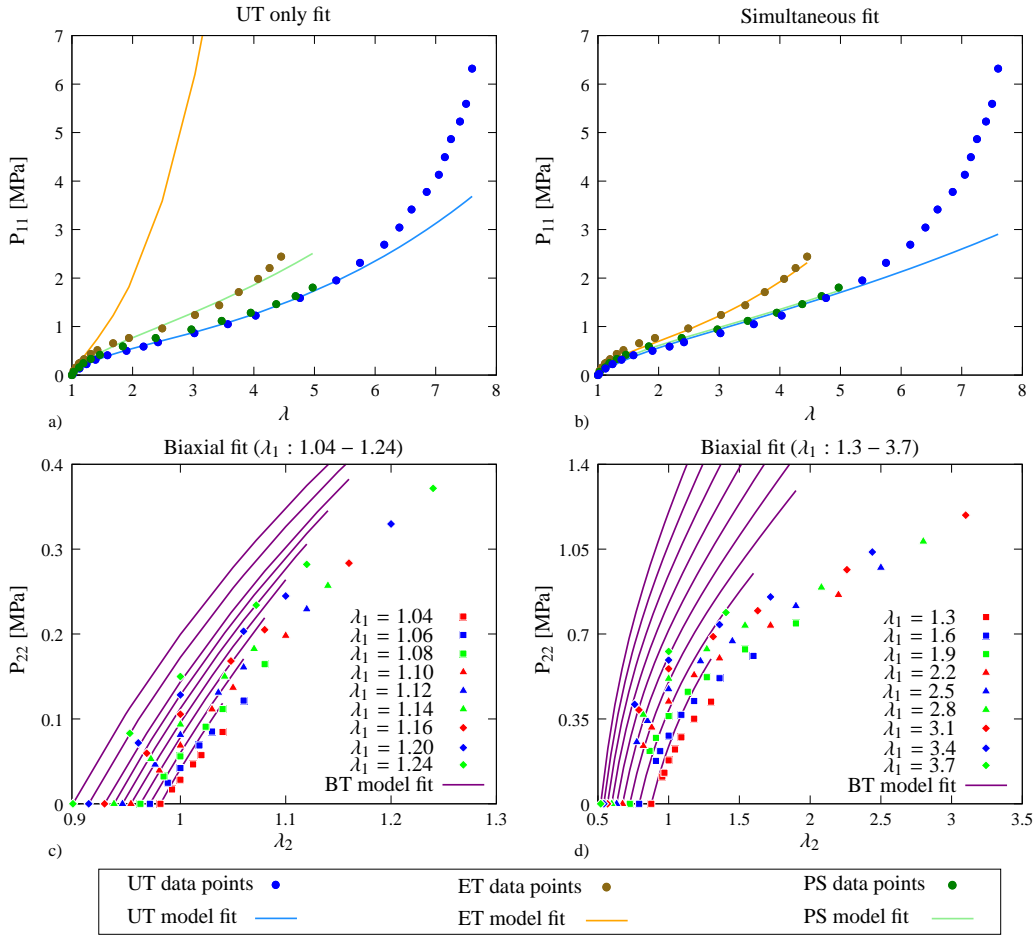


Figure 6.31: Isihara model prediction for a) uniaxial tension, b) combination of uniaxial, equibiaxial, and pure shear loadings using Treloar data c) biaxial tension loading for $\lambda_1 : 1.04 - 1.24$, d) biaxial tension loading for $\lambda_1 : 1.3 - 3.7$ using Kawabata data.

Simultaneous fitting (Treloar)					
Parameters	$C_{10}=0.1572$ [MPa]	$C_{20}=3.06e-4$ [MPa]	$C_{01}=0.0041$ [MPa]		
	Quality of fit				
	Weight	Error	Region 1	Region 2	Region 3
UT	0.0500	38.724	0.0231	0.0522	7.6180
ET	0.9000	0.0788	0.0649	0.1480	0.1583
PS	0.0500	0.0224	0.0376	0.0476	0.0550
Total	1.0000	38.826	0.1257	0.2479	7.8313

Table 6.93: Simultaneous fitting results for Isihara model.

UT only fit (Treloar)					
Parameters	$C_{10}=0.1401$ [MPa]	$C_{20}=0.0011$ [MPa]	$C_{01}=0.0964$ [MPa]		
	Quality of fit				
	Weight	Error	Region 1	Region 2	Region 3
UT	1	0.0015	0.0016	0.0021	0.0028
ET	0	1.38e3	0.0000	4.4167	1.09e3
PS	0	15.4862	0.0111	1.0180	11.7638
Total	1	1.39e3	0.127	5.4368	1.10e3

Table 6.94: Uniaxial tension results for Isihara model.

Biaxial fit (Kawabata)			
Parameters	$C_{10}=0.2393$ [MPa]	$C_{20}=1.16e-9$ [MPa]	$C_{01}=0.0229$ [MPa]
Quality of fit: 103.6728.	Biaxial error: 205.4138		

Table 6.95: Biaxial tension results for Isihara model.

6.2.32 Nunes model results

Nunes model with two material parameters shows poor performance for simultaneous fitting. The results cannot generate S-shape curve even in individual uniaxial fitting. Uniaxial fitting result is reasonable up to moderate stretch values. For biaxial tension fitting results are in good agreement with the material response curve. Fitting results are graphically given in Figure 6.32 and numerical results for simultaneous, uniaxial and biaxial fittings are given in Tables 6.96, 6.97, and 6.98, respectively.

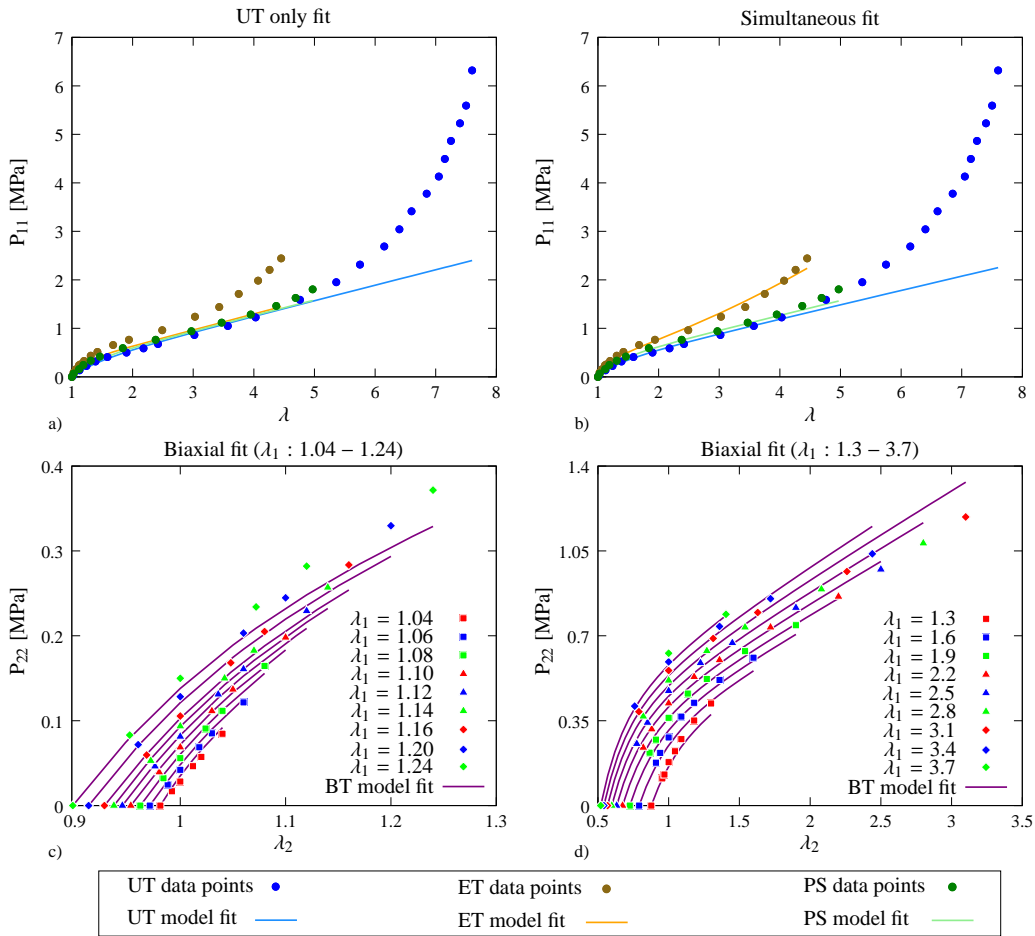


Figure 6.32: Nunes model prediction for a) uniaxial tension, b) combination of uniaxial, equibiaxial, and pure shear loadings using Treloar data c) biaxial tension loading for $\lambda_1 : 1.04 - 1.24$, d) biaxial tension loading for $\lambda_1 : 1.3 - 3.7$ using Kawabata data.

Simultaneous fitting (Treloar)					
Parameters	$C_1=0.1469$ [MPa] $C_2=0.0235$ [MPa]		Quality of fit		
	Weight	Error	Region 1	Region 2	Region 3
UT	0.8000	0.0021	0.0000	0.0051	0.0073
ET	0.1000	0.0995	0.0000	0.0024	0.1556
PS	0.1000	0.0127	0.0000	0.0099	0.0254
Total	1.0000	0.1144	0.0000	0.0174	0.1884

Table 6.96: Simultaneous fitting results for Nunes model.

UT only fit (Treloar)					
Parameters	$C_1=0.1581$ [MPa] $C_2=0.0010$ [MPa]		Quality of fit		
	Weight	Error	Region 1	Region 2	Region 3
UT	1	0.0846	0.0078	0.0269	0.0926
ET	0	2.4861	0.0000	0.4066	2.7124
PS	0	0.2740	0.0150	0.1406	0.2917
Total	1	2.8447	0.0228	0.5741	3.0967

Table 6.97: Uniaxial tension results for Nunes model.

Biaxial fit (Kawabata)		
Parameters	$C_1=0.1442$ [MPa] $C_2=0.0227$ [MPa]	
Quality of fit: 1.7811	Biaxial error: 0.8895	

Table 6.98: Biaxial tension results for Nunes model.

6.2.33 Tube model results

Tube model with three material parameters shows poor performance for simultaneous fitting. The results cannot generate S-shape curve even in individual uniaxial fitting. Uniaxial fitting result is reasonable up to moderate stretch values. For biaxial tension fitting results are in good agreement with the material response curve. Fitting results are graphically given in Figure 6.33 and numerical results for simultaneous, uniaxial and biaxial fittings are given in Tables 6.99, 6.100, and 6.101, respectively.

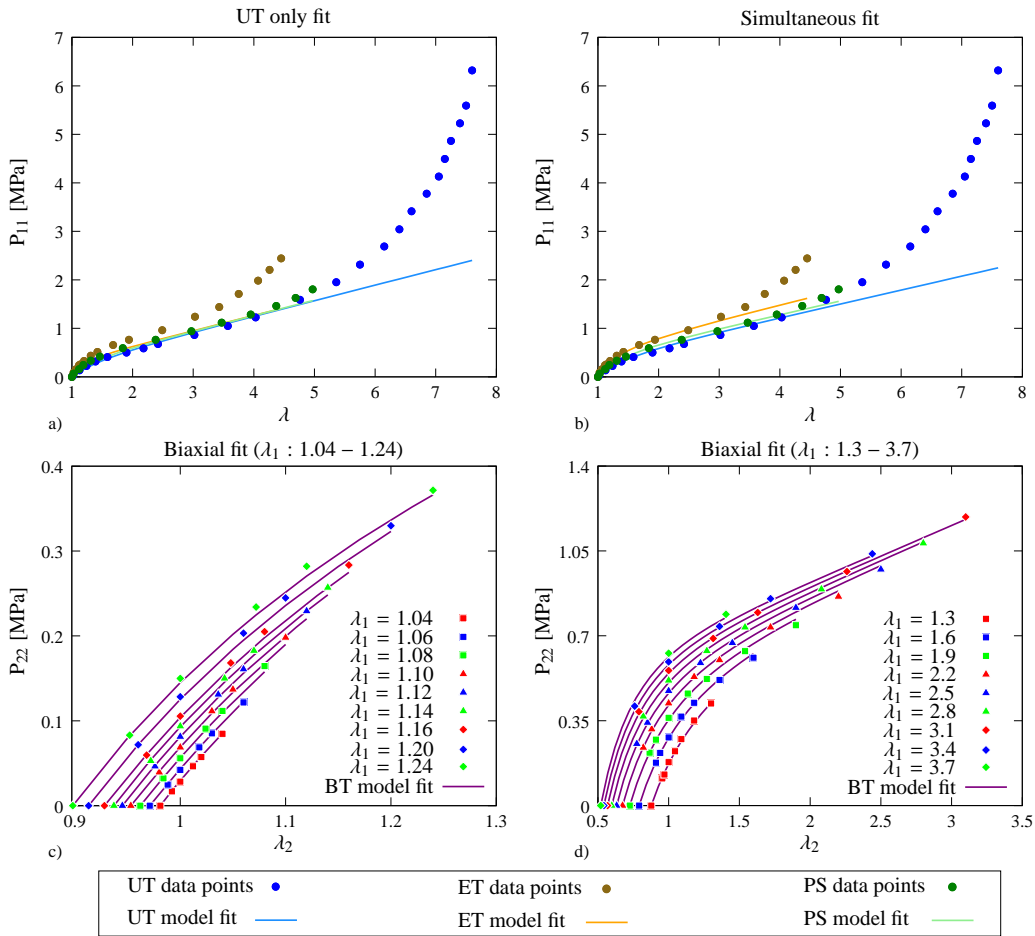


Figure 6.33: Tube model prediction for a) uniaxial tension, b) combination of uniaxial, equibiaxial, and pure shear loadings using Treloar data c) biaxial tension loading for $\lambda_1 : 1.04 - 1.24$, d) biaxial tension loading for $\lambda_1 : 1.3 - 3.7$ using Kawabata data.

Simultaneous fitting (Treloar)					
Parameters	$G_c=0.2892$ [MPa]	$G_e=0.0816$ [MPa]	$\beta=0.5832$		
	Quality of fit		Region 1	Region 2	Region 3
	Weight	Error			
UT	0.1000	0.0790	0.0000	0.0259	0.0992
ET	0.8000	0.0212	0.0000	0.0081	0.0304
PS	0.1000	0.0461	0.0000	0.0038	0.0429
Total	1.0000	0.1463	0.0000	0.0378	0.1724

Table 6.99: Simultaneous fitting results for tube model.

UT only fit (Treloar)					
Parameters	$G_c=0.3166$ [MPa]	$G_e=3.15e-8$ [MPa]	$\beta=0.5213$		
	Quality of fit		Region 1	Region 2	Region 3
	Weight	Error			
UT	1	0.0840	0.0091	0.0300	0.0946
ET	0	2.8168	0.0000	0.4338	3.0440
PS	0	0.2938	0.0171	0.1543	0.3164
Total	1	3.1946	0.0263	0.6181	3.4551

Table 6.100: Uniaxial tension results for tube model.

Biaxial fit (Kawabata)			
Parameters	$G_c=0.2840$ [MPa]	$G_e=0.1018$ [MPa]	$\beta=0.3978$
Quality of fit: 0.3875	Biaxial error: 0.1149		

Table 6.101: Biaxial tension results for tube model.

6.2.34 Slip-link model results

Slip-link model is not able to generate S-curve and its performance in simultaneous and individual fittings fitting is poor. The model results can be used in moderate strain region, however, deviation from the actual response of the material is observed in high stretches. Using Gaussian statistics and affine deformation for cross-links cause poor results. Good agreement is obtained in low stretch values of biaxial data. Fitting results are graphically given in Figure 6.34 and numerical results for simultaneous, uniaxial and biaxial fittings are given in Tables 6.102, 6.103, and 6.104, respectively.

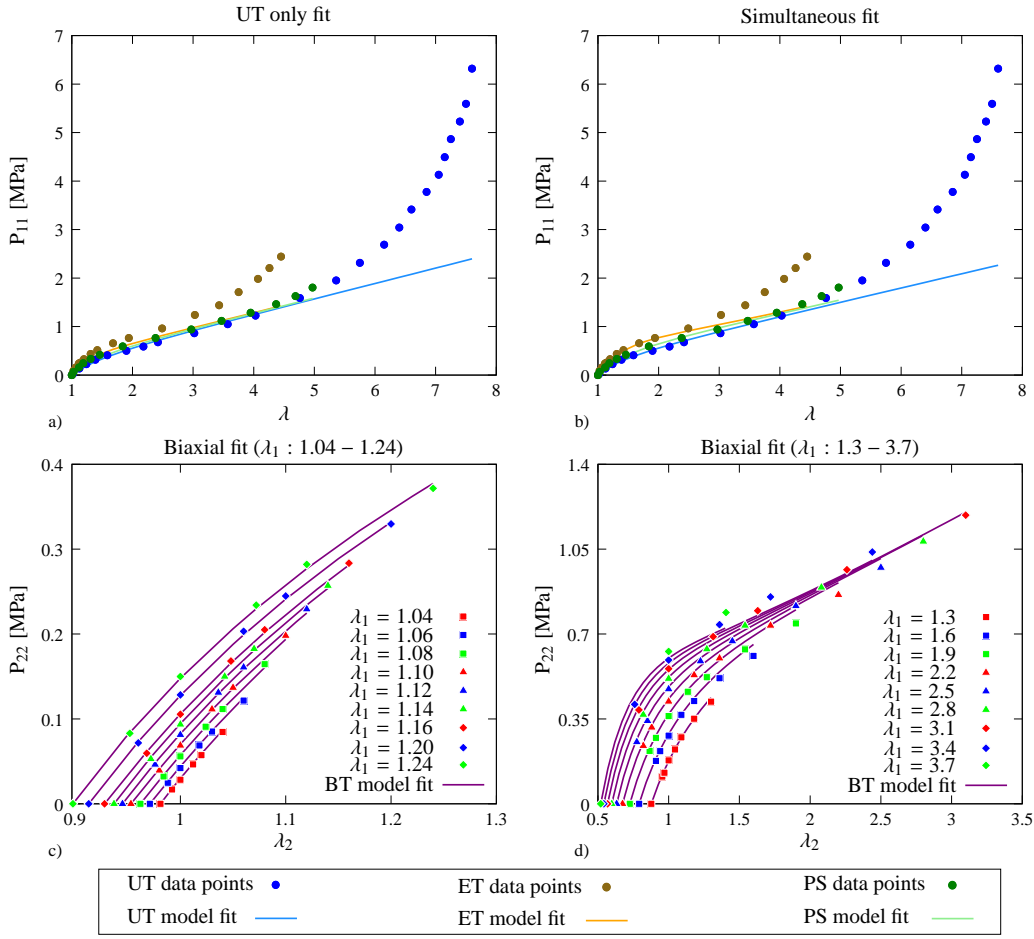


Figure 6.34: Slip-Link model prediction for a) uniaxial tension, b) combination of uniaxial, equibiaxial, and pure shear loadings using Treloar data c) biaxial tension loading for $\lambda_1 : 1.04-1.24$, d) biaxial tension loading for $\lambda_1 : 1.3-3.7$ using Kawabata data.

Simultaneous fitting (Treloar)					
Parameters	$\mu_1=0.2938$ [MPa]	$\mu_2=0.5000$ [MPa]	$\eta=1.9390$		
	Weight	Error	Quality of fit		
			Region 1	Region 2	Region 3
UT	0.8000	0.0109	0.0000	0.0049	0.0163
ET	0.1000	0.0855	0.0000	0.0062	0.0942
PS	0.1000	0.0125	0.0000	0.0085	0.0184
Total	1.0000	0.1089	0.0000	0.0195	0.1289

Table 6.102: Simultaneous fitting results for slip-link model.

UT only fit (Treloar)					
Parameters	$\mu_1=0.3153$ [MPa]	$\mu_2=0.1000$ [MPa]	$\eta=3.9997$		
	Weight	Error	Quality of fit		
			Region 1	Region 2	Region 3
UT	1	0.0857	0.0084	0.0280	0.0944
ET	0	2.1388	0.0000	0.3568	2.3007
PS	0	0.2272	0.0155	0.1253	0.2461
Total	1	2.4517	0.0239	0.5101	2.6413

Table 6.103: Uniaxial tension results for slip-link model.

Biaxial fit (Kawabata)			
Parameters	$\mu_1=0.3487$ [MPa]	$\mu_2=0.3930$ [MPa]	$\eta=2.0000$
Quality of fit: 0.5668	Biaxial error: 0.2592		

Table 6.104: Biaxial tension results for slip-link model.

6.2.35 Swanson model results

Swanson model with four material parameters is not able to generate S-curve and its performance in simultaneous fitting is poor. For individual fittings the model has reasonable results throughout the data points. Good agreement is obtained for biaxial data. Fitting results are graphically given in Figure 6.35 and numerical results for simultaneous, uniaxial and biaxial fittings are given in Tables 6.105, 6.106, and 6.107, respectively.

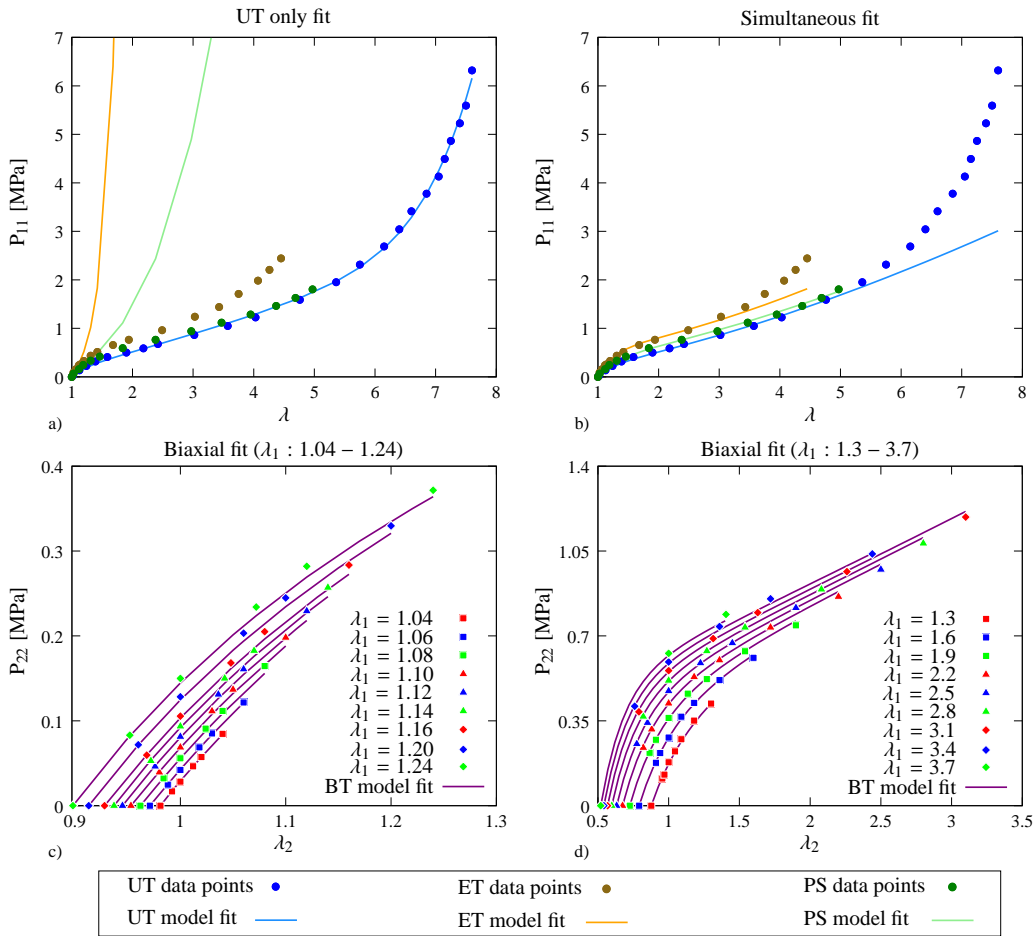


Figure 6.35: Swanson model prediction for a) uniaxial tension, b) combination of uniaxial, equibiaxial, and pure shear loadings using Treloar data c) biaxial tension loading for $\lambda_1 : 1.04-1.24$, d) biaxial tension loading for $\lambda_1 : 1.3-3.7$ using Kawabata data.

Simultaneous fitting (Treloar)					
Parameters	$A_1=0.0693$ [MPa]		$\alpha_1=0.2139$	$B_1=0.0562$ [MPa]	
	$\beta_1=-0.8748$				
			Quality of fit		
	Weight	Error	Region 1	Region 2	Region 3
UT	0.1	35.486	0.0134	0.0158	6.9206
ET	0.1	0.8187	0.0177	0.0237	0.3914
PS	0.8	0.0080	0.0113	0.0120	0.0165
Total	1	36.313	0.0425	0.0515	7.3284

Table 6.105: Simultaneous fitting results for Swanson model.

UT only fit (Treloar)					
Parameters	$A_1=8.05e-7$ [MPa]		$\alpha_1=4.0901$	$B_1=0.1277$ [MPa]	
	$\beta_1=1.2292$				
			Quality of fit		
	Weight	Error	Region 1	Region 2	Region 3
UT	1	0.1174	0.0231	0.0317	0.0540
ET	0	$3.32e8$	0.0407	$1.97e4$	$1.47e8$
PS	0	$1.48e3$	0.0126	4.1396	934.15
Total	1	$3.32e8$	0.0763	$1.97e4$	$1.47e8$

Table 6.106: Uniaxial tension results for Swanson model.

Biaxial fit (Kawabata)	
Parameters	$A_1=0.1035$ [MPa] $\alpha_1=3.98e-8$ $B_1=0.0232$ [MPa]
	$\beta_1=-0.6140$
Quality of fit: 0.4558	Biaxial error: 0.1443

Table 6.107: Biaxial tension results for Swanson model.

6.2.36 Gent-Thomas model results

Gent-Thomas model with two material parameters is not able to generate S-curve and its performance in simultaneous and individual fitting is poor. Absence of a well defined limiting chain extensibility factor results in deviation from actual material response at high strain values. Also poor agreement is obtained for biaxial data. Fitting results are graphically given in Figure 6.36 and numerical results for simultaneous, uniaxial and biaxial fittings are given in Tables 6.108, 6.109, and 6.110, respectively.

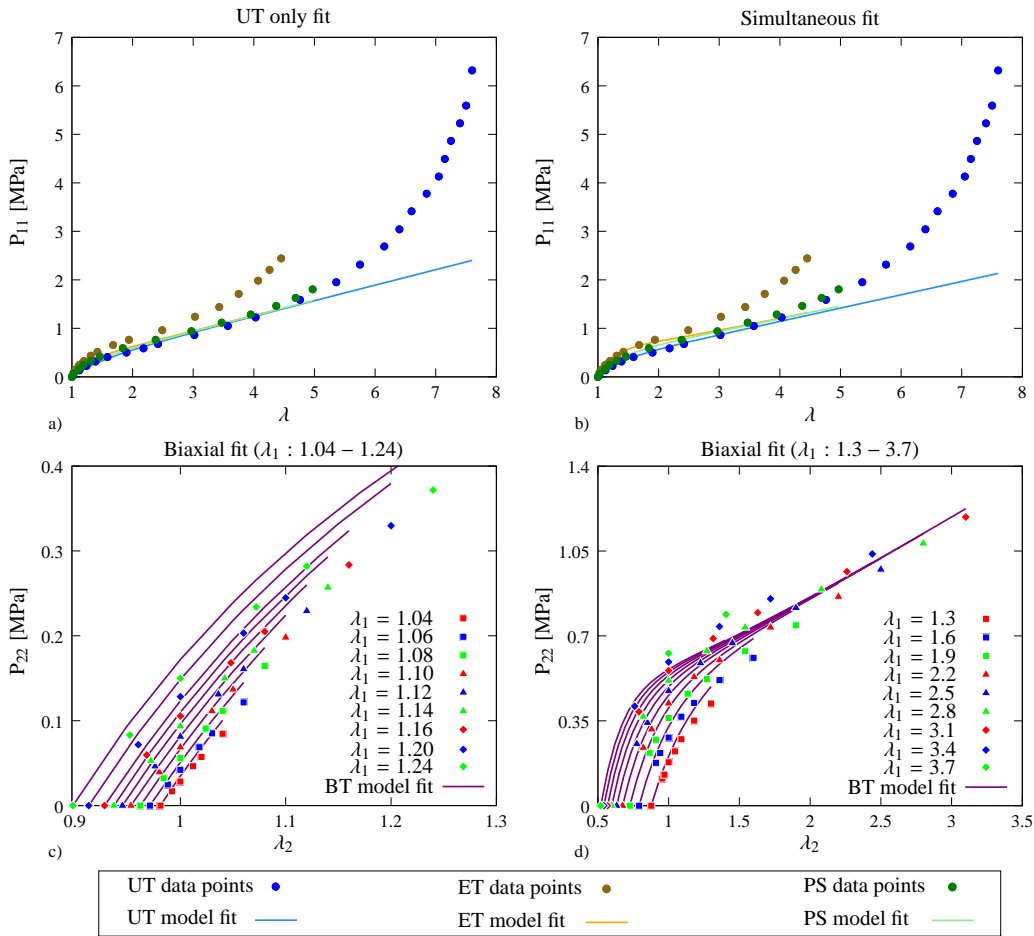


Figure 6.36: Gent-Thomas model prediction for a) uniaxial tension, b) combination of uniaxial, equibiaxial, and pure shear loadings using Treloar data c) biaxial tension loading for $\lambda_1 : 1.04 - 1.24$, d) biaxial tension loading for $\lambda_1 : 1.3 - 3.7$ using Kawabata data.

Simultaneous fitting (Treloar)					
Parameters	$C_1=0.1390$ [MPa] $C_2=0.1932$ [MPa]		Quality of fit		
	Weight	Error	Region 1	Region 2	Region 3
UT	0.6000	0.0082	0.0000	0.0061	0.0211
ET	0.2000	0.0770	0.0000	0.0000	0.1086
PS	0.2000	0.0145	0.0000	0.0096	0.0320
Total	1.0000	0.0997	0.0000	0.0157	0.1617

Table 6.108: Simultaneous fitting results for Gent-Thomas model.

UT only fit (Treloar)					
Parameters	$C_1=0.1583$ [MPa] $C_2=1.00e - 4$ [MPa]		Quality of fit		
	Weight	Error	Region 1	Region 2	Region 3
UT	1	0.0840	0.0091	0.0299	0.0946
ET	0	2.8151	0.0000	0.4331	3.0417
PS	0	0.2936	0.0171	0.1540	0.3160
Total	1	3.1926	0.0262	0.6170	3.4523

Table 6.109: Uniaxial tension results for Gent-Thomas model.

Biaxial fit (Kawabata)		
Parameters	$C_1=0.1845$ [MPa] $C_2=0.1281$ [MPa]	
Quality of fit: 1.1469	Biaxial error: 0.5662	

Table 6.110: Biaxial tension results for Gent-Thomas model.

6.2.37 Constrained-junction model results

Constrained-junction model with three material parameters has a poor fitting performance in simultaneous fitting. For individual fittings it is also observed that the constitutive relation is not able to catch actual response curve at high stretch region. In biaxial data fitting, solutions deviate from the expected results in high strain values. Fitting results are graphically given in Figure 6.37 and numerical results for simultaneous, uniaxial and biaxial fittings are given in Tables 6.111, 6.112, and 6.113, respectively.

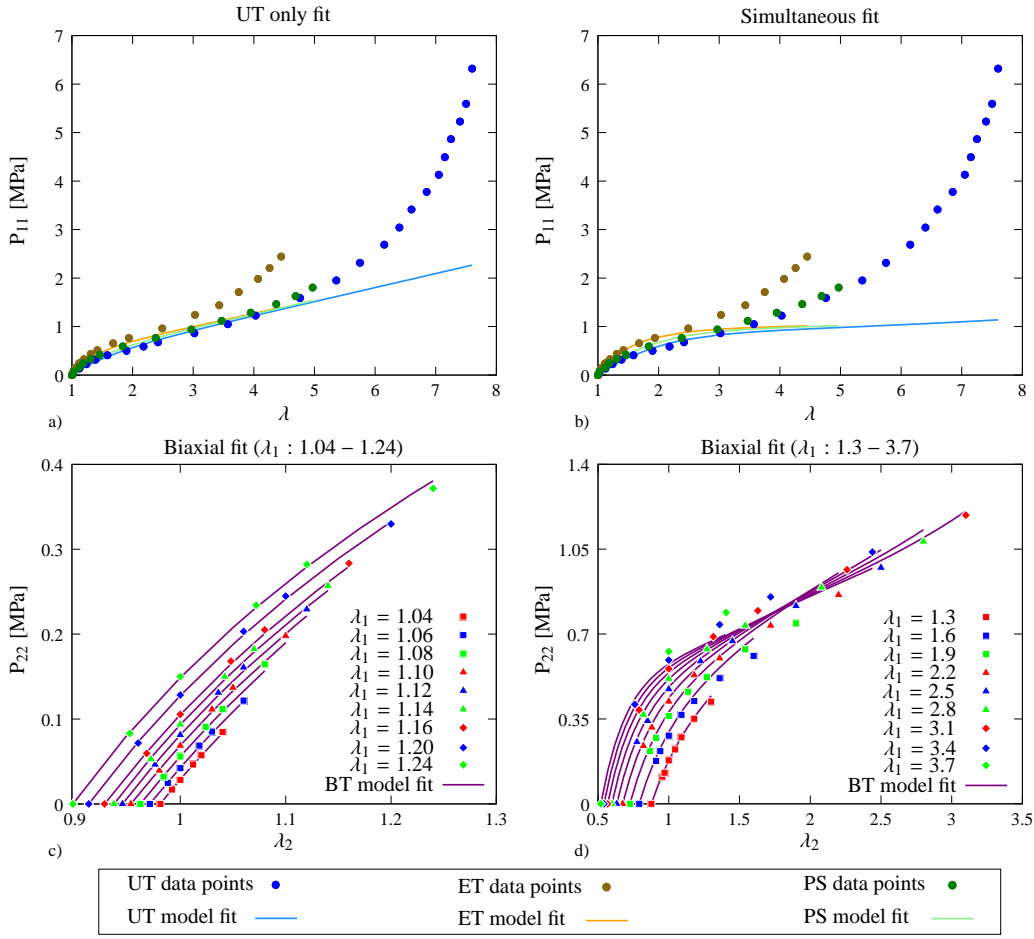


Figure 6.37: Constrained Junction model prediction for a) uniaxial tension, b) combination of uniaxial, equibiaxial, and pure shear loadings using Treloar data c) biaxial tension loading for $\lambda_1 : 1.04 - 1.24$, d) biaxial tension loading for $\lambda_1 : 1.3 - 3.7$ using Kawabata data.

Simultaneous fitting (Treloar)					
Parameters	$\mu_1=0.1308$ [MPa]	$\mu_2=0.2100$ [MPa]	$\kappa=1.6108$		
	Weight	Error	Quality of fit		
			Region 1	Region 2	Region 3
UT	0.1000	0.0432	0.0000	0.0076	0.0768
ET	0.8000	0.0081	0.0000	0.0000	0.0227
PS	0.1000	0.0380	0.0000	0.0096	0.0608
Total	1.0000	0.0893	0.0000	0.0171	0.1604

Table 6.111: Simultaneous fitting results for constrained-junction model.

UT only fit (Treloar)					
Parameters	$\mu_1=0.1461$ [MPa]	$\mu_2=0.1000$ [MPa]	$\kappa=1.0000$		
	Weight	Error	Quality of fit		
			Region 1	Region 2	Region 3
UT	1	0.0967	0.0095	0.0369	0.1167
ET	0	1.1541	0.0000	0.2103	1.2859
PS	0	0.1594	0.0095	0.0799	0.1746
Total	1	1.4102	0.0190	0.3272	1.5772

Table 6.112: Uniaxial tension results for constrained-junction model.

Biaxial fit (Kawabata)			
Parameters	$\mu_1=0.1686$ [MPa]	$\mu_2=0.1684$ [MPa]	$\kappa=1.3138$
Quality of fit: 0.8680	Biaxial error: 0.5111		

Table 6.113: Biaxial tension results for constrained-junction model.

6.2.38 WFB model results

WFB model with four material parameters has a poor fitting performance in simultaneous fitting. For individual fittings, especially in uniaxial tension, it is observed that the constitutive relation has an excellent fitting performance. Weighting function proposed by the reader should be reconsidered covering simultaneous fitting. In biaxial data fitting, solutions deviate from the expected results in high strain values. Fitting results are graphically given in Figure 6.38 and numerical results for simultaneous, uniaxial and biaxial fittings are given in Tables 6.114, 6.115, and 6.116, respectively.

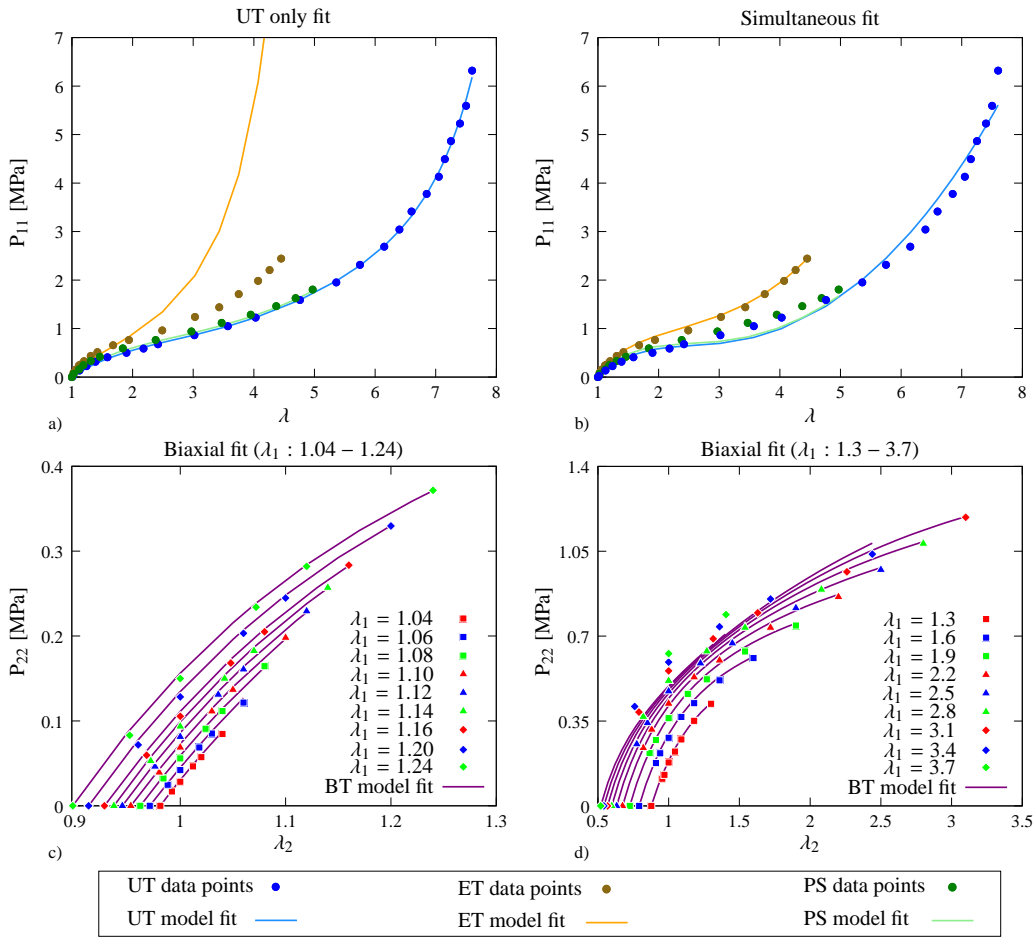


Figure 6.38: Weight Function Based (WFB) model prediction for a) uniaxial tension, b) combination of uniaxial, equibiaxial, and pure shear loadings using Treloar data c) biaxial tension loading for $\lambda_1 : 1.04 - 1.24$, d) biaxial tension loading for $\lambda_1 : 1.3 - 3.7$ using Kawabata data.

Simultaneous fitting (Treloar)					
Parameters	A=0.4921 [MPa] B=-0.0875 C=0.0112 [MPa]				
	D=-0.5284				
			Quality of fit		
	Weight	Error	Region 1	Region 2	Region 3
UT	0.4000	1.2250	0.0238	0.1619	0.4031
ET	0.3000	0.0249	0.0134	0.0365	0.0402
PS	0.3000	0.3301	0.0083	0.0220	0.2789
Total	1.0000	1.5800	0.0455	0.2204	0.7222

Table 6.114: Simultaneous fitting results for weight function based (WFB) model.

UT only fit (Treloar)					
Parameters	A=0.2369 [MPa] B=-0.1652 C=0.0629 [MPa]				
	D=0.0526				
			Quality of fit		
	Weight	Error	Region 1	Region 2	Region 3
UT	1	0.0730	0.0267	0.0270	0.0408
ET	0	118.3418	0.0831	0.2797	53.6698
PS	0	0.0242	0.0483	0.0590	0.0667
Total	1	118.4390	0.1581	0.3657	53.7773

Table 6.115: Uniaxial tension results for weight function based (WFB) model.

Biaxial fit (Kawabata)	
Parameters	A=25.9993 [MPa] B=1.9839 C=0.6443 [MPa]
	D=0.5566
Quality of fit: 1.1364	Biaxial error: 0.5035

Table 6.116: Biaxial tension results for weight function based (WFB) model.

6.2.39 neo-Hooke model results

Neo-hooke model with only one material constant has a poor fitting result for simultaneous fitting. Since the assumed distribution function for the end-to-end distances of molecular chains is Gaussian, it is not capable of generating the S-curve of rubber-like materials even for individual fittings. Results for biaxial loading also deviates from the actual response at higher stretch values. Fitting results are graphically given in Figure 6.39 and numerical results for simultaneous, uniaxial and biaxial fittings are given in Tables 6.117, 6.118, and 6.119, respectively.

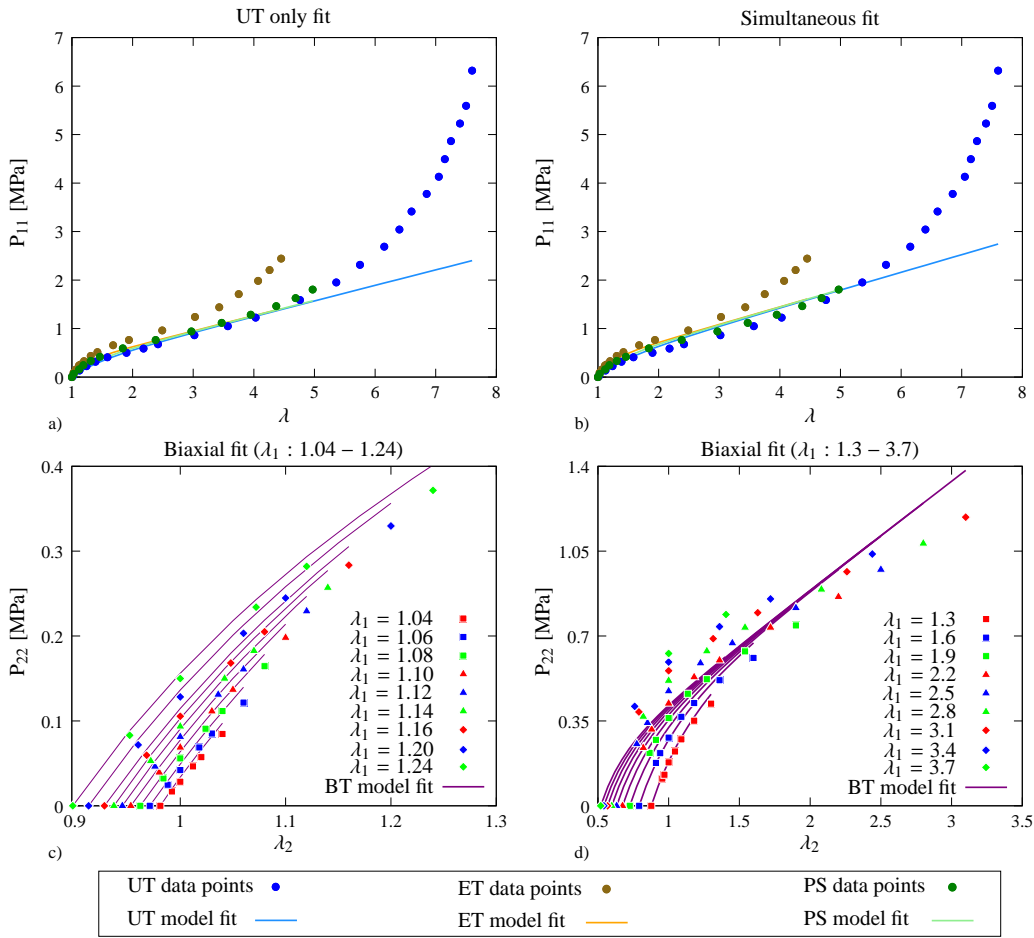


Figure 6.39: neo-Hooke model prediction for a) uniaxial tension, b) combination of uniaxial, equibiaxial, and pure shear loadings using Treloar data c) biaxial tension loading for $\lambda_1 : 1.04-1.24$, d) biaxial tension loading for $\lambda_1 : 1.3-3.7$ using Kawabata data.

Simultaneous fitting (Treloar)					
Parameters	$\mu=0.3617$ [MPa]				
	Weight	Error	Quality of fit		
			Region 1	Region 2	Region 3
UT	0.1000	0.0161	0.0000	0.0000	0.0389
ET	0.1000	0.0469	0.0000	0.0000	0.1022
PS	0.8000	$9.81e - 4$	0.0000	0.0000	0.0026
Total	1.0000	0.0640	0.0000	0.0000	0.1437

Table 6.117: Simultaneous fitting results for neo-Hooke model.

UT only fit (Treloar)					
Parameters	$\mu=0.3166$ [MPa]				
	Weight	Error	Quality of fit		
			Region 1	Region 2	Region 3
UT	1	0.0840	0.0091	0.0300	0.0946
ET	0	2.8168	0.0000	0.4338	3.0440
PS	0	0.2938	0.0171	0.1543	0.3164
Total	1	3.1946	0.0263	0.6181	3.4551

Table 6.118: Uniaxial tension results for neo-Hooke model.

Biaxial fit (Kawabata)	
Parameters	$\mu=0.4466$ [MPa]
Quality of fit: 5.3993	Biaxial error: 2.5606

Table 6.119: Biaxial tension results for neo-Hooke model.

6.2.40 Valanis-Landel model results

Like neo-Hooke model, Valanis-Landel model has only one material constant. The fitting performance of the model is poor in simultaneous fitting. The proposed model is not able to generate S-curve and for individual loading cases it has low fitting ability. Taking biaxial loading into the consideration, low fitting results can be observed even in low stretch values. Fitting results are graphically given in Figure 6.40 and numerical results for simultaneous, uniaxial and biaxial fittings are given in Tables 6.120, 6.121, and 6.122, respectively.

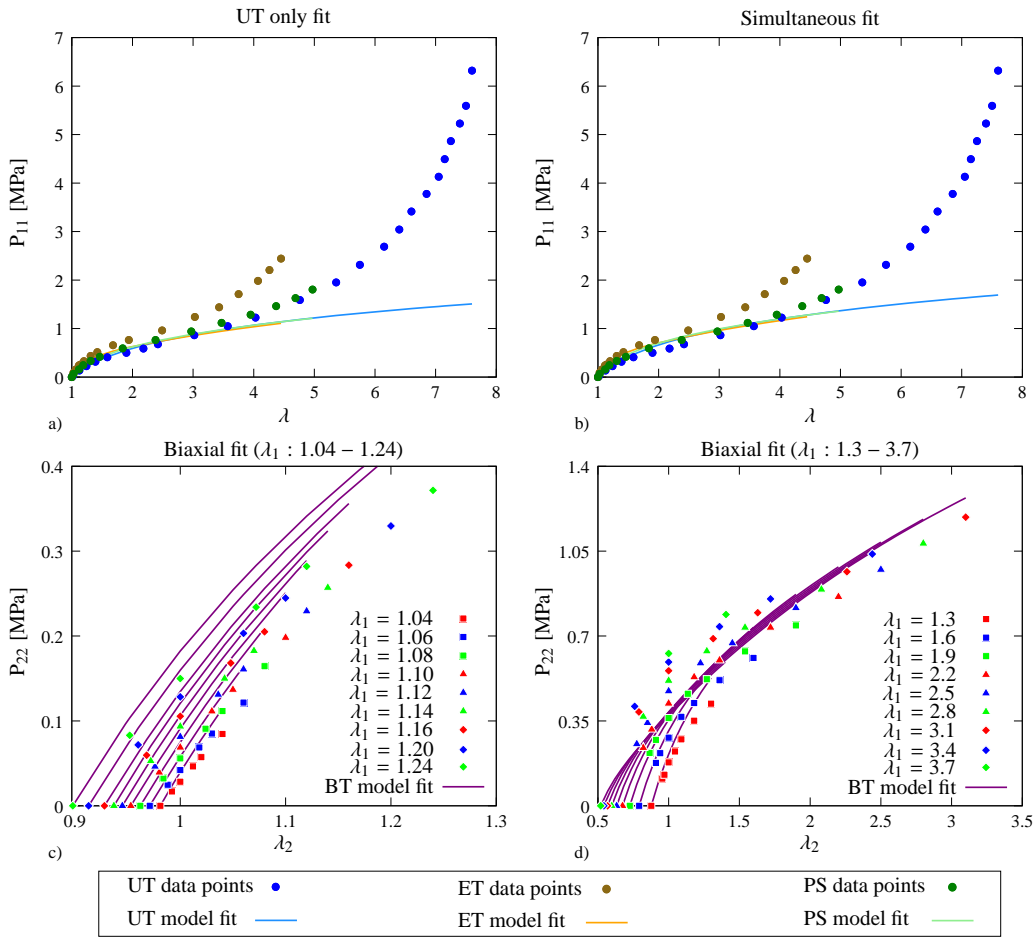


Figure 6.40: Valanis-Landel model prediction for a) uniaxial tension, b) combination of uniaxial, equibiaxial, and pure shear loadings using Treloar data c) biaxial tension loading for $\lambda_1 : 1.04-1.24$, d) biaxial tension loading for $\lambda_1 : 1.3-3.7$ using Kawabata data.

Simultaneous fitting (Treloar)					
Parameters	$\mu=0.4073$ [MPa]				
	Weight	Error	Quality of fit		
			Region 1	Region 2	Region 3
UT	0.1000	0.0287	0.0000	0.0000	0.0930
ET	0.8000	0.0024	0.0000	0.0000	0.0063
PS	0.1000	0.0125	0.0000	0.0000	0.0353
Total	1.0000	0.0436	0.0000	0.0000	0.1346

Table 6.120: Simultaneous fitting results for Valanis-Landel model.

UT only fit (Treloar)					
Parameters	$\mu=0.3631$ [MPa]				
	Weight	Error	Quality of fit		
			Region 1	Region 2	Region 3
UT	1	0.0897	0.0000	0.0150	0.1188
ET	0	1.3918	0.0000	0.0025	1.7007
PS	0	0.2591	0.0000	0.0036	0.2511
Total	1	1.7406	0.0000	0.0211	2.0706

Table 6.121: Uniaxial tension results for Valanis-Landel model.

Biaxial fit (Kawabata)	
Parameters	$\mu=0.5258$ [MPa]
Quality of fit: 7.1835	Biaxial error: 2.8856

Table 6.122: Biaxial tension results for Valanis-Landel model.

CHAPTER 7

CONCLUDING REMARKS

In this study 40 hyperelastic material models are considered and parameter optimization has been conducted on the related models. A parameter identification toolbox is developed to obtain the best fitting parameters of 40 hyperelastic material model. The toolbox can easily be adopted to different data sets and new material models. Starting with the introduction (chapter 1), general information about the necessity of the study is presented. A brief literature study on the hyperelastic material models since 1940 till 2017 has been supplied in chapter 2. Chapter 3 is composed of some preliminaries on continuum mechanics and hyperelastic material modeling. Preliminary derivations for hyperelastic response of rubber-like materials under different loading conditions has been considered. Definitions for 40 hyperelastic material models together with their strain energy functions are supplied in chapter 4. Here, the constitutive equations are categorized into phenomenological and micro-mechanically based material models as the two main categories in hyperelasticity. Models are ordered according to the publication dates. Parameter identification preliminaries and the genetic algorithm is introduced in chapter 5. A novel approach considering weight factors during the multi-objective optimization is introduced. Genetic algorithm code to be used in Matlab is developed. Genetic algorithm solutions are improved using MultiStart algorithm of Matlab software, Fmincon utility as a gradient method. Valid range of application for each model has been decided and fitting performance of each model is checked with χ^2 method. Results for the considered models are presented in chapter 6. Plots for UT only, and simultaneous fitting with Treloar data together with biaxial tension fitting with Kawabata's data are presented. For each model, numerical results of parameters, weight factors and quality of fit in three distinct regions are provided in tables. These tables include simultaneous, uniaxial and biaxial tension results.

Equibiaxial tension and pure shear fitting results are also provided in appendix A and B, respectively. An objective ranking table according to the fitting quality of the models are presented. Weakness and strength of each model is also analyzed in chapter 6.

Compressibility can also be adopted to the present work in future. The code can also be extended to compression loading mode. Also to improve the functionality of the toolbox it can be supported with an organized and well defined graphical user interface. Improving the graphical user interface and adding automatic report generating capabilities can make the toolbox commercially in used for various experiments and applications on rubber-like materials. In our work mean square error function is used as an objective function during the optimization procedure and χ^2 method is used to make comparison between the fitting performance of the constitutive relation. In the extended version of the code, instead of mean square error function, objective function can be considered as χ^2 .

REFERENCES

- [1] C. Miehe, S. Göktepe, and F. Lulei, “A micro-macro approach to rubber-like materials—part i: the non-affine micro-sphere model of rubber elasticity,” *Journal of the Mechanics and Physics of Solids*, vol. 52, no. 11, pp. 2617–2660, 2004.
- [2] L. R. G. Treloar, “The elasticity of a network of long-chain molecules-ii,” *Transactions of the Faraday Society*, vol. 39, pp. 241–246, 1943.
- [3] S. Kawabata, M. Matsuda, K. Tei, and H. Kawai, “Experimental survey of the strain energy density function of isoprene rubber vulcanizate,” *Macromolecules*, vol. 14, no. 1, pp. 154–162, 1981.
- [4] M. Mooney, “A theory of large elastic deformation,” *Journal of applied physics*, vol. 11, no. 9, pp. 582–592, 1940.
- [5] F. T. Wall, “Statistical thermodynamics of rubber,” *The Journal of Chemical Physics*, vol. 10, no. 2, pp. 132–, 1942.
- [6] M. C. Wang and E. Guth, “Statistical theory of networks of non-gaussian flexible chains,” *The Journal of Chemical Physics*, vol. 20, no. 7, pp. 1144–1157, 1952.
- [7] P. J. Flory and J. Rehner, “Statistical mechanics of cross-linked polymer networks i. rubberlike elasticity,” *The journal of chemical physics*, vol. 11, no. 11, pp. 512–520, 1943.
- [8] L. R. G. Treloar and G. Riding, “A non-gaussian theory of rubber in biaxial strain. i.mechanical properties,” vol. 369, pp. 261–280, 1979.
- [9] E. M. Arruda and M. C. Boyce, “A three-dimensional constitutive model for the large stretch behavior of rubber elastic materials,” *Journal of the Mechanics and Physics of Solids*, vol. 41, no. 2, pp. 389–412, 1993.
- [10] R. S. Rivlin and D. W. Saunders, “Large elastic deformations of isotropic materials vii. experiments on the deformation of rubber,” *Philosophical Transactions*

of the Royal Society of London. Series A, Mathematical and Physical Sciences, vol. 243, no. 865, pp. 251–288, 1951.

- [11] J. Bonet and R. D. Wood, *Nonlinear continuum mechanics for finite element analysis*. Cambridge university press, 1997.
- [12] M. C. Boyce and E. M. Arruda, “Constitutive models of rubber elasticity: a review,” *Rubber chemistry and technology*, vol. 73, no. 3, pp. 504–523, 2000.
- [13] G. Marckmann and E. Verron, “Comparison of hyperelastic models for rubber-like materials,” *Rubber chemistry and technology*, vol. 79, no. 5, pp. 835–858, 2006.
- [14] P. Steinmann, M. Hossain, and G. Possart, “Hyperelastic models for rubber-like materials: consistent tangent operators and suitability for treloar’s data,” *Archive of Applied Mechanics*, vol. 82, no. 9, pp. 1183–1217, 2012.
- [15] M. Hossain and P. Steinmann, “More hyperelastic models for rubber-like materials: consistent tangent operators and comparative study,” *Journal of the Mechanical Behavior of Materials*, vol. 22, no. 1-2, pp. 27–50, 2013.
- [16] T. Beda, “Modeling hyperelastic behavior of rubber: A novel invariant-based and a review of constitutive models,” *Journal of Polymer Science Part B: Polymer Physics*, vol. 45, no. 13, pp. 1713–1732, 2007.
- [17] T. Beda, “An approach for hyperelastic model-building and parameters estimation a review of constitutive models,” *European Polymer Journal*, vol. 50, pp. 97–108, 2014.
- [18] R. H. Gerke, “Thermodynamics of stressed vulcanized rubber,” *Industrial & Engineering Chemistry*, vol. 22, no. 1, pp. 73–77, 1930.
- [19] L. R. G. Treloar, “The elasticity of a network of long-chain molecules.—iii,” *Transactions of the Faraday Society*, vol. 42, pp. 83–94, 1946.
- [20] H. M. James, “Statistical properties of networks of flexible chains,” *The Journal of Chemical Physics*, vol. 15, no. 9, pp. 651–668, 1947.

- [21] A. Isihara, N. Hashitsume, and M. Tatibana, "Statistical theory of rubber-like elasticity. iv.(two-dimensional stretching)," *The Journal of Chemical Physics*, vol. 19, no. 12, pp. 1508–1512, 1951.
- [22] V. Biderman, "Calculation of rubber parts," *Rascheti na prochnost*, vol. 40, 1958.
- [23] A. N. Gent and A. Thomas, "Forms for the stored (strain) energy function for vulcanized rubber," *Journal of Polymer Science*, vol. 28, no. 118, pp. 625–628, 1958.
- [24] L. J. Hart-Smith, "Elasticity parameters for finite deformations of rubber-like materials," *Zeitschrift für angewandte Mathematik und Physik ZAMP*, vol. 17, no. 5, pp. 608–626, 1966.
- [25] K. C. Valanis and R. F. Landel, "The strain-energy function of a hyperelastic material in terms of the extension ratios," *Journal of Applied Physics*, vol. 38, no. 7, pp. 2997–3002, 1967.
- [26] H. Alexander, "A constitutive relation for rubber-like materials," *International Journal of Engineering Science*, vol. 6, no. 9, pp. 549–563, 1968.
- [27] R. W. Ogden, "Large deformation isotropic elasticity-on the correlation of theory and experiment for incompressible rubberlike solids," *Proc. R. Soc. Lond. A*, vol. 326, no. 1567, pp. 565–584, 1972.
- [28] A. G. James, A. Green, and G. M. Simpson, "Strain energy functions of rubber. i. characterization of gum vulcanizates," *Journal of Applied Polymer Science*, vol. 19, no. 7, pp. 2033–2058, 1975.
- [29] D. Haines and W. Wilson, "Strain-energy density function for rubberlike materials," *Journal of the Mechanics and Physics of Solids*, vol. 27, no. 4, pp. 345–360, 1979.
- [30] R. C. Ball, M. Doi, S. F. Edwards, and M. Warner, "Elasticity of entangled networks," *Polymer*, vol. 22, no. 8, pp. 1010–1018, 1981.

- [31] B. Erman and P. J. Flory, "Relationships between stress, strain, and molecular constitution of polymer networks. comparison of theory with experiments," *Macromolecules*, vol. 15, no. 3, pp. 806–811, 1982.
- [32] S. R. Swanson, "A constitutive model for high elongation elastic materials," *Journal of engineering materials and technology*, vol. 107, no. 2, pp. 110–114, 1985.
- [33] H.-G. Kilian, H. F. Enderle, and K. Unseld, "The use of the van der waals model to elucidate universal aspects of structure-property relationships in simply extended dry and swollen rubbers," *Colloid and Polymer Science*, vol. 264, no. 10, pp. 866–876, 1986.
- [34] O. H. Yeoh, "Characterization of elastic properties of carbon-black-filled rubber vulcanizates," *Rubber chemistry and technology*, vol. 63, no. 5, pp. 792–805, 1990.
- [35] Y. Yamashita and S. Kawabata, "Approximated form of the strain energy-density function of carbon-black filled rubbers for industrial applications," *Nippon Gomu Kyokaishi (Journal of the Society of Rubber Industry, Japan)*, vol. 65, no. 9, pp. 517–528, 1992.
- [36] L. R. G. Treloar, "The physics of rubber elasticity," *Oxford University Press*, 1975.
- [37] A. N. Gent, "A new constitutive relation for rubber," *Rubber chemistry and technology*, vol. 69, no. 1, pp. 59–61, 1996.
- [38] S. F. Edwards and T. A. Vilgis, "The tube model theory of rubber elasticity," *Reports on Progress in Physics*, vol. 51, no. 2, p. 243., 1988.
- [39] M. Doi, *Introduction to polymer physics*. 1996.
- [40] G. Heinrich and M. Kaliske, "Theoretical and numerical formulation of a molecular based constitutive tube-model of rubber elasticity," *Computational and Theoretical Polymer Science*, vol. 7, no. 3-4, pp. 227–241, 1997.
- [41] A. Lion, "On the large deformation behaviour of reinforced rubber at different

- temperatures,” *Journal of the Mechanics and Physics of Solids*, vol. 45, no. 11-12, pp. 1805–1834, 1997.
- [42] O. H. Yeoh and P. D. Fleming, “A new attempt to reconcile the statistical and phenomenological theories of rubber elasticity,” *Journal of Polymer Science Part B: Polymer Physics*, vol. 35, no. 12, pp. 1919–1931, 1997.
- [43] J. Lambert-Diani and C. Rey, “New phenomenological behavior laws for rubbers and thermoplastic elastomers,” *European Journal of Mechanics-A/Solids*, vol. 18, no. 6, pp. 1027–1043, 1999.
- [44] L. R. G. Treloar, “Stress-strain data for vulcanized rubber under various types of deformation,” *Rubber Chemistry and Technology*, vol. 17, no. 4, pp. 813–825, 1944.
- [45] M. Kaliske and G. Heinrich, “An extended tube-model for rubber elasticity: statistical-mechanical theory and finite element implementation,” *Rubber Chemistry and Technology*, vol. 72, no. 4, pp. 602–632, 1999.
- [46] M. H. B. M. Shariff, “Strain energy function for filled and unfilled rubberlike material,” *Rubber chemistry and technology*, vol. 73, no. 1, pp. 1–18, 2000.
- [47] P. Haupt and K. Sedlan, “Viscoplasticity of elastomeric materials: experimental facts and constitutive modelling,” *Archive of Applied Mechanics*, vol. 71, no. 2-3, pp. 89–109, 2001.
- [48] L. Chevalier and Y. Marco, “Tools for multiaxial validation of behavior laws chosen for modeling hyper-elasticity of rubber-like materials,” *Polymer Engineering & Science*, vol. 42, no. 2, pp. 280–298, 2002.
- [49] E. Pucci and G. Saccomandi, “A note on the gent model for rubber-like materials,” *Rubber chemistry and technology*, vol. 75, no. 5, pp. 839–852, 2002.
- [50] M. Doi and S. F. Edwards, *The theory of polymer dynamics*, vol. 73. 1988.
- [51] M. M. Attard and G. W. Hunt, “Hyperelastic constitutive modeling under finite strain,” *International Journal of Solids and Structures*, vol. 41, no. 18-19, pp. 5327–5350, 2004.

- [52] A. F. Amin, S. I. Wiraguna, A. R. Bhuiyan, and Y. Okui, “Hyperelasticity model for finite element analysis of natural and high damping rubbers in compression and shear,” *Journal of engineering mechanics*, vol. 132, no. 1, pp. 54–64, 2006.
- [53] H. Bechir, L. Chevalier, M. Chaouche, and K. Boufala, “Hyperelastic constitutive model for rubber-like materials based on the first seth strain measures invariant,” *European Journal of Mechanics-A/Solids*, vol. 25, no. 1, pp. 110–124, 2006.
- [54] O. Lopez-Pamies, “A new il-based hyperelastic model for rubber elastic materials,” *Comptes Rendus Mecanique*, vol. 338, no. 1, pp. 3–11, 2010.
- [55] M. M. Carroll, “A strain energy function for vulcanized rubbers,” *Journal of Elasticity*, vol. 103, no. 2, pp. 173–187, 2011.
- [56] L. C. S. Nunes, “Mechanical characterization of hyperelastic polydimethylsiloxane by simple shear test,” *Materials Science and Engineering: A*, vol. 528, no. 3, pp. 1799–1804, 2011.
- [57] H. Khajehsaeid, J. Arghavani, and R. Naghdabadi, “A hyperelastic constitutive model for rubber-like materials,” *European Journal of Mechanics-A/Solids*, vol. 38, pp. 144–151, 2013.
- [58] V. N. Khiêm and M. Itskov, “Analytical network-averaging of the tube model:: Rubber elasticity,” *Journal of the Mechanics and Physics of Solids*, vol. 95, pp. 254–269, 2016.
- [59] A. G. Korba and M. E. Barkey, “New model for hyper-elastic materials behavior with an application on natural rubber,” in *ASME 2017 12th International Manufacturing Science and Engineering Conference collocated with the JSME/ASME 2017 6th International Conference on Materials and Processing*, pp. V002T03A020–V002T03A020, American Society of Mechanical Engineers, 2017.
- [60] H. Dal, Y. Badienia, K. Açıkğöz, and F. A. Denli, “A novel parameter identification toolbox for the selection of hyperelastic constitutive models from experimental data,” *eps*, vol. 11, no. P11, p. 2.

- [61] H. Dal, Y. Badienia, K. Açikgöz, and F. A. Denli, “A comparative study on hyperelastic constitutive models on rubber: State of the art after 2006,” 2019.
- [62] H. Dal, “A quasi-incompressible and quasi-inextensible element formulation for transversely isotropic materials,” *International Journal for Numerical Methods in Engineering*, vol. 117, no. 1, pp. 118–140, 2019.
- [63] W. Kuhn and F. Grün, “Beziehungen zwischen elastischen konstanten und dehnungsdoppelbrechung hochelastischer stoffe,” *Kolloid-Zeitschrift*, vol. 101, no. 3, pp. 248–271, 1942.
- [64] H. Pak and P. J. Flory, “Relationship of stress to uniaxial strain in crosslinked poly (dimethylsiloxane) over the full range from large compressions to high elongations,” *Journal of Polymer Science: Polymer Physics Edition*, vol. 17, no. 11, pp. 1845–1854, 1979.
- [65] R. T. Deam and S. F. Edwards, “The theory of rubber elasticity,” *Philosophical Transactions of the Royal Society of London. Series A Mathematical and Physical Sciences (1934-1990)*, vol. 280, no. 1296, pp. 317–353, 1976.
- [66] B. Flory, Paul J.; Erman, “Theory of elasticity of polymer networks. 3,” *Macromolecules*, vol. 15, no. 3, pp. 800–806, 1982.
- [67] L. J. Hart-Smith, “Elasticity parameters for finite deformations of rubber-like materials,” *Zeitschrift für angewandte Mathematik und Physik ZAMP*, vol. 17, no. 5, pp. 608–626, 1966.

Appendix A

EQUIBIAXIAL TENSION RESULTS FOR HYPERELASTIC MODELS

ET only fit (Treloar)					
Parameters	$\mu=0.2919$ [MPa]		$N=27.0855$	$p=3.2767$	
	$U=0.4394$		$q=0.0878$		
			Quality of fit		
	Weight	Error	Region 1	Region 2	Region 3
UT	0	277.7764	0.2131	1.3015	54.3806
ET	1	0.0025	0.0088	0.0097	0.0104
PS	0	1.9997	0.0130	0.1017	1.4040
Total	1	279.7785	0.2350	1.4130	55.7950

Table A.1: Equibiaxial tension results for Micro-Sphere model.

ET only fit (Treloar)					
Parameters	$C_1=0.1764$ [MPa]		$C_2=0.0655$ [MPa]	$C_3=7.95e-4$ [MPa]	
	$\gamma=2.2576$		$k=2.78e-4$		
			Quality of fit		
	Weight	Error	Region 1	Region 2	Region 3
UT	0	1.5733	0.0640	0.3100	0.6853
ET	1	0.0028	0.0120	0.0129	0.0135
PS	0	0.3021	0.0071	0.0306	0.2329
Total	1	1.8781	0.0831	0.3534	0.9316

Table A.2: Equibiaxial tension fitting results for Alexander model.

ET only fit (Treloar)					
Parameters	$exp(a_0)=0.2430$ [MPa]		$a_1=0.0283$ [MPa]	$a_2=-1.16e-4$ [MPa]	
	$exp(b_0)=-0.0254$ [MPa]		$b_1=-0.0801$		
			Quality of fit		
	Weight	Error	Region 1	Region 2	Region 3
UT	0	338.9997	0.5239	7.8807	89.2520
ET	1	0.0022	0.0089	0.0096	0.0102
PS	0	15.5327	0.0160	0.2863	10.3068
Total	1	354.5347	0.5488	8.1766	99.5689

Table A.3: Equibiaxial tension results for Diani and Ray model.

ET only fit (Treloar)					
Parameters	$G_c=0.2206$ [MPa] $\delta=0.0941$ [MPa] $G_e=0.1566$ $\beta=2.11e-6$				
	Quality of fit				
	Weight	Error	Region 1	Region 2	Region 3
UT	0	1.5311	0.0061	0.0180	0.3877
ET	1	0.0051	0.0226	0.0241	0.0247
PS	0	0.0289	0.0113	0.0114	0.0287
Total	1	1.5651	0.0400	0.0535	0.4410

Table A.4: Equibiaxial tension results for Extended-Tube model.

ET only fit (Treloar)					
Parameters	$E=1.3542$ [MPa] $\alpha_1=-4.3742$ $\alpha_2=6.2276$ $\alpha_3=-0.0015$ $\alpha_4=-2.2508$				
	Quality of fit				
	Weight	Error	Region 1	Region 2	Region 3
UT	0	$1.98e6$	0.4497	629.6295	$4.05e5$
ET	1	0.0027	0.0077	0.0089	0.0096
PS	0	$2.50e3$	0.0195	0.2590	$1.48e3$
Total	1	$1.99e6$	0.4770	629.8974	$4.06e5$

Table A.5: Equibiaxial tension results for Shariff model.

ET only fit (Treloar)					
Parameters	$A=0.1983$ [MPa] $B=3.11e-7$ [MPa] $C=2.04e-5$ [MPa]				
	Quality of fit				
	Weight	Error	Region 1	Region 2	Region 3
UT	0	5.5904	0.1175	0.6492	1.9545
ET	1	0.0063	0.0184	0.0223	0.0232
PS	0	0.6571	0.0074	0.0489	0.4946
Total	1	6.2542	0.1433	0.7204	2.4724

Table A.6: Equibiaxial tension results for Carroll model.

ET only fit (Treloar)					
Parameters	$\mu_c k = 0.1447$ [MPa]		$n = 15.2554$ $q = 0.8582$		
	$\mu_l = 2.19e - 6$ [MPa]				
	Weight	Error	Quality of fit		
			Region 1	Region 2	Region 3
UT	0	16.8384	0.1588	0.6569	4.0330
ET	1	0.0030	0.0102	0.0111	0.0118
PS	0	0.6170	0.0098	0.0658	0.4773
Total	1	17.4584	0.1788	0.7338	4.5185

Table A.7: Equibiaxial tension results network averaging tube model.

ET only fit (Treloar)					
Parameters	$a_0 = 0.4845$ [MPa]		$a_1 = 0.1100$ [MPa]		$a_2 = 5.94e - 5$ [MPa]
	$b_0 = -0.2185$ [MPa]		$b_1 = 0.1613$ [MPa]		$b_2 = -0.5625$ [MPa]
	Weight	Error	Quality of fit		
			Region 1	Region 2	Region 3
UT	0	3.32e4	12.2765	667.0533	1.53e4
ET	1	0.0016	0.0040	0.0043	0.0050
PS	0	1.73e3	0.1451	9.9151	1.11e3
Total	1	6.49e4	12.4256	686.9728	1.64e4

Table A.8: Equibiaxial tension results for Chevalier and Marco model.

ET only fit (Treloar)					
Parameters	$\mu_1 = 0.4165$ [MPa]		$\mu_2 = 0.0548$ [MPa]		$\mu_3 = 0.0604$ [MPa]
	$\alpha_1 = 1.9701$		$\alpha_2 = 4.9307$		$\alpha_3 = -2.4208$
	Weight	Error	Quality of fit		
			Region 1	Region 2	Region 3
UT	0	1.47e5	4.5506	654.3110	3.35e4
ET	1	0.0022	0.0064	0.0076	0.0082
PS	0	1.95e3	0.0514	4.0965	1.22e3
Total	1	1.45e5	4.6084	658.4152	3.47e4

Table A.9: Equibiaxial tension results for Ogden model.

ET only fit (Treloar)					
Parameters	$C_2=0.0028$ [MPa]	$C_3=1.92e-6$ [MPa]	$C_4=-94.6990$ [MPa]		
	$C_5=94.8998$ [MPa]	$M=1.06e-4$	$N=2.8475$		
	Quality of fit				
	Weight	Error	Region 1	Region 2	Region 3
UT	0	3.5901	0.1234	0.2945	0.9153
ET	1	0.0026	0.0040	0.0059	0.0065
PS	0	0.1058	0.0140	0.0473	0.1153
Total	1	3.6985	0.1414	0.3477	1.0371

Table A.10: Equibiaxial tension results for Amin model.

ET only fit (Treloar)					
Parameters	$C_{10}=0.4037$ [MPa]	$C_{01}=-0.1599$ [MPa]	$C_{11}=-0.0526$ [MPa]		
	$C_{20}=0.1182$ [MPa]	$C_{30}=0.0132$ [MPa]			
	Quality of fit				
	Weight	Error	Region 1	Region 2	Region 3
UT	0	$2.11e7$	31.8252	$3.12e4$	$4.56e6$
ET	1	0.0022	0.0055	0.0066	0.0071
PS	0	$1.07e5$	0.1126	41.1770	$6.46e4$
Total	1	$2.12e7$	31.9432	$3.13e4$	$4.63e6$

Table A.11: Equibiaxial tension results for James model.

ET only fit (Treloar)					
Parameters	$C_{10}=0.3342$ [MPa]	$C_{01}=-0.1003$ [MPa]	$C_{11}=-0.0272$ [MPa]		
	$C_{02}=-1.55e-6$ [MPa]	$C_{20}=0.0649$ [MPa]	$C_{30}=0.0068$ [MPa]		
	Quality of fit				
	Weight	Error	Region 1	Region 2	Region 3
UT	0	$5.73e6$	11.3043	$8.75e3$	$1.24e6$
ET	1	0.0021	0.0067	0.0076	0.0081
PS	0	$2.96e4$	0.0581	13.4249	$1.80e4$
Total	1	$5.75e6$	11.3691	$8.77e3$	$1.26e6$

Table A.12: Equibiaxial tension results for Haines and Wilson model.

ET only fit (Treloar)					
Parameters	$A_1=0.4550$ [MPa]	$A_2=-0.0219$ [MPa]	$A_3=0.0022$ [MPa]		
	$B_1=1.23e-4$ [MPa]	$B_2=-5.46e-5$ [MPa]	$B_3=2.29e-8$ [MPa]		
		Quality of fit			
	Weight	Error	Region 1	Region 2	Region 3
UT	0	1.03e4	0.1258	11.4912	2.22e3
ET	1	0.0025	0.0117	0.0121	0.0127
PS	0	39.2720	0.0081	0.0589	23.7168
Total	1	1.04e4	0.1456	11.5622	2.24e3

Table A.13: Equibiaxial tension results for Attard and Hunt model.

ET only fit (Treloar)					
Parameters	$C_1^1=0.0596$ [MPa]	$C_2^1=-0.0220$ [MPa]	$C_1^2=0.0443$ [MPa]		
	$C_2^2=1.19e-6$ [MPa]				
		Quality of fit			
	Weight	Error	Region 1	Region 2	Region 3
UT	0	1.56e4	2.9156	129.3340	3.65e3
ET	1	0.0030	0.0062	0.0080	0.0087
PS	0	324.5130	0.0487	2.1177	207.8771
Total	1	1.59e4	2.9705	131.4598	3.86e3

Table A.14: Equibiaxial tension results for 4-term Bechir model.

ET only fit (Treloar)					
Parameters	$C_2=0.1378$ [MPa]	$\mu=0.3072$ [MPa]	$J_m=88.6946$		
		Quality of fit			
	Weight	Error	Region 1	Region 2	Region 3
UT	0	3.1673	0.0237	0.2268	1.0415
ET	1	0.0031	0.0141	0.0151	0.0158
PS	0	0.3591	0.0071	0.0161	0.2521
Total	1	3.5295	0.0449	0.2581	1.3094

Table A.15: Equibiaxial tension results for Pucci and Saccomandi model.

ET only fit (Treloar)					
Parameters	$C_{10}=0.2072$ [MPa]	$C_{01}=7.11e-5$ [MPa]	$C_{20}=-9.22e-4$ [MPa]		
	$C_{30}=3.34e-5$ [MPa]				
		Quality of fit			
	Weight	Error	Region 1	Region 2	Region 3
UT	0	3.6072	0.1527	0.6527	1.5413
ET	1	0.0031	0.0128	0.0136	0.0142
PS	0	0.5886	0.0080	0.0647	0.4570
Total	1	4.1990	0.1736	0.7309	2.0124

Table A.16: Equibiaxial tension results for Biderman model.

ET only fit (Treloar)					
Parameters	$G=0.4461$ [MPa]	$\lambda_m=11.1104$	$\beta=1.57e-4$		
	$\alpha=0.2340$				
		Quality of fit			
	Weight	Error	Region 1	Region 2	Region 3
UT	0	3.5784	0.1621	0.6343	1.5217
ET	1	0.0023	0.0082	0.0092	0.0098
PS	0	0.5844	0.0116	0.0673	0.4507
Total	1	4.1651	0.1819	0.7108	1.9823

Table A.17: Equibiaxial tension results for Kilian (van der Waals) model.

ET only fit (Treloar)					
Parameters	$C_2=0.0011$ [MPa]	$C_3=3.03e-7$ [MPa]	$C_5=0.1939$ [MPa]		
	$N=3.3820$				
		Quality of fit			
	Weight	Error	Region 1	Region 2	Region 3
UT	0	2.1591	0.0970	0.4834	0.9224
ET	1	0.0087	0.0209	0.0268	0.0282
PS	0	0.3994	0.0079	0.0397	0.3174
Total	1	2.5672	0.1258	0.5499	1.2681

Table A.18: Equibiaxial tension results for Yamashita and Kawabata model.

ET only fit (Treloar)					
Parameters	$C_{10}=0.1952$ [MPa]	$C_{01}=0.0012$ [MPa]	$C_{03}=6.48e-9$ [MPa]		
			Quality of fit		
	Weight	Error	Region 1	Region 2	Region 3
UT	0	7.7762	0.1035	0.4983	2.0072
ET	1	0.0095	0.0198	0.0250	0.0269
PS	0	0.3935	0.0077	0.0430	0.3183
Total	1	8.1792	0.1310	0.5662	2.3525

Table A.19: Equibiaxial tension results for Lion model.

ET only fit (Treloar)					
Parameters	$C_{10}=0.1790$ [MPa]	$B=4.99e-5$ [MPa]	$K=0.0747$ [MPa]		
	$\alpha=3.0883$				
			Quality of fit		
	Weight	Error	Region 1	Region 2	Region 3
UT	0	2.6879	0.0702	0.3893	1.0991
ET	1	0.0027	0.0131	0.0136	0.0142
PS	0	0.4542	0.0071	0.0340	0.3345
Total	1	3.1448	0.0904	0.4369	1.4482

Table A.20: Equibiaxial tension results for Beda model.

ET only fit (Treloar)					
Parameters	$G=0.1834$ [MPa]	$k_1=2.96e-4$	$k_2=0.3317$		
			Quality of fit		
	Weight	Error	Region 1	Region 2	Region 3
UT	0	5.5854	0.0819	0.4461	1.7516
ET	1	0.0031	0.0135	0.0140	0.0147
PS	0	0.4944	0.0071	0.0387	0.3685
Total	1	6.0828	0.1025	0.4989	2.1348

Table A.21: Equibiaxial tension results for Hart-Smith model.

ET only fit (Treloar)					
Parameters	$c_1=0.2527$ [MPa]	$c_2=-0.0303$ [MPa]	$c_3=0.0044$ [MPa]		
	$c_4=-2.53e-6$ [MPa]	$c_5=-0.0011$ [MPa]			
			Quality of fit		
	Weight	Error	Region 1	Region 2	Region 3
UT	0	$1.08e5$	0.4026	87.3263	$2.30e4$
ET	1	0.0022	0.0083	0.0091	0.0097
PS	0	337.4034	0.0184	0.1452	200.7400
Total	1	$1.08e5$	0.4293	87.4806	$2.32e4$

Table A.22: Equibiaxial tension results for Haupt and Sedlan model.

ET only fit (Treloar)					
Parameters	$A=0.2278$ [MPa]	$a=0.0137$	$b=0.1247$ [MPa]		
			Quality of fit		
	Weight	Error	Region 1	Region 2	Region 3
UT	0	2.8791	0.1683	0.5998	1.3120
ET	1	0.0047	0.0077	0.0113	0.0125
PS	0	0.5833	0.0172	0.0698	0.4439
Total	1	3.4671	0.1933	0.6810	1.7684

Table A.23: Equibiaxial tension results for Exp-Ln model.

ET only fit (Treloar)					
Parameters	$C_{10}=0.2071$ [MPa]	$C_{20}=-8.94e-4$ [MPa]	$C_{30}=3.33e-5$ [MPa]		
			Quality of fit		
	Weight	Error	Region 1	Region 2	Region 3
UT	0	3.8303	0.1527	0.6629	1.6107
ET	1	0.0031	0.0129	0.0137	0.0142
PS	0	0.6085	0.0080	0.0647	0.4701
Total	1	4.4419	0.1736	0.7413	2.0950

Table A.24: Equibiaxial tension results for Yeoh model.

ET only fit (Treloar)					
Parameters	$\alpha_1=0.9003$	$\alpha_2=3.0016$	$\mu_1=0.4279$ [MPa]		
	$\mu_2=0.0012$ [MPa]				
			Quality of fit		
	Weight	Error	Region 1	Region 2	Region 3
UT	0	3.1431	0.1658	0.6425	1.4394
ET	1	0.0023	0.0099	0.0106	0.0112
PS	0	0.5876	0.0103	0.0692	0.4535
Total	1	3.7330	0.1861	0.7223	1.9041

Table A.25: Equibiaxial tension results for two-term model.

ET only fit (Treloar)					
Parameters	$A=0.2116$ [MPa]	$B=31.6895$	$C_{10}=4.2914$ [MPa]		
	$I_m=714.1750$				
			Quality of fit		
	Weight	Error	Region 1	Region 2	Region 3
UT	0	2.9946	0.1664	0.6466	1.3936
ET	1	0.0024	0.0109	0.0114	0.0120
PS	0	0.5820	0.0093	0.0702	0.4508
Total	1	3.5791	0.1867	0.7282	1.8565

Table A.26: Equibiaxial tension results for Yeoh-Fleming model.

ET only fit (Treloar)					
Parameters	$\mu=0.1192$ [MPa]		$N=30.4174$		
			Quality of fit		
	Weight	Error	Region 1	Region 2	Region 3
UT	0	2.5312	0.0613	0.5722	1.2156
ET	1	0.0258	0.0334	0.0561	0.0615
PS	0	0.7451	0.0134	0.0290	0.5302
Total	1	3.3020	0.1081	0.6573	1.8073

Table A.27: Equibiaxial tension results for Arruda-Boyce model.

ET only fit (Treloar)					
Parameters	$\mu=0.3437$ [MPa] $J_m=118.2802$				
	Weight	Error	Quality of fit		
			Region 1	Region 2	Region 3
UT	0	3.1376	0.0568	0.5749	1.2900
ET	1	0.0319	0.0357	0.0618	0.0694
PS	0	0.7758	0.0147	0.0287	0.5493
Total	1	3.9453	0.1072	0.6654	1.9087

Table A.28: Equibiaxial tension results for Gent model.

ET only fit (Treloar)					
Parameters	$\mu=0.3574$ [MPa] $N=45.5545$				
	Weight	Error	Quality of fit		
			Region 1	Region 2	Region 3
UT	0	$6.11e3$	0.0853	1.9276	$1.59e3$
ET	1	0.0253	0.0325	0.0547	0.0600
PS	0	4.4234	0.0124	0.0410	2.8233
Total	1	$6.11e3$	0.1302	2.0232	$1.59e3$

Table A.29: Equibiaxial tension results for three-chain model.

ET only fit (Treloar)					
Parameters	$C_{10}=0.1847$ [MPa] $C_{01}=0.0031$ [MPa]				
	Weight	Error	Quality of fit		
			Region 1	Region 2	Region 3
UT	0	40.527	0.0616	0.2767	8.0857
ET	1	0.1153	0.0275	0.0404	0.0869
PS	0	0.1563	0.0106	0.0264	0.1425
Total	1	40.799	0.0996	0.3435	8.3152

Table A.30: Equibiaxial tension results for Mooney model.

ET only fit (Treloar)						
Parameters	$C_{10}=0.3915$ [MPa]	$C_{20}=0.0347$ [MPa]	$C_{01}=-0.1371$ [MPa]	Quality of fit		
	Weight	Error	Region 1	Region 2	Region 3	
UT	0	5.93e3	0.7331	114.1330	4.19e3	
ET	1	0.0408	0.0000	0.0541	0.0779	
PS	0	4.8317	0.3146	64.3727	3.28e3	
Total	1	1.07e4	1.0478	178.5598	7.47e3	

Table A.31: Equibiaxial tension results for Isihara model.

ET only fit (Treloar)					
Parameters	$C_1=0.1877$ [MPa]	$C_2=0.0045$ [MPa]	Quality of fit		
	Weight	Error	Region 1	Region 2	Region 3
UT	0	3.0911	0.0159	0.5669	3.1010
ET	1	0.0703	0.0000	0.0370	0.0810
PS	0	1.8016	0.0045	0.3321	1.6404
Total	1	4.9631	0.0204	1.2360	4.8224

Table A.32: Equibiaxial tension results for Nunes model.

ET only fit (Treloar)						
Parameters	$G_c=0.4009$ [MPa]	$G_e=1.56e-7$ [MPa]	$\beta=0.7531$	Quality of fit		
	Weight	Error	Region 1	Region 2	Region 3	
UT	0	6.1397	0.0299	1.5152	5.9214	
ET	1	0.0838	0.0000	0.0130	0.0765	
PS	0	3.8622	0.0104	0.6720	3.4163	
Total	1	10.0857	0.0403	2.2002	9.4143	

Table A.33: Equibiaxial tension results for tube model.

ET only fit (Treloar)					
Parameters	$\mu_1=0.3899$ [MPa] $\mu_2=0.1000$ [MPa] $\eta=3.9998$		Quality of fit		
	Weight	Error	Region 1	Region 2	Region 3
UT	0	4.7611	0.0209	1.2168	4.6468
ET	1	0.1081	0.0000	0.0105	0.0959
PS	0	3.0767	0.0062	0.5511	2.7520
Total	1	7.9459	0.0271	1.7784	7.4947

Table A.34: Equibiaxial tension results for slip-link model.

ET only fit (Treloar)					
Parameters	$A_1=0.1327$ [MPa] $\alpha_1=7.07e-5$ $B_1=1.47e-5$ [MPa]		Quality of fit		
	Weight	Error	Region 1	Region 2	Region 3
UT	0	34.005	0.1213	0.5584	6.9520
ET	1	0.0063	0.0178	0.0213	0.0223
PS	0	0.3883	0.0073	0.0506	0.3276
Total	1	34.400	0.1464	0.6303	7.3019

Table A.35: Equibiaxial tension results for Swanson model.

ET only fit (Treloar)					
Parameters	$C_1=0.2004$ [MPa] $C_2=1.01e-4$ [MPa]		Quality of fit		
	Weight	Error	Region 1	Region 2	Region 3
UT	0	6.1364	0.0299	1.5150	5.9187
ET	1	0.0838	0.0000	0.0129	0.0764
PS	0	3.8605	0.0104	0.6721	3.4152
Total	1	10.0807	0.0403	2.2000	9.4103

Table A.36: Equibiaxial tension results for Gent-Thomas model.

ET only fit (Treloar)					
Parameters	$\mu_1=0.1783$ [MPa]	$\mu_2=0.1000$ [MPa]	$\kappa=1.0000$		
			Quality of fit		
	Weight	Error	Region 1	Region 2	Region 3
UT	0	3.0956	0.0087	1.0527	3.2452
ET	1	0.2051	0.0000	0.0056	0.1799
PS	0	2.0953	0.0014	0.5644	2.0316
Total	1	5.3960	0.0102	1.6228	5.4567

Table A.37: Equibiaxial tension results for constrained-junction model.

ET only fit (Treloar)					
Parameters	$A=0.4832$ [MPa]	$B=-0.0486$	$C=0.0372$ [MPa]		
			$D=-0.3035$		
			Quality of fit		
	Weight	Error	Region 1	Region 2	Region 3
UT	0	30.0420	0.0333	0.3613	8.3432
ET	1	0.0045	0.0181	0.0188	0.0200
PS	0	0.9673	0.0080	0.0124	0.5918
Total	1	31.0138	0.0594	0.3926	8.9550

Table A.38: Equibiaxial tension results for weight function based (WFB) model.

ET only fit (Treloar)					
Parameters	$\mu=0.4009$ [MPa]				
			Quality of fit		
	Weight	Error	Region 1	Region 2	Region 3
UT	0	6.1397	0.0299	1.5152	5.9215
ET	1	0.0838	0.0000	0.0130	0.0765
PS	0	3.8623	0.0104	0.6720	3.4164
Total	1	10.0858	0.0403	2.2002	9.4143

Table A.39: Equibiaxial tension results for neo-Hooke model.

ET only fit (Treloar)					
$\mu=0.4848$ [MPa]					
Parameters	Weight	Error	Quality of fit		
			Region 1	Region 2	Region 3
UT	0	4.2051	0.1279	2.9803	5.6992
ET	1	0.3980	0.0000	0.1764	0.4721
PS	0	2.5146	0.0877	1.7969	3.2121
Total	1	7.1177	0.2156	4.9536	9.3833

Table A.40: Equibiaxial tension results for Valanis-Landel model.

Appendix B

PRURE SHEAR RESULTS FOR HYPERELASTIC MODELS

PS only fit (Treloar)					
Parameters	$\mu=0.1285$ [MPa]	$N=32.3906$	$p=6.6449$		
	$U=0.1360$	$q=0.9990$			
		Quality of fit			
	Weight	Error	Region 1	Region 2	Region 3
UT	0	986.2659	0.0018	0.0174	163.7452
ET	0	0.0934	0.0188	0.0417	0.0855
PS	1	$8.07e-4$	0.0067	0.0069	0.0070
Total	1	986.3601	0.0273	0.0660	163.8377

Table B.1: Pure shear results for Micro-Sphere model.

PS only fit (Treloar)					
Parameters	$C_1=0.0145$ [MPa]	$C_2=0.0643$ [MPa]	$C_3=0.1381$ [MPa]		
	$\gamma=1.2550$	$k=0.0020$			
		Quality of fit			
	Weight	Error	Region 1	Region 2	Region 3
UT	0	$1.71e4$	0.2078	2.0950	$2.95e3$
ET	0	$1.62e3$	0.0215	15.6632	796.0377
PS	1	$6.83e-4$	0.0064	0.0066	0.0067
Total	1	$1.87e4$	0.2357	17.7648	$3.75e3$

Table B.2: Pure Shear results for Alexander model.

PS only fit (Treloar)					
Parameters	$exp(a_0)=0.0656$ [MPa]	$a_1=-0.3288$ [MPa]	$a_2=0.0119$ [MPa]		
	$exp(b_0)=0.1174$ [MPa]	$b_1=0.1038$			
		Quality of fit			
	Weight	Error	Region 1	Region 2	Region 3
UT	0	$4.20e15$	0.1544	2.6320	$6.69e14$
ET	0	$7.09e3$	0.0156	23.9587	$3.21e3$
PS	1	$8.30e-4$	0.0075	0.0078	0.0078
Total	1	$4.20e15$	0.1776	26.5985	$6.69e14$

Table B.3: Pure shear results for Diani and Ray model.

PS only fit (Treloar)					
Parameters	$G_c=0.2030$ [MPa] $\delta=0.0934$ [MPa] $G_e=0.1876$ $\beta=0.1244$				
	Quality of fit				
	Weight	Error	Region 1	Region 2	Region 3
UT	0	0.3330	0.0034	0.0038	0.0597
ET	0	0.0299	0.0166	0.0299	0.0381
PS	1	0.0011	0.0083	0.0085	0.0087
Total	1	0.3641	0.0283	0.0422	0.1066

Table B.4: Pure shear results for Extended-Tube model.

PS only fit (Treloar)					
Parameters	$E=1.1963$ [MPa] $\alpha_1=-0.4853$ $\alpha_2=0.1529$ $\alpha_3=-0.1340$ $\alpha_4=0.3373$				
	Quality of fit				
	Weight	Error	Region 1	Region 2	Region 3
UT	0	$4.01e3$	0.0281	19.4816	908.5265
ET	0	$4.15e6$	0.0135	744.7868	$1.87e6$
PS	1	$7.26e-4$	0.0071	0.0073	0.0074
Total	1	$4.15e6$	0.0487	764.2757	$1.87e6$

Table B.5: Pure shear results for Shariff model.

PS only fit (Treloar)					
Parameters	$A=0.1261$ [MPa] $B=5.05e-7$ [MPa] $C=0.2205$ [MPa]				
	Quality of fit				
	Weight	Error	Region 1	Region 2	Region 3
UT	0	15.0585	0.0053	0.0199	3.0564
ET	0	1.7330	0.0181	0.1125	0.9265
PS	1	0.0016	0.0100	0.0103	0.0106
Total	1	16.7930	0.0334	0.1427	3.9936

Table B.6: Pure shear results for Carroll model.

PS only fit (Treloar)					
Parameters	$\mu_c k=0.0351$ [MPa] $n=33.0269$ $q=1.1768$ $\mu_l=0.7588$ [MPa]				
	Quality of fit				
	Weight	Error	Region 1	Region 2	Region 3
UT	0	8.38e3	0.0426	0.1974	1.34e3
ET	0	8.6040	0.0146	0.7853	4.9532
PS	1	9.72e-4	0.0079	0.0081	0.0083
Total	1	8.39e3	0.0651	0.9907	1.35e3

Table B.7: Pure shear results network averaging tube model.

PS only fit (Treloar)					
Parameters	$a_0=0.1395$ [MPa] $a_1=-0.0032$ [MPa] $a_2=1.34e-4$ [MPa] $b_0=0.0527$ [MPa] $b_1=-0.2217$ [MPa] $b_2=0.7603$ [MPa]				
	Quality of fit				
	Weight	Error	Region 1	Region 2	Region 3
UT	0	1.0860	9.28e-4	0.1079	0.3576
ET	0	210.9443	0.0123	1.4178	103.2765
PS	1	7.330e-4	0.0066	0.0068	0.0069
Total	1	212.0310	0.0198	1.5325	103.6409

Table B.8: Pure shear results for Chevalier and Marco model.

PS only fit (Treloar)					
Parameters	$\mu_1=1.5108$ [MPa] $\mu_2=1.39e-5$ [MPa] $\mu_3=-0.1074$ [MPa] $\alpha_1=0.3346$ $\alpha_2=7.0853$ $\alpha_3=-2.5156$				
	Quality of fit				
	Weight	Error	Region 1	Region 2	Region 3
UT	0	41.7210	0.1036	1.6617	11.1918
ET	0	4.63e3	0.0154	17.6400	2.21e3
PS	1	0.0011	0.0084	0.0086	0.0088
Total	1	4.67e3	0.1274	19.3503	2.21e3

Table B.9: Pure shear results for Ogden model.

PS only fit (Treloar)					
Parameters	$C_2=1.1861$ [MPa]	$C_3=1.88e-5$ [MPa]	$C_4=-2.8493$ [MPa]		
	$C_5=1.8430$ [MPa]	$M=0.0035$	$N=2.3978$		
		Quality of fit			
	Weight	Error	Region 1	Region 2	Region 3
UT	0	$2.35e4$	20.2393	179.4903	739.2803
ET	0	$1.17e5$	1.1021	$1.26e3$	$8.81e4$
PS	1	$5.40e-4$	0.0034	0.0035	0.0036
Total	1	$1.20e5$	21.3448	$1.44e3$	$5.89e4$

Table B.10: Pure shear results for Amin model.

PS only fit (Treloar)					
Parameters	$C_{10}=0.1775$ [MPa]	$C_{01}=0.0044$ [MPa]	$C_{11}=-1.00e-4$ [MPa]		
	$C_{20}=-0.0017$ [MPa]	$C_{30}=5.37e-5$ [MPa]			
		Quality of fit			
	Weight	Error	Region 1	Region 2	Region 3
UT	0	8.4930	0.0242	0.0494	1.9146
ET	0	0.3295	0.0343	0.0783	0.2304
PS	1	0.0031	0.0146	0.0152	0.0160
Total	1	8.8256	0.0731	0.1430	2.1610

Table B.11: Pure shear results for James model.

PS only fit (Treloar)					
Parameters	$C_{10}=0.0934$ [MPa]	$C_{01}=0.0886$ [MPa]	$C_{11}=-3.05e-4$ [MPa]		
	$C_{02}=-0.0012$ [MPa]	$C_{20}=-9.26e-4$ [MPa]	$C_{30}=5.42e-5$ [MPa]		
		Quality of fit			
	Weight	Error	Region 1	Region 2	Region 3
UT	0	11.8164	0.0394	0.2595	2.6773
ET	0	$4.11e4$	0.0205	0.6189	$1.83e4$
PS	1	0.0031	0.0144	0.0152	0.0159
Total	1	$4.11e4$	0.0744	0.8936	$1.83e4$

Table B.12: Pure shear results for Haines and Wilson model.

PS only fit (Treloar)					
Parameters	$A_1=0.1905$ [MPa]	$A_2=-0.0043$ [MPa]	$A_3=1.63e-4$ [MPa]		
	$B_1=0.1899$ [MPa]	$B_2=-0.0043$ [MPa]	$B_3=1.63e-4$ [MPa]		
	Quality of fit				
	Weight	Error	Region 1	Region 2	Region 3
UT	0	27.1247	0.0439	0.5710	6.4834
ET	0	6.56e6	0.0203	13.8971	2.83e6
PS	1	0.0031	0.0144	0.0152	0.0159
Total	1	6.56e6	0.0787	14.4832	2.83e6

Table B.13: Pure shear results for Attard and Hunt model.

PS only fit (Treloar)					
Parameters	$C_1^1=2.1279$ [MPa]	$C_2^1=0.4864$ [MPa]	$C_1^2=-0.4875$ [MPa]		
	$C_2^2=8.80e-7$ [MPa]				
	Quality of fit				
	Weight	Error	Region 1	Region 2	Region 3
UT	0	1.03e3	13.6093	119.8938	376.3074
ET	0	7.85e4	0.6105	848.0354	3.89e4
PS	1	0.0047	0.0177	0.0190	0.0202
Total	1	7.95e4	14.2375	967.9482	3.93e4

Table B.14: Pure shear results for 4-term Bechir model.

PS only fit (Treloar)					
Parameters	$C_2=0.2213$ [MPa]	$\mu=0.2534$ [MPa]	$J_m=89.0821$		
	Quality of fit				
	Weight	Error	Region 1	Region 2	Region 3
UT	0	1.9229	0.0021	0.0030	0.3534
ET	0	0.4754	0.0128	0.0260	0.2585
PS	1	0.0012	0.0069	0.0072	0.0076
Total	1	2.3996	0.0217	0.0362	0.6195

Table B.15: Pure shear results for Pucci and Saccomandi model.

PS only fit (Treloar)					
Parameters	$C_{10}=0.0911$ [MPa]	$C_{01}=0.0909$ [MPa]	$C_{20}=-0.0018$ [MPa]		
	$C_{30}=5.42e-5$ [MPa]				
	Quality of fit				
	Weight	Error	Region 1	Region 2	Region 3
UT	0	2.5990	0.0503	0.7343	1.3931
ET	0	669.7721	0.0203	6.2479	330.0228
PS	1	0.0031	0.0144	0.0152	0.0159
Total	1	672.3742	0.0850	6.9974	331.4317

Table B.16: Pure shear results for Biderman model.

PS only fit (Treloar)					
Parameters	$G=0.4024$ [MPa]	$\lambda_m=10.2460$	$\beta=0.5003$		
	$a=0.2939$				
	Quality of fit				
	Weight	Error	Region 1	Region 2	Region 3
UT	0	83.9494	0.0322	0.6459	18.5211
ET	0	$1.35e5$	0.0130	6.3157	$7.55e4$
PS	1	$9.42e-4$	0.0073	0.0075	0.0077
Total	1	$1.35e5$	0.0525	6.9690	$7.55e4$

Table B.17: Pure shear results for Kilian (van der Waals) model.

PS only fit (Treloar)					
Parameters	$C_2=0.0821$ [MPa]	$C_3=5.73e-8$ [MPa]	$C_5=0.0821$ [MPa]		
	$N=4.0178$				
	Quality of fit				
	Weight	Error	Region 1	Region 2	Region 3
UT	0	43.1106	0.0964	0.6085	8.6632
ET	0	544.5772	0.0377	4.9766	267.9724
PS	1	0.0118	0.0335	0.0413	0.0427
Total	1	587.6996	0.1676	5.6264	276.6783

Table B.18: Pure shear results for Yamashita and Kawabata model.

PS only fit (Treloar)					
Parameters	$C_{10}=0.0649$ [MPa]	$C_{01}=0.0990$ [MPa]	$C_{03}=1.29e-8$ [MPa]		
			Quality of fit		
	Weight	Error	Region 1	Region 2	Region 3
UT	0	46.7771	0.1395	0.9458	9.7012
ET	0	799.2474	0.0347	7.4637	393.6284
PS	1	0.0117	0.0340	0.0421	0.0433
Total	1	846.0362	0.2082	8.4516	403.3730

Table B.19: Pure shear results for Lion model.

PS only fit (Treloar)					
Parameters	$C_{10}=0.1431$ [MPa]	$B=3.25e-5$ [MPa]	$K=0.1588$ [MPa]		
	$\alpha=3.2084$				
			Quality of fit		
	Weight	Error	Region 1	Region 2	Region 3
UT	0	0.6372	0.0057	0.0102	0.1237
ET	0	0.3669	0.0156	0.0332	0.2208
PS	1	$9.60e-4$	0.0078	0.0080	0.0082
Total	1	1.0051	0.0291	0.0514	0.3527

Table B.20: Pure shear results for Beda model.

PS only fit (Treloar)					
Parameters	$G=0.1423$ [MPa]	$k_1=4.03e-4$	$k_2=1.1377$		
			Quality of fit		
	Weight	Error	Region 1	Region 2	Region 3
UT	0	5.7363	0.0053	0.0096	1.1572
ET	0	0.2971	0.0154	0.0325	0.1894
PS	1	$9.28e-4$	0.0078	0.0079	0.0081
Total	1	6.0343	0.0285	0.0500	1.3547

Table B.21: Pure shear results for Hart-Smith model.

PS only fit (Treloar)					
Parameters	$c_1=0.1256$ [MPa]	$c_2=0.0564$ [MPa]	$c_3=0.4963$ [MPa]		
	$c_4=-0.4982$ [MPa]	$c_5=5.42e-5$ [MPa]			
		Quality of fit			
	Weight	Error	Region 1	Region 2	Region 3
UT	0	1.18e5	15.7672	1.76e3	2.96e4
ET	0	7.73e9	0.0654	7.91e5	3.46e9
PS	1	0.0031	0.0144	0.0152	0.0159
Total	1	7.73e9	15.8469	7.93e5	3.46e9

Table B.22: Pure shear results for Haupt and Sedlan model.

PS only fit (Treloar)					
Parameters	$A=0.2002$ [MPa]	$a=0.0134$	$b=0.1427$ [MPa]		
		Quality of fit			
	Weight	Error	Region 1	Region 2	Region 3
UT	0	6.8204	0.0264	0.0511	1.2829
ET	0	0.7676	0.0186	0.1072	0.4655
PS	1	0.0011	0.0069	0.0072	0.0075
Total	1	7.5891	0.0519	0.1654	1.7558

Table B.23: Pure shear results for Exp-Ln model.

PS only fit (Treloar)					
Parameters	$C_{10}=0.1820$ [MPa]	$C_{20}=-0.0018$ [MPa]	$C_{30}=5.39e-5$ [MPa]		
		Quality of fit			
	Weight	Error	Region 1	Region 2	Region 3
UT	0	7.6973	0.0288	0.0621	1.7526
ET	0	0.3315	0.0352	0.1194	0.2861
PS	1	0.0031	0.0145	0.0152	0.0159
Total	1	8.0319	0.0784	0.1967	2.0545

Table B.24: Pure shear results for Yeoh model.

PS only fit (Treloar)					
Parameters	$\alpha_1=0.7602$	$\alpha_2=2.4004$	$\mu_1=0.3820$ [MPa]		
	$\mu_2=0.0066$ [MPa]				
			Quality of fit		
	Weight	Error	Region 1	Region 2	Region 3
UT	0	6.5263	0.0290	0.0551	1.2239
ET	0	0.7188	0.0228	0.1083	0.4457
PS	1	0.0012	0.0083	0.0085	0.0088
Total	1	7.2463	0.0601	0.1720	1.6784

Table B.25: Pure shear results for two-term model.

PS only fit (Treloar)					
Parameters	$A=0.2062$ [MPa]	$B=0.0169$	$C_{10}=0.0763$ [MPa]		
	$I_m=1.0003$				
			Quality of fit		
	Weight	Error	Region 1	Region 2	Region 3
UT	0	16.7429	0.0224	0.0456	3.1888
ET	0	1.0345	0.0148	0.1102	0.5842
PS	1	0.0022	0.0063	0.0070	0.0079
Total	1	17.7795	0.0435	0.1629	3.7809

Table B.26: Pure shear results for Yeoh-Fleming model.

PS only fit (Treloar)					
Parameters	$\mu=0.1057$ [MPa]		$N=59.5721$		
			Quality of fit		
	Weight	Error	Region 1	Region 2	Region 3
UT	0	31.5855	0.0242	0.0656	6.1779
ET	0	1.5616	0.0683	0.2050	0.6033
PS	1	0.0215	0.0391	0.0504	0.0563
Total	1	33.1686	0.1316	0.3210	7.1376

Table B.27: Pure shear results for Arruda-Boyce model.

PS only fit (Treloar)					
Parameters	$\mu=0.3137$ [MPa] $J_m=263.0011$				
	Weight	Error	Quality of fit		
			Region 1	Region 2	Region 3
UT	0	33.3852	0.0242	0.0663	6.5342
ET	0	1.6008	0.0679	0.2034	0.9196
PS	1	0.0218	0.0389	0.0498	0.0562
Total	1	35.0078	0.1310	0.3196	7.5099

Table B.28: Pure shear results for Gent model.

PS only fit (Treloar)					
Parameters	$\mu=0.3183$ [MPa] $N=177.3919$				
	Weight	Error	Quality of fit		
			Region 1	Region 2	Region 3
UT	0	31.1220	0.0244	0.0686	6.0839
ET	0	2.1957	0.0685	0.2158	1.2133
PS	1	0.0215	0.0391	0.0504	0.0563
Total	1	33.3392	0.1320	0.3347	7.3535

Table B.29: Pure shear results for three-chain model.

PS only fit (Treloar)					
Parameters	$C_{10}=0.0855$ [MPa] $C_{01}=0.0854$ [MPa]				
	Weight	Error	Quality of fit		
			Region 1	Region 2	Region 3
UT	0	0.5860	0.0000	0.0093	0.9237
ET	0	12.2850	0.0000	0.0000	15.9620
PS	1	0.0179	0.0000	0.0048	0.0400
Total	1	12.8888	0.0000	0.0141	16.9256

Table B.30: Pure shear results for Mooney model.

PS only fit (Treloar)					
Parameters	$C_{10}=0.0807$ [MPa]	$C_{20}=3.23e-4$ [MPa]	$C_{01}=0.0803$ [MPa]		
	Weight	Error	Quality of fit		
			Region 1	Region 2	Region 3
UT	0	81.312	0.1056	0.5617	17.570
ET	0	481.83	0.0421	4.7777	239.071
PS	1	0.0224	0.0382	0.0486	0.0557
Total	1	563.17	0.1859	5.3880	256.697

Table B.31: Pure shear results for Isihara model.

PS only fit (Treloar)					
Parameters	$C_1=0.1577$ [MPa]		$C_2=0.0143$ [MPa]		
	Weight	Error	Quality of fit		
			Region 1	Region 2	Region 3
UT	0	0.1001	0.0011	0.0209	0.1191
ET	0	0.1414	0.0000	0.0824	0.2300
PS	1	0.0297	0.0009	0.0105	0.0320
Total	1	0.2713	0.0020	0.1138	0.3811

Table B.32: Pure shear results for Nunes model.

PS only fit (Treloar)					
Parameters	$G_c=0.3164$ [MPa]	$G_e=0.0314$ [MPa]	$\beta=0.0065$		
	Weight	Error	Quality of fit		
			Region 1	Region 2	Region 3
UT	0	0.1756	0.0005	0.0251	0.2116
ET	0	0.8253	0.0000	0.0771	0.9670
PS	1	0.0216	0.0003	0.0171	0.0310
Total	1	1.0225	0.0008	0.1194	1.2097

Table B.33: Pure shear results for tube model.

PS only fit (Treloar)					
Parameters	$\mu_1=0.3237$ [MPa]	$\mu_2=0.1000$ [MPa]	$\eta=0.8401$		
			Quality of fit		
	Weight	Error	Region 1	Region 2	Region 3
UT	0	0.2059	0.0006	0.0415	0.2415
ET	0	1.0882	0.0000	0.0958	1.1577
PS	1	0.0330	0.0010	0.0104	0.0354
Total	1	1.3271	0.0016	0.1477	1.4346

Table B.34: Pure shear results for slip-link model.

PS only fit (Treloar)					
Parameters	$A_1=0.0022$ [MPa]	$\alpha_1=1.4009$	$B_1=0.1273$ [MPa]		
	$\beta_1=-0.2397$				
			Quality of fit		
	Weight	Error	Region 1	Region 2	Region 3
UT	0	35.904	0.2304	1.6113	9.1460
ET	0	295.15	0.0215	8.5802	154.67
PS	1	0.0012	0.0083	0.0085	0.0088
Total	1	331.05	0.2603	10.200	168.83

Table B.35: Pure shear results for Swanson model.

PS only fit (Treloar)					
Parameters	$C_1=0.1630$ [MPa]	$C_2=0.0353$ [MPa]			
			Quality of fit		
	Weight	Error	Region 1	Region 2	Region 3
UT	0	0.2114	0.0009	0.0385	0.2449
ET	0	1.2386	0.0000	0.1193	1.3428
PS	1	0.0314	0.0014	0.0157	0.0376
Total	1	1.4814	0.0023	0.1735	1.6253

Table B.36: Pure shear results for Gent-Thomas model.

PS only fit (Treloar)					
Parameters	$\mu_1=0.1498$ [MPa] $\mu_2=0.1000$ [MPa] $\kappa=1.2122$		Quality of fit		
	Weight	Error	Region 1	Region 2	Region 3
UT	0	0.0796	0.0000	0.0132	0.1168
ET	0	0.3511	0.0000	0.0126	0.4979
PS	1	0.0192	0.0000	0.0353	0.0450
Total	1	0.4498	0.0000	0.0611	0.6597

Table B.37: Pure shear results for constrained-junction model.

PS only fit (Treloar)					
Parameters	$A=0.3366$ [MPa] $B=-0.0515$ $C=0.1317$ [MPa] $D=0.1895$		Quality of fit		
	Weight	Error	Region 1	Region 2	Region 3
UT	0	22.3858	0.0361	0.0643	4.2765
ET	0	2.6816	0.0399	0.0730	1.3467
PS	1	0.0035	0.0151	0.0161	0.0170
Total	1	25.0709	0.0911	0.1534	5.6402

Table B.38: Pure shear results for weight function based (WFB) model.

PS only fit (Treloar)					
Parameters	$\mu=0.3377$ [MPa]		Quality of fit		
	Weight	Error	Region 1	Region 2	Region 3
UT	0	0.1071	0.0000	0.0026	0.1575
ET	0	0.4457	0.0000	0.0000	0.7078
PS	1	0.0179	0.0000	0.0048	0.0400
Total	1	0.5706	0.0000	0.0074	0.9052

Table B.39: Pure shear results for neo-Hooke model.

PS only fit (Treloar)					
$\mu=0.3820$ [MPa]					
Parameters	Weight	Error	Quality of fit		
			Region 1	Region 2	Region 3
UT	0	0.1687	0.0000	0.0202	0.2845
ET	0	0.5544	0.0000	0.0000	0.7310
PS	1	0.0181	0.0000	0.0015	0.0237
Total	1	0.7411	0.0000	0.0216	1.0393

Table B.40: Pure shear results for Valanis-Landel model.

Appendix C

STRAIN ENERGY FUNCTIONS FOR HYPERELASTIC MODELS

Rank	model name	n_p	model definition
1	Micro-sphere model	5	$\psi = \mu N \left(\langle \lambda_r \rangle_p \mathcal{L}^{-1}(\langle \lambda_r \rangle_p) + \ln \frac{\mathcal{L}^{-1}(\langle \lambda_r \rangle_p)}{\sinh \mathcal{L}^{-1}(\langle \lambda_r \rangle_p)} \right) + \mu NU \langle \overline{\gamma^d} \rangle$
2	Alexander model	5	$\psi = C_1 \int \exp(k [I_1 - 3]^2) dI_1 + C_2 \ln \left[\frac{(I_2 - 3)^{1+2}}{\gamma} \right] + C_3 (I_2 - 3)$
3	Diani-Rey model	5	$\psi = \int \exp \left(\sum_{i=0}^m a_i (I_1 - 3)^i \right) dI_1 + \int \exp \left(\sum_{i=0}^m b_i (\ln I_2)^i \right) dI_2$
4	Extended tube model	4	$\psi = \frac{C_c}{2} \frac{(1-\delta^2)(D-3)}{1-\delta^2(D-3)} + \ln(1-\delta^2(D-3)) + \frac{2C_c}{\beta^2} \sum_{A=1}^3 (\lambda_{\frac{A}{\lambda}}^{-\beta} - 1)$, with $D = \sum_{A=1}^3 \lambda_A^2$
5	Shariff model	5	$\psi = E \sum_{i=0}^3 \alpha_i \phi_i$ $\phi_0 = \frac{2 \ln(D)}{3}$, $\phi_1 = \exp(1-\lambda) + \lambda - 2$, $\phi_2 = \exp(\lambda-1) - \lambda$, $\phi_3 = \frac{(\lambda-1)^3}{\lambda^3 \delta^6}$, and $\phi_j = (\lambda-1)^{j-1}$ for $j=4,5,\dots,n$
6	Carroll model	3	$\psi = A I_1 + B I_1^4 + C \sqrt{I_2}$
7	Network averaging tube model	4	$\psi = (\mu_c k) n \ln \frac{\sin(\frac{\pi l}{\sqrt{D}})(l_1/3)^{3/2}}{\sin(\frac{\pi l}{\sqrt{D}})(l_1/3)^{3/2}} + \mu_l \left(\frac{l_2}{3} \right)^{1/2} - 1$
8	Chevalier-Marco model	6	$\frac{\partial \psi}{\partial I_1} = \sum_{i=0}^n a_i (I_1 - 3)^i$ and $\frac{\partial \psi}{\partial I_2} = \sum_{i=0}^n \frac{b_i}{I_2^i}$
9	Ogden model	6	$\psi = \sum_{i=1}^N \frac{\mu_i}{\alpha_i} (\lambda_1^{\alpha_i} + \lambda_2^{\alpha_i} + \lambda_3^{\alpha_i} - 3)$
10	Amin model	6	$\psi = C_5 (I_1 - 3) + \frac{C_3}{N+1} (I_1 - 3)^{N+1} + \frac{C_4}{M+1} (I_1 - 3)^{M+1} + C_2 (I_2 - 3)$
11	James-Green-Simpson model	5	$\psi = C_{10} (I_1 - 3) + C_{01} (I_2 - 3) + C_{11} (I_1 - 3)(I_2 - 3) + C_{20} (I_1 - 3)^2 + C_{30} (I_1 - 3)^3$
12	Hains-Wilson model	6	$\psi = C_{10} (I_1 - 3) + C_{01} (I_2 - 3) + C_{11} (I_1 - 3)(I_2 - 3) + C_{02} (I_2 - 3)^2 + C_{20} (I_1 - 3)^2 + C_{30} (I_1 - 3)^3$
13	Attard-Hunt model	6	$\psi = \sum_{i=1}^m \left[\frac{A_i}{2n} (\lambda_1^{2n} + \lambda_2^{2n} + \lambda_3^{2n} - 3) + \frac{B_i}{2n} (\lambda_1^{-2n} + \lambda_2^{-2n} + \lambda_3^{-2n} - 3) \right]$
14	Bechir-4term model	4	$\psi = C_1^1 (I_1 - 3) + \sum_{i=2}^{\infty} C_i^i \left(\lambda_1^{2n} + \lambda_2^{2n} + \lambda_3^{2n} - 3 \right)^i$
15	Pucci-Saccomandi model	3	$\psi = -\frac{\mu}{2} J_m \log \left(1 - \frac{I_1 - 3}{J_m} \right) + C_2 \log \left(\frac{I_2}{3} \right)$
16	Biderman model	4	$\psi = C_{10} (I_1 - 3) + C_{01} (I_2 - 3) + C_{20} (I_1 - 3)^2 + C_{30} (I_1 - 3)^3$
17	van der waals model	4	$\psi = G \left\{ - \left(\lambda_m^2 - 3 \right) \left[\ln(1-\theta) + \theta \right] - \frac{2}{3} a \left(\frac{I_2 - 3}{2} \right)^{3/2} \right\}$ with $\theta = \sqrt{\frac{(I_2 - 3)}{(2I_m - 3)}}$, and $\tilde{I} = \beta I_1 + (1 - \beta) I_2$
18	Yamashita-Kawabata model	4	$\psi = C_5 (I_1 - 3) + C_2 (I_2 - 3) + \frac{C_3}{N+1} (I_1 - 3)^{N+1}$
19	Lion model	3	$\psi = C_{10} (I_1 - 3) + C_{01} (I_2 - 3) + C_{03} (I_1 - 3)^5$
20	Beda model	4	$\psi = C_{10} (I_1 - 3) + \frac{B}{a} (I_1 - 3)^a + K \ln \frac{I_2}{3}$

Table C.1: Free energy functions of first 20 models sorted by quality of fit metric.

Rank	model name	n_p	model definition
21	Hart-Smith-Crisp model	3	$\frac{\partial \psi}{\partial I_1} = G \exp(k_1 (I_1 - 3)^2)$ and $\frac{\partial \psi}{\partial I_2} = G \frac{k_2}{I_2}$
22	Haupt-Sedlan model	5	$\psi = C_{10} (I_1 - 3) + C_{01} (I_2 - 3) + C_{11} (I_1 - 3)(I_2 - 3) + C_{02} (I_2 - 3)^2 + C_{30} (I_1 - 3)^3$
23	Exp-Ln model	3	$\psi = A \frac{1}{a} \exp(a(I_1 - 3)) + b(I_1 - 2)(1 - \ln(I_1 - 2)) - \frac{1}{a} - b$
24	Yeoh model	3	$\psi = C_{10} (I_1 - 3) + C_{20} (I_1 - 3)^2 + C_{30} (I_1 - 3)^3$
25	Two-Term model	4	$\psi = \frac{3^{1-\alpha_1}}{2\alpha_1} \mu_1 (I_1^{\alpha_1} - 3^{\alpha_1}) + \frac{3^{1-\alpha_2}}{2\alpha_2} \mu_2 (I_1^{\alpha_2} - 3^{\alpha_2})$
26	Yeoh-Fleming model	4	$\psi = \frac{A}{B} (I_m - 3) (1 - e^{-BR}) - C_{10} (I_m - 3) \ln(1 - R)$ with $R = \frac{(I_1 - 3)}{(I_m - 3)}$
27	Arruda-Boyce model	2	$\psi = \mu \sqrt{N} \left[\beta_{ch} \lambda_{ch} + \sqrt{N} \ln \left(\frac{\beta_{ch}}{\sinh \beta_{ch}} \right) \right]$, where $\beta_{ch} = \mathcal{L}^{-1} \left(\frac{\lambda_{ch}}{\sqrt{N}} \right)$
28	Three Chain model	2	$\psi = \frac{\mu \sqrt{N}}{3} \sum_{i=1}^3 \left(\lambda_i \beta_i + \sqrt{N} \ln \left(\frac{\beta_i}{\sinh \beta_i} \right) \right)$ with $\beta_i = \mathcal{L}^{-1} \left(\frac{\lambda_i}{\sqrt{N}} \right)$
29	Mooney model	2	$\psi = C_{10} (I_1 - 3) + C_{01} (I_2 - 3)$
30	Ishihara model	3	$\psi = C_{10} (I_1 - 3) + C_{20} (I_1 - 3)^2 + C_{01} (I_2 - 3)$
31	Nunes model	2	$\psi = C_1 (I_1 - 3) + \frac{4}{3} C_2 (I_2 - 3)^{3/4}$
32	Tube model	3	$\psi = \sum_{i=1}^3 \frac{G_c}{2} (\lambda_i^2 - 1) + \frac{2G_c}{\beta^2} (\lambda_i^{-\beta} - 1)$
33	Slip-Link model	3	$\psi = \frac{\mu_1}{2} \sum_{i=1}^3 \lambda_i^2 + \frac{\mu_2}{2} \sum_{i=1}^3 \frac{(1+\eta)\lambda_i^2}{1+\eta\lambda_i^2} + \ln(1 + \eta\lambda_i^2)$
34	Swanson model	4	$\psi = \frac{3}{2} \sum_{i=1}^n \frac{A_i}{1+\alpha_i} \left[\frac{I_1}{3} \right]^{1+\alpha_i} + \frac{3}{2} \sum_{j=1}^n \frac{B_j}{1+\beta_j} \left[\frac{I_2}{3} \right]^{1+\beta_j}$
35	Gent-Thomas model	2	$\psi = C_1 (I_1 - 3) + C_2 \ln \left(\frac{I_2}{3} \right)$
36	Constrained Junction model	3	$\psi = \mu_1 (I_1 - 3) + \mu_2 \sum_{i=1}^3 [B_i + D_i - \ln(B_i + 1) - \ln(D_i + 1)]$, where $B_i = \kappa^2 (\lambda_i^2 + \kappa)^{-2}$ and $D_i = \lambda_i^2 \kappa^{-1} B_i$
37	WFB model	4	$\psi = \int_{I_1}^{I_1^*} \{ F(\lambda) A (\lambda e^{-B\lambda}) + C (\lambda I^{-D}) \} \left(\lambda - \frac{1}{\lambda} \right) d\lambda$ where $F(\lambda) = 2.378e8 (\lambda^2 + 15.5128)^{-7.0574}$
38	Gent model	2	$\psi = -\frac{\mu}{2} J_m \ln \left(1 - \frac{I_1 - 3}{J_m} \right)$
39	neo-Hooke model	1	$\psi = \frac{\mu}{2} (I_1 - 3)$
40	Valanis-Landel model	1	$\frac{d\psi}{d\lambda} = 2\mu \ln(\lambda)$

Table C.2: Free energy functions of the remaining 20 models sorted by quality of fit metric.